

EDSC

Ecole Doctorale des
Sciences Chimiques

UNIVERSITÉ DE STRASBOURG



UNIVERSITE DE STRASBOURG

ECOLE DOCTORALE DES SCIENCES CHIMIQUES

THESE DE DOCTORAT

pour obtenir le grade de
DOCTEUR DE L'UNIVERSITE DE STRASBOURG

Synthesis, physicochemical and biological evaluation studies of ruthenium(II) and osmium(II) anticancer organometallic complexes

Présentée par

Bastien BOFF

Ingénieur de l'Ecole Européenne
de Chimie, Polymères et Matériaux (E.C.P.M)

Soutenue le 11 Février 2012 devant la commission d'examen:

Rapporteur externe: Dr. Eric MEGGERS, Philipps-Universität Marburg (Allemagne)

Rapporteur externe: Dr. John SPENCER, University of Greenwich (Royaume-Uni)

Rapporteur interne: Dr. Dominique MATT, Université de Strasbourg

Directeur de thèse: Dr. Michel PFEFFER, Université de Strasbourg

Personnalité invitée: Dr. Christian GAIDDON, Université de Strasbourg

- Laboratoire de Synthèses Métallo Induites (LSMI) -

EDSC

Ecole Doctorale des
Sciences Chimiques

UNIVERSITÉ DE STRASBOURG



Synthesis, physicochemical and biological evaluation studies of ruthenium(II) and osmium(II) anticancer organometallic complexes

BOFF Bastien

E.C.P.M. Chemical engineer

Ecole Européenne de Chimie, Polymères et Matériaux de Strasbourg, France

M. Sc. Molecular and Supramolecular Chemistry

Université de Strasbourg I

Ecole Doctorale des Sciences Chimiques de Strasbourg (ED 222), Université de Strasbourg I.

The synthetic work described in this thesis was carried out at the Institut de Chimie (UMR 7177) in the **Laboratoire de Synthèses Metallo-Induites** (LSMI), 4 rue Blaise Pascal, 67000 Strasbourg.

Biological evaluation was carried out at the Inserm Institute (U692) in the **Laboratoire de Signalisation moléculaire et Neurodégénérescence** (LSMN), 11 rue Humann, 67085 Strasbourg.

This research was financially supported by the C.N.R.S and the Région Alsace through B.D.I. fellowship.

***à mes parents, Mireille et Bernard,
pour leur soutien, leur amour inconditionnel,
et leurs encouragements.***

Remerciements

A tous les "curieux" ouvrant ce mémoire, qu'ils soient scientifiques ou non, ce préambule me permet de saluer les personnes qui, de près ou de loin, ont contribué à la concrétisation de ce travail de thèse de doctorat. Soucieux d'exprimer ma reconnaissance et ma gratitude le plus sincèrement possible, j'espère que les mots employés ici seront à la hauteur de l'estime que j'ai pour les personnes concernées.

Au terme de ce doctorat, je tiens tout d'abord à remercier Dr. Michel Pfeffer, Directeur du Laboratoire de Synthèses Métallo-Induites (LSMI, Université de Strasbourg), pour ces trois années à superviser mon travail de thèse. Michel, je tiens à te faire part de ma profonde reconnaissance pour m'avoir accueilli au sein du laboratoire et pour l'attention, ainsi que la réelle confiance que tu as su me témoigner dans ma liberté d'action et mes initiatives personnelles qui se sont d'ailleurs souvent révélées prometteuses. En plus de ta compétence, je garderai de toi le souvenir d'un homme passionné, tout comme moi, par la chimie et fervent défenseur des anticancéreux cyclométallés, sujet qui te tient particulièrement à cœur. Par amour du travail bien fait, tu as le souci permanent d'approcher la perfection. Tu as toujours fait preuve d'une grande disponibilité et lors de nos échanges tu as à chaque fois été compréhensif et tu as su m'encourager dans mes prises de décision. C'est déjà la fin d'une belle aventure, mais je garderai un excellent souvenir de ces années passées à tes côtés.

Je tiens également à remercier les Membres du jury, Prof. Dr. Eric Meggers (Philipps-Universität Marburg, Allemagne) Dr. John Spencer (University of Greenwich, Royaume-Uni) pour avoir lu attentivement le présent manuscrit et Dr. Dominique Matt pour avoir accepté d'être le Président du jury. Je les remercie tous aussi pour leurs remarques et questions ouvrant de nouvelles perspectives à ce travail.

Je ne peux, bien entendu, pas oublier de remercier Dr. Claude Sirlin, Maître de conférences (Université de Strasbourg) pour son soutien. Claude, tu as réussi à faire preuve de souplesse et d'ouverture d'esprit à mon égard, notamment dans mes choix de méthodes de travail, me permettant ainsi d'évoluer plus efficacement et de satisfaire ma curiosité. Nos discussions amicales "entre ingénieurs" autour d'un verre ou d'un bon repas resteront présentes dans ma mémoire. Je me souviendrai toujours de ton humour quelque fois décapant voire aussi caustique... que la soude mais tellement empreint de sincérité et d'authenticité sundgauvienne. Malgré ton caractère parfois "bien trempé", tes frasques m'ont souvent fait mourir de rire... Maintes fois imitées, mais jamais égalées!

Cette thèse m'a permis de collaborer de manière fructueuse avec de nombreuses personnes, contribuant chacune à son caractère interdisciplinaire. En effet, je n'aurais jamais pu réaliser ce travail doctoral sans le soutien d'un grand nombre de personnes dont la générosité, la bonne humeur et l'intérêt manifesté à l'égard de ma recherche m'ont permis de progresser.

Je remercie le Dr. Jean-Philippe Loeffler, Directeur du Laboratoire de Signalisations Moléculaires et Neurodégénérescence (LSMN, INSERM UM692) et plus particulièrement les Drs. Christian Gaidon et Marjorie Sidhoum pour m'avoir initié à la biologie cellulaire et m'avoir permis de réaliser les mesures *in vitro* sur l'ensemble de mes composés. Leur sympathie mais également leurs conseils avisés ont su enrichir mes connaissances.

J'adresse aussi toute ma gratitude au Dr. Jean-Paul Collin, Directeur de recherche émérite (Université de Strasbourg), pour m'avoir transmis son savoir faire dans les mesures d'électrochimie de mes complexes. Malgré ta retraite, tu restes toujours autant passionné par la chimie et tu as su trouver du temps pour me conseiller et me guider.

Je remercie également Dr. Anne Vessières, Directrice du Laboratoire Charles Friedel, (ENSCP Chimie ParisTech) et Marie-Aude Plamont (AI CNRS) pour la formation aux mesures de lipophilie sur HPLC. Anne, je vous remercie pour les discussions scientifiques que nous avons pu avoir et pour l'accueil très chaleureux que vous m'avez réservé au sein de votre équipe.

Mes vifs remerciements vont aussi au Dr. Michel Mehrenberger, Maître de conférences (Institut de Recherche Mathématique Avancée IRMA), pour m'avoir fait profiter de ses connaissances en mathématique et pour ses précieux conseils apportés dans la programmation de la résolution du problème d'optimisation non-linéaire.

Je ne peux oublier de remercier les membres des services communs d'analyses pour leurs compétences et leur savoir-faire dans leurs domaines respectifs. J'exprime ainsi particulièrement ma reconnaissance à:

- Jean-Daniel Sauer et Maurice Coppe du service de Résonance Magnétique Nucléaire
- Lydia Brelot et Corinne Bailly du service de Radiocristallographie
- Hélène Nierengarten et Romain Carriere du service de Spectrométrie de Masse.

J'associe bien entendu ces remerciements à vous tous, acteurs du LSMI et du LSMN que j'ai côtoyés. Vous avez tous contribué de près ou de loin à la bonne ambiance de ces trois années passées en votre compagnie. C'est avec nostalgie, que je vais regretter cette mixité culturelle et scientifique. Quant à la liste de tous les apports non-scientifiques, je m'abstiendrai de la dévoiler ici, pour des raisons évidentes de "confidentialité" !

Je m'excuse par avance pour tous ceux que j'aurais pu avoir oubliés, mais soyez sûrs que vous resterez tous dans mon cœur. Du côté des chimistes, un grand merci aux Drs. Laurent Barloy et Jean-Pierre Djukic, à Pape, Ksénia, Dusan, Ludivine, Ali, Jean-Thomas, Wissam, Nicolas, Stéphane, Predrag, Christophe, Noël... Du côté des biologistes, merci également à Pauline, Yannick, Cynthia, Vania et Orphée pour leur soutien à un chimiste lors de ses premiers pas en biologie cellulaire.

Un petit clin d'œil également à mes étudiants que j'ai eu en cours ou que j'ai encadrés lors de leurs stages au laboratoire et plus particulièrement Ozlem, Hugo, Estelle, Benjamin et Nathan avec qui j'ai pu partager bien plus qu'un simple bout de paillasse. Je pense avoir réussi à vous communiquer ma passion pour la recherche et je souhaite vous remercier pour votre implication quotidienne dans votre travail au laboratoire.

Il y a pour finir tous ceux qui n'étaient pas nécessairement et physiquement présents au laboratoire. Je remercie bien sûr ma famille et plus particulièrement mes parents qui m'ont appris qu'il faut rêver, persévérer et toujours avoir foi en ce que l'on fait. Même si les plus belles réussites se doivent d'être méritées, Maman, Papa, vous y avez contribué tous les deux en ayant toujours su trouver les mots justes pour m'encourager et me soutenir tout au long de ce chemin. Je ne vous en serai jamais assez reconnaissant.

Bastien

Résumé

Suite au succès clinique des composés du platine (*cis*platine et de ses dérivés) en tant qu'agent anticancéreux, la chimie inorganique médicinale a connu un essor considérable offrant ainsi une alternative à la conception d'agents thérapeutiques. Bien que le *cis*platine et ses dérivés soient sans doute une des classes la plus réussie de médicaments anticancéreux, leur utilisation n'est pas efficace contre tous les types de cancer. De plus, ils sont à l'origine d'effets secondaires très invalidants (neurotoxicité, néphrotoxicité, perte de poids, nausées...) et sont également inactifs contre certains cancers présentant une résistance innée ou induite. Par conséquent, la recherche a développé des composés possédant des activités améliorées et des profils de toxicité plus acceptables. Ceci a ainsi stimulé l'intérêt pour les complexes contenant d'autres métaux de la mine du platine tels que le ruthénium, car ces composés présentent une plus faible toxicité que les complexes existants. Certains composés du ruthénium ont déjà montré une activité anticancéreuse prometteuse et deux complexes du Ru^{III} le *trans*-[RuCl₄-(DMSO)(Im)]ImH (NAMI-A) et le *trans*-[RuCl₄(Ind)₂]IndH (KP1019) sont entrés récemment en phase clinique.

Dans le but d'améliorer l'activité et de réduire les effets secondaires des agents anticancéreux existants, le Laboratoire de Synthèses Métallo-Induites a développé depuis plusieurs années des complexes organométalliques du ruthénium **RDC** (**R**uthenium **D**erivative **C**ompound) dans lesquels un des ligands est fortement lié au métal par une liaison covalente σ C-Ru qui est elle-même stabilisée par une liaison intramoléculaire N-Ru. Cette thèse présente les avancées récentes du laboratoire dans ce domaine et plus particulièrement le développement d'une chimiothèque de **RDC** de seconde génération dans laquelle le ligand cyclométallé est stabilisé par deux liaisons N-Ru. Plusieurs complexes ont ainsi atteint des IC₅₀ significativement inférieur à la micromole. En parallèle, le même type d'études a été réalisé sur des complexes de l'osmium aboutissant à une chimiothèque **ODC** (**O**smium **D**erivative **C**ompound) d'une quarantaine de composés. Cette étude est d'un intérêt particulier car non seulement elle complète la famille des **RDC**, mais elle permet également de vérifier l'impact du changement de métal. Les études biologiques ont ainsi montré que l'osmium présente un réel intérêt dans le développement de nouveaux médicaments antitumoraux particulièrement efficaces. Les mesures des propriétés physico-chimiques telles que le potentiel d'oxydo-réduction et la lipophilie ($\log(P_{o/w})$) ont permis de corréler ces paramètres à leur activité *in vitro*, se rapprochant ainsi d'une éventuelle relation propriété-activité (P.A.R.). Le réel rôle du potentiel d'oxydo-réduction deviendra probablement plus clair au fur et à mesure de notre avancée dans la résolution du mécanisme d'action de ces espèces.

Mots clés

ruthénium / osmium / complexes organométalliques / cyclométallation / potentiel d'oxydo-réduction / lipophilie / chimie inorganique médicinale / cancer / agents anticancéreux / chimiothérapie / stabilité / évaluation *in vitro* et *in vivo* / relation propriété activité (P.A.R.)

List of abbreviations

A172	human glioblastoma
ADME	Absorption, Distribution, Metabolism and Excretion
AI	active ingredient
ampy	2-pyridinylmethanamine
A2780cis / A2780	human ovarian cancer cell line <i>cisplatin</i> resistant or not
AMMN	N-nitroso-acetoxymethyl-methylamine
Azpy Nme₂	4-(2-pyridylazo)- <i>N,N</i> -dimethylaniline
bip	biphenyl
bp	base pair(s)
[<i>n</i>-Bu₄N][PF₆]	tetrabutylammonium hexafluorophosphate
bpy	2,2'-bipyridyl
carboxy-H₂DCFDA	5-(and-6)-carboxy-2',7'-dichlorodihydrofluorescein diacetate
CDKs	cyclin-dependent kinases
Cp	cyclopentadienyl
DMEM	Dulbecco's Modified Eagle Medium
DMSO	dimethyl sulfoxide
DNA	deoxyribonucleic acid
dppz	2,5-bis(2-pyridyl)pyrazine
ECACC	European Collection of Culture
E. Coli.	<i>Escherichia coli</i>
en	ethylenediamine
E°_{1/2}	absolute peak potential
E_{pa}	anodic peak potential
E_{pc}	cathodic peak potential
ERK	Extracellular signal-Regulated Kinase
FCS	Foetal calf serum
F.D.A.	(or USFDA) Food and Drugs Administration
GSK	Glycogen Synthase Kinase
Hbzim	1 <i>H</i> -benzimidazole
HInd	1 <i>H</i> -indazole
HIm	1 <i>H</i> -imidazole
Hpz	1 <i>H</i> -pyrazole
Htrz	1 <i>H</i> -1,2,4-triazole
HCT116	colorectal carcinoma
IC₅₀	half-maximal Inhibitory Concentration
InCa	Institut National du Cancer
InVs	Institut de Veille Sanitaire (French sanitary surveillance institute)
IP	intraperitoneal injection
k'_(Φ)	capacity factor

LD₅₀	dose inducing 50% lethality
log(P_{o/w})	Partition coefficient
log(k'_w)	logarithm of capacity factor at 100% water
LMCT	Ligand-Metal Charge Transfer
Log(P_{o/w})	Partition coefficient factor (octanol/water)
MCa	mucine-like carcinoma-associated antigen
MLCT	Metal-Ligand Charge Transfer
MND	menadione
MOPS	3-morpholinopropane-1-sulfonic acid
mppy	pinene-2-phenylpyridine
MTD	Maximal Tolerated Dose
MTT	3-(4,5-Dimethylthiazol-2-yl)-2,5-diphenyltetrazolium bromide
NHE	Normal hydrogen electrode
NCI	National Cancer Institute
NSCL	Non-small cell lung
ODC	Osmium Derivatibe Compound
p53	protein 53 or tumour protein 53
p21/WAF1	cyclin-dependent kinase inhibitor 1
p-cym	<i>para</i> -cymene
P.A.R.	Property Activity Relationship
PDT	Photodynamic Therapy
PGMs	Platinum Group Metals
phen	1,10-phenanthroline
pta	1,3,5-triaza-7-phosphatricyclo[3.3.1.1]decane
Q.S.P.R.	Quantitative Structure-Property Relationship
RCS	Royal Chemical Society
RDC	Ruthenium Derivative Compound
RFU	Rate of Fluorescence
ROS	Reactive Oxygen Species
R.T.	Room temperature
S.A.R.	Structure Activity Relationship
SCE	Saturated calomel electrode
T/C ratio	Percentage of tumour volume in treated condition (T) compared to the control condition (C)
THA	1,4,9,10-tetrahydroanthracene
terpy	2,2',6',2''-terpyridine (IUPAC 2,6-bis(2-pyridyl)pyridine)
t_r / t₀	retention time / dead time
U87	human glioblastoma
UV	Ultraviolet
vis	visible light
W.H.O.	World Health Organization

Table of contents

Foreword:	19
Chapter 1: General Introduction	21
1.1. Generalities about cancer	23
1.1.1. Definition of cancer	23
1.1.2. Cancer epidemiology worldwide: Some facts and figures	24
1.1.3. Formation of cancer cells (Tumorigenesis).....	27
1.1.4. The different existing cancer treatments	30
1.2. Cancer treatment by platinum drugs: cisplatin and its analogues	32
1.2.1. Introduction: How organometallic chemistry established the bases of modern chemotherapy?.....	32
1.2.2. Clinically used anticancer platinum drugs: A success story?.....	32
1.2.3. Cisplatin limitations: Side effects and resistance in chemotherapy	34
1.3. Ruthenium complexes: an ongoing alternative to existing treatments?	36
1.3.1. Introduction.....	36
1.3.2. Ru(III)-based drugs under clinical trials: NAMI-A and KP1019.....	38
1.3.3. Ru(III) complexes vs. cisplatin: Highlight of another activity pattern?	43
1.3.4. Non-cyclometalated arene Ruthenium(II) compounds as potential anticancer agents.....	44
1.3.5. Cyclometalated Ruthenium(II) compounds developed by the Laboratoire de Synthèses Métallo-induites: State of the art.....	52
1.3.6. Ruthenium(II) compounds: A controversial activity pattern?.....	56
1.3.7. Perspectives for ruthenium in cancer treatment	56
1.4. Osmium analogues: a new step towards anticancer therapeutics?	57
1.4.1. Introduction.....	57
1.4.2. NAMI-A osmium analogues	57
1.4.3. En route to KP1019 osmium analogues	59
1.4.4. Half-sandwich arene osmium(II) analogues.....	60
1.4.5. Perspectives for osmium drug in cancer treatment.....	66
1.5. Concluding remark and aim of the present thesis	67
1.6. References Chapter 1	69
Chapter 2: Second-generation cycloruthenated complexes: Extension of RDC chemical library and evaluation of their biological properties as potential anticancer drugs	75
2.1. Achievement of second-generation Ru(II) chemical library	77
2.1.1. Introduction.....	77
2.1.2. Synthesis of second generation complexes	77

Table of contents

2.1.3.	Cytotoxic activity of second generation complexes.....	80
2.1.4.	Electrochemical properties of first- and second-generation RDCs	91
2.2.	Study of the exchange of MeCN vs. DMSO in piano-stool cycloruthenated complexes.....	95
2.2.1.	Introduction.....	95
2.2.2.	Synthesis of piano-stool cycloruthenated complexes.....	95
2.2.3.	Preliminary results: kinetic evolution of RDC 49 in DMSO.....	96
2.2.4.	Synthesis and characterization of RDC 49-DMSO	103
2.2.5.	Cytotoxic activity of RDC 49 vs. RDC 49-DMSO	107
2.2.6.	Exchange of the counter ion PF_6^- vs. Cl^- in RDC 49	108
2.2.7.	Conclusion	109
2.3.	Chirality induction in RDC 11 lead compound.....	110
2.3.1.	Introduction: importance of chirality in everyday science	110
2.3.2.	Synthesis of RDC 8*.....	111
2.3.3.	Synthesis and separation of RDC 11* isomers	113
2.3.4.	Conclusion	116
2.4.	References Chapter 2.....	117
 Chapter 3: Library of first & second-generation cyclometalated osmium complexes and evaluation of their biological properties as anticancer agents..... 119		
3.1.	Introduction: Osmium as an alternative to Ruthenium?	121
3.2.	Achievement of first-generation piano-stool Os(II) chemical library	122
3.2.1.	Synthesis of cyclometalated Os(II) piano-stool complexes	122
3.2.2.	Cytotoxic activity of cyclometalated piano-stool osmacycles	126
3.2.3.	Study of the exchange of MeCN vs. DMSO in piano-stool ODCs	128
3.3.	Completed first-generation Os(II) chemical library	137
3.3.1.	Synthesis of other cyclometalated Os(II) complexes	137
3.3.2.	Cytotoxic activity of completed first generation Os(II) chemical library	139
3.4.	Achievement of second-generation Os(II) chemical library.....	143
3.4.1.	Synthesis of cyclometalated second-generation Os(II) complexes	143
3.4.2.	Cytotoxic activity of second generation ODCs.....	147
3.5.	Electrochemical properties of first and second generation ODCs.....	154
3.6.	References Chapter 3.....	157
 Chapter 4: Complementary stability studies and evaluation of bio-physicochemical properties..... 159		
4.1.	Complementary stability studies	161
4.1.1.	Introduction.....	161
4.1.2.	UV stability study in different solvent conditions.....	161
4.1.3.	Study of the exchange of MeCN vs. DMSO in other complexes	162

4.2. Lipophilicity properties of RDCs and ODCs	165
4.2.1. Introduction: Importance of lipophilicity in the drug design	165
4.2.2. Partition coefficient: Definition and techniques	166
4.2.3. Correlation between activity, lipophilicity and red-ox potentials: A rational approach in the drug design?	168
4.3. Complementary <i>in vitro</i> biological results	174
4.3.1. Direct DNA interaction	174
4.3.2. Detection of Reactive Oxygen Species (ROS)	175
4.4. Preliminary <i>in vivo</i> biological results	177
4.4.1. <i>In vivo</i> toxicities: Determination of LD ₅₀ and MTD	177
4.4.2. <i>In vivo</i> anticancer activity	179
4.5. References Chapter 4	181
 Conclusion and perspectives:	 183
 Chapter 5: Experimental part	 189
5.1. General remarks	191
5.1.1. Generalities	191
5.1.2. Analytical instruments	192
5.1.3. Electrochemical measurements	192
5.1.4. Hydrophobic properties measurement	192
5.1.5. Biological assays	193
5.2. Synthesis protocols	194
5.3. References Chapter 5	211
 Appendix	 213

Foreword:

Cancer is one of the most serious health problems in the Western hemisphere. Significant progress in the development of surgery, early diagnosis as well as novel drugs and therapies has occurred in the last 60 years. Thanks to the discovery of drugs such as *cisplatin*, taxanes, nitrogen mustards and the generation of targeted therapies over the last century, the treatment of some forms of the disease has a high success rate, although patients must often tolerate severe side effects. However, despite these advances, the treatment of most type of solid tumours remains problematic and survival rates are in general disappointingly low.

Statistics from the Institut de Veille Sanitaire (InVS) and from the Institut National du Cancer (INCa) show that in France, one man out of two and one women out of three will develop at least one cancer during their lives. According to the government, the fight against this disease has become a national priority. The “crab” – a term used by Hippocrate in the IVth and Vth centuries to describe the aspect of a malignant tumour because the cut surface of a solid malignant tumour with “stretched veins in all directions” resembles the legs of a crab – has become since 2004 the leading cause of death in France and will be soon the first cause of death in industrialized countries.

Cancer is not a disease like any other. People still do not talk about it overtly because in ancient times it was considered as a “divine punishment”. Now, it is often evoked with euphemism as “a long and painful illness...” Why do people have such a reaction when they speak about cancer? Perhaps because, even cured, people are often considered like a dead man with a suspended sentence. An attitude that is not easy to change. As a leading cause of death in France since 2004, cancer can objectively scare people. Indeed, the other fatal diseases (infections, cardiovascular disease...) continue to decline thanks to advances in medicine, hygiene and food. In contrast, due to ageing of population, pollution and changes in lifestyle of emerging countries, figures of the population affected by cancer will still increase in the next decades.

But even if this ancient scourge is expanding rapidly, the research is also making important progress. Cancer treatment often encompasses more than one approach, and the strategy depends largely on the nature of the cancer and how far it has progressed. Moreover, development of drug resistance is one of the most significant problems encountered in cancer chemotherapy, since up to 50% of tumours have either *de novo* drug resistance (acquired

resistance) or otherwise develop resistance to anticancer drugs after initial treatment (induced resistance).

Among surgery, radiotherapy and conventional chemotherapy, now new molecules are able to attack malignant tumours. At the same time, researchers are trying to isolate substances, among thousands of each we are exposed, to determine if they could have a carcinogenic effect. Moreover, early detection and diagnosis offer now to the patients better chance of survival.

Hence this hopeful conclusion: Although the “crab” is more and more striking, it does not lead inevitably to death. Nearly one fight out of two ends in the victory of the patient. However, this victory is sometimes temporary because unfortunately, a defeated tumour can give the way to a new one. In the therapeutic area, the hope is to turn many cases of fatal cancer into « manageable » chronic illness, as it has happened with other disease entities. In short, learning not to beat cancer but to live with it will be the great health challenge of this XXIst century.

This work is the result of a collaboration between the Laboratoire de Synthèses Metallo-Induites (LSMI) and the Laboratoire de Signalisation Moléculaire et de Neurodégénérescence (LSMN) which allowed me to evaluate the anticancer properties of newly synthesized compounds *in vitro* and provided me some *in vivo* data. This thesis follows previous results obtained by the laboratory which has developed, for more than ten years, cytotoxic ruthenium based complexes in which one of the ligands is strongly bound to the metal *via* a strong covalent bond.

In this context, this thesis explores the chemistry of osmium and ruthenium cyclometalated complexes and investigates their application in the field of cytotoxic drugs. The increased understanding and demonstration of how physico-chemical properties such as red-ox potential and lipophilicity can affect the anticancer activity will initiate many new projects in the development of these promising chemotherapeutics.

Chapter 1:

General Introduction

Do you think that the immortality, which created so much phantasm, is always desirable? The cellular world has answered "No" to this question and cancer, this disease with multiple faces, is certainly the most fatal demonstration of this theory.



Chapter 1: General Introduction..... 21

1.1. Generalities about cancer.....	23
1.1.1. Definition of cancer	23
1.1.2. Cancer epidemiology worldwide: Some facts and figures	24
1.1.3. Formation of cancer cells (Tumorigenesis).....	27
1.1.4. The different existing cancer treatments	30
1.2. Cancer treatment by platinum drugs: cisplatin and its analogues.....	32
1.2.1. Introduction: How organometallic chemistry established the bases of modern chemotherapy?	32
1.2.2. Clinically used anticancer platinum drugs: A success story?.....	32
1.2.3. Cisplatin limitations: Side effects and resistance in chemotherapy	34
1.3. Ruthenium complexes: an ongoing alternative to existing treatments?.....	36
1.3.1. Introduction.....	36
1.3.2. Ru(III)-based drugs under clinical trials: NAMI-A and KP1019.....	38
1.3.3. Ru(III) complexes vs. cisplatin: Highlight of another activity pattern?	43
1.3.4. Non-cyclometalated arene Ruthenium(II) compounds as potential anticancer agents.....	44
1.3.5. Cyclometalated Ruthenium(II) compounds developed by the Laboratoire de Synthèses Métallo-induites: State of the art.....	52
1.3.6. Ruthenium(II) compounds: A controversial activity pattern?.....	56
1.3.7. Perspectives for ruthenium in cancer treatment	56
1.4. Osmium analogues: a new step towards anticancer therapeutics?	57
1.4.1. Introduction.....	57
1.4.2. NAMI-A osmium analogues	57
1.4.3. En route to KP1019 osmium analogues	59
1.4.4. Half-sandwich arene osmium(II) analogues.....	60
1.4.5. Perspectives for osmium drug in cancer treatment	66
1.5. Concluding remark and aim of the present thesis	67
1.6. References Chapter 1.....	69

Chapter 1: General Introduction

1.1. Generalities about cancer

1.1.1. Definition of cancer

Cancer is a large and heterogeneous class of diseases in which the control of growth in a group of cells is lost, leading to a solid mass of cells known as **tumour**. The initial tumour, also called **primary tumour**, often becomes life-threatening by obstructing organs or vessels. However, death in the case of malignant neoplasm is most commonly caused by the spreading of the primary tumour to vital organs (by a process called **metastasis**) *via* the lymphatic system or through the bloodstream. In this case, surgery is no more used and a pharmacological approach is the remaining treatment. In some cases, patients die due to severe toxicities induced by chemotherapies that damage vital organs such as kidneys, liver and hematopoietic tissue.

If we classify cancers according to the most affected organ or to the type of cancerous cells, we can identify more than 200 different types of cancers. Scientists have realized that this “anatomical” classification is too simplistic because two cancers apparently identical and affecting the same organ can respond very differently to the same treatment or progress at varying speeds. Scientists generally distinguish six types of cancers (**Table 1**):

Principal type of cancer	Origin of the tumour	Frequency (estimation)	Localisation
Adenocarcinoma	Epithelium (surface tissue of many glands)	85% of all cancers	Breast, liver, kidney, prostate, pancreas, ovary, thyroid, colon, stomach, salivary glands, lungs ...
Squamous-cell Carcinoma	Squamous epithelial cells (epidermis)		Skin, gastrointestinal tract, lung, uterus, pancreas ...
Sarcoma	Connective tissues (bones, muscles...)	2-4% of all cancers	Bone, cartilage, lungs, fat tissue, blood vessels ...
Hodgkin's Lymphoma	B and T lymphocyte , (large atypical cells)	5-7% of all cancers	Lymph nodes, spleen
Non-Hodgkin's Lymphoma	B and T lymphocyte		Lymph nodes, gastrointestinal tract, skin, brain, bones, reproductive organs, lungs
Leukaemia	Bone marrow cells (blast)	4-6% of all cancers	Blood
Myeloma	Bone marrow cells (plasmocyte)		Bone marrow

Table 1: Classification by type of cancer

After more than 50 years of chemotherapy research, cancer remains one of the most difficult life-threatening diseases to treat because of tumour diversity, drug resistance and side effects of the different treatments. Collectively, these diseases represent one of the most pressing challenges of the XXIst century.

1.1.2. Cancer epidemiology worldwide: Some facts and figures

All around the world, **25 million people** are suffering from cancer (**Figure 3**), and 30 new cases are diagnosed each minute according to the World Health Organization (W.H.O). Data from the W.H.O. estimate that the most common scourge is lung cancer (1.2 million new cases per year), followed by breast (about 1 million cases), colorectal (940,000 cases), stomach (870,000 cases) and liver cancers (560,000 cases). The incidence of cancer is increasing partially due to ageing population¹ in most countries and it has been estimated that within 20 years, there will be **20 million new cancer patients** worldwide each year.²

According to the French sanitary surveillance institute – Institut National de Veille Sanitaire (INVS) – 1 200,000 French people are suffering from cancer and this disease, which caused the death of more than **145,000 people in 2008**, has become the leading cause of death in France since 2004 (**Figure 1**).

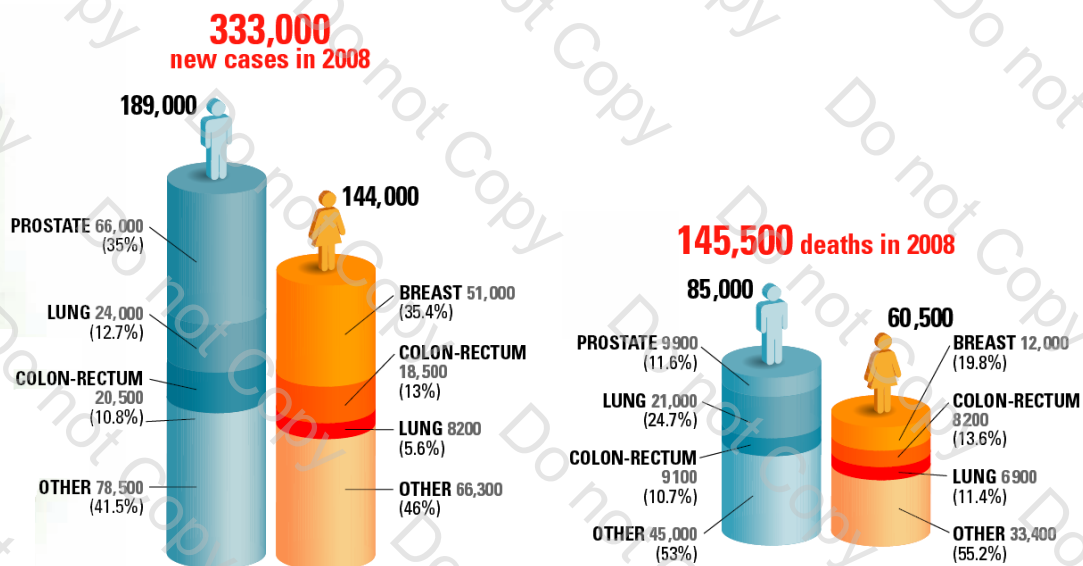


Figure 1: Cancer in France (from INVS)

Survival rates vary widely between different kinds of cancer and the stage of the disease at diagnosis: later stage diagnosis and metastatic disease correspond invariably to poorer survival. An optimistic view however is, that the coming decades advance in prevention, detection and treatment will see cancer being considered not as a fatal, but as a chronic disease.²

However, cancer rates are predicted to further increase not only due to steadily ageing populations, but also due to trends in smoking prevalence, to the adoption of unhealthy lifestyles (poor diet, obesity, lack of physical activity...) and to other environmental factors (radiations, environmental pollutants...).³ All these environmental factors can cause or enhance abnormalities in the genetic material of the cells.⁴

Indeed, according to Aggarwal *et al.*³ (Figure 2), cancers are primarily an “environmental” disease. **90-95% of all cases are attributed to environmental factor**, whereas only 5-10% are purely genetic. The word “environmental” is used in this study to characterize non-genetic causes. **Therefore, our way of life is directly put into question.**

Common environmental factors that contribute to cancer development include: tobacco use (25-30%), diet and obesity (30-35%), infections (15-20%), radiation (up to 10%), lack of physical activity, stress and environmental pollutants.

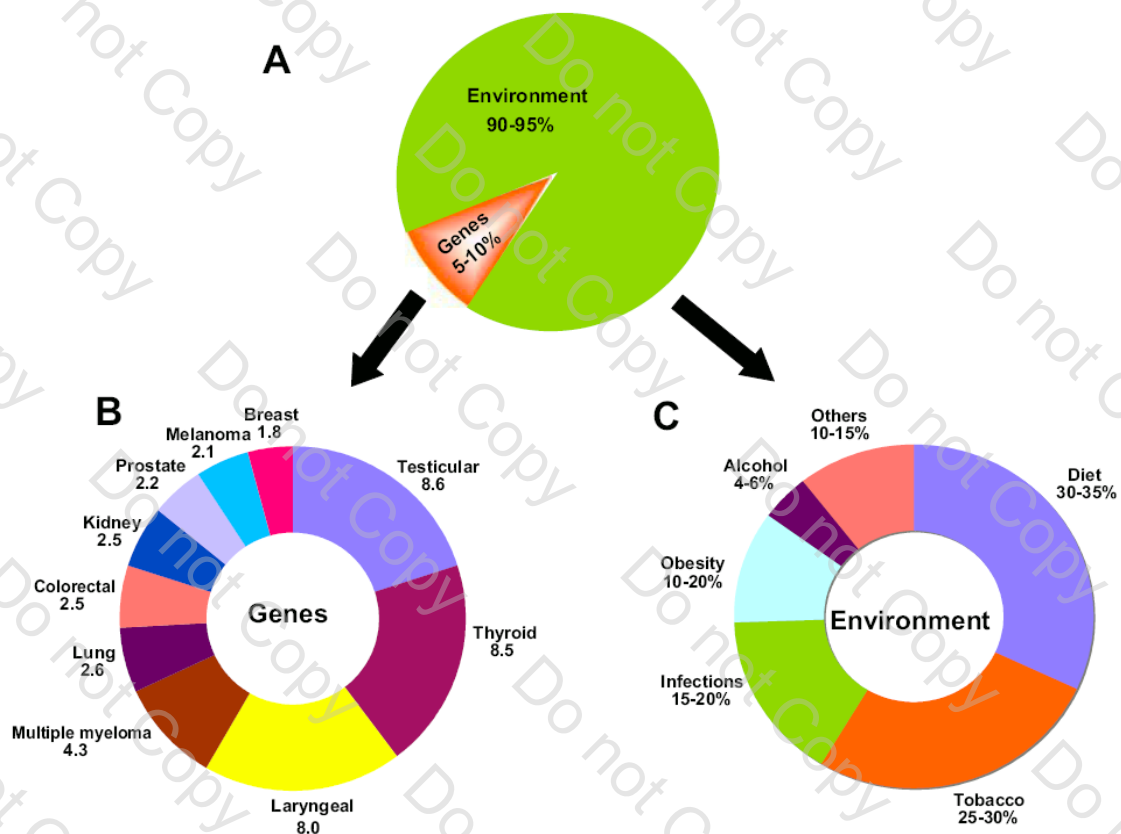
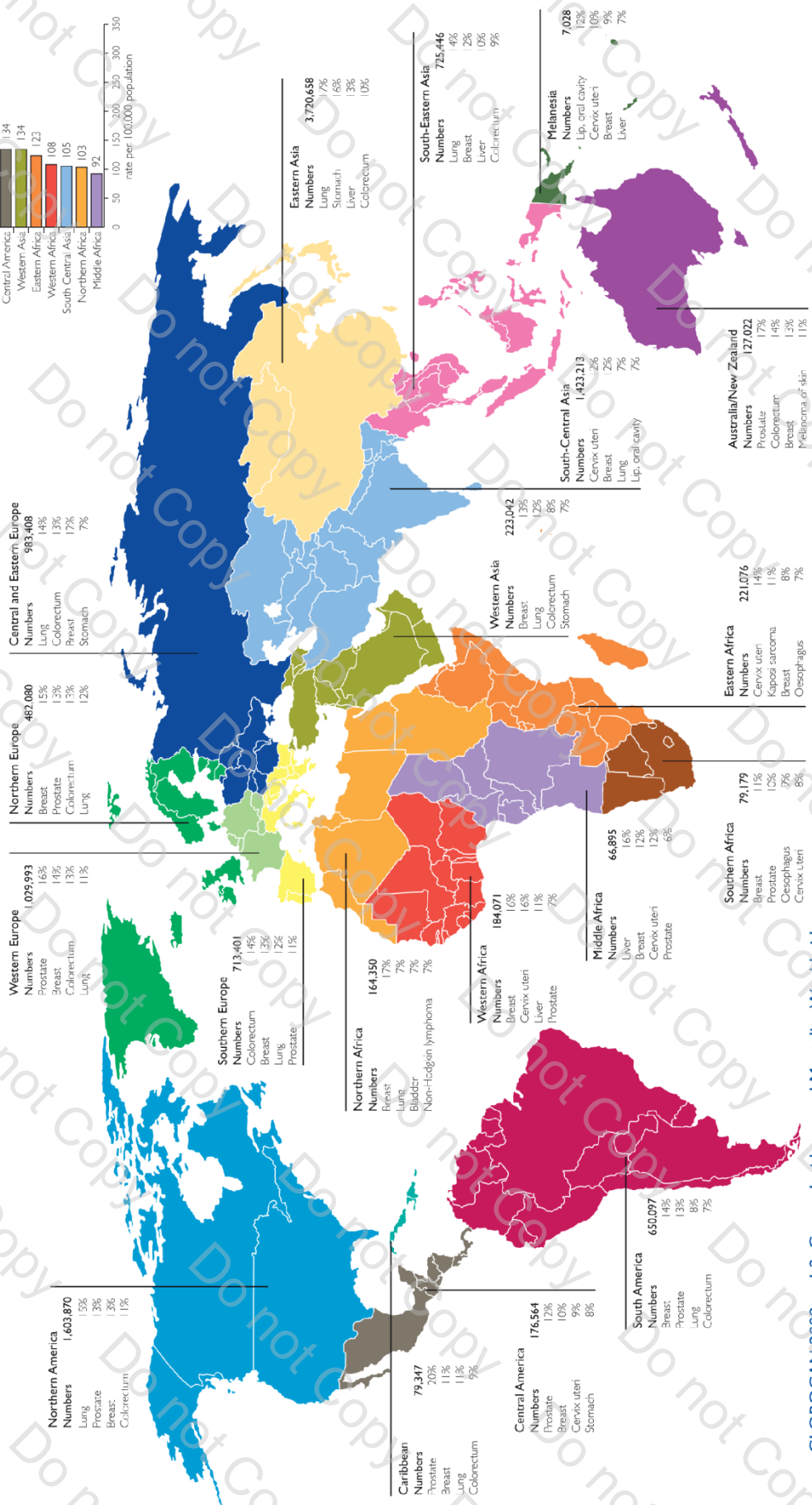
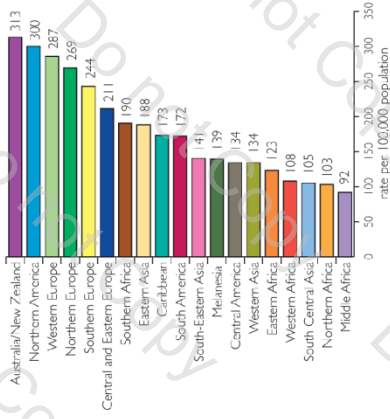


Figure 2: The role of genes and environment in the development of cancer

- A:** The percentage contribution of genetic and environmental factors to cancer. The contribution of genetic factors and environmental factors towards cancer risk is 5–10% and 90–95% respectively.
- B:** Family risk ratios for selected cancers. The numbers represent familial risk ratios, defined as the risk to a given type of relative of an affected individual divided by the population prevalence. The familial risk ratios were assessed as the ratio of the observed number of cancer cases among the first degree relatives divided by the expected number derived from the control relatives, based on the years of birth (cohort) of the case relatives.
- C:** Percentage contribution of each environmental factor. The percentages represented here indicate the attributable-fraction of cancer deaths due to the specified environmental risk factor.

Cancer Incidence Worldwide

Breakdown of the estimated 12.7 million new cases, World-age standardised incidence rates and the most commonly diagnosed cancers by the different regions of the world, 2008.



Source: GLOBOCAN 2008, v. 1.2, Cancer Incidence and Mortality Worldwide. IARC, 2010 (<http://globocan.iarc.fr>)
Map updated February 2011

<http://info.cancerresearchuk.org/cancerstats/>

© Cancer Research UK
Registered charity no 1094847 (England & Wales)
& 15011466 (Scotland)

Figure 3: Cancer incidence worldwide

1.1.3. Formation of cancer cells (Tumorigenesis)

Robert A. Weinberg⁵ suggested that numerous tumour cell genotypes may result from essential modifications to cell physiology leading to the induction of malignancy. According to him, all cancers share six common marks that distinguish them from other diseases:

- Self-sufficiency in growth signal
- Insensitivity to growth-inhibitory signals
- Evasion of programmed cell death (apoptosis)
- Limitless reproductive potential
- Sustained angiogenesis
- Tissue invasion and metastasis

How does gene expression fail?

From a molecular and cell biological conception, cancer is caused by molecular defects in cell function resulting from common types of alteration to a cell's gene. Genetic changes can occur at different levels and by different mechanisms. The gain or loss of partial or total chromosome can occur through errors in mitosis. More common are mutations, in which changes occur in the nucleotide sequence of genomic DNA. These mutations which avoid or alter the expression of some genes may be caused by five major factors (**Figure 4**).

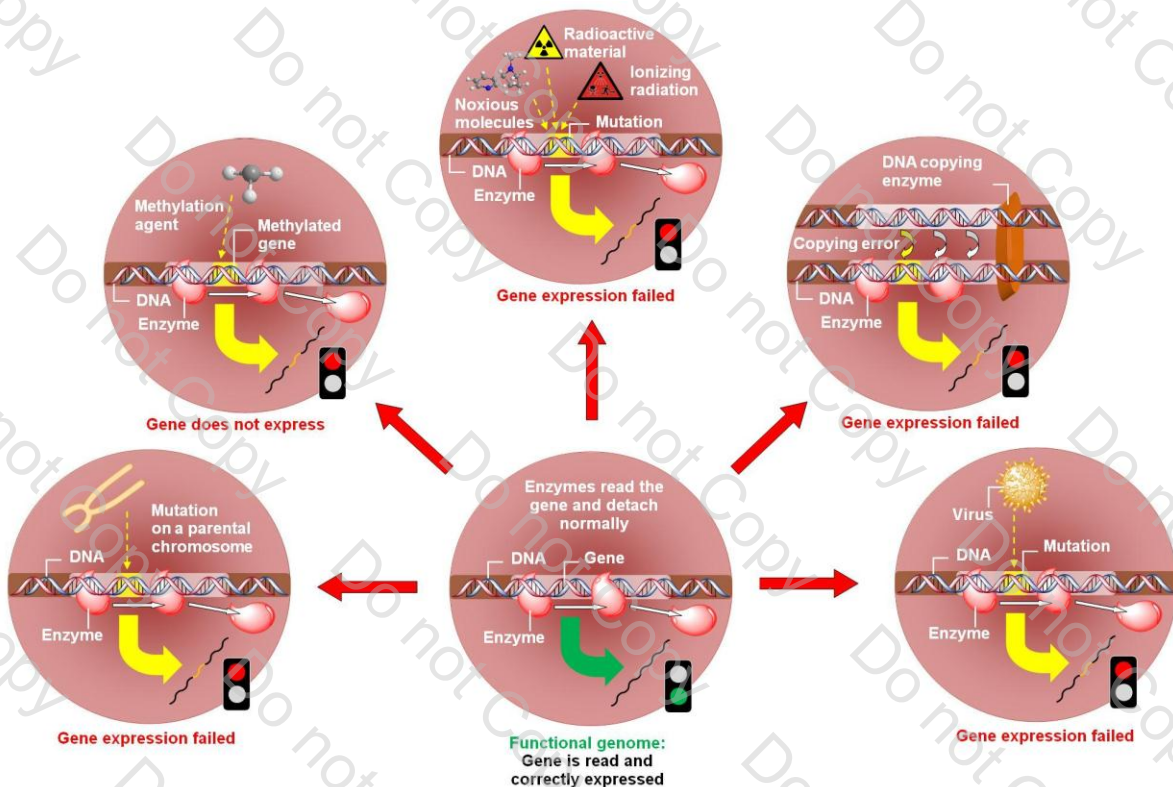


Figure 4: Zoom on 5 factors leading to gene expression failure

Heredity:

Some people inherit from their parents a predisposition to develop a cancer. Hence, one or more of their genes present some mutations. The enzyme responsible for reading the gene fulfils its mission but the expression of the gene is altered.

Viruses:

When a virus infects a cell, it introduces its genetic material into the genome of its host. Some of this material may contain oncogenes. A virus can also inactivate essential genes or activate cell proliferation genes. In all cases, gene expression is perturbed.

Mutagenic factors:

UV, X-rays, and all ionizing radiations produce mutations within the DNA. Many molecules from the environment also create mutations by chemical reaction with DNA. Consequently, the gene cannot express normally anymore.

Copying errors:

When cells divide, the DNA is fully copied. During this operation, copying errors can occur and may not be detected, leading to carcinogenic mutations. Thus, the gene cannot express normally anymore.

Epigenetic:

A small molecule (usually methyl) can bind to the gene. The enzymes responsible for DNA reading do not read the entire gene anymore and detach prematurely. Therefore, the gene cannot be expressed properly.

How does a normal cell become a cancer cell?

As previously discussed, it is now accepted that cancer is a disease with genetic component resulting from changes to DNA sequence information in one or more genes. These alterations can occur through internal, external, or hereditary process. The transformation of normal cell into cancer cell is due to a chain reaction caused by initial errors (**Figure 5**).

Once growth and differentiation-regulating genes are altered,⁶ it can lead to more severe errors, progressively allowing the cell to **get out of control** to the detriment of normal cells. In this rebellion-like process, cancer cells will grow anarchically at the expense of normal cells.

The overall result is an **imbalance of cell replication** and cell death in a tumour cell population that leads to an expansion of tumour tissue. Once cancer has begun, the ongoing process will progress towards more invasive stages.⁷

As already described (see Chapter 1, 1.1.2.) causes of cancer are not clearly defined yet, but both external (e.g. environmental chemicals, radiation...) and internal (e.g. immune system defects, genetic predisposition) factors play a role. These casual factors may act together to **initiate** (initial genetic insult) and **promote** (stimulation of growth of initiated cells) carcinogenesis. Hence, 10 to 20 years may elapse before initiated neoplastic cells become a clinically detectable tumour.

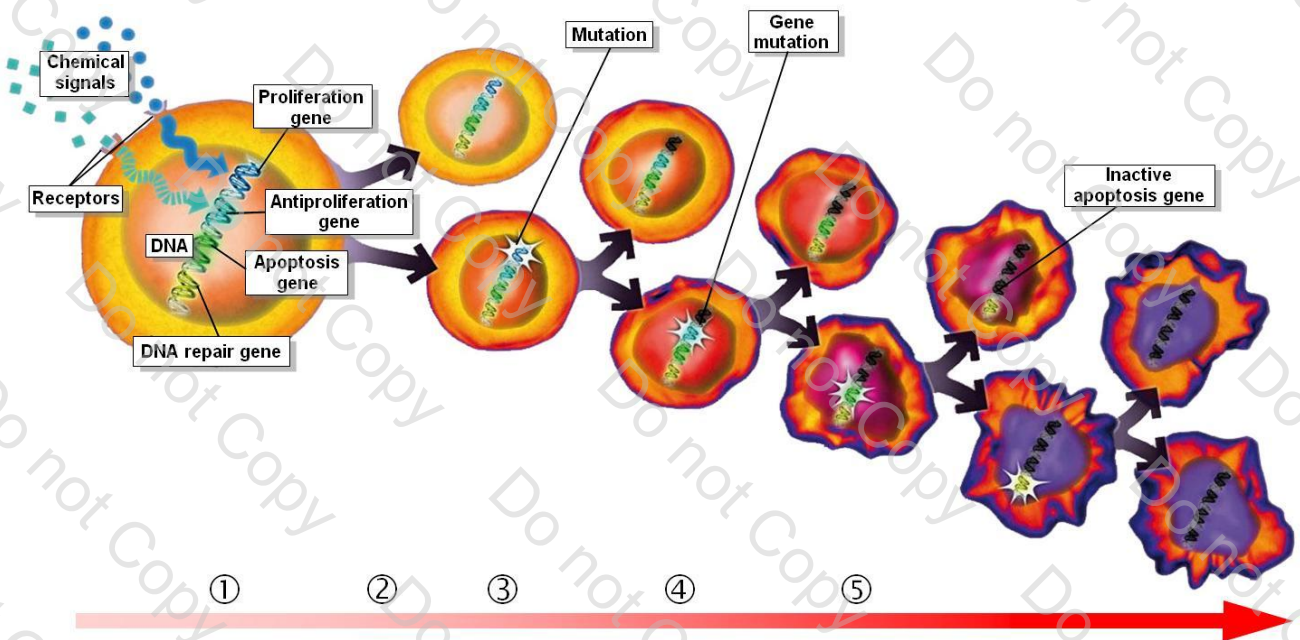


Figure 5: Simplified scheme representing the neoplastic cell growth

- ① A healthy cell continuously receives chemical signals from the other cells. They can regulate the cell division *via* a **proliferation gene** or order to rest *via* an **antiproliferation gene**. In response to a signal, the cell can also self-destruct *via* the **apoptosis gene**.
- ② During cell division, DNA is duplicated so that daughter cells receive a copy from the mother cell. **DNA repair gene** continuously verifies that the copy is identical to the original. However, an error may still occur.
- ③ In this case, a **proliferation gene** has just mutated. It has been activated without being solicited. Fortunately, the **antiproliferation gene** remains intact and can slow down cell division or order the self-destruction of the cell *via* the **apoptosis gene**.
- ④ The **proliferation gene** may also undergo a mutation. Thus, it can neither respond to proliferation stop order nor order self-destruction. Now, the mutated cell refuses to die and is dividing anarchically: it has become a **cancer cell**.
- ⑤ Protection systems of the cell collapse one after the other. DNA repair genes are also damaged, and as a consequence, cancer cells accumulate more and more errors in their DNA.

Mutant cells pack themselves in their origin tissue and begin to form a **tumour**. Some of them can undergo supplementary mutations that allow cancer cells to reach blood vessels. Cancer cells are intensively fed with glucose by the blood vessels and can then migrate in the rest of the body *via* blood stream. Through this **metastasis process**, they can affect other organs, hence creating new tumours.

1.1.4. The different existing cancer treatments

In order to treat cancer, a good diagnosis from the medical team must be first established, taking into account the type of cancer, its size, the presence or absence of metastases and of course the general health state of the patient. Cancer treatment often encompasses more than one approach, and the strategy depends largely on the cancer type and how far it has progressed. Although some new approaches in cancer treatments are under development, its treatment is still mainly focused on surgery, radiotherapy and chemotherapy.

Surgery: If a tumour is small or reasonably well defined, it can sometimes be surgically removed. Although this technique has been widely used in the past because it was the only existing treatment against cancer, it is still the most common form of treatment. Indeed, these techniques are constantly becoming more efficient thanks to the advance of medicine and medical imaging, leading to less invasive interventions. However, additional treatment with radiotherapy or chemotherapy is often needed to eliminate hidden remaining cancer cells that can still metastasize.

Radiotherapy: Radiotherapy is a local treatment that uses radiation to destroy cancer cells specifically. It involves the use of X-rays or radiopharmaceuticals (radionuclides) that act as γ -rays source to induce DNA irreparable damages in the cancerous cells. In X-ray therapy, beams are precisely oriented so that radiation is delivered locally on the tumour without damaging healthy tissues. This approach is used to eliminate primary tumour, but is more difficult to use in case of metastatic process.

Hormone therapy: Hormone therapy is an important form of therapy in the treatment of hormone-dependent cancers. It involves the manipulation of the endocrine system through administration of specific hormones (particularly steroid hormones). Indeed, steroid hormones are powerful drivers of gene expression in certain cancer cells. Hence, the change of the levels or activity of some hormones can cause cancers to cease growing, or even undergo cell death.

Immunotherapy: Immunotherapy is a treatment that involves the use of an antibody as a treatment of cancer by inducing, enhancing, or suppressing an immune response. The use of these antibodies allows preventing cell proliferation by blocking the activity of some receptors encoded by oncogenes.

Phototherapy: The Photodynamic Therapy (PDT) is based on a chemical reaction activated by light energy that is used to destroy tissue selectively. The reaction requires the presence of a photosensitive substance (a photosensitizer) in the target tissue and a light source that can emit radiation at wavelengths absorbed by these substances. The reaction produces singlet oxygen and other free radicals with cytotoxic effects.

Chemotherapy: Chemotherapy involves the use of low molecular weight drugs to selectively destroy a tumour or at least limit its growth. Originally, nitrogen mustards were the first agents to be used clinically and resulted from the observation that mustard gas used during World War I had antileukemic properties. Since this discovery, important advances have been made in the development of new chemotherapeutics. A large number of chemotherapeutic agents (**Figure 6**) have been granted regulatory approval and in 2004 approximately 1000 chemotherapeutic agents were undergoing clinical trials.²

Cancer treatments:

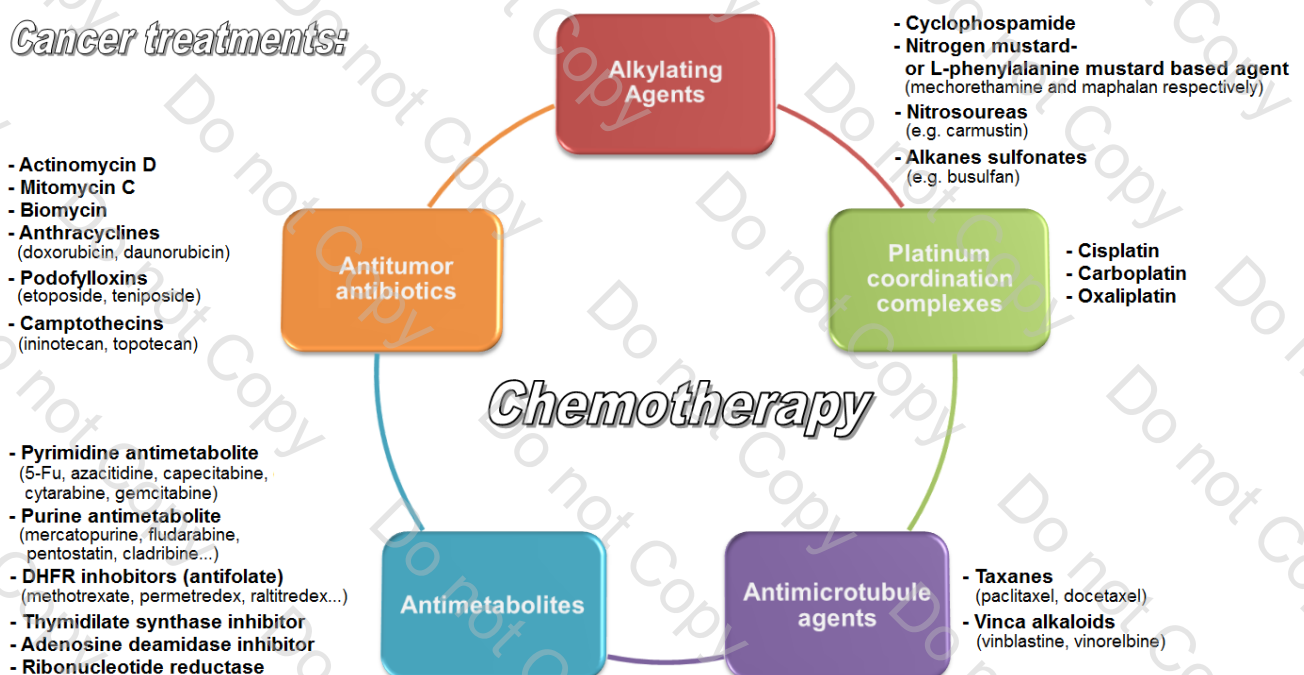


Figure 6: Classification of chemotherapeutic drugs

1.2. Cancer treatment by platinum drugs: *cisplatin* and its analogues

1.2.1. Introduction: How organometallic chemistry established the bases of modern chemotherapy?

Since the serendipitous discovery by Rosenberg in the 1960s,⁸ there has been an increasing interest in the application of organometallic chemistry to medicine and biology.⁹ During the second half of the XXth century the organometallic chemistry evolved rapidly,¹⁰ and it is now established that **bio-organometallic chemistry** is an important branch of modern medicine.¹¹ Medicinal organometallic chemistry can thus design new drugs by exploiting the properties of metal ion. This has led to clinical application of **antitumour drugs** such as *cisplatin* and its analogues including carboplatin (ParaplatinTM), oxaliplatin (EloxatinTM) and satraplatin (OrplatnaTM) which were later developed in the attempt to reduce the problematic side effects of *cisplatin* (**Figure 7**). Thanks to this great success story of cancer chemotherapy, thousands of novel platinum and also non platinum complexes have been synthesized and biologically evaluated.¹² However, from over 3000 platinum-based compounds tested *in vitro*, only about 30 entered into clinical trials (1%). Only 10% of these compounds will make it to registration, so that the success rate for designing new platinum drugs is less than 1 out of 1000 compounds. This is a classical figure in the drug discovery process according to the regulation of therapeutics goods.

1.2.2. Clinically used anticancer platinum drugs: A success story?

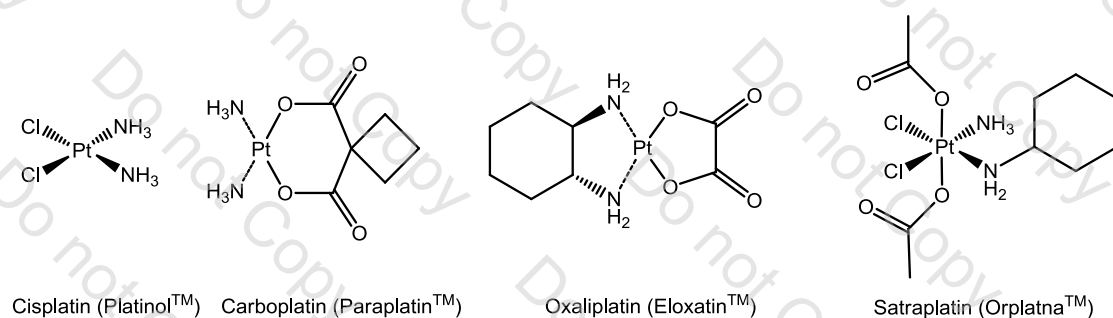


Figure 7: Structures of *cisplatin*, carboplatin (ParaplatinTM), oxaliplatin (EloxatinTM) and satraplatin (OrplatnaTM)

Like many other clinically useful drugs, *cis*-diaminedichloroplatinum(II), more commonly known as *cisplatin*, was discovered by serendipity rather than by design. It is used to treat various types of cancer including sarcomas, carcinomas (non-small cell lung and ovarian cancers), lymphomas and germ cell tumours.

Cisplatin was first synthesized in 1845 by Peyrone¹³ and has been known for a long time as Peyrone's salt. Its structure was only elucidated in 1893 by Alfred Werner,¹⁴ who established

the basis of **coordination chemistry** and demonstrated that ammonia can bond to a metal ion like platinum +II by donating its lone pair of electrons in a coordinate bond.

In 1965, Rosenberg discovered,^{15,16} while studying the effect of an electric field on the growth of bacteria, that platinum electrodes generated soluble platinum complexes (*cis*-diaminedichloroplatinum(II) and *cis*-diaminetetrachloroplatinum(IV)) which inhibited cellular division in *Escherichia coli* (*E. coli*). This discovery led to the finding that *cis*-diaminedichloroplatinum(II) was highly effective at regressing sarcomas in rats.¹⁷

In order to confirm its medical application, *cis*platin entered into clinical trials in 1971¹⁸ and was approved as chemotherapeutic in 1978 by U.S. Food and Drug Administration (F.D.A).

Cytotoxic action of *cis*platin: Interaction with DNA

The mode of cytotoxic action of *cis*platin on cell division is still poorly understood and many studies are being conducted on this subject. Indeed Jon Steed (from RCS interview “Chemistry in its Element – *cis*platin”) likes making fun on *cis*platin saying about it that “Square planar it may be; but square and plain it’aint!”. Although the mechanism has not yet been fully elucidated, *cis*platin is generally believed to kill cancer cells by binding to major groove of DNA, forming intrastrand cross-links and interfering with the cell's repair mechanism, which ultimately triggers apoptosis.¹⁹

Platinum antineoplastic complexes have a common structure: platinum is bound by covalent bonds to four substituents: two small labile nitrogen substituents and two labile chloride or oxygen substituents. Hydrolysis of square planar *cis*platin leads to the substitution of two chlorides by one or two water molecules.

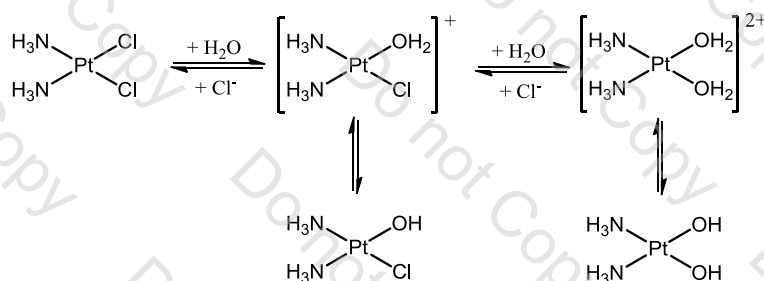


Figure 8: Hydrolysis of *cis*platin

This hydrolysis is facilitated by the low intracellular concentration of chloride ions (in the blood around 100 mM and in the cell between 3 and 20 mM).²⁰ Highly reactive electrophilic complexes thus formed (**Figure 8**), interact with DNA mainly at nitrogen (N7) of guanine and adenine (**Figure 9**).²¹

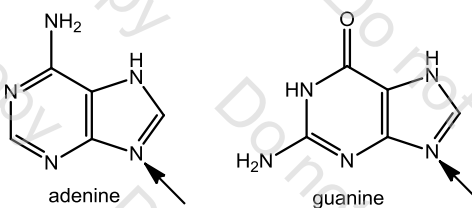


Figure 9: N7 nitrogen atom of adenine and guanine reacting with *cisplatin*

Cisplatin form bridges (adducts) in intra-strand between two adjacent purine bases (mainly guanine).²² Three modes of interaction have been described: (Figure 10)

- Intra-strand interaction (between two GG or GXG or GA or on the same strand)
- Inter-strand interaction (between GG and GA on two different strands)
- DNA-protein interactions (between G protein and sulphur).²³

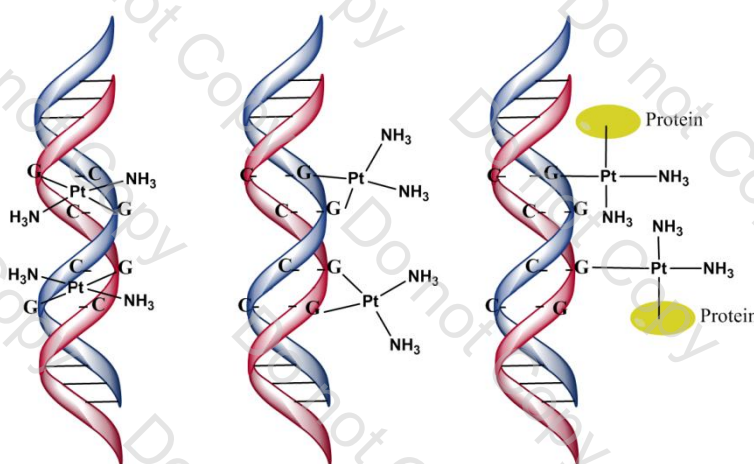


Figure 10: Three mode of interaction of *cisplatin* with DNA, inter-strand (left), intra-strand (centre) and DNA-proteins (right)²⁰

However, it should be argued that this DNA binding is not sufficient to explain the differences of activities of platinum based drugs on human tumours. Where *cisplatin* and carboplatin display the same activity on same tumours (*e.g.* lungs, head and neck, ovarian),²⁴ oxaliplatin is active on colorectal tumours²⁵ and satraplatin affects prostate cancer.²⁶

1.2.3. *Cisplatin* limitations: Side effects and resistance in chemotherapy

Platinum-based compounds are a reference in chemotherapy and are widely used in many cancers (including lungs, colon, glioma, testicles, ovaries...) and are often associated with other therapies (see Chapter 1, 1.1.4.). *Cisplatin* is one of the three most commonly used anticancer agents in the world²⁷ but, as it is the case for the majority of chemotherapeutics, *cisplatin* has two major drawbacks in its clinical use.

On the one hand, it has significant toxicity, involving numerous side effects for treated patients and resulting sometimes in serious consequences. Thus, its use remains limited according to the doses tolerated by the patients.

On the other hand, it was found that some tumours have **innate resistance** against *cisplatin* or can develop an **acquired resistance** against this drug after an initial treatment. However, *cisplatin* remains the cornerstone of antineoplastic agents and is increasingly given in day care settings.

Cisplatin side effects:

Clinical observations show that patients treated with *cisplatin* can develop more or less important side effects that may be sometimes irreversible. These observations lead clinicians to reduce the doses of treatment but this can result in a risk of ineffective cure. The disadvantages of this technique include **unpleasant side effects** for the patient including gastro-intestinal tract lesions, hair loss, skin changes (redness, itching...), nausea, vomiting, diarrhoea, and often a rapid development of clinical resistance.²⁸ In more severe cases, sensory neuropathies resulting in ataxia, paresthesia and loss of hearing (ototoxicity) have been reported, as well as **hematologic toxicities, renal** and hepatic toxicities that can be fatal in some cases. Although there have been successes, especially in the treatment of testicular cancer,²⁹ chemotherapy can currently still offer **only** a modest increase in survival time in the majority of advanced cases.³⁰

Cisplatin resistance:

One of the main limitations in clinical application is the development of *cisplatin* resistance. In some cases, initial platinum reactivity is high but **10% of patients** display **innate resistance** to the drug and **20% of patients** treated with *cisplatin* will eventually relapse with ***cisplatin-resistant cancer***. Indeed, studies conducted by Ozols *et al.*³¹ demonstrated that during the first treatment of ovarian cancer by *cisplatin*, over 70% of patients responded favourably to the treatment. However, 5 years after the initial treatment, the use of the same drug only enables to get 15 to 20% positive response. These observations indicate that cancer cells can develop resistance against drugs,³² and sometimes in a very rapid way, as it is the case for bacteria during treatment with antibiotics.

Cisplatin resistance occurs by expansion of tumour cells in the heterogeneous tumour cell population with acquired resistance to *cisplatin* during initial treatment. The mutagenic effect of *cisplatin* can favour the development of mutations in various genes leading to over expression or other mechanisms in specific genes that **confer resistance**. Since the observation of this **acquired resistance**, many studies have been undertaken to understand the phenomenon using for example cellular models.³³ Details about the different resistance mechanisms which are more related to biology will not be discussed here. However, many

mechanisms have been proposed to explain *cisplatin* resistance including changes in cellular uptake and efflux of the drug, deregulation or inhibition of apoptosis, increased detoxification of the drug, and increased DNA repair. Today, toxicities and resistances induced by platinum complexes and more widely by the majority of chemotherapies lead clinicians and pharmaceutical industry to investigate new therapeutic approaches to develop innovative anticancer therapies.

1.3. Ruthenium complexes: an ongoing alternative to existing treatments?

1.3.1. Introduction

Medicinal inorganic chemistry can use the different properties of metal ions for designing new anticancer agents. However, current **metal-based chemotherapeutics** have some limitations which have lead the chemists to search new antitumour drugs with fewer side effect and enhanced activity.^{34,35,36} Notwithstanding the widespread application of platinum-based drug, there is an important need for the development of new metal-based drugs with unprecedented feature.

The clinical success of *cisplatin* as an anticancer agent has promoted the search for cytotoxic compounds with enhanced activities and more acceptable toxicity profiles. This has stimulated interest in complexes containing other heavy metals of groups 8, 9, 10 of the periodic table (formerly known as Group VIII or **Platinum Group Metals PGMs**). Due to their different chemical characteristics, these complexes can differ significantly from *cisplatin* in their mode of action and their activity pattern.

For many years, many scientific groups have actively worked in the field of inorganic drugs and numerous new platinum and non-platinum complexes have been synthesized and tested for their antitumour and antimetastatic properties.¹² Among the non-platinum complexes, **ruthenium(II)** and **ruthenium(III) compounds** are of promising interest because these compounds show a lower toxicity than platinum-based drugs and therefore are better tolerated *in vivo*.^{37,38} Indeed, ruthenium possesses several properties that make this metal applicable to medicine:

Slow ligand exchange kinetics: A key element explaining why platinum can act as an anticancer drug relies on its ligand-exchange kinetics. This confers a high kinetic stability and avoids rapid equilibration reactions.³⁹ It has been demonstrated that the ligand-exchange process for the same ligand is linked to the metallic ion. Thus Ru(II) and Ru(III) complexes have similar exchange kinetics to those of Pt(II).⁴⁰ Moreover, for most small ligands (*e.g.*

water), the ligand-exchange process for metallic ions like Pt(II), Ru(II), Ru(III) takes several hours, which mimics the time scale for many division cells.⁴¹

Multiple accessible oxidation states: The chemistry of ruthenium complexes, and especially the study of their electron-transfer properties, has been receiving great attention for the last decades. Ruthenium is a particular metal characterized by the fact that oxidation states Ru(II), Ru(III) and Ru(IV) are all accessible under **physiological conditions**. In these states, the ruthenium centre is predominantly hexacoordinated with an octahedral geometry. Around the ruthenium, the coordination environment plays a key factor in stabilizing the complexes in their oxidation states and thus influences the red-ox properties of the central metal atom.⁴² Metabolisms altered by cancer result in a tumour tissue containing lower oxygen concentration, hence promoting a **reductive environment (Figure 11)**. Additionally, cancer cells contain a lower pH than normal cells and higher level of glutathione further generates a strongly reducing environment.⁴³ The red-ox potential of ruthenium complexes can also be modified in order to increase the selectivity of ruthenium species towards cancer cells and to reduce damages to healthy cells. One of the example is to administer relatively inert Ru(III) complexes (considered as pro-drugs) which are then **activated by reduction** within cancerous cells (see Chapter 1, 1.3.2.).

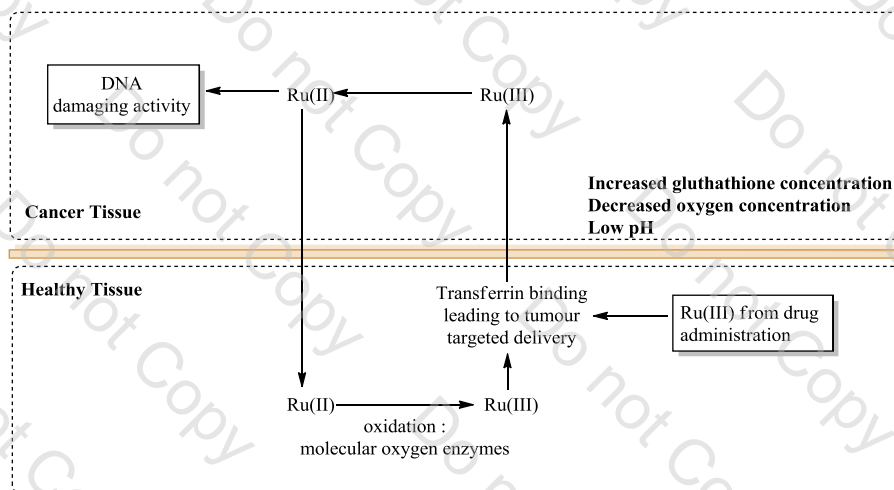


Figure 11: Oxidation state changes of ruthenium in cancer and healthy cells

Ability of ruthenium to mimic iron to some bio-molecules: Ruthenium complexes are able to **mimic iron** in binding to serum transferrin and albumin⁴⁴ which solubilise and transport iron in plasma. Given that rapidly dividing cells (like malignant cells) required more iron, this leads to an up-regulation of the number of transferrin receptors on the cell surface, (**Figure 12**) resulting in an uptake of more circulating iron-loaded transferrin. *In vivo* studies indeed show an increase of ruthenium concentration in malignant cells rather than in healthy cells.⁴⁵ Since ruthenium seems to target cancer cells, its acute toxicity is expected to be decreased.

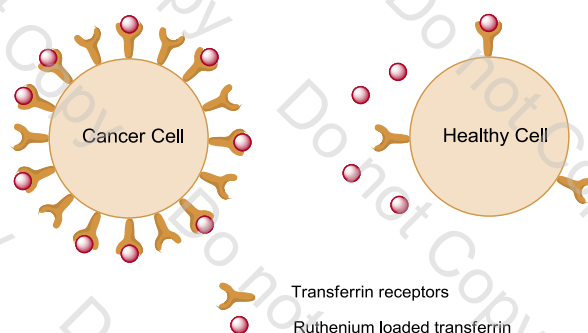


Figure 12: Schematic representation of the selective uptake of transferrin by cancer cells.

In this context some **ruthenium compounds**^{38,46} have already shown promising activity towards different types of cancer that cannot be treated with conventional platinum based compounds. This difference is probably due to a different mode of action, biodistribution and toxicity (see **Chapter 1, 1.3.2.**). Thus, they might be active against human *cisplatin* resistant malignancies and exhibit lower host toxicity. These compounds therefore represent a new class of antitumour drugs endowed with a potent ability for the treatment of human tumours.

1.3.2. Ru(III)-based drugs under clinical trials: NAMI-A and KP1019

Ruthenium(III) complexes are among the most intensively studied alternatives to platinum drugs in cancer chemotherapy. These were originally synthesised as compounds selectively toxic for solid tumours, because of the selective activation to cytotoxic species into these tissues (see **Chapter 1, 1.3.1.**). In recent years, two Ru(III)-based drugs of promising interest, *trans*-[RuCl₄(DMSO)(Im)]ImH (NAMI-A, where Im = imidazole, Imidazolium-*trans*-dimethylsulfoxyd-imidazole-tetrachlororuthenate)⁴⁷ and *trans*-[RuCl₄(Ind)₂]IndH (KP1019, where Ind = indazole, Indazolium-*trans*-bis(1*H*-indazole)-tetrachlororuthenate),⁴⁸ are in **clinical trials**. Despite their structural and chemical similarities, these two Ru(III) complexes show different antitumour behaviours.

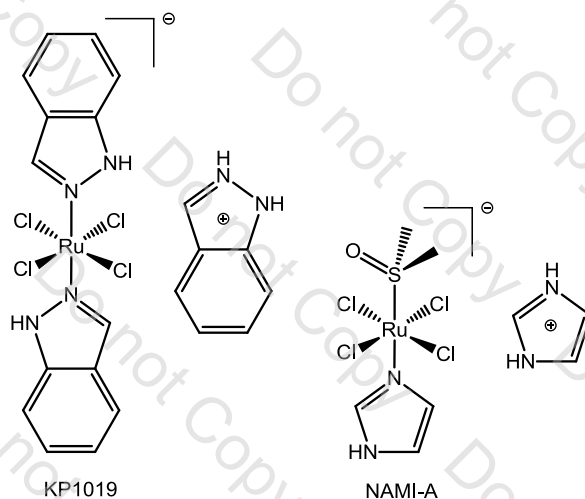


Figure 13: Chemical structures of KP1019 and NAMI-A

NAMI-A and **KP1019** were selected as lead candidates out of a large number of ruthenium complexes, which were tested for their therapeutic potential. Many studies on their Structure Activity Relationship (S.A.R.) and on their mode of action were undertaken. However, many aspects of the tumour-inhibiting action are still rather obscure.

NAMI type complexes

Several Ru(III) complexes with a coordinated dimethyl sulfoxide have demonstrated good antimetastatic properties against animal model. After extensive preclinical investigation, **NAMI-A** exhibited specific antimetastatic properties in a large variety of tumour animal models without direct cytotoxic effects on the primary tumour⁴⁹ (**Figure 14**). The synthetic procedure of **NAMI-A** was reported and its rights are protected by the referenced patent.⁵⁰

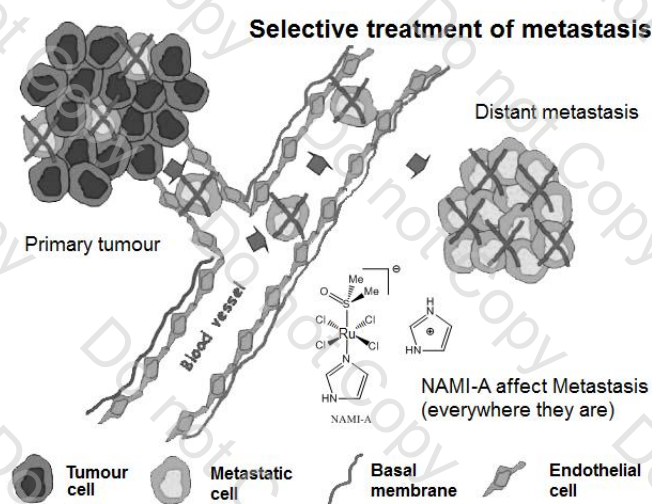


Figure 14: Selective metastatic removal by NAMI-A^{47(b)}

NAMI-A was the first ruthenium based drug to reach human trials. A phase I clinical trial and pharmacokinetic study starting in 1999 was reported in 2004.⁵¹ In this study, 24 patients displaying a wide variety of metastatic solid tumours (including lung, melanoma, colorectal, ovarian and pancreatic cancers) refractory to conventional therapies were treated according to a dose escalation protocol. Details concerning this study will not be discussed here. However, 20 out of 24 patients (83%) were evaluable for tumour response. One heavily pretreated patient with progressive metastatic non-small cell lung cancer achieved stable disease for 21 weeks. Unfortunately, the remainder of the patients show disease progression. A phase II clinical trial evaluating **NAMI-A** has not yet been conducted.

NAMI-A appears to alter protein expression, either by binding to proteins or to RNA, causing thickening of the protein layer surrounding tumours and metastases.⁵² As a consequence, the tumour becomes isolated, preventing escape of metastasizing cells and reducing blood flow,

which ultimately suffocates it. Only a very small portion of the drug reaches the tumour target and its activity appears to be independent of its concentration in tumour cells.

According to P.J. Dyson, **NAMI-A** has an extracellular mode of activity centring on interaction with proteins.⁵² Extensive research was undertaken to collect data on the chemical properties⁵³ of **NAMI-A** and its effects on a cellular level,⁵⁴ but its exact mechanism of action still remains obscure, even if **NAMI-A** is supposed to differ from platinum-based anticancer agents in its mode of action. It is purported to entirely inhibit neoangiogenesis induced by endothelial growth factor resulting from apoptosis of endothelial cells *via* the modulation of protein kinase C, dephosphorylation of extracellular signal-regulated kinase (ERK) and inhibition of c-myc transcription.⁵⁵ **NAMI-A** has thus attracted significant attention and at least 30 various reviews and research papers concerning use of **NAMI-A** in clinical trial have been published. Although the mode of action is still unclear, most of them highlight the great progress in the understanding of the mode of action of this compound.

In parallel with these biological studies, numerous analogues of **NAMI-A** were synthesised. These compounds differ from their **NAMI-A** congener in the nature of coordinated ligands, such as pyrazole, thiazole and pyrazine. This modification conferred to the new **NAMI-A** type complexes a better stability in aqueous solution compared to the parent compound. These complexes have been also patented⁵⁶ and behave similarly to **NAMI-A**. They display very effective activity on *in vitro* metastases despite having no effects on primary tumour growth nor *in vitro* cytotoxicity. In **phase I clinical trials**, **NAMI-A** did not reach the Maximal Tolerated Dose (MTD) and no feedback concerning a possible change in formulation or a possible **clinical phase II** on **NAMI-A** have been published yet.

KP1019 type complexes

Unlike **NAMI-A**, **KP1019** (**Figure 14**) shows direct cytotoxicity by inducing apoptosis in a number of cell lines as well as in tumour models (especially colorectal cancer) including explanted human tumours.^{57,58} Astonishingly **KP1019** reduces colorectal tumours where *cisplatin* is inactive but has no pronounced antimetastatic activity.⁵⁹ The procedure of synthesis of **NAMI-A** and its anticancer activity were first reported by Keppler *et al.* in 1989⁶⁰ and its rights are protected by a patent.⁶¹

This patent, which covers the anionic ruthenium(III) complexes with different counter ion, describes 15 drugs with a mono- or multi-cyclic basic heterocycle. These complexes were tested on different cancer cells including P388 and 1210 leukaemia, B16 melanoma and

AMMN colon carcinoma and display antitumour activity coupled with favourable toxicity. Keppler *et al.* investigated also the hydrolysis of these Ru(III) complexes under different conditions (varying pH, temperature, NaCl concentration) by means of NMR-spectroscopy, UV/Vis, HPLC, pH- and conductivity measurements.⁶² It appears that **KP1019** is more stable towards aquation and hydrolysis and is thus more readily taken up by cells than **NAMI-A**.⁶³

KP1019 was the second ruthenium based drug to reach human trials. A phase I clinical trial and pharmacokinetic study was recently reported.⁶⁴ In this study, 8 patients with advanced and refractory solid tumours (including colorectal, endometrial, melanoma and bladder carcinomas) were treated by **KP1019** according to a dose escalation protocol. Details concerning this study will not be discussed here. However, out of six evaluable patients presenting progressive disease at trial entry, five had disease stabilization that lasted for 8-10 weeks, despite the fact that the majority of patients were not treated with the therapeutically optimal dose in this study (**Table 2**). Stable disease was achieved even at the lowest dose level^{64(a)} and only mild toxicities related to treatment have been observed.

Patient N°	Diagnosis at study entry	Additional cycles	Dose	Outcome
1	Site: Sigmoid colon Histology: Adenocarcinoma	Yes (Cycle 2)	25 mg	Stable disease duration: 9 weeks
2	Site: Rectum Histology: Adenocarcinoma	No	50 mg	Not evaluable
3	Site: Colon Histology: Adenocarcinoma	No	50 mg	Stable disease duration: 10 weeks
4	Site: Bladder cancer	No	100 mg	Progressive disease
5	Site: Liver Histology: Cholangiocellular carcinoma	Yes (Cycle 2)	200 mg	Stable disease duration: 8 weeks
6	Site: Endometrium Histology: Carcinoma	No	400 mg	Stable disease duration: 10 weeks
7	Site: Left eye melanoma of the choroidea Histology: Spindle B-cell melanoma	No	600 mg	Not evaluable
8	Site: Tongue Histology: Carcinoma	Yes (Cycle 2)	600 mg	Stable disease duration: 8weeks

Table 2: Results of the clinical phase I trials with KP1019

KP1019 is supposed to induce oxidative stress and DNA damage comparable to that for the other metal-based drugs like *cisplatin*.⁶⁵ Moreover, **KP1019** treatment seems to induce apoptosis *via* a mitochondrial pathway (**Figure 15**).⁶⁶ However, **KP1019** is also known to strongly bind to serum proteins, including albumin and transferrin.⁶⁷ As a consequence, it has been assumed that serum protein binding, which can occur through transferrin pathway, is necessary for drug accumulation into the tumour.⁶⁷ Given that cancer cells generally over express transferrin receptors to serve the higher need for iron (see **Chapter 1, 1.3.1**), **KP1019** is expected to accumulate preferentially in tumour tissues rather than in healthy ones.

This has been highlighted by the observation done during clinical phase I trial.⁶⁴ Although numerous studies focused on the interaction of **KP1019** with proteins have done significant progress in the understanding of its mode of action, the intracellular fate of this drug after uptake into tumour cells is definitively still unclear. Keppler *et al.* reported also analogues of **KP1019** of type $[\text{Ru}^{\text{III}}\text{Cl}_{(6-n)}(\text{Hind})_n]^{(3-n)-}$ ($n=0$ to 4). Their antiproliferative activities were evaluated in CH1 (ovarian cancer) and SW480 (colon cancer) cells and were correlated with their $\text{Ru}^{\text{III}}/\text{Ru}^{\text{II}}$ red-ox potential in the following order : $[\text{Ru}^{\text{III}}\text{Cl}_4(\text{Hind})_2] < [\text{Ru}^{\text{III}}\text{Cl}_5(\text{Hind})]^{2-} < [\text{Ru}^{\text{III}}\text{Cl}_3(\text{Hind})_3] < [\text{Ru}^{\text{III}}\text{Cl}_2(\text{Hind})_4]^+ \approx [\text{Ru}^{\text{II}}\text{Cl}_2(\text{Hind})_4]$.⁶⁸

In **phase I clinical trials**, **KP1019** did not reach the MTD and no feedback on a possible **clinical phase II** on **KP1019** has been published yet. However, on the basis of its higher water solubility, the sodium salt of **KP1019**, sodium trans-[tetrachlorobis(1H-indazole)ruthenate(III)] (**KP1339**),⁶⁹ has been selected as a lead candidate for further clinical development.

As a conclusion, although these Ru^{III} compounds obviously differ from *cisplatin* in their mode of action (see **Chapter 1, 1.3.2.**), many aspects of the tumour-inhibitory effects of these ruthenium(III) complexes are still not completely understood.

Indeed **NAMI-A** and **KP1019** are stated to be active because of interactions with cell components different from DNA and responsible for the destruction of malignancy of tumour cells (**NAMI-A** modifies cell invasion and metastasis)⁷⁰ or for activation of apoptosis due to interaction with molecules responsible for cell survival (**KP1019** promotes apoptosis through a possible mitochondrial pathway) (**Figure 15**).^{65,66,71}

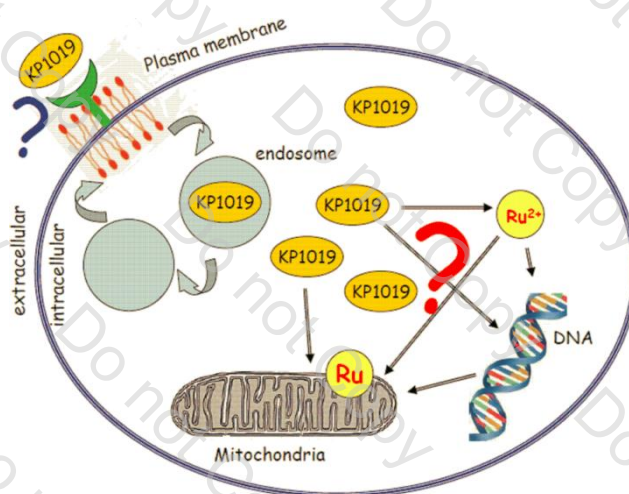


Figure 15: Schematic representation of the hypothetical mode of action of KP1019⁷¹

1.3.3. Ru(III) complexes vs. cisplatin: Highlight of another activity pattern?

Initially, ruthenium was believed to act by direct interaction with DNA like its platinum congener. However, three major findings were made in the 80's that lead to an important number of publications dealing with the mode of action of ruthenium(III) species:

- The hypothesis proposed by M. J. Clarke⁷² of “**activation by reduction**” mechanism in which a ruthenium(III) species can circulate in the body as an “inert chemical” until it reaches the tumour where the pH (lower than 7) will transform the complex into an active molecule (*i.e.* act as a prodrug).
- The initial study and the hypothesis proposed by S.C. Srivastava⁷³ that transferrin allows ruthenium transportation to cancer cells.
- The study done by V. Brabec⁷⁴ on ruthenium binding mode on DNA which differs from conventional platinum drugs.

For now, it has been demonstrated⁷⁵ that ruthenium shows a large number of differences compared with conventional platinum drugs:

- 1) Ruthenium(III) seems to accumulate preferentially in neoplasms rather than in normal tissues, possibly by using transferrin to enter tumours.⁴⁵ It has been postulated that transferrin-ruthenium complexes are transported into neoplastic tissue which contains high transferrin receptor densities. Once bound to **transferrin receptor**, the complex can liberate ruthenium(II) which is **internalized** by the tumour.⁷⁶ Although this postulate is very exciting and is strengthened by molecular demonstration, it remains to show, how the transferrin can easily link to a ruthenium complex, which is much larger than the iron atom usually shuttled by the transferrin.
- 2) Ru(III) species remain relatively non active until they reach the tumour site. In the tumour environment, where there is a lower oxygen content and a higher acidity compared to normal tissues, **reduction** to the more reactive Ru(II) occurs.⁷⁷ This activation by reduction process can selectively target tumour cells.
- 3) Some ruthenium drugs exhibit greater activity against metastases than against primary tumours. This effect is possible thanks to the inhibition of tumour cell detachment, invasion/migration and re-adhesion to a new growth substrate.⁷⁸

Regarding these properties (activation by reduction, transferrin transportation, DNA binding and activity on metastases), ruthenium species **must have different activity patterns** from those of platinum drugs.

1.3.4. Non-cyclometalated arene Ruthenium(II) compounds as potential anticancer agents

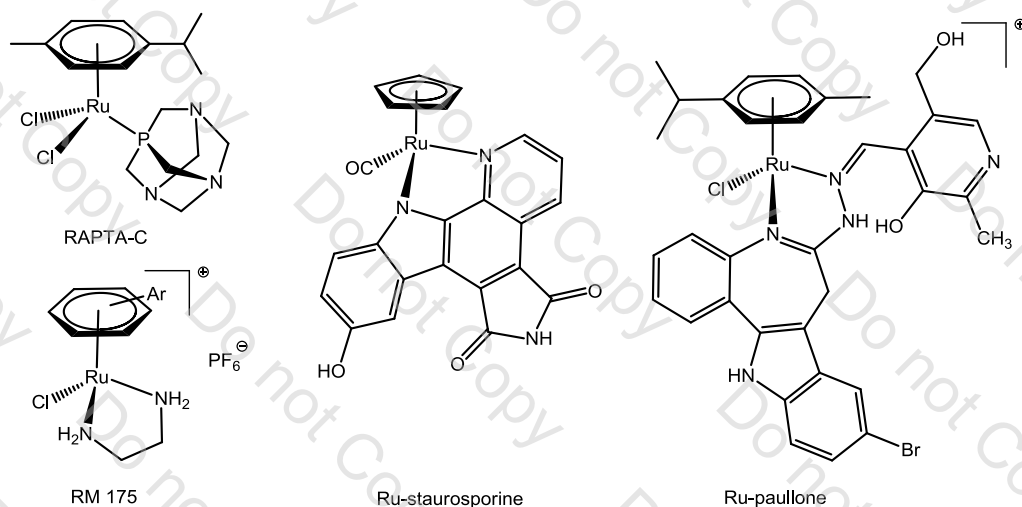
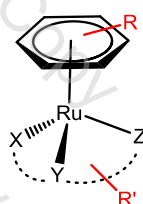


Figure 16: Examples of some non-cyclometalated Ru-arene complexes with biological activity

More recently, **half-sandwich** organometallic Ru(II)-arene complexes have been intensively studied for their possible application in cancer chemotherapy. These complexes also known as “**piano-stool**” complexes have a general formula $[(\eta^6\text{-arene})\text{Ru}(\text{X})(\text{Y})(\text{Z})]$, where (X) is a monodentately bound moiety, often a leaving group (*e.g.* chloride) and (Y) and (Z) are bidentate chelating or two monodentate ligands, resulting in neutral or positively charged complexes (bearing Cl^- , BF_4^- , PF_6^- ... as counter ions).



R, R': functional groups
X, Y, Z: monodentate ligands
or bidentate ligands
or tridentate ligands

Figure 17: General structure of half-sandwich arene ruthenium complexes

The nature of the half-sandwich complexes allows to introduce numerous biologically active groups and the hydrophobic arene part can undergo various substitutions.⁷⁹ The three remaining coordination sites (X, Y, Z) on the metal centre are amenable to a variety of coordination including three monodentate (X= Y= Z), one monodentate (X) and a bidentate (ZY) or even tridentate (XYZ) ligands (**Figure 17**). Various approaches have been investigated to introduce additional functionalities to the coordination sphere including coordination of ethylenediamine (en),⁸⁰ paullone derivatives,⁸¹ 1,3,5-triaza-7-phosphatricyclo[3.3.1.1]decane (pta),⁸² pyridinones⁸³ or *per se* bioactive groups, like staurosporine derivatives (**Figure 16**).⁸⁴

In this section, **only the mononuclear arene-ruthenium complexes** cited above will be discussed in order to draw a parallel with their arene-osmium analogues (**see Chapter 1, 1.4.**).

There are of course many other forms of arene ruthenium complexes summarized by Therrien B. and Smith G.S. in a recent perspective review⁸⁵ focused on arene-ruthenium chemotherapeutics:

Multinuclear arene compounds:

- Heteronuclear arene ruthenium complexes containing a ferrocene or a titanocene moiety.
- Dinuclear arene ruthenium complexes bridged with pyridinone, thiophenolato, 2,3-bis(2-pyridyl) pyrazine and thiosemicarbazone ligands.
- Trinuclear arene ruthenium cluster and metalla-cycle.
- Dendritic cores decorated with four or eight arene ruthenium complexes.
- Tetranuclear, Hexanuclear and Octanuclear arene ruthenium complexes.

Ruthenium porphyrin compounds:

- Pentafluorophenyl porphyrin ruthenium complex and tetranuclear porphyrin ruthenium conjugate.
- Bis-porphyrin sawhorse-type diruthenium complex and tetra-porphyrin derivative.
- Water soluble ruthenium-arene [porphine-cage]ⁿ⁺ (n=6,8) system.
- Mononuclear and tetranuclear arene ruthenium porphyrin complexes.

1.3.4.1. Coordination with N,N chelating ligands:

In 2001, Sadler *et al.* developed a new group of arene ruthenium(II) diamine complexes $[(\eta^6\text{-arene})\text{Ru}(\text{X})(\text{Y})(\text{Z})]$ (**Figure 17**) where the π -arene is benzene or substituted benzene and X, Y, Z are monodentate ligands such as halide, acetonitrile, or isonicotinamide, or Y, Z is chelating ligand **ethylenediamine** (en) or **N-ethylenediamine** (**Table 3**).^{80(a)} These compounds show *in vitro* cytotoxic effect in ovarian cancer cells (against A2780 cells), associated with DNA interaction.⁸⁶

A broad range of IC₅₀ values was obtained with two compounds (**RM 175** and **HC29**) comparable to carboplatin (6 μ M), one compound (**HC11**) comparable to cisplatin (0.6 μ M) and one compound (**HC27**) intermediate in activity between the two platinum complexes (**Table 3**).

Compound	Arene	X	Y	Z	IC ₅₀ (μM)
RM 100	<i>p</i> -cymene	Cl	CH ₃ CN	CH ₃ CN	>100
RM 101	<i>p</i> -cymene	Br	CH ₃ CN	CH ₃ CN	>100
RM 114	<i>p</i> -cymene	Cl	Cl	isonicotamide	>100
RM 116	<i>p</i> -cymene	Cl	H ₂ NCH ₂ CH ₂ NH ₂		10 ± 1.1
RM 118	C ₆ H ₆	I	H ₂ NCH ₂ CH ₂ NH ₂		20 ± 8.9
RM 119	C ₆ H ₆	Cl	H ₂ NCH ₂ CH ₂ NH ₂		17 ± 8.3
RM 121	<i>p</i> -cymene	I	H ₂ NCH ₂ CH ₂ NH ₂		9 ± 1.6
RM 125	C ₆ H ₅ CO ₂ CH ₃	Cl	H ₂ NCH ₂ CH ₂ NH ₂		56 ± 0.7
RM 168	C ₆ H ₅ CO ₂ CH ₂ CH ₃	Cl	H ₂ NCH ₂ CH ₂ NH ₂		52 ± 2.3
RM 175	C ₆ H ₅ C ₆ H ₅	Cl	H ₂ NCH ₂ CH ₂ NH ₂		5 ± 0.4
HC 11	Tetrahydroanthracene	Cl	H ₂ NCH ₂ CH ₂ NH ₂		0.5 ± 0.1
HC 27	Dihydroanthracene	Cl	H ₂ N(CH ₂) ₂ NH(CH ₂ CH ₃)		2 ± 0.4
HC 29	C ₆ H ₅ C ₆ H ₅	Cl	H ₂ N(CH ₂) ₂ NH(CH ₂ CH ₃)		6 ± 0.7
Cisplatin	-	-	-	-	0.6 ± 0.06
Carboplatin	-	-	-	-	6 ± 0.7

Table 3: IC₅₀ values of Ru(II) arene complexes on A2780 cell line after 24h drug exposure^{80(a)}

The recently published inventions of Sadler's group, describing the use of Ru(II) arene complexes in medicine, particularly for the treatment and/or prevention of cancer, are protected by the referenced patents.⁸⁷

One of the lead compounds in this arene ruthenium class, the **RM 175**, demonstrated a p53 and p21/WAF1-dependent early growth arrest in HCT116 colorectal cells.⁸⁸ Our laboratory (see Chapter 1, 1.3.5.) has also demonstrated for cycloruthenated compounds both p53-dependent and p53-independent mechanisms of cytotoxicity in neuroblastoma and glioblastoma cell lines with G₁ arrest and apoptosis induction.⁸⁹ This suggests that these Ru(II) arene complexes have a mechanism of action which differs from those of Ru(III) complexes currently in clinical trials.

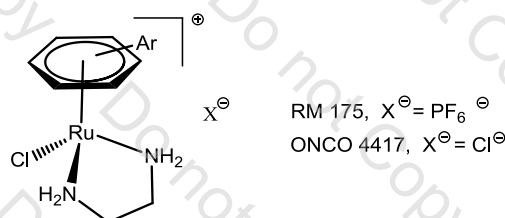


Figure 18: Chemical structure of arene Ru(II) diamine complexes **RM 175** and **ONCO 4417**

The substitution of the hexafluorophosphate (PF₆) anion by a chloride anion in **RM 175** leads to another Ru(II) salt **ONCO 4417** (Figure 18) which possesses antineoplastic properties and can induce DNA damage (at similar levels to cisplatin).^{80(b)} According to Sadler *et al.*,^{80(b)} this

complex induces apoptosis in cancer cells and arrests cell cycle at the G₂/M phase. Moreover, *in vitro* studies have demonstrated that **ONCO 4417** is at least as efficient as *cisplatin* in numerous cell lines (including lung, colorectal, ovarian, oesophageal, pancreatic and melanoma). In addition, **ONCO 4417** still remains active against *cisplatin* resistant ovarian cancer cell lines (A2780cis) which suggests that this compound does not share cross resistance mechanisms with *cisplatin*.

1.3.4.2. Coordination with 1,3,5-triaza-7-phosphaadamantane (pta):

The work of Dyson *et al.* on a distinct series of arenes-Ru(II) characterized by the presence of **phosphaadamantane coordinates**, called **RAPTA** (acronym for **Ru**thenium-**A**rene-**P**TA) (**Figure 19**), were developed in 2005⁹⁰ and brought many contribution to the development of cytotoxic arene-ruthenium complexes. This group of arene ruthenium(II) complexes of general formula $[(\eta^6\text{-arene})\text{RuCl}_2(\text{pta})]$ is characterized by the use of different π -arene derivatives such as *p*-cymene, toluene, benzene, benzo-15-crown-5, 1-ethylbenzene-2,3-dimethylimidazolium tetrafuloroborate, ethyl benzoate and hexamethylbenzene.

Compound	Arene	X	Y	Z	IC ₅₀ TS/A(μM)	IC ₅₀ HBL-100 (μM)
RAPTA-C	$\eta^6\text{-C}_{10}\text{H}_{14}$	Cl	Cl	pta	>300	>300
RAPTA-B	$\eta^6\text{-C}_6\text{H}_6$	Cl	Cl	pta	231	>300
RAPTA-H	$\eta^6\text{-C}_{12}\text{H}_{18}$	Cl	Cl	pta	199	>300
RAPTA-T	$\eta^6\text{-C}_7\text{H}_8$	Cl	Cl	pta	74	>300
RAPTA-BI	$\eta^6\text{-C}_6\text{H}_5\text{-(CH}_2)_2\text{Im}$	Cl	Cl	pta	66	>300
RAPTA-BC	$\eta^6\text{-benzo-15-crown-5}$	Cl	Cl	pta	159	>300
RAPTAMe ⁺ -T	$\eta^6\text{-C}_7\text{H}_8$	Cl	Cl	Me-pta	110	77
RAPTA-CO ₂ Et	$\eta^6\text{-C}_6\text{H}_5\text{CO}_2\text{Et}$	Cl	Cl	pta	103	>300

Table 4: IC₅₀ values of the RAPTA type complexes on TS/A and HBL-100 cell lines after 72h incubation^{90(a)}

RAPTA complexes exhibit weak and heterogeneous *in vitro* cytotoxicity towards the TS/A tumourigenic cell line with practically no effect in non-tumourigenic HBL-100 (**Table 4**). The *in vivo* effect on the growth of lung metastases was also established for **RAPTA-C** and **RAPTA-B** complexes.

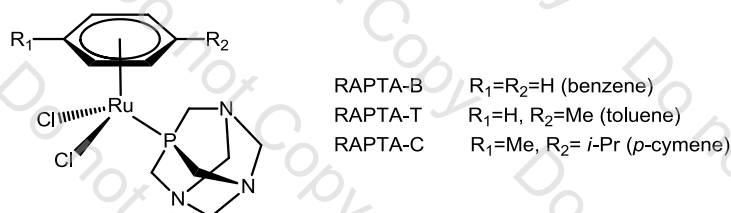


Figure 19: Chemical structures of three arene-ruthenium(II) complexes (RAPTA)

This study confirmed that these compounds reduce significantly the growth of lung metastases in CBA mice bearing MCa mammary carcinoma.^{90(a)} It is important to notice that the pta ligand provides a degree of water solubility (dependent on the nature of the arene ligand) which facilitates administration and transport in the body.

In vitro studies on **RAPTA-T** showed inhibition of some key steps of the metastatic process such as detachment from the primary tumour cell mass, migration/invasion, and re-adhesion to a new growth substrate in breast cancer cell lines. *In vivo*, **RAPTA-T** selectively reduces the growth of lung metastases.⁷⁸ It is quite striking, that two such different compounds **RAPTA-T** (ruthenium(II) organometallic compound) and **NAMI-A** (a ruthenium(III) coordinated complex) exhibit such similar activities, both being inactive towards primary tumours, but active towards secondary metastasis tumours.

These RAPTA complexes were also functionalized at the π -arene with substitutes able to generate hydrogen bonds in order to increase the interaction with DNA and increase their cytotoxicity. These structurally diverse analogues have been studied and their *in vitro* cytotoxicity has been evaluated.⁹¹ These new compounds are also weakly cytotoxic against tumour cells *in vitro* and are also usually **free of toxicity to healthy cells** as their first generation congeners. All these RAPTA complexes show low, to very low general toxicity, what makes them highly attractive for their therapeutic potential.

1.3.4.3. Coordination with protein kinase inhibitors:

Coordination with Indolo[3,2-*d*]benzazepines (Paullones) and Indolo[3,2-*c*]quinoline

More recently, metal complexes with biologically active ligands have become a challenging subject of current research effort. Since their discovery, the **indolo[3,2-*d*]benzazepines**, also referred as **paullones**, were referred as cyclin-dependent kinase (CDKs).⁹² These latter compounds have also shown inhibition of other intracellular proteins such as glycogen kinase-3 and mitochondrial malate dehydrogenase.⁹³

In 2007, Keppler *et al.*⁹⁴ developed a new group of **arene ruthenium(II) paullone complexes** $[(\eta^6\text{-arene})\text{Ru}(\text{X})(\text{Y})(\text{Z})]$ where the π -arene is *p*-cymene, X is a monodentate ligand such as chloride and Y,Z is chelating **paullone-type** ligand. These paullones contain a seven-member folded azepine ring, which makes the whole molecule nonplanar (**Figure 20**).

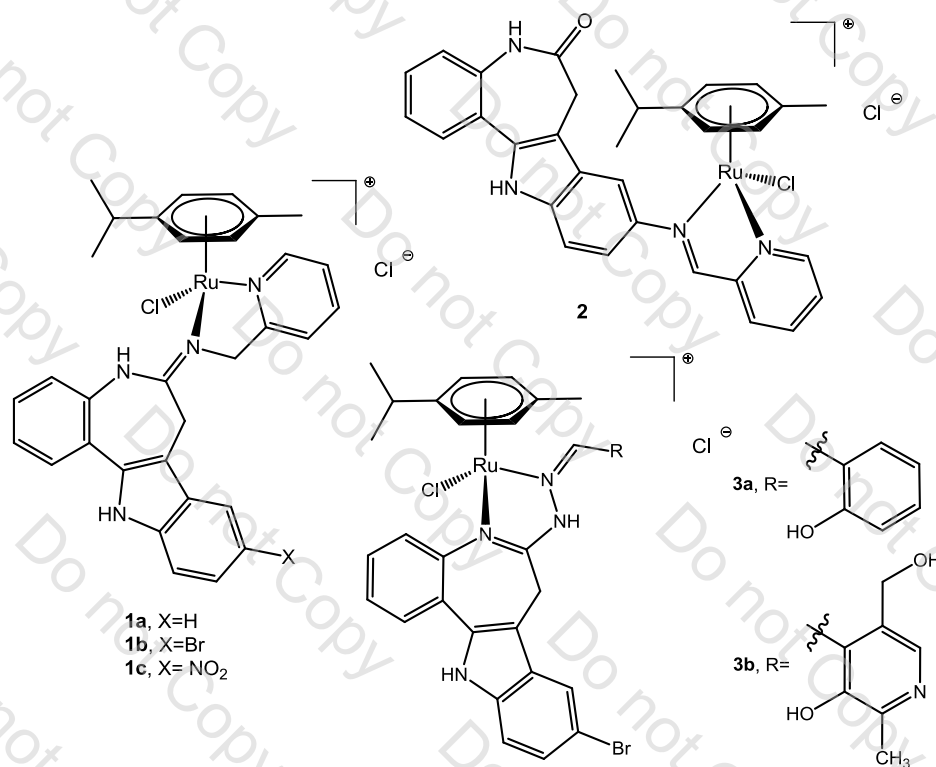


Figure 20: Chemical structures of some paullone-type arene-ruthenium(II) complexes

The antiproliferative activity was tested in three human cancer cell lines (A529 non-small-cell lung cancer, CH1 ovarian carcinoma and SW480 colon adenocarcinoma) (**Table 5**). The IC₅₀ (in the submicromolar to very low micromolar concentration range) indicate that these metal-based paullone derivatives are **potential candidates** for further development and medical application as antitumour chemotherapeutics.

<i>Ru-paullone</i> <i>compounds</i>	<i>IC</i> ₅₀ (<i>μM</i>)		
	<i>A549</i>	<i>CH1</i>	<i>SW480</i>
1a	5.2 ± 0.9	1.6 ± 0.5	1.6 ± 0.3
1b	8.5 ± 1.6	1.9 ± 0.4	1.2 ± 0.5
1c	12 ± 4	1.8 ± 0.2	3.9 ± 0.3
2	32 ± 1	9.7 ± 1.6	28 ± 5
3a	1.7 ± 0.4	0.53 ± 0.18	0.59 ± 0.19
3b	2.5 ± 0.2	0.58 ± 0.08	1.0 ± 0.2

Table 5: IC₅₀ values of the paullone type complexes on several cell lines after 96h incubation⁸⁴

Building on his success with paullone-type arene-ruthenium(II) complexes, Keppler *et al.* developed in 2010⁹⁵ a new group of **arene ruthenium(II) indoloquinoline complexes** [(η⁶-arene)Ru(X)(Y)(Z)] where the π-arene is *p*-cymene, X is a monodentate ligand such as chloride and Y,Z is chelating **indolo[3,2-*c*]quinoline-type ligand** (**Figure 21**).

These indoloquinolines have a similar framework to that of paullones but are composed of a flat six-membered ring instead of the folded seven-membered azepine ring, which confers to the indoloquinoline a planar heteroaromatic system. These biologically active ligands displaying antiproliferative properties⁹⁶ are a challenging subject of current research effort.

However, results of this first⁹⁵ study show much lower stability in both organic and aqueous media than the paullone derivatives. This can lead to a rapid dissociation of the ligands to the metal-arene scaffold. More recently in 2011,⁹⁷ Keppler *et al.* developed novel arene-ruthenium(II) with **modified indolo[3,2-*c*]quinoline**, looking for elucidation of structure-activity relationship of this class of compounds (**Figure 21**).

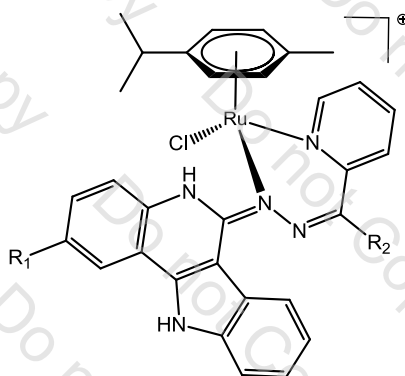


Figure 21: Chemical structures of indoloquinoline-type arene-ruthenium(II) complexes

The antiproliferative activity was tested, like their paullone congeners, in three human cancer cell lines (A529, CH1 and SW480) (**Table 6**) leading to IC_{50} values in the submicromolar to low micromolar range.

Indoquinoline compounds	R_1	R_2	IC_{50} (μM)		
			A549	CHI	SW480
1	H	H	6.0 ± 1.5	2.2 ± 0.6	2.1 ± 0.4
2	H	CH ₃	4.6 ± 0.8	0.7 ± 0.06	1.0 ± 0.2
3	F	CH ₃	14 ± 3	2.8 ± 0.9	2.3 ± 1.0
4	Cl	H	5.1 ± 1.8	0.32 ± 0.13	0.76 ± 0.03
5	Cl	CH ₃	9.3 ± 3.4	3.8 ± 0.6	5.0 ± 1.0
6	Br	CH ₃	7.2 ± 1.7	1.3 ± 0.2	1.5 ± 0.6
7	CH ₃	CH ₃	2.0 ± 0.4	0.19 ± 0.02	0.28 ± 0.2

Table 6: IC_{50} values of the indoloquinoline-type complexes on several cell lines after 96h incubation⁹⁷

Coordination with biologically active Staurosporine

Protein kinases are a large family of homologous proteins with 518 members in the human genome.⁹⁸ They regulate most aspects of cellular life and are one of the main drug targets. The natural microbial **alkaloid staurosporine** is a highly potent inhibitor for various kinases, and many staurosporine derivatives have been developed as anticancer drugs. It has been demonstrated that its effect can also be mimicked by an octahedral ruthenium complex.⁹⁹

Meggers *et al.* have exploited the strategy to develop a new group of **arene ruthenium(II) staurosporine complexes**, where the π -arene is a cyclopentadienyl (Cp), X is a monodentate carbonyl ligand CO and Y,Z is chelating bidentate N,N' **staurosporine-type ligand** (**Figure 22**). Meggers *et al.* showed that by replacing indolocarbazole alkaloid scaffold with a metal complex, these arene ruthenium(II) staurosporine complexes can be used as protein kinase inhibitor including glycogen synthase kinase (GSK)-3 β .⁸⁴

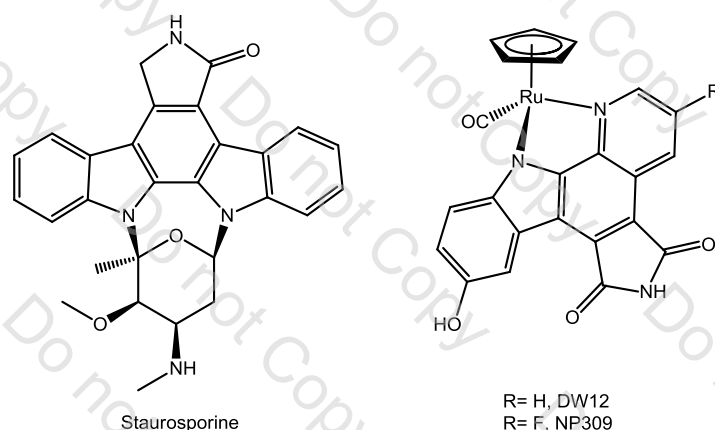


Figure 22: Indolocarbazole natural product (here staurosporine) and metallo-pyridocarbazole as protein kinase inhibitors

Thus, elaborate structures, which differ from purely organic molecules, could be built up by variation of the ligands. These complexes and especially **DW12** and **NP309** are potent activators of p53 and induce p53-activated apoptosis *via* the mitochondrial pathway through down-regulation of Mdm2 and Mdm4 in vincristine- and cytarabine highly resistant human B-cell melanoma cell lines.^{84,100,101} Hence, ruthenium staurosporine-type complexes have shown increased activity compared to their purely organic congeners. However, no *in vivo* studies evaluating **DW12** or other compounds of this group have been conducted yet.

Such properties of organometallic complexes demonstrate that the use of kinetically inert metal centres, as rigid structural scaffolds for enzyme inhibitor design, will broaden the synthetic scope of new antitumour drugs.

1.3.5. Cyclometalated Ruthenium(II) compounds developed by the Laboratoire de Synthèses Métallo-induites: State of the art

In the essential aim of increasing activity and reducing side effects of this compound, our laboratory has developed over several years organometallic ruthenium compounds named **RDC** (acronym for **R**uthenium **D**erivative **C**ompound). The laboratory has been involved in this field since the discovery that some cyclometalated ruthenium(II) compounds can display interesting antitumour activity.¹⁰²

Contrary to the existing antitumour compounds which are usually built up with a ligand weakly coordinated to the metal, our laboratory has prepared and tested¹⁰³ ruthenacycle in which one ligand is **strongly bound to the metal** via a strong carbon-ruthenium (C-Ru) σ bond which is stabilized by a nitrogen-ruthenium (N-Ru) intramolecular bond (**Figure 23**).

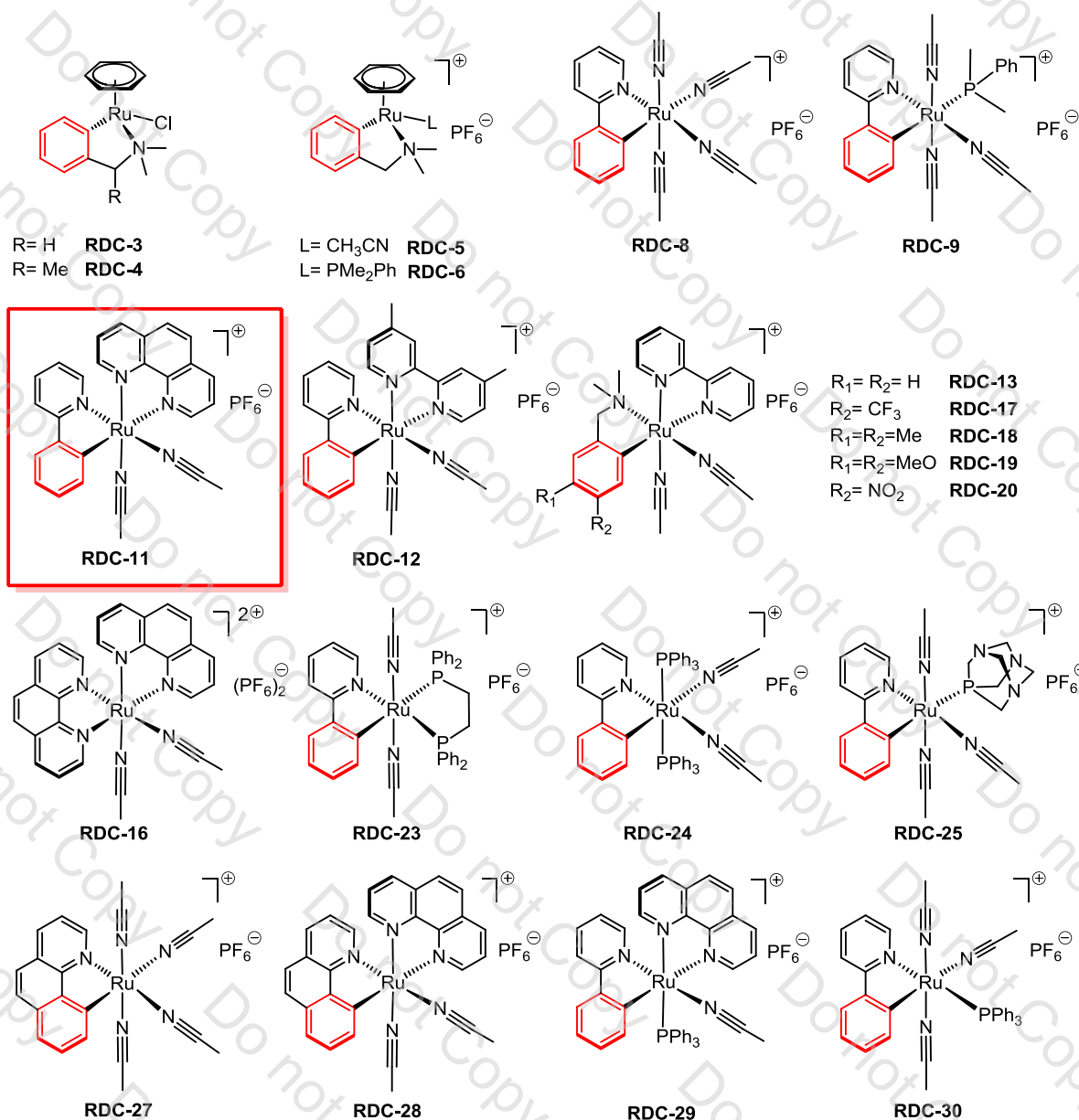


Figure 23: Extract of the chemical library

We have demonstrated that these thermodynamically and kinetically (towards substitution reactions) stable cyclometalated complexes containing 2-phenylpyridine derivatives have a Red-Ox potential of particular interest that may allow them to interact with the **oxido-reductase enzymes**.¹⁰⁴ Moreover, some of these complexes have good lipophilicities that allow them to enter malignant cells and may likely display mechanisms of action that differ from that of more classical platinum derivatives.¹⁰⁵

In vitro and *in vivo* studies

An extensive chemical library has been developed in which most of the compounds have shown *in vitro* antitumour activity. These preliminary studies led to the selection of several candidates as anticancer drugs and **RDC 11** [Ru(o-C₆H₄py-κC,N)(phen)(NCMe)₂]PF₆ was selected for further *in vivo* biological studies (**Figure 24**).¹⁰⁵

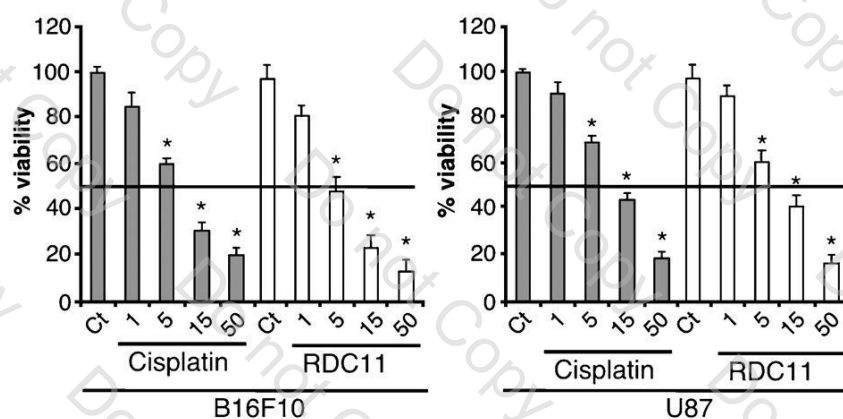


Figure 24: *In vitro* evaluation of RDC 11 on B16F10 and U87 cell lines by MTT tests¹⁰⁵

RDC 11's *in vivo* activity was also evaluated on syngeneic tumour models B16F10 (subcutaneous melanoma) and 3LL (Lewis Lung carcinoma) and also on xenograft models U87 (human glioblastoma). In all of those models, both **RDC 11** and *cisplatin* demonstrated similar tumour growth inhibition of up to 40% compared with untreated mice (**Figure 25**).

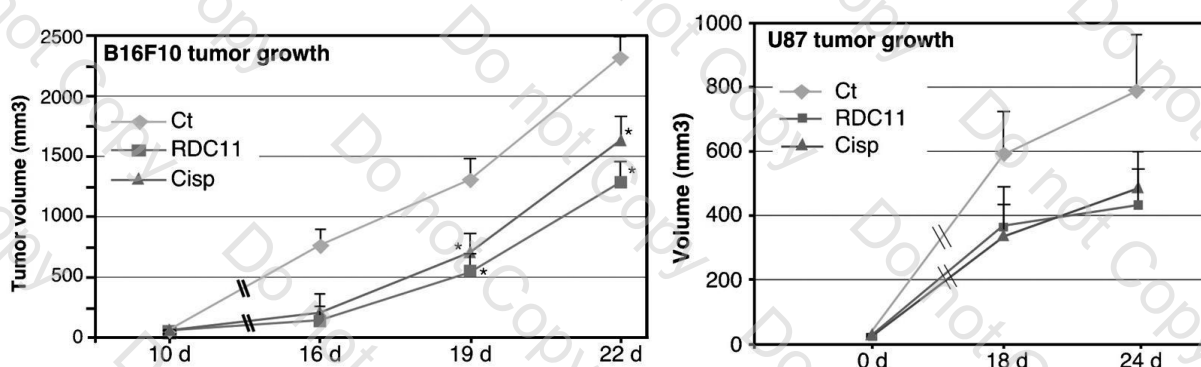


Figure 25: Example of *in vivo* evaluation of RDC 11 on B16F10 and U87 cell lines¹⁰⁵

A major drawback of chemotherapy is the lack of selectivity, leading to significant side effects (see Chapter 1, 1.2.3). Therefore, two criteria were used to analyze the toxicity induced by **RDC 11** in mice: the acute and chronic toxicity. In one single dose experiment, the lethal dose (LD₅₀) of **RDC 11** is comparable to those of *cisplatin* (LD₅₀ = 54 $\mu\text{mol.kg}^{-1}$) (Figure 26). To assess the chronic toxicity of **RDC 11**, mice were regularly treated with equimolar doses of *cisplatin* or **RDC 11**. After 3 weeks, *cisplatin*-treated mice had lost about 20% of their body weight in contrast to **RDC 11**-treated mice, which maintained their body mass.¹⁰⁵

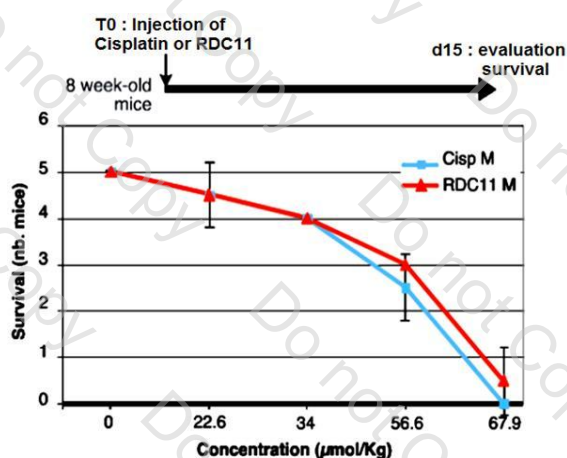


Figure 26: Comparison of LD₅₀ between *cisplatin* and **RDC 11**¹⁰⁵

Based on the classical toxicities observed in clinic on specific organs, several **markers** have been monitored to assess the tolerance of **RDC 11** towards those specific tissues. Liver, kidney and hematopoietic functions have been evaluated based on blood marker analysis (Figure 27). Biochemistry analyses of the blood showed that *cisplatin* induced changes in uric acid, ASAT, ALAT, α -Amylase, glucose, bicarbonate and iron, corresponding to an alteration in liver and kidneys function. No significant changes were observed on several blood markers from **RDC 11**-treated mice, except a drop in creatine enzyme concentration. Furthermore, after a chronic treatment, liver and kidneys from *cisplatin*-treated mice lost mass, further demonstrating that toxicities had arisen.

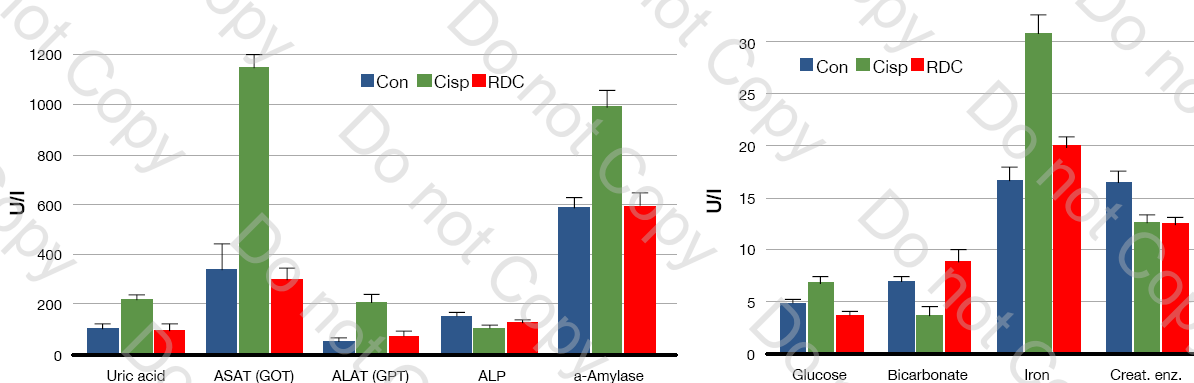


Figure 27: Blood marker analysis

To analyze the toxicity on the sensory system, which is a classical toxicity triggered by *cisplatin* in clinic, an electromyography was used to record the speed of propagation of nerve impulses. After three weeks of treatment, *cisplatin* significantly reduces the speed conduction of sensory nerves, whereas **RDC 11** has a modest effect on the nervous system (**Figure 28**).

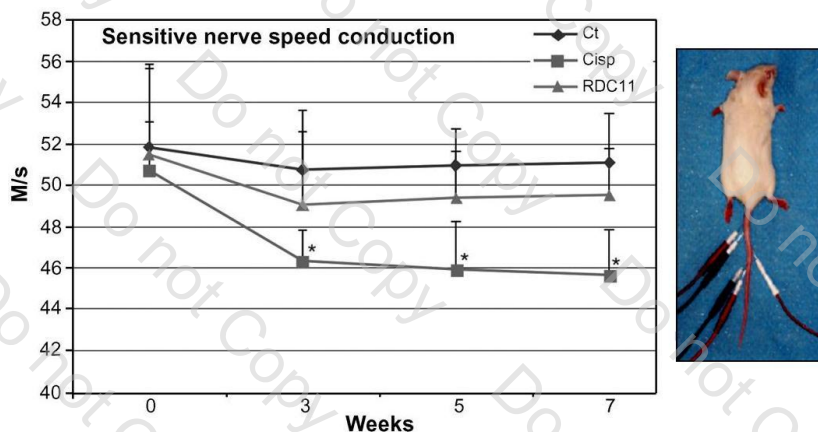


Figure 28: *Cisplatin* reduces the speed of propagation of nerve impulses compared to **RDC 11**¹⁰⁵

As a conclusion, **RDC 11** shows significant inhibition of the growth of mouse and human tumours implanted in mice without affecting the body weight, liver and kidney functions, or the neuronal sensory system, in striking contrast with *cisplatin*.

The C-Ru bond as the corner-stone of the activity?

Several studies have been conducted in the laboratory to understand the antiproliferative activity of the **RDCs**. The carbon-ruthenium bond appears to be a prerequisite for biological activity in this family of compounds. The results show that cyclometalated complexes are cytotoxic while their non-cyclometalated analogues are not. By comparing the activities of **RDC 11** and its non-cyclometalated **RDC 16** analogue (**Figure 23**), it appears that the complex without a C-Ru bond displays no cytotoxic activity (**Figure 29**). However, this result should be confirmed, because of the dicationic nature of **RDC 16**.

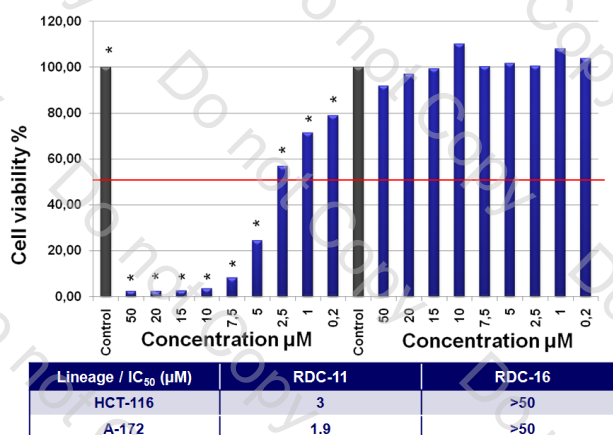


Figure 29: Influence of the C-Ru bond

1.3.6. Ruthenium(II) compounds: A controversial activity pattern?

The rapid development of anticancer drugs has spurred chemists to employ different strategies in synthesizing new metal-based compounds in which the ruthenium is directly linked to the carbons atoms of structural ligands (*e.g.* non-leaving groups). In these complexes, Clarke's theory of "activation by reduction" does not apply.⁷² Indeed, the metal is kept at a +II oxidation state (the lowest state available for ruthenium in biological fluids) and these complexes are reactive *per se*. In these Ru(II) compounds we can distinguish three main groups of complexes, where it is possible to extract biological data, referring respectively to:

- Sadler's **RM-type** complexes (see Chapter 1, 1.3.4.1.)
- Dyson's **RAPTA-type** complexes (see Chapter 1, 1.3.4.2.)
- Pfeffer's **RDC-type** complexes (see Chapter 1, 1.3.5.).

As described by Sadler *et al.*¹⁰⁶ for **RM-type** complexes, these Ru(II) complexes do not need any activation process to exchange their chloride ligands with water to target DNA.

Paradoxically, **RAPTA-type** complexes from Dyson *et al.* exhibit low cytotoxicity, suggesting that Ru(II) does not necessarily contribute to more reactive species than those with the Ru(III) oxidation state.

In short, it must be realized, that Ru(II) compounds have a rather **controversial activity pattern** associated with likely different mechanisms of action. Hence, the concept of "activation by reduction" mechanism is not a rule to be generalized to any ruthenium complex. However, at the present time, no mechanism of action has yet been unanimously adopted given that these complexes display a broad anticancer activity spectrum towards primary or secondary metastasis tumours.

1.3.7. Perspectives for ruthenium in cancer treatment

Inorganic compounds have been used in medicine for centuries, but often in an **empirical fashion**¹⁰⁷ with little attempt defining the molecular basis of their mechanisms of action. The interaction of transition metal ions with biological molecules provides one of the most captivating fields of coordination chemistry.

For now, it is still difficult to establish rules for particularly active ruthenium compounds with innovative mechanisms of action. Although ruthenium anticancer drugs have attracted an increasing interest in the last twenty years, the collected data on chemical and biological properties (especially the mechanism of action), do not allow formulating a leading compound. Examples such as **NAMI-A**, **KP1019**, **RM-175**, and **RAPTA-C** and **RDC 11**

In 2007 Keppler *et al.* reported a comparative study on ruthenium(III) **NAMI-A-type** complexes and their heavier and kinetically stable osmium(III) analogues (**Figure 30**).¹¹² These different analogues differ from the **osmium(III) NAMI-A** complex $trans-[OsCl_4(DMSO)(azole)]^- azoleH^+$ in the nature of coordinated azole ligand, such as 1*H*-indazole (Hind), 1*H*-pyrazole (Hpz), 1*H*-benzimidazole (Hbzim), 1*H*-imidazole (Him) or 1*H*-1,2,4-triazole (Htrz) (**Figure 31**).



Figure 31: Heterocyclic azole ligands used to build up NAMI-A osmium analogues

Surprisingly, this study revealed that osmium(III) analogues display *in vitro* **antiproliferative activity** in two human cell lines HT29 (colon carcinoma) and SK-BR-3 (mammary carcinoma) with IC_{50} in the 10^{-5} M range.

Comparison of antiproliferative activity of closely related ruthenium and osmium compounds shows that the behaviour of these compounds is **quite different**. Indeed, where the antimetastatic drug candidate $trans-[RuCl_4(DMSO)(Im)]ImH$ (**NAMI-A**, where Im = imidazole) displays an $IC_{50} = 212 \mu M \pm 22$, the IC_{50} of its heavier congener (**compound 2**, **Table 7**) in the human HT29 cell line is ten times lower ($IC_{50} = 21 \mu M \pm 1$) in HT29 cell line.

<i>Os</i> NAMI-A type compounds	<i>L</i>	<i>L</i> ⁺ counter ion	IC_{50} (μM)	
			HT29	SK-BR-3
1	DMSO	H(DMSO) ₂ ⁺	75 ± 11	241 ± 57
2	Hind	H₂ind⁺	21 ± 1	119 ± 41
3	Hpz	H ₂ pz ⁺	39 ± 10	325 ± 141
4	Hbzim	H ₂ bzim ⁺	36 ± 2	194 ± 19
5	Him	H ₂ im ⁺	103 ± 15	930 ± 45
6	Htrz	H ₂ trz ⁺	214 ± 61	>1000
Ruthenium analogues	Hind	H₂ind⁺	212 ± 22	169 ± 10
	Him	H ₂ im ⁺	339 ± 68	472 ± 25
	Htrz	H ₂ trz ⁺	322 ± 32	415 ± 48

Table 7: IC_{50} values of osmium(III) NAMI-A type complexes and ruthenium(III) congeners in several cell lines after 96h incubation¹¹²

1.4.3. En route to KP1019 osmium analogues

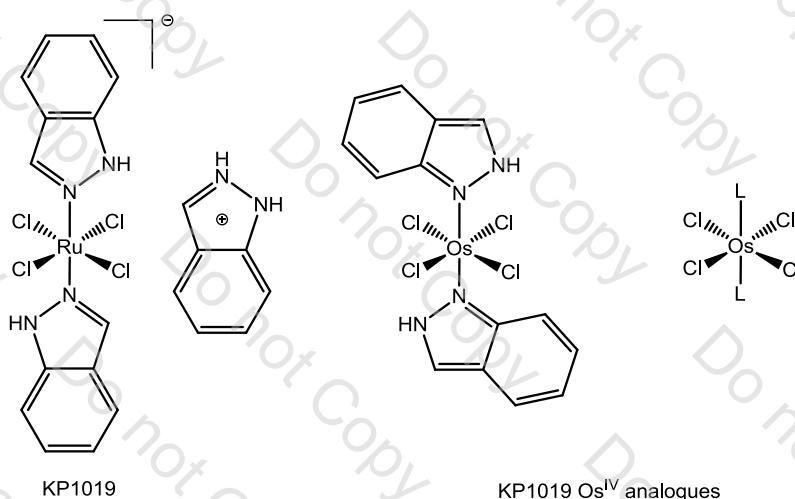


Figure 32: KP1019 and anticancer osmium(IV) analogues

In the aim of further exploring the structure-activity of **osmium azole complexes**,^{108(d, f)} Keppler *et al.* reported in 2011 a recent comparative study on **KP1019 osmium analogues** which display a cytotoxic activity in range comparable to that of clinically studied **KP1019** *trans*-[RuCl₄(Ind)₂]IndH (**Figure 32**).¹¹³ The new family of general formula *trans*-[Os^{IV}Cl₄(azole)] where the coordinated ligand is an azole, such as *2H*-indazole, *1H*-pyrazole, *1H*-benzimidazole or *1H*-imidazole (**Figure 33**) was synthesized by Anderson's type rearrangement reaction.

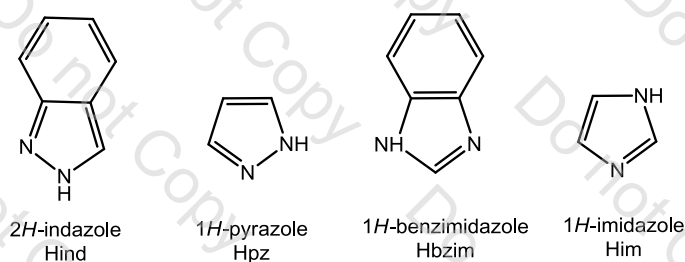


Figure 33: Heterocyclic azole ligands used to build up KP1019 osmium analogues

These osmium(IV) complexes are **appropriate precursors** for the synthesis of **osmium(III) analogues** of **KP1019**. The cytotoxicity of these complexes was evaluated in three human cancer cell lines (**Table 8**): CH1 (ovarian carcinoma), A549 (non-small lung carcinoma) and SW480 (colon carcinoma). IC₅₀ values are mostly in the 10⁻⁵ M range in the rather chemosensitive CH1 cell line, but mostly higher to 100 μM or even higher in the less chemosensitive A529 and SW480 cell lines. The best results are observed for **compound 2** (**Table 8**) which displays antiproliferative effects on two cell lines in a range comparable to the clinically studied ruthenium complex **KP1019**.

<i>Os</i> KP1019 type compounds	<i>L</i>	<i>IC</i> ₅₀ (μM)		
		A549	CHI	SW480
1	Hpz	>160	115 ± 14	120 ± 5
2	Hind	181 ± 11	53 ± 4	41 ± 14
3	Him	>640	46 ± 1	173 ± 9
4	Hbzim	>160	36 ± 16	>160
KP1019	Hind	-	44 ± 11	79 ± 5

Table 8: IC₅₀ values of osmium(IV) KP1019 type complexes and KP1019 in several cell lines after 96h incubation

1.4.4. Half-sandwich arene osmium(II) analogues

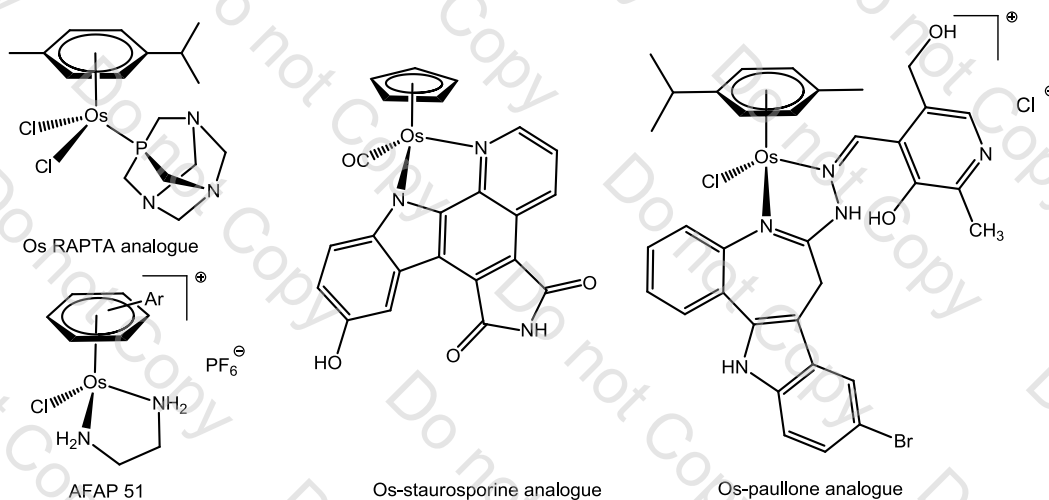


Figure 34: Example of some non-cyclometalated Os-arene analogues with biological activity

As it is the case for ruthenium, **half-sandwich** complexes of their heavier congener osmium have been studied for their possible application in cancer chemotherapy. These “**piano-stool**” complexes analogues have also a general formula $[(\eta^6\text{-arene})\text{Os}(\text{X})(\text{Y})(\text{Z})]$, where (X) is a monodentately bound moiety, often a leaving group (*e.g.* chloride) and (Y) and (Z) are bidentate chelating or two monodentate ligands, resulting in neutral or positively charged complexes (bearing Cl^- , BF_4^- , PF_6^- ... as counter ions) (**Figure 35**).

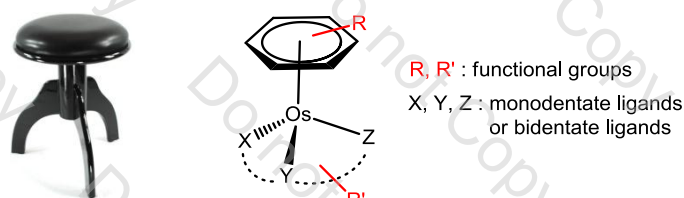


Figure 35: General structure of half-sandwich arene osmium complexes

Osmium analogues of many of these “piano-stool” complexes have been synthesized by introducing functionalities to the coordination sphere using coordination of N,N or N,O chelating ligands,¹¹⁰ 1,3,5-triaza-7-phosphatrimethylene (pta),^{109,111} paullone derivatives^{94,97} or *per se* bioactive groups, like staurosporine derivatives.¹⁰⁰ Despite numerous

studies on this metal as anticancer agent, a clear structure-activity relationship does not exist allowing one to predict the effect of exchanging ruthenium for osmium.

1.4.4.1. Coordination with N,N chelating ligands:

Sadler *et al.* reinvestigated in 2007^{110(c)} a new group of **arene osmium(II)** $[(\eta^6\text{-arene})\text{Os}(\text{X})(\text{Y})(\text{Z})]$ (**Figure 36**) where the π -arene is benzene or substituted benzene, X is a chloride and Y,Z is **chelating N,N ligand** such as ethylenediamine (en), 2-pyridinylmethanamine (ampy), 2,2'-bipyridyl (bpy), 1,10-phenanthroline (phen), [3,2-*a*:2',3'-*c*]phenazine (dppz) or 4-(2-pyridylazo)-*N,N*-dimethylaniline (azpy NME₂). Indeed, in previous studies^{110(a)} the non antiproliferative activity of $[(\eta^6\text{-bip})\text{Os}(\text{en})(\text{Cl})]^+ \text{BF}_4^-$ was misinterpreted, because of partial decomposition of the complex in stock solution prepared in DMSO.^{110(c)}

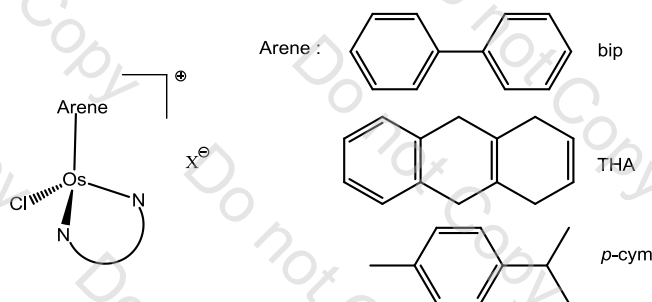


Figure 36: Osmium(II) arene complexes containing N-donor ligands

These complexes were tested *in vitro* in A549 (lung carcinoma) and in A2780 (ovarian cancer) cell lines. Some of them display an $\text{IC}_{50} \approx 6\text{-}10\mu\text{M}$, comparable to carboplatin.

<i>Os(II) arene compounds</i>	<i>Arene</i>	<i>N,N</i>	<i>Counter ion</i>	<i>IC₅₀ (μM)</i>				
				<i>A549</i>	<i>A2780</i>	<i>MDA-MB-231</i>	<i>MCF-7</i>	<i>HBL-100</i>
				<i>References</i>	<i>110 (c)</i>	<i>110 (c)</i>	<i>110 (n)</i>	<i>110 (n)</i>
AFAP51	bip	en	PF₆	10	7.0	48	15	16
1	bip	en	BF ₄	10	7.6	-	-	-
2	THA	en	BF ₄	6.4	9.4	-	-	-
3	<i>p</i> -cymene	ampy	PF ₆	>100	-	-	-	-
4	<i>p</i> -cymene	bipy	PF ₆	>100	-	-	-	-
5	<i>p</i> -cymene	phen	PF ₆	>100	-	-	-	-
6	bip	dppz	PF ₆	<40	<2	-	-	-
7	bip	azpy NME ₂	PF ₆	>100	-	-	-	-
8	<i>p</i> -cymene	azpy NME ₂	PF ₆	>100	-	-	-	-
RM175	bip	en	PF₆	-	5	62	93	54

Table 9: IC₅₀ values of Os(II) arene complexes and RM175 congener in different cell lines after 24h drug exposure

A more complete study was also undertaken recently, studying *in vivo* tumour and metastasis reduction and *in vitro* effects on invasion assays of the ruthenium **RM175** and osmium **AFAP51** complexes in the mammary cancer model.¹¹⁰⁽ⁿ⁾ Comparison of antiproliferative activity of ruthenium and osmium analogues (**Table 9**) shows that the behaviour of these complexes **can be very similar**^{110(c)} against certain human cancer cells, while completely different in respect to other cancer cells.¹¹⁰⁽ⁿ⁾

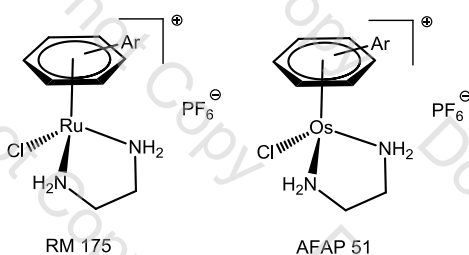


Figure 37: Chemical structure of RM 175 and its osmium(II) analogue AFAP 51

The osmium complex **AFAP51** is up to six times more active than **RM175** towards highly invasive MDA-MB-231 (human breast carcinoma), MCF-7 (human breast adenocarcinoma) and HBL-100 (epithelial human breast cancer). However, **RM175** was active against MCa (mammary carcinoma) *in vivo* and caused metastasis reduction, where **AFAP51** was not.¹¹⁰⁽ⁿ⁾ Thus, as in most cases, the congruency reasoning between observed effect *in vivo* and the behaviour of the compounds *in vivo* is not applicable.

1.4.4.2. Coordination with 1,3,5-triaza-7-phosphaadamantane (pta):

Dyson *et al.*^{111(a)} reported for the first time in 2005 a series of anticancer *p*-cymene osmium(II) dichloride complexes characterized by the presence of phosphadamantane (pta) or [Me-pta]Cl ligand. This group of arene osmium(II) complexes of general formula $[(\eta^6\text{-arene})\text{Os}(\text{Cl})_2(\text{pta})]$ is characterized by the use of different π -arene derivatives such as benzene or *p*-cymene.

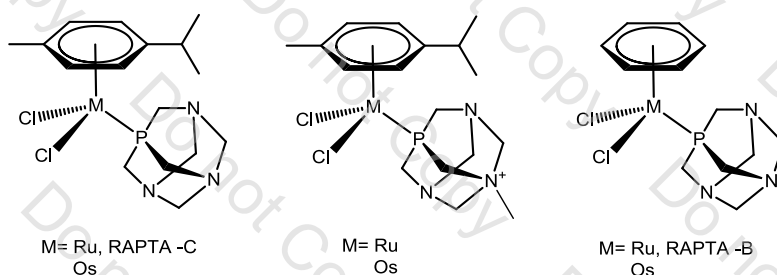


Figure 38: Chemical structure of three arene-ruthenium(II) complexes (RAPTA) and their osmium(II) analogues

Only a few studies were undertaken to evaluate the *in vitro* cytotoxicity of these compounds. *In vitro* evaluation of $[(\eta^6\text{-C}_{10}\text{H}_{14})\text{Os}(\text{Cl})_2(\text{pta})]$ together with the well characterised antimetastasis drug $[(\eta^6\text{-C}_{10}\text{H}_{14})\text{Ru}(\text{Cl})_2(\text{pta})]$ also known as **RAPTA-C**, was undertaken using HT29 (colon carcinoma), A549 (lung carcinoma) and T47D (breast carcinoma) cells.^{109(a)} The two congeners show similar cytotoxicity profiles in the HT29 cell line.

Compounds	Arene	X	Y	Z	IC_{50} (μM)		
					HT29	A549	T47D
RAPTA-C	$\eta^6\text{-C}_{10}\text{H}_{14}$	Cl	Cl	pta	441	1105	1034
Os analogue	$\eta^6\text{-C}_{10}\text{H}_{14}$	Cl	Cl	pta	456	1430	>1600

Table 10 : IC_{50} values of **RAPTA-C** and its osmium analogue^{109(a)}

Although these data suggest that the development of these analogues should not be overlooked, neither extensive *in vitro* nor *in vivo* studies on the **osmium(II) RAPTA** analogues were conducted yet. Structurally diverse **osmium(II) RAPTA** analogues should be therefore synthesized and evaluated in order to develop a chemical library of **RAPTA analogues** which may be attractive for their therapeutic potential.

1.4.4.3. Coordination with protein kinase inhibitors:

Coordination with Indolo[3,2-*d*]benzazepines (Paullones) and Indolo[3,2-*c*]quinoline

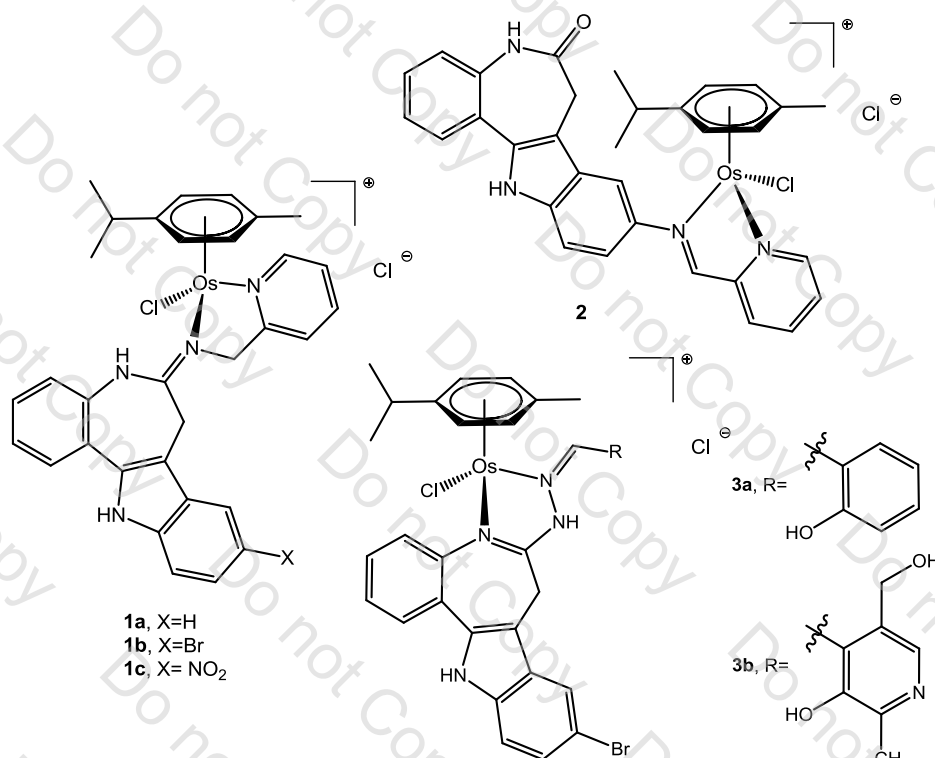


Figure 39: Chemical structures of some paullone-type arene-osmium(II) complexes

At the same time Keppler *et al.*⁹⁴ developed a new group of arene ruthenium(II) paullone complexes for their medical applications, this team also synthesized new **arene osmium(II) paullone complexes** $[(\eta^6\text{-arene})\text{Os}(\text{X})(\text{Y})(\text{Z})]$ where the π -arene is *p*-cymene, X is a monodentate ligand such as chloride and Y, Z is a chelating **paullone type** ligand.

The antiproliferative activity was tested in three human cancer cell lines (A529 non-small-cell lung cancer, CH1 ovarian carcinoma and SW480 colon adenocarcinoma) (**Table 5**). As for ruthenium compounds, the paullone complexes with a derivatized lactam unit showed higher antiproliferative activity, than the first paullone complexes with unmodified lactam unit.

The IC_{50} in the low micromolar concentration range indicate **no significant improvement** comparatively to **ruthenium congeners** (see **Chapter 1, 1.3.3.3**). However, these osmium metal-based paullone derivatives are potential candidates for further development.

<i>Os-paullone</i> <i>compounds</i>	<i>IC</i> ₅₀ (μM)		
	<i>A549</i>	<i>CH1</i>	<i>SW480</i>
1a	9.2 ± 1.6	3.7 ± 1	3.7 ± 0.6
1b	16 ± 3	4.5 ± 1	6.7 ± 1.0
1c	23 ± 4	5.5 ± 1.0	8.7 ± 1.0
2	15 ± 2	7.9 ± 1.3	9.0 ± 1.0
3a	2.2 ± 0.5	0.75 ± 0.07	1.2 ± 0.4
3b	2.0 ± 0.2	0.63 ± 0.09	1.0 ± 0.1

Table 11: IC_{50} values of the paullone type complexes on several cell lines after 96h of incubation⁹⁴

Building on his success with paullone-type arene-osmium(II) complexes, Keppler *et al.*⁹⁵ developed in 2010 a new group of **arene osmium(II) indoloquinoline complexes** $[(\eta^6\text{-arene})\text{Ru}(\text{X})(\text{Y})(\text{Z})]$ where the π -arene is *p*-cymene, X is a monodentate ligand such as chloride and Y,Z is chelating **indolo[3,2-*c*]quinoline-type** ligand (**Figure 40**). The framework of these indoloquinoline and the fact that they are a subject of current research effort, have already been discussed (see **Chapter 1, 1.3.4.3**).

More recently in 2011, Keppler *et al.*⁹⁷ developed novel arene-osmium (II) complexes with **modified indolo[3,2-*c*]quinoline**, looking for elucidation of structure-activity relationship of this class of compounds (**Figure 40**).

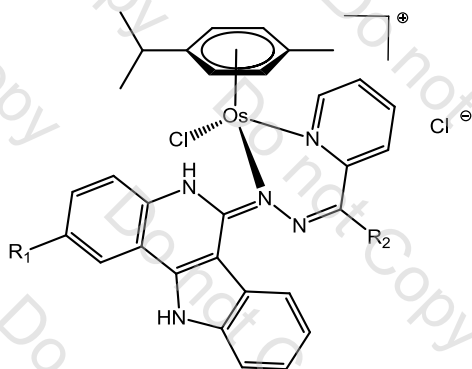


Figure 40: Chemical structure of indoloquinoline-type arene-osmium(II) complexes

The antiproliferative activity was tested, like their paullone congeners, in three human cancer cell lines (A529, CH1 and SW480) (**Table 12**). All osmium(II) arene-based indoloquinoline complexes show IC_{50} values in the 10^{-7} to 10^{-5} M concentration range, which is a little bit better than its ruthenium(II) analogues. As expected by the authors,⁹⁷ osmium(II) complexes were **more stable** than the ruthenium congeners and practically remained intact over 24h according to optical measurement. Hence, binding an indoloquinoline to a ruthenium-arene or osmium-arene moiety makes this class **of particular interest**, whatever the role the metal may play in the mechanism of action.

Indoquinoline compounds	R_1	R_2	IC_{50} (μM)		
			A549	CH1	SW480
1	H	H	0.83 ± 0.19	0.19 ± 0.06	0.26 ± 0.03
2	H	CH ₃	1.8 ± 0.3	0.24 ± 0.02	1.0 ± 0.2
3	F	CH ₃	10 ± 3	1.2 ± 0.5	2.9 ± 0.6
4	Cl	H	1.8 ± 0.2	0.42 ± 0.05	0.51 ± 0.04
5	Cl	CH ₃	3.9 ± 0.5	0.55 ± 0.14	1.2 ± 0.3
6	Br	CH ₃	7.8 ± 2.1	1.0 ± 0.4	2.3 ± 0.4
7	CH ₃	CH ₃	3.2 ± 0.4	0.19 ± 0.08	0.57 ± 0.2

Table 12: IC_{50} values of the indoloquinoline-type complexes in several cell lines after 96h of incubation⁹⁷

Coordination with biologically active staurosporine

In previous section (see **Chapter 1, 1.3.4.3.**), a glimpse at the role of staurosporine on protein kinase was caught, and studies from Meggers *et al.* demonstrated that the staurosporine can also be mimicked by an octahedral ruthenium complex.⁹⁹

Meggers *et al.* believe that ruthenium centre has a solely structural role, and that it is rather the shape of the organometallic complex that is responsible for the bioactivity.¹¹⁴

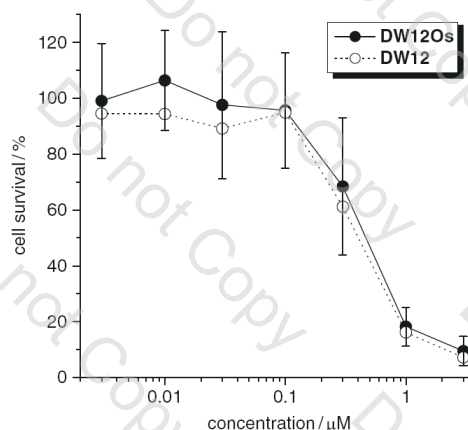
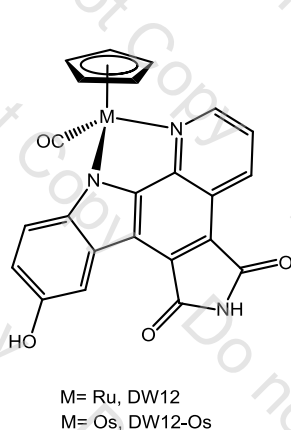


Figure 41: Anticancer activities of the isostructural kinase inhibitors DW12 and DW12-Os in 1205Lu melanoma after 72h drug exposure¹⁰⁰

In order to prove this assumption, Meggers *et al.* decided to develop an analogue **arene osmium(II) staurosporine complex**, where the π -arene is a cyclopentadienyl (Cp), X is a monodentate carbonyl ligand CO and Y, Z is chelating bidentate N,N' **staurosporine-type** ligand. Replacing the ruthenium with osmium in the kinase inhibitor DW12 complex afforded the isostructural **DW12-Os** complex (**Figure 41**).

Therefore, ruthenium and osmium should differ significantly in their bioactivity, if the reactivity of the metal plays a role in the mode of action. In contrast, ruthenium and osmium species must display closely related properties, if the three dimensional structures of these organometallic scaffolds determine the activity.¹⁰⁰

The replacement of ruthenium for its heavier osmium congener in this organometallic kinase inhibitor scaffold **shows almost indistinguishable biological activity (Figure 41)**. Detailed investigations¹⁰⁰ revealed an apoptic effect by strong activation of the p53 suppressor protein. Thus, Meggers *et al.* concluded that the role of the metal in **DW12** and **DW12-Os** is solely structural and that the biological effect of these complexes are essentially due to the rigid and inert shape of these complexes.

1.4.5. Perspectives for osmium drug in cancer treatment

As it is the case for ruthenium, osmium medicinal inorganic chemistry is a field of increasing interest, given that metal-based osmium compounds are also an alternative for the design of therapeutic agents that are not readily available to organic compounds. Osmium analogues of many of these “piano-stool” or “half-sandwich” organometallic ruthenium complexes have been synthesized. Examples such as osmium type- **NAMI-A**, **KP1019**, **RAPTA** and **AFAP51** have in common an osmium metal centre, but show a number of differences in their reactivity pattern.

They all exhibit anticancer properties *in vitro* and in some cases, they proved to be as efficient as clinical drugs such as cisplatin and carboplatin.^{81, 84, 109(b), 110(d, i, k)} However, there are no evident structure-activity relationships allowing to predict the effects of change of the metal and it is still difficult to establish rules for particularly active osmium compounds. Indeed, it has been observed by Sadler *et al.*,^{110(d)} that osmium complexes can be more active than their ruthenium congeners, whereas in other cases, changing the metal by its heavier homologue does not significantly improve the biological activity.^{81, 84}

Given that osmium is a platinum group metal which seems to display a completely different mode of action, the comparison of these complexes with its ruthenium analogues can provide useful information for the understanding of the mechanism of action of ruthenium compounds. These osmium complexes – as it is the case for ruthenium ones – appear to operate *via* red-ox mechanisms, making these complexes good candidates for further investigations and potentially clinical trials.

1.5. Concluding remark and aim of the present thesis

In this introduction, I tried to highlight that medicinal inorganic chemistry is a field of increasing interest given that metal-based compounds offer many possibilities for the design of therapeutic agents. The wide range of geometries, the different red-ox states all accessible under physiological conditions, the kinetic and thermodynamic characteristics, and the intrinsic properties of the cationic metal ion and/or the ligand itself, provide to the medicinal inorganic chemistry a wide spectrum of reactivity. In this context, the aim of my thesis had a dual purpose. In **Chapter 2**, an extended second generation ruthenium chemical library was synthesized. These elements have been chosen according to criteria of activity and toxicity that we identified through the previous chemical library and also according to preliminary results that we recently obtained. This second generation ruthenium based chemical library **RDCs (Ruthenium Derived Complexes)** consists of new complexes, in which the C-Ru bond is stabilized by two intramolecular N-Ru bonds, instead of only one N-Ru bond in first generation complexes.

These complexes were tested *in vitro* and several complexes have thus reached an IC₅₀ in the order or significantly lower than one micromole, indicating a **critical improvement**. These complexes were also compared to Sadler *et al.* lead compounds **RM175** and **ONCO4417**, which appear to be poorly active on the same cell line. At the same time, biologists were faced with non-reproducible *in vivo* measurements. Hence, a stability study was undertaken

on first generation arene **RDCs**, especially on the exchange of MeCN vs. DMSO in stock solution, in order to determine if this non-reproducibility can be imputable to this exchange. The final section of **Chapter 2** is focused on chiral resolution, which is an important tool in the production of optically active drugs. At biological level, two enantiomers of a molecule may have different physiological effects, even antagonistic ones. The lead compound **RDC 11** is chiral and obtained under two non-separable enantiomeric forms **RDC 11 (Δ isomer)** and **RDC 11 (Λ isomer)**. In an attempt to verify the bioactivity of each form in cell lines, different strategies using chiral resolution were undertaken to separate the two forms of **RDC 11**.

In **Chapter 3**, the same kind of study was carried out on new osmium based complexes which resulted in a new chemical library **ODCs (Osmium Derived Complexes)** of about forty compounds. This study is of particular interest, not only because it completes the **RDC** chemical library but also because it enables to verify the impact of exchanging the metal. **First and second generation** osmium based complexes **ODCs** in which the C-Os bond is respectively stabilized by one or two intramolecular N-Os bonds were tested *in vitro* and compared to their **RDCs** congeners. These complexes are at least as efficient as **RDCs** or even better, reaching an IC_{50} significantly lower than one micromole.

Finally, **Chapter 4** is mainly focused on complementary **stability studies** and on the determination of **physicochemical properties**. The use of the *n*-octanol/water partition coefficient (expressed as $\log(P_{o/w})$) has become the cornerstone of predicting the biological effects of organic chemicals from physical properties. Therefore, measurement of lipophilicity and red-ox potential, related to the biological *in vitro* activity has allowed me to establish a three-dimensional correlation for **RDCs** and **ODCs**. Through this possible property activity relationship (P.A.R.), it was demonstrated for the first time that both **Ru(III/II)** or **Os(III/II)** **red-ox potentials** (that allow possibly complexes to efficiently interfere with oxido-reductase enzymes), and good **lipophilicities** (that allow their entries into the cells) are somehow closely related, even this rationalization is not clear yet.

At the same time, biologists studied some **RDCs** and **ODCs** *in vivo* in order to characterize the acute toxicity, the antiproliferative properties and the mechanism of action of these complexes. These studies have enabled to see how the change in structure and/or metal can modify the mechanisms of action responsible for the cytotoxicity. They have also shown, as expected from three-dimensional correlation, that even minor structural and/or metal related modification can drastically modify physico-chemical properties and thus, modify the cytotoxicity.

1.6. References Chapter 1

- 1 Jemal, A.; Bray, F.; Center, M.; Ferlay, J.; Ward, E.; Forman, D. *CA-Cancer J. Clin.* **2011**, *61*, 69–90.
- 2 Sikira, K.; Timbs, O. *Exp. Rev. Anticancer Ther.* **2004**, *4*, S11–S12.
- 3 Anand, P.; Kunnumakara, A.; Sundaram, C.; Harikumar, K.; Tharakan, S.; Lai, O.; Sung, B.; Aggarwal, B. *Pharmaceut. Res.* **2008**, *25*, 2097–2116.
- 4 National Cancer Institute (at the National Institute of Health) <http://www.cancer.gov/cancertopics/>
- 5 Hanahan, D.; Weinberg, R.A. *Cell* **2000**, *100*, 57–70.
- 6 Croce, C.M. *New Eng. J. Med.* **2008**, *358*, 502–511.
- 7 Merlo, L.; Pepper, J.; Reid, B.; Maley C. *Nat. Rev. Cancer* **2006**, *6*, 924–935.
- 8 Rosenberg, B.; Van Camp, L.; Krigas, T. *Nature* **1965**, *205*, 698–699.
- 9 Ronconia, L.; Sadler, P.J. *Coord. Chem. Rev.* **2007**, *251*, 1633–1648.
- 10 Halpern, J. *Pure Appl. Chem.* **2001**, *73*, 209–220.
- 11 Fish, R.; Jaouen, G. *Organometallics* **2003**, *22*, 2166–2177.
- 12 Guo, Z.; Sadler, P.J. *Angew. Chem., Int. Ed.* **1999**, *38*, 1512–1531.
- 13 Peyrone, M. *Justus Liebigs Ann. Chem.* **1844**, *51*, 1–29.
- 14 Werner, A. *Z. Anorg. Allg. Chem.* **1893**, *3*, 267–330.
- 15 Rosenberg, B.; Van Camp, L.; Grimley, E.B.; Thompson, A.J. *J. Biol. Chem.* **1967**, *242*, 1347–1352.
- 16 Rosenberg, B. *Platinum Met. Rev.* **1971**, *15*, 42–51.
- 17 Mansour, V.H.; Rosenberg, B.; Van Camp, L.; Trosko, J.E. *Nature* **1969**, *222*, 385–386.
- 18 Higby, D.; Wallace, H.; Albert, D.; Holland, J. *Cancer* **1974**, *33*, 1219–1225.
- 19 Siddik, Z. *Oncogene* **2003**, *22*, 7265–7279.
- 20 Lippard, S. *Pure & Appl. Chem.* **1987**, *6*, 731–42.
- 21 Baik, M.; Friesner, R.; Lippard, S. J. *J. Am. Chem. Soc.* **2003**, *125*, 14082–14092.
- 22 Legendre, F.; Bas, V.; Kozelka, J.; Chottard, J. *Chem. Eur. J.* **2000**, *6*, 2002–2010.
- 23 Chválová, K.; Brabec, V.; Kaspárková, J. *Nucleic Acids Res.* **2007**, *35*, 1812–1821.
- 24 (a) Joo, W. D.; Lee, J. Y.; Kim, J. H.; Yoo, H. J.; Roh, H. J.; Park, J. Y.; Kim, D. Y.; Kim Y. T.; Nam, J. H. *Journal of Gynecologic Oncology* **2009**, *20*, 96–100.
(b) Fan, Y.; Lin, N.M.; Ma, S. L.; Luo, L.H.; Fang, L.; Huang, Z.Y.; Yu, H. F.; Wu, F. Q. *Acta Pharmacol. Sin.* **2010**, *31*, 746–752.
(c) Souquet, P. J.; Krzakowski, M.; Ramlau, R.; Sun, X. S.; Lopez-Vivanco, G.; Puozzo, C.; Pouget, J. C.; Pinel, M. C.; Rosell, R. *Clin. Lung Cancer* **2010**, *11*, 105–113.
(d) Kim, H. S.; Lee, G. W.; Kim, J. H.; Kim, H. Y.; Kwon, J. H.; Song, H. H.; Kim, H. J.; Jung, J. Y.; Jang, G.; Choi, D. R.; Park, S. M.; Shin, T. R.; Lee, H. S.; Zang, D. Y. *Lung Cancer* **2010**, *70*, 71–76.
(e) Gridelli, C.; Maione, P.; Rossi, A.; Ferrara, M. L.; Castaldo, V.; Palazzolo, G.; Mazzeo, N. *Lung Cancer* **2009**, *66*, 282–286.
- 25 (a) Morelli, M. F.; Santomaggio, A.; Ricevuto, E.; Cannita, K.; De Galitiis, F.; Tudini, M.; Bruera, G.; Mancini, M.; Pelliccione, M.; Calista, F.; Guglielmi, F.; Martella, F.; Lanfiuti Baldi, P.; Porzio, G.; Russo, A.; Gebbia, N.; Iacobelli, S.; Marchetti P.; Ficorella, C. *Oncol. Rep.* **2010**, *23*, 1635–1640.
- 26 (a) Sonpavde, G.; Sternberg, C.N. *Future Oncol.* **2009**, *5*, 931–940.
(b) Choy, H.; Park C.; Yao, M. *Clin. Cancer Res.* **2008**, *14*, 1633–1638.
- 27 Wong, E.; Giandomenico, C.M. *Chem. Rev.* **1999**, *99*, 2451–2466.
- 28 Markman, M. *Expert Opin. Drug Saf.* **2003**, *6*, 597–607
- 29 Bosl, G.; Motzer, R. *New Eng. J. Med.* **1997**, *337*, 242–254.
- 30 McVie, G.; Schipper, H.; Sikora, K. *Exp. Rev. Anticancer Ther.* **2004**, *4*, S43–S50.
- 31 Ozols, R.; Young, R. *Semin. Oncol.* **1991**, *18*, 222–232.
- 32 Ozols, R. *Curr. Probl. Cancer* **1992**, *16*, 61–126.
- 33 Stordal, B.; Davey, M. *IUBMB Life* **2007**, *59*, 696–699.
- 34 Galanski, M.; Jakupec, M. A.; Keppler, B. K. *Curr. Med. Chem.* **2005**, *12*, 2075–2094.
- 35 Heffeter, P.; Jungwirth, U.; Jakupec, M.; Hartinger, C.; Galanski, M.; Elbling, L.; Micksche, M.; Keppler B.; Berger, W. *Drug Resist. Updates* **2008**, *11*, 1–16.
- 36 Sadler, P. J. Themed issue on Metal Anticancer Compounds, *J. Chem. Soc., Dalton Trans.* **2009**, 10629–10936.
- 37 Hartinger, C.G.; Zorbas-Seifried, S.; Jakupec, M.A.; Kynast, B.; Zorbas, H.; Keppler, B.K. *J. Inorg. Biochem.* **2006**, *100*, 891–904.
- 38 Hartinger, C.G.; Dyson, P.J. *Chem. Soc. Rev.* **2009**, *38*, 391–401.
- 39 Bloemink, M.J.; Reejick, J. *Met. Ions. Biol. Syst.* **1996**, *32*, 641–685.

- ⁴⁰ Reejick, J. *Proc. Nat. Acad. Sci.* **2003**, *100*, 3611–3616.
- ⁴¹ Yamada, H.; Koike, T.; Hurst, J.K. *J. Am. Chem. Soc.* **2001**, *123*, 12775–12780.
- ⁴² (a) Chakravarty, J.; Bhattacharya, S. *Polyhedron* **1996**, *15*, 1047–1055.
(b) Baitalik, S.; Adhikary, B. *Polyhedron* **1997**, *16*, 4073–4080.
- ⁴³ Schluga, P.; Hartinger, C.G.; Egger, A.; Reisner, E.; Galanski M.; Jakupec, M.; Keppler, B.K. *J. Chem. Soc., Dalton Trans.* **2006**, *14*, 1796–1802.
- ⁴⁴ Kratz, F.; Messori, L. *J. Inorg. Biochem.* **1993**, *49*, 79–82.
- ⁴⁵ Sava, G.; Bergamo, A. *Int. J. Oncol.* **2000**, *17*, 353–365.
- ⁴⁶ (a) Yan, Y. K.; Melchart, M.; Habtemariam, A.; Sadler, P. J. *Chem. Comm.* **2005**, 4764–4776.
(b) Ang, W.H.; Dyson P.J. *Eur. J. Inorg. Chem.* **2006**, *20*, 4003–4018.
(c) Dyson, P. J.; Sava, G. *J. Chem. Soc., Dalton Trans.* **2006**, 1929–1933.
(e) Gianferrara, T.; Bratsos, I.; Alessio, E. *J. Chem. Soc., Dalton Trans.* **2009**, 7588–7598.
(f) Levina, A.; Mitra, A.; Lay, P. A. *Metallomics* **2009**, *1*, 458–470.
(g) Suess-Fink, G. *J. Chem. Soc., Dalton Trans.* **2010**, 1673–1688.
(h) Gasser, G.; Ott, I.; Metzler-Nolte, N. *J. Med. Chem.* **2011**, *54*, 3–25.
- ⁴⁷ (a) Sava, G.; Zorzet, S.; Turin, C.; Vita, F.; Soranzo, M.; Zabucchi, G.; Cocchietto, M.; Bergamo, A.; Digiovine, S.; Pezzoni, G.; Sartor, L.; Garbisa, S. *Clin. Cancer Res.* **2003**, *9*, 1898–1905
(b) Bergamo, A.; Sava, G.; *J. Chem. Soc., Dalton Trans.* **2007**, 1267–1272
- ⁴⁸ (a) Hartinger, C.G.; Zorbas-Seifried, S.; Jakupec, M.A.; Groessl, M.; Egger, A.; Berger, W.; Zorbas, H.; Dyson P.J.; Keppler, B.K. *Chem. Biodiversity* **2008**, *5*, 2140–2155.
(b) Heffeter, P.; Böck, K.; Atil, B.; Reza Hoda, A.; Körner, W.; Bartel, C.; Jungwirth U.; Keppler, B.K.; Micksche, M.; Berger, W.; Koellensperger, G. *J. Biol. Inorg. Chem.* **2010**, *15*, 737–748.
- ⁴⁹ Sava, G.; Pacor, S.; Bergamo, A.; Cocchietto, M.; Mestroni, G.; Alessio, E. *Chem. Biol. Interact.* **1995**, *95*, 109–126.
- ⁵⁰ Mestroni, G.; Alessio, E.; Sava, G. Int. Patent PCT C 07F 15/00, A61K 32/28; WO 94/00431, **1998**.
- ⁵¹ Rademaker-Lakhai, J.M.; van den Bongard, D.; Pluim, D; Beijnen, J.H.; Schnellens, J.H. *Clin. Cancer Res.* **2004**, *10*, 3717–3727
- ⁵² Allardyce, C.S.; Dyson, P.J. *Platinum Metals Rev.* **2001**, *45*, 62–69.
- ⁵³ (a) Sava, G.; Bergamo, A.; Zorzet, S.; Gava, B.; Casarsa, C.; Cocchietto, M.; Furlani, A.; Scarcia, V.; Serli, B.; Iengo, E.; Alessio, E.; Mestroni, G. *Eur. J. Cancer* **2002**, *38*, 427–435.
(b) Bouma, M.; Nuijen, B.; Jansen, M. T.; Sava, G.; Bult, A.; Beijnen, J. H. *J. Pharm. Biomed. Anal.* **2002**, *30*, 1287–1296.
(c) Bouma, M.; Nuijen, B.; Jansen, M. T.; Sava, G.; Flaibani, A.; Bult, A.; Beijnen, J. H. *Int. J. Pharm.* **2002**, *248*, 239–246.
(d) Alessio, E. *Chem. Rev.* **2004**, *104*, 4203–4242.
- ⁵⁴ (a) Bergamo, A.; Gagliardi, R.; Scarcia, V.; Furlani, A.; Alessio, E.; Mestroni, G.; Sava, G. *J. Pharmacol. Exp. Ther.* **1999**, *289*, 559–564.
(b) Bergamo, A.; Zorzet, S.; Cocchietto, M.; Carotenuto, M. E.; Magnarin, M.; Sava, G. *Anticancer Res.* **2001**, *21*, 1893–1898.
(c) Vacca, A.; Bruno, M.; Boccarelli, A.; Coluccia, M.; Ribatti, D.; Bergamo, A.; Garbisa, S.; Sartor, L.; Sava, G. *Br. J. Cancer* **2002**, *86*, 993–998.
(d) Zorzet, S.; Bergamo, A.; Cocchietto, M.; Sorc, A.; Gava, B.; Alessio, E.; Iengo, E.; Sava, G. *J. Pharmacol. Exp. Ther.* **2000**, *295*, 927–933.
(e) Pacor, S.; Zorzet, S.; Cocchietto, M.; Bacac, M.; Vadori, M.; Turrin, C.; Gava, B.; Castellarin, A.; Sava, G. *J. Pharmacol. Exp. Ther.* **2004**, *310*, 737–744.
(f) Casarsa, C.; Mischis, M. T.; Sava, G. *J. Inorg. Biochem.* **2004**, *98*, 1648–1654.
- ⁵⁵ (a) Pintus, G.; Tadolini, B.; Posadino, A. M.; Sanna, B.; Debidda, M.; Bennardini, F.; Sava G.; Ventura, C. *Eur. J. Biochem.*, **2002**, *269*, 5861–5870.
(b) Sanna, B.; Debidda, M.; Pintus, G.; Tadolini, B.; Posadino, A. M.; Bennardini, F.; Sava G.; Ventura, C. *Arch. Biochem. Biophys.*, **2002**, *403*, 209–218.
(c) Debidda, M.; Sanna, B.; Cossu, A.; Posadino, A.M.; Tadolini, B.; Ventura C.; Pintus, G.; *Int. J. Oncol.*, **2003**, *23*, 477–482.
- ⁵⁶ (a) Alessio, E.; Mestroni, G.; Pocar, S.; Sava, G.; Spinelli, S. *US Patent, 5409893*, **1995**.
(b) Mestroni, G.; Alessio, E.; Sava, G. *US Patent, 6221905*, **2001**.
- ⁵⁷ Galanski, M.; Arion, V.B.; Jakupec, M.A.; Keppler, B.K. *Curr. Pharm. Des.* **2003**, *9*, 2078–2089.
- ⁵⁸ Kapitza, S.; Pongratz, M.; Jakupec, M.A.; Heffeter, P.; Berger, W.; Lackinger, L.; Keppler, B.K.; Marian, B.J. *Cancer Res. Clin. Oncol.* **2005**, *131*, 101–110.

- ⁵⁹ Reisner, E.; Arion, V.B.; Keppler, B.K.; Pombeiro, A.J.L. *Inorg. Chim. Acta.* **2008**, *361*, 1569–1583.
- ⁶⁰ Keppler, B.K.; Henn, M.; Juhl, U.M.; Berger, M.R.; Niebl, R.; Wagner, F.E. *Progr. Clin. Biochem. Med.* **1989**, *10*, 41–69.
- ⁶¹ Keller, H.; Keppler, B. *US Patent*, 4843069, **1989**.
- ⁶² (a) Chatlas, J.; van Eldik, R.; Keppler, B.K. *Inorg. Chim. Acta* **1995**, *233*, 59–63.
(b) Ni Dhubhghaill, O.M.; Hagen, W.R.; Keppler, B.K.; Lipponer, K.G.; Sadler, P.J. *J. Chem. Soc., Dalton Trans.* **1994**, 3305–3310.
- ⁶³ Vargiu, A.; Robertazzi, A.; Magistrato, A.; Ruggerone, P.; Carloni, P. *J. Phys. Chem. B* **2008**, *112*, 4401–4409.
- ⁶⁴ (a) Hartinger, C.G.; Jakupec, M.A.; Zorbas-Seifried, S.; Groessl, M.; Egger, A.; Berger, W.; Haralabos, Z.; Dyson, P.J.; Keppler, B.K. *Chem. Biodivers.* **2008**, *5*, 2140–2155.
(b) Lentz, F.; Drescher, A.; Lindauer, A.; Henke, M.; Hilger, R.A.; Hartinger, C.G.; Scheulen, M.E.; Dittrich, C.; Keppler, B.K.; Jaehde, U. *Anti-Cancer Drugs* **2009**, *20*, 97–103.
(c) Henke, M.M.; Richly, H.; Drescher, A.; Grubert, M.; Alex, D.; Thyssen, D.; Jaehde, U.; Scheulen, M.E.; Hilger, R.A.; *Int. J. Pharmacol. Ther.* **2009**, *47*, 58–60.
- ⁶⁵ (a) Kapitza, S.; Jakupec, M.A.; Uhl, M.; Keppler, B.K.; Marian, B. *Cancer Lett.* **2005**, *226*, 115–121.
- ⁶⁶ Kapitza, S.; Pongratz, M.; Jakupec, M.A.; Heffeter, P.; Berger, W.; Lackinger, L.; Keppler, B.K.; Marian, B. *J. Cancer Res. Clin. Oncol.* **2005**, *131*, 101–110.
- ⁶⁷ (a) Hartinger, C.G.; Zorbas-Seifried S.; Jakupec, M.A.; Kynast, B.; Zorbas, H.; Keppler, B.K. *J. Inorg. Biochem.* **2006**, *100*, 891–904.
(b) Cetinbas, N.; Webb, M.I.; Dubland, J.A.; Walsby, C.J. *J. Biol. Inorg. Chem.* **2010**, *15*, 131–145.
- ⁶⁸ Jakupec, M. A.; Resiner, E.; Eichinger, A.; Pongratz, M.; Arion, V. B.; Galanski, M.; Hartinger, C. G.; Keppler, B. K. *J. Med. Chem.* **2005**, *48*, 2831–2837.
- ⁶⁹ (a) Heffeter, P.; Böck, K.; Atil, B.; Hoda, M.A.R.; Körner, W.; Bartel, C.; Jungwirth, U.; Keppler, B.K.; Michsche, M.; Berger, W.; Koellensperger, G. *J. Biol. Inorg. Chem.* **2010**, *15*, 737–748.
(b) Hudej, R.; Turel, I.; Kanduser, M.; Scancar, J.; Kranjc, S.; Sersa, G.; Miklavcic, D.; Jakupec, M.A.; Keppler, B.K.; Cemazar, M. *Anticancer Res.* **2010**, *30*, 2055–2063
- ⁷⁰ (a) Vacca, A.; Bruno, M.; Boccarelli, A.; Coluccia, M.; Ribatti, D.; Bergamo, A.; Garbisa, S.; Sartor L.; Sava, G.; *Br. J. Cancer* **2002**, *86*, 993–998.
(b) Sava, G.; Zorzet, S.; Turrin, C.; Vita, F.; Soranzo, M.R.; Zabucchi, G.; Cocchietto, M.; Bergamo, A.; DiGiovine, S.; Pezzoni, G.; Sartor, L.; Garbisa, S. *Clin. Cancer Res.*, **2003**, *9*, 1898–1905.
(c) Sava, G.; Frausin, F.; Cocchietto, M.; Vita, F.; Podda, E.; Spessotto, P.; Furlani, A.; Scarcia, V.; Zabucchi, G. *Eur. J. Cancer* **2004**, *40*, 1383–1392.
- ⁷¹ Bergamo, A.; Sava, G. *Dalton Trans.* **2011**, *40*, 7817–7823.
- ⁷² (a) Clarke, M. J.; Bitler, S.; Rennert, D.; Buchbinder M.; Kelman, A. D. *J. Inorg. Biochem.* **1980**, *12*, 79–87.
(b) Frasca, D.; Ciampa, J.; Emerson, J.; Umans R. S.; Clarke, M. J. *Met. Based Drugs* **1996**, *3*, 197–209.
(c) Clarke, M. J. *Coord. Chem. Rev.* **2003**, *236*, 209–233.
- ⁷³ Som, P.; Oster, Z. H.; Matsui, K.; Guglielmi, G.; Persson, B. R.; Pellettieri, M. L.; Srivastava, S. C.; Richards, P.; Atkins, H. L.; Brill, A. B. *Eur. J. Nucl. Med. Mol. Imaging* **1983**, *8*, 491–494.
- ⁷⁴ (a) Brabec, V. *Prog. Nucleic Acid Res. Mol. Biol.* **2002**, *71*, 1–68.
(b) Brabec, V.; Novakova, O. *Drug Resist. Updates* **2006**, *9*, 111–122.
- ⁷⁵ Heffeter, P.; Jungwirth, U.; Jakupec, M.; Hartinger, C.; Galanski, M.; Elbling, L.; Micksche, M.; Keppler, B.K.; Berger, W. *Drug Resist. Update* **2008**, *11*, 1–16
- ⁷⁶ Sava, G.; Bergamo, A. *Int. J. Oncol.* **2000**, *17*, 353–365
- ⁷⁷ Schluga, P.; Hartinger, C. G.; Egger, A.; Reisner, E.; Galanski, M.; Jakupec, M. A.; Keppler, B. K. *Dalton Trans.* **2006**, *14*, 1796–1802.
- ⁷⁸ Bergamo, A.; Masi, A.; Dyson, P.J.; Sava, G. *Int J Oncol* **2008**, *33*, 1281–1289.
- ⁷⁹ Therrien, B. *Coord. Chem. Rev.* **2009**, *253*, 493–519.
- ⁸⁰ (a) Morris, R.E.; Aird, R.E.; Murdoch, P.d.S.; Chen, H.; Cummings, J.; Hughes, N. D.; Parsons, S.; Parkin, A.; Boyd, G.; Jodrell D. I.; Sadler, P. J. *J. Med. Chem.*, **2001**, *44*, 3616–3621.
(b) Aird, R. E.; Cummings, J.; Ritchie, A.A.; Muir, M.; Morris, R.E.; Chen, H.; Sadler P. J.; Jodrell, D. I. *Br. J. Cancer*, **2002**, *86*, 1652–1657.
- ⁸¹ Schmid, W.F.; John, R.O.; Arion, V.B.; Jakupec, M.A.; Keppler B.K. *Organometallics* **2007**, *26*, 6643–6652.
- ⁸² Sclaro, C.; Bergamo, A.; Brescacin, L.; Delfino, R.; Cocchietto, M.; Laurenczy, G.; Geldbach, T. J.; Sava, G.; Dyson, P. J. *J. Med. Chem.* **2005**, *48*, 4161–4171.
- ⁸³ (a) Mendoza-Ferri, M.G.; Hartinger, C.G.; Nazarov, A.A.; Eichinger, R.E.; Jakupec, M.A.; Severin, K.; Keppler, B. K. *Organometallics* **2009**, *28*, 6260–6265.

- (b) Kandioller, W.; Hartinger, C.G.; Nazarov, A.A.; Bartel, C.; Skocic, M.; Jakupec, M.A.; Arion, V.B.; Keppler, B.K. *Chem. Eur. J.* **2009**, *15*, 12283–12291.
- (c) Mendoza-Ferri, M.G.; Hartinger, C.G.; Mendoza, M.A.; Groessl, M.; Egger, A.E.; Eichinger, R.E.; Mangrum, J.B.; Farrell, N.P.; Maruszak, M.; Bednarski, P.J.; Klein, F.; Jakupec, M.A.; Nazarov, A.A.; Severin, K.; Keppler, B.K. *J. Med. Chem.* **2009**, *52*, 916–925.
- ⁸⁴ Smalley, K.S.M.; Contractor, R.; Haas, N.K.; Kulp, A.N.; Atilla-Gokcumen, G.E.; Williams, D.S.; Bregman, H.; Flaherty, K.T.; Soengas, M.S.; Meggers, E.; Herlyn, M. *Cancer Res.* **2007**, *67*, 209–217.
- ⁸⁵ Smith, G.S.; Therrien, B. *J. Chem. Soc., Dalton Trans.* **2011**, Advance Article DOI: 10.1039/C1DT11007A.
- ⁸⁶ (a) Chen, H.; Parkinson, J.A.; Parsons, S.; Coxall, R.A.; Gould, R.O.; Sadler, P.J. *J. Am. Chem. Soc.* **2002**, *124*, 3064–3082.
- (b) Chen, H.; Parkinson, J.A.; Morris, R.E.; Sadler, P.J. *J. Am. Chem. Soc.* **2003**, *125*, 173–186.
- ⁸⁷ (a) Habtemariam, A.; Bugarcic, T.; Sadler, P. J. *PCT Int. Appl.* **2007**, WO 2007135410 A1 20071129
- (b) Dougan, S.; Habtemariam, A.; Melchart, M.; Sadler, P.J. *PCT Int. Appl.* **2007**, WO 2007101997 A1 20070913.
- (c) Habtemariam, A.; Sadler, P. J. *PCT Int. Appl.* **2006**, WO 2006018649 A1 20060223.
- (d) Habtemariam, A.; Sadler, P. J. *PCT Int. Appl.* **2004**, WO 2004096819 A1 20041111.
- (e) Sadler, P. J.; Fernandez Lainez, R.; Habtemariam, A.; Melchart, M.; Jodrell, D. I. *PCT Int. Appl.* **2004**, WO 2004005304 A1 20040115.
- (f) Morris, R. E.; Sadler, P. J.; Jodrell, D.I.; Chen, H. *PCT Int. Appl.* **2002**, WO 2002002572 A1 20020110.
- ⁸⁸ Hayward, R. L.; Schornagel, Q. C.; Tente, R.; Macpherson, J. S.; Aird, R. E.; Guichard, S.; Habtemariam, A.; Sadler, P.J.; Jodrell, D. I. *Cancer Chemoth. Pharm.* **2005**, *55*, 577–583
- ⁸⁹ Gaiddon, C.; Jeannequin, P.; Bischoff, P.; Pfeffer, M.; Sirlin, C.; Loeffler, J.-P. *J. Pharmacol Exp Ther.* **2005**, 1403–1411.
- ⁹⁰ (a) Scolaro, C.; Bergamo, A.; Brescacin, L.; Delfino, R.; Cochietto, M.; Laurenczy, G.; Geldbach, T.J.; Sava, G.; Dyson, P.J. *J. Med. Chem.* **2005**, *48*, 4161–4171.
- (b) Vock, C.A.; Ang, W.H.; Scolaro, C.; Phillips, A.D.; Lagopoulos, L.; Juillerat-Jeanerret, L.; Sava, G.; Scopelliti, R.; Dyson, P.J. *J. Med. Chem.* **2006**, *49*, 5552–5561.
- ⁹¹ (a) Scolaro, C.; Geldbach, T. J.; Rochat, S.; Dorcier, A.; Gossens, C.; Bergamo, A.; Cocchietto, M.; Tavernelli, I.; Sava, G.; Rothlisberger U.; Dyson, P. J. *Organometallics* **2006**, *25*, 756–765.
- (b) Scolaro, C.; Chaplin, A.B.; Hartinger, C.G.; Bergamo, A.; Cocchietto, M.; Keppler, B.K. Sava, G.; Dyson, P.J. *J. Chem. Soc., Dalton Trans.* **2007**, *43*, 5065–5072.
- ⁹² (a) Zaharewitz, D. W.; Gussio, R.; Leost, M.; Senderowitz, A. M.; Lahusen, T.; Kunick, C.; Meijer, L.; Sausville, E. A. *Cancer Res.* **1999**, *59*, 2566–2569.
- (b) Huwe, A.; Mazitschek, R.; Giannis, A. *Angew. Chem., Int. Ed.* **2003**, *19*, 2122–2138.
- ⁹³ Knockaert, M.; Wieking, K.; Schmitt, S.; Leost, M.; Grant, K. M.; Mottram, J. C.; Kunick, C.; Meijer, L. *J. Biol. Chem.* **2002**, *277*, 25493–25501.
- ⁹⁴ (a) Schmid, W.F.; John, R.O.; Arion, V.B.; Jakupec, M. A.; Keppler, B.K. *Organometallics* **2007**, *26*, 6643–6652.
- (b) Schmid, W.F.; John, R.O.; Mühlgassner, G.; Heffeter, P.; Jakupec, M. A.; Galanski, M.; Berger, W.; Arion, V.B.; Keppler, B.K. *J. Med. Chem.* **2007**, *50*, 6343–6355.
- ⁹⁵ Filak, L.K.; Mühlgassner, G.; Jakupec, M. A.; Heffeter, P.; Berger, W.; Arion, V.B.; Keppler, B.K. *J. Biol. Inorg. Chem.* **2010**, *15*, 903–918.
- ⁹⁶ Chien, C.-M.; Yang, S.-H.; Lin, K.-L.; Chen, Y.-L.; Chang, L.-S.; Lin S.-R., *Chem.-Biol. Interact.* **2008**, *176*, 40–47.
- ⁹⁷ Filak, L.K.; Mühlgassner, G.; Bacher, F.; Roller, A.; Galanski, M.; Jakupec, M. A.; Arion, V.B.; Keppler, B.K. *Organometallics* **2011**, *30*, 273–283.
- ⁹⁸ Cohen, P. *Nat. Rev. Drug. Discov.* **2002**, *1*, 309–315.
- ⁹⁹ Meggers, E.; Atilla-Gokcumen, G.E.; Bregman, H.; Maksimoska, J.; Mulcahy, S.P.; Pagano, N.; Williams, D.S. *Synlett* **2007**, *8*, 1177–1189.
- ¹⁰⁰ Maksomiska, J.; Williams, D.S.; Atilla-Gokcumen, G.E.; Smalley, K.S.M.; Carroll, P.J.; Webster, R.D.; Filippakopoulos, P.; Knapp, S.; Herlyn M.; Meggers, E. *Chem. Eur. J.* **2008**, *14*, 4816–4822.
- ¹⁰¹ Meggers, E.; Atilla-Gokcumen, G.E.; Gründler, K.; Frias, C.; Prokop, A. *J. Chem. Soc., Dalton Trans.* **2009**, 10882–10888.
- ¹⁰² Gaiddon, C.; Jeannequin, P.; Bischoff, P.; Pfeffer, M.; Sirlin, C.; Loeffler, J.-P. *J. Pharmacol. Exp. Ther.* **2005**, *315*, 1403–1411.
- ¹⁰³ Leyva, L.; Sirlin, C.; Rubio, L.; Franco, C.; Le Lagadec, R.; Spencer, J.; Bischoff, P.; Gaiddon, C.; Loeffler, J.-P.; Pfeffer, M. *Eur. J. Inorg. Chem.* **2007**, 3055–3066.

- ¹⁰⁴ (a) Ryabov, A. D.; Sukharev, V. S.; Alexandrova, L.; Le Lagadec, R.; Pfeffer, M. *Inorg. Chem.* **2001**, *40*, 6529–6532.
- (b) Le Lagadec, R.; Rubio, L.; Alexandrova, L.; Toscano, R. A.; Ivanova, E. V.; Meskys, R.; Laurinavicius, V.; Pfeffer, M.; Ryabov, A. D. *J. Organomet. Chem.* **2004**, *689*, 4820–4832.
- (c) Ryabov, A. D.; Le Lagadec, R.; Estevez, H.; Toscano, R. A.; Hernandez, S.; Alexandrova, L.; Kurova, V. S.; Fischer, A.; Sirlin, C.; Pfeffer, M. *Inorg. Chem.* **2005**, *44*, 1626–1634.
- (d) Le Lagadec, R.; Alexandrova, L.; Estevez, H.; Pfeffer, M.; Laurinavicius, V.; Razumiene, J.; Ryabov, A. D. *Eur. J. Inorg. Chem.* **2006**, 2735–2738.
- (e) Ryabov, A. D.; Kurova, V. S.; Ivanova, E. V.; Le Lagadec, R.; Alexandrova, L. *Anal. Chem.* **2005**, *77*, 1132–1139.
- (f) Ivanova, E. V.; Kurnikov, I. V.; Fischer, A.; Alexandrova, L.; Ryabov, A. D. *J. Mol. Catal. B* **2006**, *41*, 110–116.
- ¹⁰⁵ Meng, X.; Leyva, M. L.; Jenny, M.; Gross, I.; Benosman, S.; Fricker, B.; Harlepp, S.; Hebraud, P.; Boos, A.; Wlosik, P.; Bischoff, P.; Sirlin, C.; Pfeffer, M.; Loeffler, J. P.; Gaiddon, C. *Cancer Res.*, **2009**, *69*, 5458–5466.
- ¹⁰⁶ Novakova, O.; Chen, H.; Vrana, O.; Rodger, A.; Sadler, P.J.; Brabec, V. *Biochemistry* **2003**, *42*, 11544–11554.
- ¹⁰⁷ Thompson, K.H.; Orvig, C. *J. Chem. Soc., Dalton Trans.* **2006**, 761–764.
- ¹⁰⁸ (a) Schmid, W. F.; John, R. O.; Arion, V. B.; Jakupec, M. A.; Keppler, B. K. *Organometallics* **2007**, *26*, 6643–6652.
- (b) Schmid, W.F.; John, R.O.; Mühlgassner, G.; Heffeter, P.; Jakupec, M.A.; Galanski, M.; Berger, W.; Arion, V.B.; Keppler, B.K. *J. Med. Chem.* **2007**, *50*, 6343–6355.
- (c) Schuecker, R.; John, R.O.; Jakupec, M.A.; Arion, V.B.; Keppler, B.K. *Organometallics* **2008**, *27*, 6587–6595.
- (d) Stepanenko, I.N.; Krokhin, A.A.; John, R.O.; Roller, A.; Arion, V.B.; Jakupec, M.A.; Keppler, B.K. *Inorg. Chem.* **2008**, *47*, 7338–7347.
- (e) Reisner, E.; Arion, V.B.; Keppler, B.K.; Pombeiro A.J.L. *Inorg. Chim. Acta.* **2008**, *361*, 1569–1583.
- (f) Buchel, G.E.; Stepanenko, I.N.; Hejl, M.; Jakupec, M.A.; Arion, V.B.; Keppler, B.K., *Inorg. Chem.* **2009**, *48*, 10737–10747.
- (g) Hanif, M.; Henke, H.; Meier, S.M.; Martic, S.; Labib, M.; Kandioller, W.; Jakupec, M.A.; Arion, V.B.; Kraatz, H.-B.; Keppler, B.K. *Inorg. Chem.* **2010**, *49*, 7953–7963.
- (h) Filak, L.K.; Muehlgassner, G.; Bacher, F.; Roller, A.; Galanski, M.; Jakupec, M.A.; Keppler, B.K.; Arion, V.B. *Organometallics* **2011**, *30*, 273–283.
- ¹⁰⁹ (a) Dorcier, A.; Ang, W.H.; Bolano, S.; Gonsalvi, L.; Juillerat-Jeannerat, L.; Laurency, G.; Peruzzini, M.; Phillips, A.D.; Zanobini, F.; Dyson, P.J. *Organometallics* **2006**, *25*, 4090–4096.
- (b) Renfrew, A.K.; Phillips, A.D.; Egger, A.E.; Hartinger, C.G.; Bosquain, S.S.; Nazarov, A.A.; Keppler, B.K.; Gonsalvi, L.; Peruzzini, M.; Dyson, P.J. *Organometallics* **2009**, *28*, 1165–1172.
- (c) Barry, N.P.E.; Edafe, F.; Dyson, P.J.; Therrien, B. *Dalton Trans.* **2010**, *39*, 2816–2820.
- (d) Hanif, M.; Nazarov, A.A.; Hartinger, C.G.; Kandioller, W.; Jakupec, M.A.; Arion, V.B.; Dyson, P.J.; Keppler, B.K. *Dalton Trans.* **2010**, *39*, 7345–7352.
- ¹¹⁰ (a) Peacock, A.F.A.; Habtemariam, A.; Fernandez, R.; Walland, V.; Fabbiani, F.P.A.; Parsons, S.; Aird, R. E.; Jodrell, D.I.; Sadler, P. J. *J. Am. Chem. Soc.* **2006**, *128*, 1739–1748.
- (b) Peacock, A.F.A.; Melchart, M.; Deeth, R.J.; Habtemariam, A.; Parsons, S.; Sadler, P.J. *Chem. Eur. J.* **2007**, *13*, 2601–2613.
- (c) Peacock, A.F.A.; Habtemariam, A.; Moggach, S.A.; Prescimone, A.; Parsons, S.; Sadler, P.J. *Inorg. Chem.* **2007**, *46*, 4049–4059.
- (d) Peacock, A.F.A.; Parsons, S.; Sadler, P.J. *J. Am. Chem. Soc.* **2007**, *129*, 3348–3357.
- (e) Ronconi, L.; Sadler, P.J. *Coord. Chem. Rev.* **2007**, *251*, 1633–1648.
- (f) Kostrhunova, H.; Florian, J.; Navakova, O.; Prescimone, Peacock, A.F.A.; Sadler, P.J.; Brabec, V. *J. Med. Chem.* **2008**, *51*, 3635–3643.
- (g) Sadler, P.J., Peacock, A.F.A.; Van Rijt, S.H.; Habtemariam, A.; *PCT Int. Appl.* **2008**, WO 2008017855 A1 20080214.
- (h) Peacock, A.F.A.; Sadler, P.J.; *Chem. Asian J.* **2008**, *3*, 1890–1899.
- (i) Van Rijt, S.H.; Peacock, A.F.A.; Johnstone, R.D.L.; Parsons, S.; Sadler, P.J. *Inorg. Chem.* **2009**, *48*, 1753–1752.
- (j) Bruijninx, P.C.A.; Sadler, P.J.; *Adv. Inorg. Chem.* **2009**, *61*, 1–62.

- (k) Van Rijt, S.H.; Hebden, A.J.; Amaresekera, T.; Deeth, R.J.; Clarkson, G.J.; Parsons, S.; McGowan, P.C.; Sadler, P.J. *J. Med. Chem.* **2009**, *52*, 7753–7764.
- (l) Van Rijt, S.H.; Sadler, P.J. *Drug Discovery Today* **2009**, *14*, 1089–1097.
- (m) Van Rijt, S.H.; Mukherjee, A.; Pizarro, A.M.; Sadler, P.J. *J. Med. Chem.* **2010**, *53*, 840–849.
- (n) Bergamo, A.; Masi, A.; Peacock, A.F.A.; Habtemariam, A.; Sadler, P.J.; Sava, G. *J. Inorg. Biochem.* **2010**, *104*, 79–86.
- (o) Fu, Y.; Habtemariam, A.; Pizarro, A.M.; Van Rijt, S.H.; Healey, D.J.; Cooper, P.A.; Shnyder, S.D.; Clarkson, G.J.; Sadler, P.J. *J. Med. Chem.* **2010**, *53*, 8192–8196.
- (p) Pizarro, A.M.; Habtemariam, A.; Sadler, P.J. *Top. Organomet. Chem.* **2010**, *32*, 21–56.
- (q) Van Rijt, S.H.; Kostrhunova, H.; Brabec, V.; Sadler, P.J. *Bioconjugate Chem.* **2011**, *22*, 218–226.
- ¹¹¹ (a) Dorcier, A.; Dyson, P.J.; Gossens, C.; Rothlisberger, U.; Scopelliti, R.; Tavernelli, I. *Organometallics* **2005**, *24*, 2114–2123.
- (b) Dorcier, A.; Hartinger, C. J.; Scopelliti, R.; Fish, R.H.; Keppler, B.K.; Dyson, P.J. *J. Inorg. Biochem.* **2008**, *102*, 1066–1076.
- ¹¹² (a) Cebrian-Losantos, B.; Krokhin, A.A.; Stepanenko, I.N.; Eichinger, R.; Jakupec, M.A.; Arion, V.B.; Keppler, B.K. *Inorg. Chem.* **2007**, *46*, 5023–5033.
- (b) Egger, A.; Cebrián-Losantos, B.; Stepanenko, I.N.; Krokhin, A.A.; Eichinger, R.; Jakupec, M.A.; Arion, V.B.; Keppler, B.K. *Chem. Biodiv.* **2008**, *5*, 1588–1593.
- ¹¹³ Büchel, G.E.; Stepanenko, I.N.; Hejl, M.; Jakupec, M.A.; Keppler, B.K.; Arion, V.B. *Inorg. Chem.* **2011**, *50*, 7690–7697.
- ¹¹⁴ Debreczeni, J.E.; Bullock, A.N.; Atilla, G.E.; Williams, D.S.; Bregman, H.; Knapp, E.; Meggers, E. *Angew. Chem., Int. Ed.* **2006**, *45*, 1580–1585

Chapter 2:

Second-generation cyclo ruthenated complexes

Is medicinal organometallic chemistry science or art? In fact it is both and especially regarding chemotherapeutic field. Its science side offers mankind perspectives and the best hopes for improving treatments and quality of life. Its art side allows challenging its practitioners with the need for intuition, design and experience to discover new drugs.



Chapter 2: Second-generation cycloruthenated complexes: Extension of RDC chemical library and evaluation of their biological properties as potential anticancer drugs	75
2.1. Achievement of second-generation Ru(II) chemical library	77
2.1.1. Introduction	77
2.1.2. Synthesis of second generation complexes	77
2.1.3. Cytotoxic activity of second generation complexes	80
2.1.4. Electrochemical properties of first- and second-generation RDCs	91
2.2. Study of the exchange of MeCN vs. DMSO in piano-stool cycloruthenated complexes.....	95
2.2.1. Introduction	95
2.2.2. Synthesis of piano-stool cycloruthenated complexes	95
2.2.3. Preliminary results: kinetic evolution of RDC 49 in DMSO	96
2.2.4. Synthesis and characterization of RDC 49-DMSO	103
2.2.5. Cytotoxic activity of RDC 49 vs. RDC 49-DMSO	107
2.2.6. Exchange of the counter ion PF ₆ ⁻ vs. Cl ⁻ in RDC 49	108
2.2.7. Conclusion	109
2.3. Chirality induction in RDC 11 lead compound	110
2.3.1. Introduction: importance of chirality in everyday science	110
2.3.2. Synthesis of RDC 8*	111
2.3.3. Synthesis and separation of RDC 11* isomers	113
2.3.4. Conclusion	116
2.4. References Chapter 2.....	117

Chapter 2: Second-generation cycloruthenated complexes: Extension of RDC chemical library and evaluation of their biological properties as potential anticancer drugs

2.1. Achievement of second-generation Ru(II) chemical library

2.1.1. Introduction

In order to enhance activity and reduce side effects in anticancer agents, the Laboratoire de Synthèses Métallo-Induites has developed for several years ruthenium complexes termed **RDCs** (**R**uthenium **D**erived **C**ompound) in which one ligand is bound to the metal *via* a strong C-Ru covalent bond stabilized by an N-Ru intramolecular bond. The laboratory has been involved in this field since the discovery that some cyclometalated ruthenium compounds might become good anticancer drug candidates.¹

Indeed, previous studies demonstrated that these cyclometalated compounds are stable towards substitution reactions² and have interesting Ru^{III/II} red-ox potential that enables them to interact with oxido-reductase enzymes.³ Thus, these latter seem to have a mechanism of action likely different from that of more classical platinum derivatives.⁴ So far, the biological properties of only a few of these cyclometalated complexes have been exploited. However, studies have led to the selection of several candidates as anticancer drugs from a library of twenty compounds.⁵ The *in vivo* results we have accumulated so far on one of them, **RDC 11**, have indeed convinced us that further development of this class of compounds is worthwhile (see Chapter 1, 1.3.5.).⁴

The other ligands bound to ruthenium also play an important role in the anticancer activity of the complexes. In our quest for ideal drug candidate, we thought to extend the family of complexes which may exhibit the same properties. Therefore, a second generation **RDC** chemical library has been developed by synthesizing complexes in which the C-Ru is stabilized by two intramolecular N-Ru bonds instead of one for the first generation complexes. Several complexes have thus reached an IC₅₀ in the order or significantly lower than one micromole, indicating a critical improvement.

2.1.2. Synthesis of second generation complexes

A series of cyclometalated ruthenium compounds bearing either a tridentate N[^]C[^]N[']- or N[^]N['][^]C-cyclometalated ligand and one bidentate N[^]N or tridentate N[^]N[^]N ligand was synthesized and characterized. Some of them have been recently published by van Koten *et*

al. and are used for their photochemical properties.⁶ This new generation of **RDCs** enabled us to diversify and complement the existing chemical library of a dozen compounds.

All substituted $N^{\wedge}C(H)^{\wedge}N^{\wedge}$ and $C(H)^{\wedge}N^{\wedge}N^{\wedge}$ -cyclometalating ligands and substituted terpyridine ligands used in **second generation RDC** complexes were prepared according to literature procedures: 1,3-di(pyridin-2-yl)benzene ($N^{\wedge}C(H)^{\wedge}N^{\wedge}$),^{7,8} methyl-3,5-di(2-pyridyl)benzoate ($MeO_2C-N^{\wedge}C(H)^{\wedge}N^{\wedge}$),^{9,10,11} 3,5-di(2-pyridyl)toluene ($Me-N^{\wedge}C(H)^{\wedge}N^{\wedge}$),¹¹ 6-phenyl-2,2'-bipyridine ($C(H)^{\wedge}N^{\wedge}N^{\wedge}$),^{12,13} 4-ethoxycarbonyl-6-phenyl-2,2'-bipyridine ($EtO_2C-C(H)^{\wedge}N^{\wedge}N^{\wedge}$),^{6,14} 4,4'-di(methoxycarbonyl)-6-phenyl-2,2'-bipyridine ($(MeO_2C)_2-C(H)^{\wedge}N^{\wedge}N^{\wedge}$),⁶ 4'-ethoxycarbonyl-2,2':6',2''-terpyridine (EtO_2C -terpy),^{6,15,16} trimethyl 2,2':6',2''-terpyridine-4-4'-4''-tricarboxylate ($(MeO_2C)_3$ -terpy),¹⁷ 4'-(4-methylphenyl)-2,2':6',2''-terpyridine ($MePh$ -terpy).¹⁸

Monocationic complexes **RDC 51-54** were prepared by reacting activated $[RuCl_3(R_1\text{-terpy})]$ by $AgBF_4$ with the corresponding $R_2-N^{\wedge}C^{\wedge}N^{\wedge}$ ligand in *n*-BuOH according to a published procedure (**Figure 1**).⁶ Notice that coordination of potentially C,N,N^{\wedge} -binding ligand can be solvent dependent, as described by Constable *at al.*¹⁹ The use of solvents with high dielectric constants such as DMF or MeOH favours a cyclometallation process. Hence, monocationic complexes **RDC 57-59** were finally synthesized in EtOH in the presence of *N*-methylmorpholine as a sacrificial reducing agent (**Figure 1**) according to recently published procedure.⁶

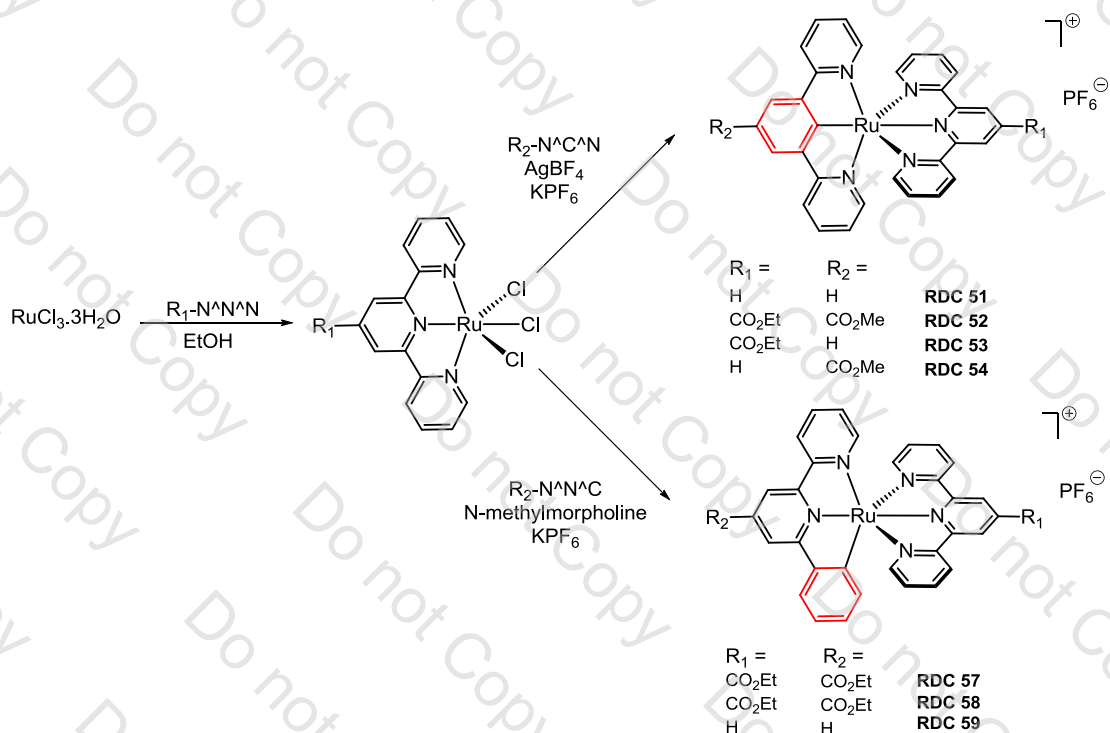


Figure 1: Synthesis of second generation RDCs containing $N^{\wedge}C^{\wedge}N^{\wedge}$ or $N^{\wedge}N^{\wedge}C^{\wedge}$ pincers and substituted terpy ligand

The synthesis of the compounds containing one MeCN ligand was achieved with the starting material $[\eta^6\text{-}(\text{C}_6\text{H}_6)\text{RuCl}(\mu\text{Cl})_2]$. From previous work,²⁰ it is known that the latter dimeric reagent treated by 2-phenylpyridine in the presence of NaOH and KPF_6 yielded to the corresponding $[\text{Ru}(o\text{-C}_6\text{H}_4\text{py-}\kappa\text{C,N})(\text{NCMe})_4]\text{PF}_6$ C,N-cyclometalated complex.

In a similar way, $[\eta^6\text{-}(\text{C}_6\text{H}_6)\text{RuCl}(\mu\text{Cl})_2]$ reacts with substituted R-N^{^C}(H)^{^N} in a refluxing MeCN solution for 12h in the presence of NaOH and KPF_6 forming the tridentate corresponding complex $[\text{Ru}(\text{R-N}^{\wedge}\text{C}^{\wedge}\text{N})(\text{NCMe})_3]\text{PF}_6$ (**Figure 2**). This result is in contrast to that observed by van Koten *et al.*²¹ who found that the above reaction leads to a mixture of two compounds showing the same high degree of symmetry. Nevertheless, no structure for these two compounds was proposed by the author since no suitable crystals for X-ray diffraction have been obtained. Notice that same procedure can be used to synthesize **RDC 52** and **RDC 54** using respectively EtCO₂-terpy and terpy as further chelating agents.

However, when $[\eta^6\text{-}(\text{C}_6\text{H}_6)\text{RuCl}(\mu\text{Cl})_2]$ is treated with non-substituted N^{^C}(H)^{^N}, a complex mixture is obtained, as evidenced by ¹H NMR spectroscopy. Indeed, cyclometallation can occur either inside the pincer (as it is the case for substituted R-N^{^C}(H)^{^N}) or outside the pincer. Although the exact composition of this mixture still remained unknown, it must likely contain species in which the tridentate ligand is bound as bidentate C,N-cyclometalated ligand at either 1- or 3-positions of the phenyl ring, in addition to the desired product. Hence, cyclometallation of non-substituted N^{^C}(H)^{^N} (*e.g.* **RDC 51** and **RDC 53**) must be performed using reaction depicted in **Figure 1** in order to avoid by-products formation.

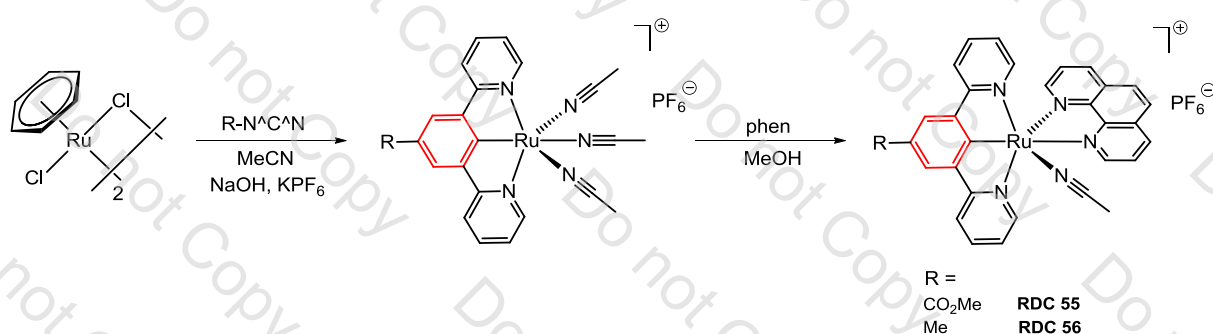


Figure 2: Synthesis of second generation RDCs containing N^{^C}^{^N} substituted pincers and bidentate 2,2'-phenanthroline

Sadler *et al.* lead compounds **RM 175** and **ONCO 4417** were synthesized from $[\text{RuCl}(\mu\text{Cl})(\eta^6\text{-C}_{12}\text{H}_{10})]^{22}$ according to a reported procedure.²³ Note that by using standard methods,²⁰ cyclometallation of 2-phenylpyridine by $[\text{RuCl}(\mu\text{Cl})(\eta^6\text{-C}_{12}\text{H}_{10})]$ involves the dissociation of the η^6 -benzene and the formation of $[\text{Ru}(\text{N}\sim\text{C})(\text{NCMe})_4]\text{PF}_6$.

2.1.3. Cytotoxic activity of second generation complexes

2.1.3.1. Introduction

The cytotoxic activity of **second generation RDCs** was evaluated against two cell lines. The cell lines HCT116 and A172 from the European Collection of Culture (ECACC, Salisbury, UK), were matured in a Petri dish containing DMEM with 10% foetal calf serum (FCS), and 1% antibiotic (PS) in an incubator under a moist atmosphere 5% CO₂ at 37 ° C for 24h. The determination of the initial number of cells is necessary in order:

- to prevent excessive confluence, causing a decrease in the proliferation and/or cell death.
- to reach sufficient number of cells in exponential progression to measure the cytotoxicity.

After 24h to 48h the cells are detached from the Petri dish thanks to 0.25% trypsin and then diluted 10 times in the culture medium and placed into 96-wells dishes, at a concentration of approximately 10⁶ cells.mL⁻¹. After 24h incubation, cells at 70% confluence in exponential growth are treated with the different complexes at given concentrations. After 48h treatment, the viability of the cells was determined by measuring the mitochondrial succinic hydrogenase activity by MTT assay on the remaining living cells in order to determine the IC₅₀ of the complexes (*i.e.* inhibitory concentration causing 50% cancer cells death).

2.1.3.2. Principle of the MTT test:

In order to determine the cytotoxicity of the **RDC** complexes, MTT test was used to assess the viability and the proliferation of the cells. The **MTT test** is a colorimetric assay for measuring the activity of enzymes that reduce tetrazolium salt 3-(4,5-Dimethylthiazol-2-yl)-2,5-diphenyltetrazolium bromide (0.5mg/mL, yellow tetrazole) to purple **formazan** crystals in living cells, giving a purple colour (**Figure 3**).

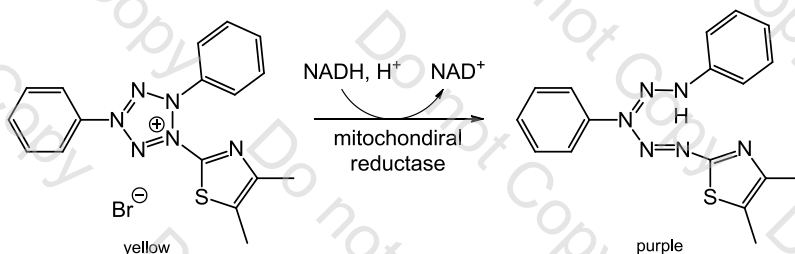


Figure 3: Reduction of tetrazolium salt into formazan by dehydrogenase succinate

The intensity of the colour is directly proportional to the number of living cells during the test. Formazan crystals are then solubilised in an acidified *iso*-propanol solution (0.04M HCl). The absorbance of this coloured solution can be quantified by measuring at a given wavelength $\lambda=570\text{nm}$ the optical density with a multiwell Elisa plate reader (iEMS Reader MF,

Labsystem, US). The percentage of surviving cells was calculated from the ratio of absorbance of treated to untreated cells. The experiments were repeated at least three times and the mean deviation was determined by considering the extreme values found over all experiments. This semi-quantitative method was developed by Tim Mosmann²⁴ in 1983 and is nowadays widely used.

2.1.3.2. *In vitro* antiproliferative activity results:

The IC₅₀ of various second generation **RDCs** have been evaluated by measuring their effects on the cell proliferation in A172 (human glioblastoma) and in HCT116 (colorectal carcinoma) cell lines (**Figure 4**). Results are presented as a percentage compared with the control condition. Graphs represent mean values with standard deviation of eight wells from one out of three independent experiments. The thick line corresponds to 50% viability (IC₅₀) (**Figure 5**). The IC₅₀ results are compared to those obtained with the previously reported¹ compound **RDC 11** at 5μM and are summarized in **Table 1**. Antiproliferative activity of the newly synthesized **RDCs** was also compared to Sadler's lead compounds (**RM175** and **ONCO4417**) in an A172 cell line (**Figure 6**).

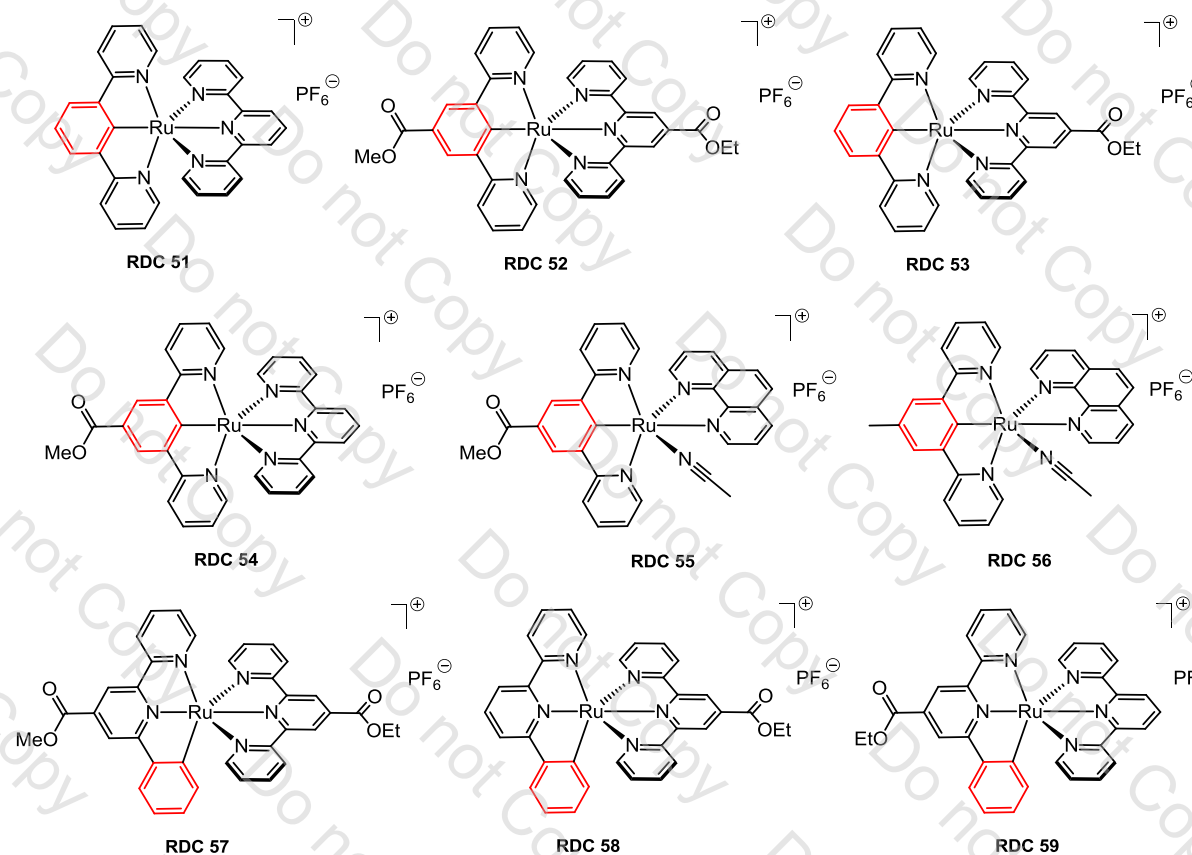


Figure 4: Chemical library of second generation RDCs complexes



Figure 5: Antiproliferative *in vitro* activity of second generation RDC on an A172 cell line

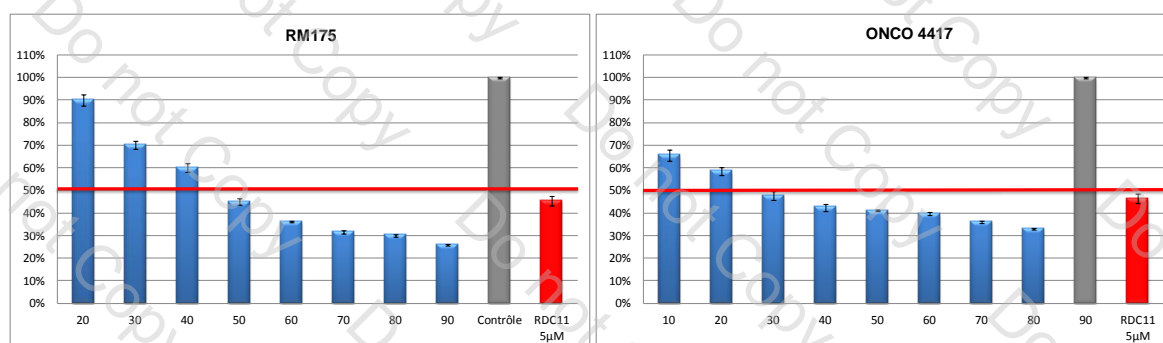


Figure 6: IC_{50} on synthesized Sadler *at al.* leading compounds (RM175 and ONCO 4417) on an A172 cell line

<i>RDCs second generation</i>	<i>IC₅₀ (µM)</i>	
	<i>HCT 116</i>	<i>A172</i>
RDC 51	0.7 ± 0.1	0.6 ± 0.1
RDC 52	2.8 ± 0.3	1.5 ± 0.2
RDC 53	1.3 ± 0.3	0.6 ± 0.1
RDC 54	1.2 ± 0.1	1.2 ± 0.2
RDC 55	2.9 ± 0.4	1.7 ± 0.5
RDC 56	1.4 ± 0.3	0.8 ± 0.2
RDC 57	1.2 ± 0.2	0.9 ± 0.2
RDC 58	2.8 ± 0.3	1.0 ± 0.2
RDC 59	1.3 ± 0.2	1.2 ± 0.2
Sadler RM175	-	45 ± 5.0
Sadler ONCO 4417	-	30 ± 5.0
RDC 11	5 ± 0.5	5 ± 0.5
Cisplatin	5 ± 0.5	5 ± 0.5

Table 1: Recapitulative table of the IC_{50} values on HCT116 and A172 cell lines

This new generation of **RDCs** complexes enabled us to diversify and complement the existing chemical library of a dozen compounds. As it was the case for compounds previously described,⁵ we found that all **second generation RDCs** display good to very good cytotoxicities against HCT116 and A172 cell lines. Several compounds of **second generation RDCs** (using N-C-N or N-N-C pincers) cross the symbolic barrier of the nanomolar range for their IC_{50} , indicating a critical improvement relative to the **first generation RDCs**.

Given that no clear-cut **Structure Activity Relationship** (S.A.R.) can be rationalized from these results, we checked whether the red-ox potential (see **Chapter 2, 2.1.4.**) and the lipophilicities (see **Chapter 4, 4.2.**) of our compounds could be correlated with their *in vitro* activity. Indeed, substitution of the ligands with electron-withdrawing ester functionalities fine-tuned the electronic properties with slight modifications of the *in vitro* activity.

However, to emphasize the importance of the C-Ru bond and that of the Ru^{III/II} red-ox potential, it is also interesting to compare the results of the previous chemical library with those of structurally related compounds such as [Ru(bipy)₃](PF₆)₂,^{1,25} [Ru(phen)₃](PF₆)₂, or [Ru(phen)₂(MeCN)₂](PF₆)₂. The latter all have IC₅₀ > 50 μM and E°_{1/2} (Ru^{III/II}) > 1.3V. However, one has to take into account that they are dicationic species and thus might be less lipophilic than the monocationic organoruthenium derivatives studied here.

We can note that the cellular response can also be plotted in terms of IC₅₀ as a function of log₁₀([concentration of complex in μM]) to draw sigmoids whose functions can easily be calculated using non-linear regression of the experimental points. Fitting of the curves based on a 4-parameter sigmoid function was performed using Maple and Sigma Plot softwares. Nevertheless, no correlation between the IC₅₀ and the slope of the tangent at the inflexion point of the curve can be observed.

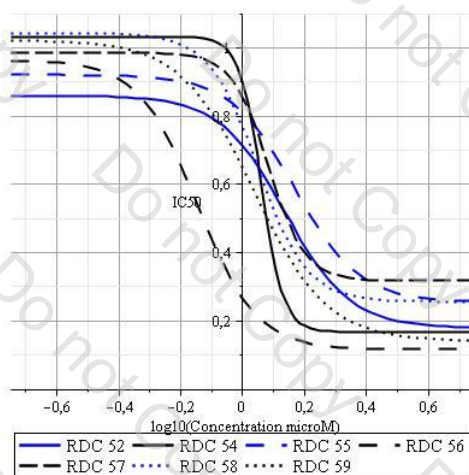


Figure 7: Fittings of the curves were based on a 4-parameter sigmoid function of type $y = y_0 + \frac{a}{1 + e^{-\left(\frac{x-x_0}{b}\right)}}$

2.1.3.3. Results from the National Cancer Institute:

The National Cancer Institute (NCI) has carried out a screening cascade since the 1960s and developed in the late 1980s a 60 human tumour cell lines anticancer drug screen (NCI60) as an *in vitro* drug-discovery tool intended to supplant the use of transplantable animal tumours in anticancer drugs. This screening was rapidly recognized as a rich source of information about the mechanisms of growth inhibition and tumour-cell kill.²⁶

Compounds sent to the NCI from academic and industrial sources are initially screened in this 60-cell line panel, representing nine distinct tumour types: leukemia, colon, lungs, central nervous system, renal, melanoma, ovarian, breast and prostate. The NCI has now established a substantial database of information and uses a computer algorithm known as “COMPARE”

to establish whether the characteristics of a novel agent evaluated in the 60-cell line panel are similar to any existing families of agents, thus predicting the likely mechanism of action.

Our laboratory sent to the NCI already described new first generation **RDCs (RDC 11, RDC 34 and RDC 41** whose structure is depicted on the graphs) and also two new second generation complexes (**RDC 55 and RDC 56**). Mean graphs are constructed at each level of effect, with bars depicting the deviation of individual cell lines from the overall mean value for all the tested cells. The graphs can be interpreted as follows:

- The bars situated in the 0 area (growth inhibition) indicate a **cytostatic activity**.
- The bars situated between -100 and 0 (tumour regression) indicate a **cytotoxic activity**.
- The bars situated between 0 and 100 (slower tumour proliferation) indicate a **decrease in the speed** of proliferation.
- The bars situated in the 100 area (tumour proliferation) indicate **no *in vitro* activity**.

As expected by previous studies, **RDC 11** seems to be a good drug candidate, given that it is cytotoxic against several cell lines with different activity potentials. It is particularly active against one ovarian cancer (OVCAR-3), several melanomas (UAC-62, SK-MEL-5, SK-MEL-2, MALME 3M), one colon cancer (COLO 205) and also against one non-small-cell lung carcinoma (NSCLC NCI-H522) (**Figure 8**).

Results from NCI demonstrated that **RDC 34** displays high cytotoxic properties in practically all tested cell lines (**Figure 9**). However, previous *in vivo* studies showed that **RDC 34** is not well accepted in animal models because of its important chronic and acute toxicity.

In **RDC 41**, the incorporation of an NH₂ electron donating group leads to the decrease of red-ox potential (see **Chapter 2, 2.1.4.**) $E^{\circ}_{1/2}$ (**RDC 41**) = 200mV compared to $E^{\circ}_{1/2}$ (**RDC 34**) = 410mV and also to the decrease of lipophilicity (see **Chapter 4, 4.2.**). Hence, as expected by previous *in vitro* studies, a decrease of cytotoxicity should be observed. Measures from the NCI in different cell lines agree with preliminary *in vitro* activity measurements (**Figure 10**).

RDC 55 seems also to be a good drug candidate, for the same reasons discussed above for **RDC 11**. However, **RDC 55** is active against fewer cell lines and with reduced activity compared to **RDC 11**. **RDC 55** is particularly active against melanoma (SK-MEL-5, SK-MEL-2) and colon cancer (COLO 205) (**Figure 11**). Replacement of ester group in **RDC 55** by a methyl group leads to the compound **RDC 56**. **RDC 56** shows enhanced *in vitro* activity compared to **RDC 55**. It is more cytotoxic, but not as toxic as **RDC 34** and interestingly shows also cytostatic properties against several cell lines including prostate, ovarian, central nervous system, non-small-cell lung carcinoma and leukemia (**Figure 12**).

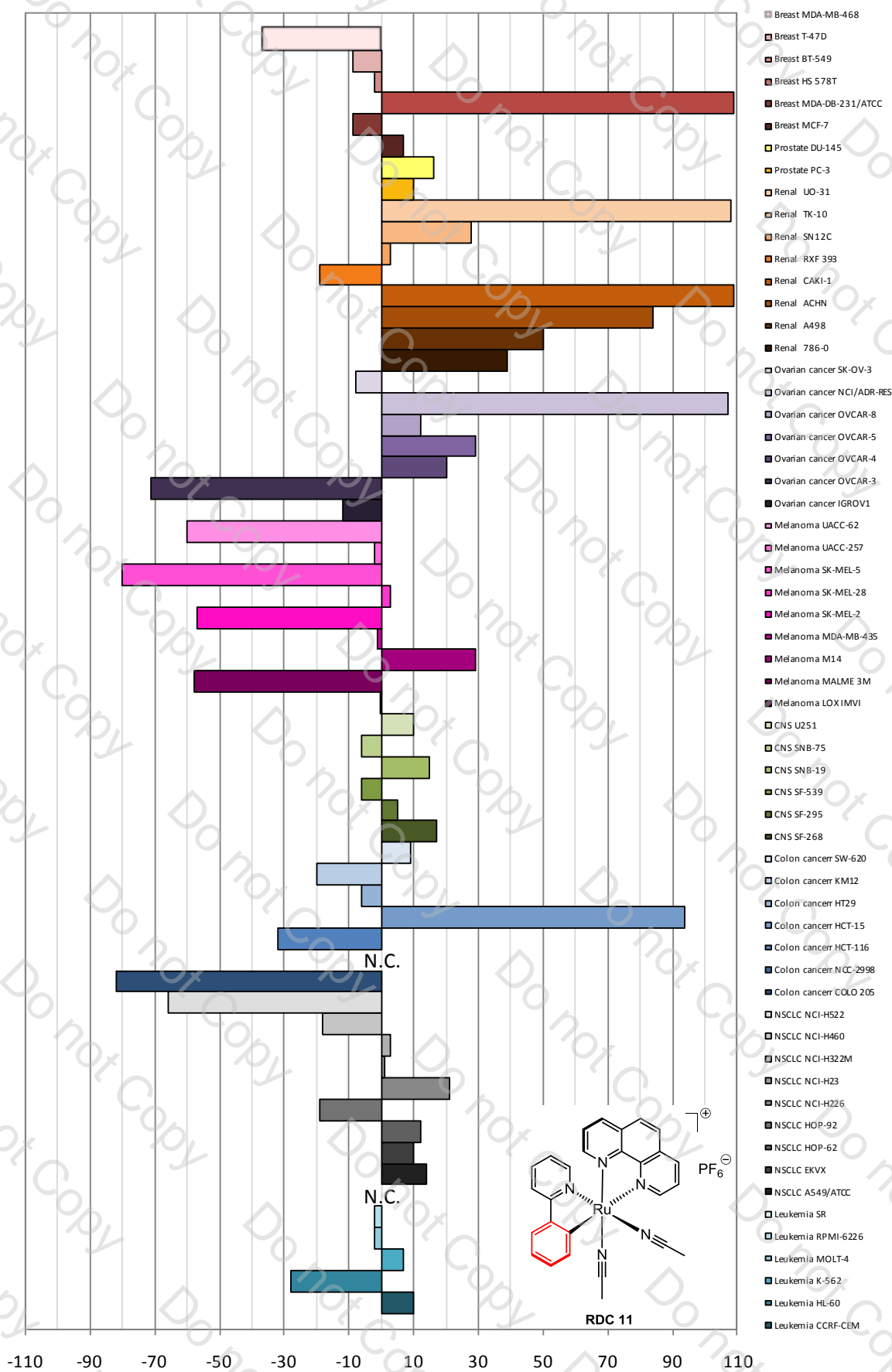


Figure 8: Cellular response towards RDC 11 treatment on 60 cancerous cell lines

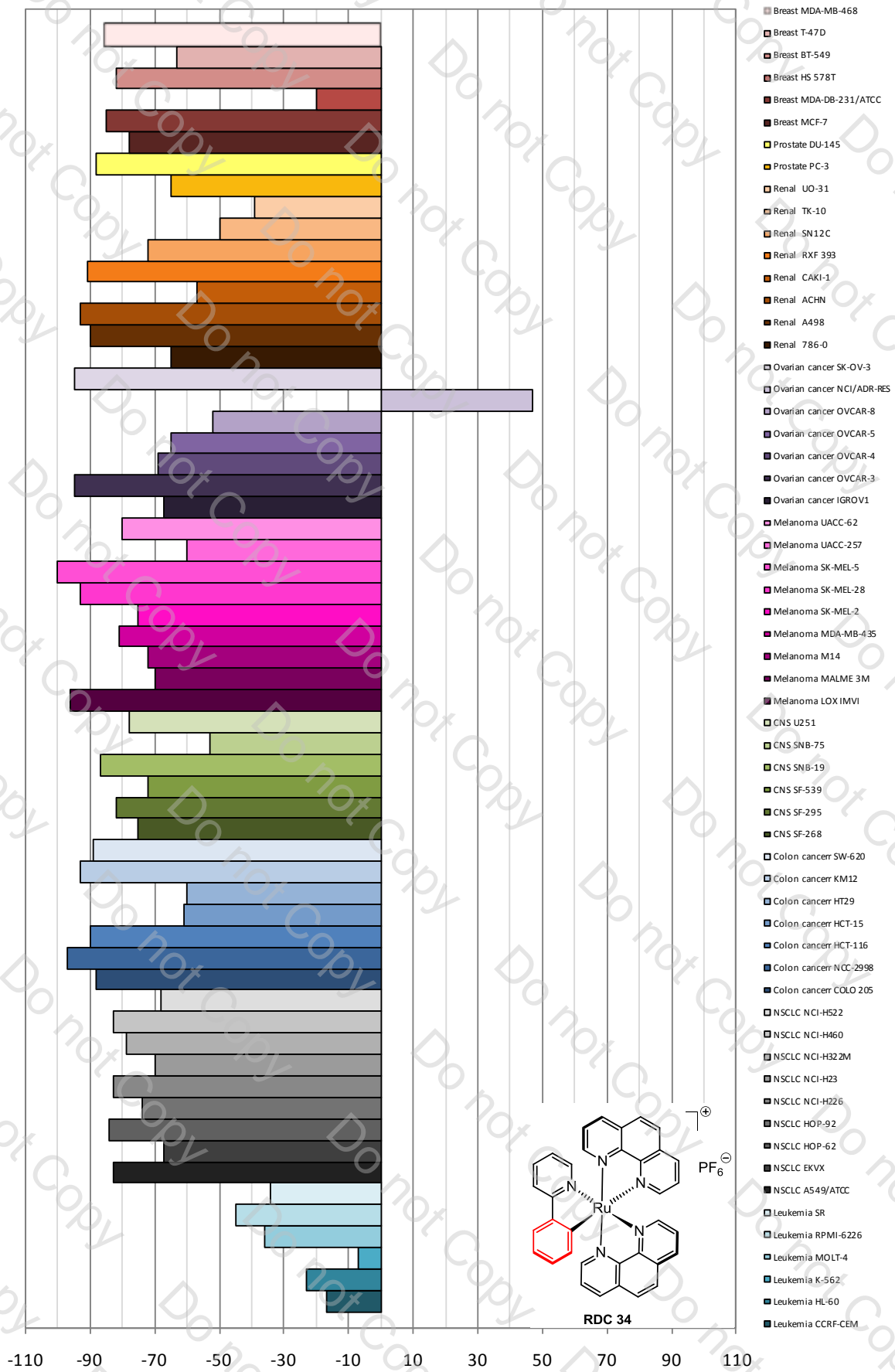


Figure 9: Cellular response towards RDC 34 treatment on 60 cancerous cell lines

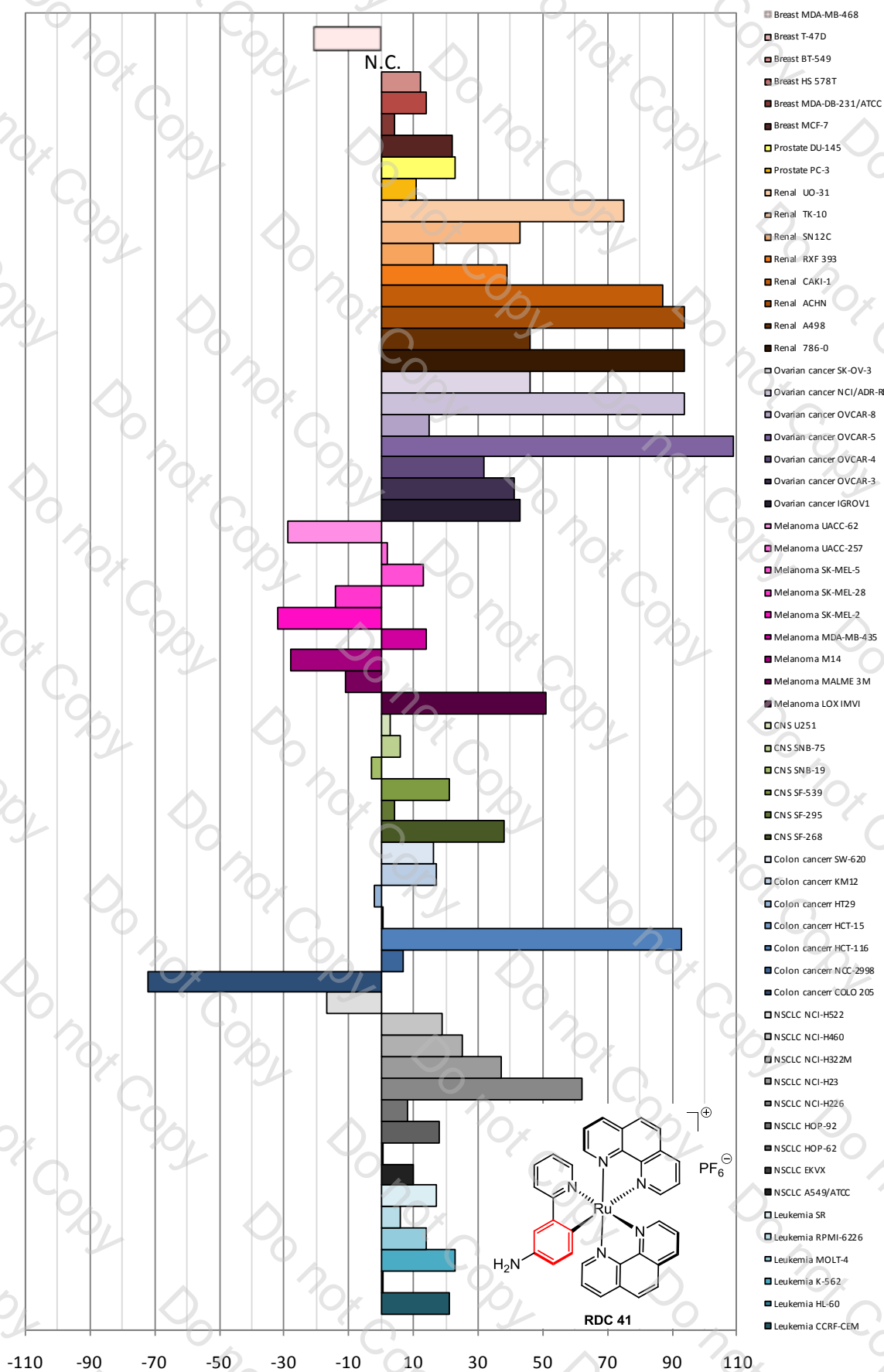


Figure 10: Cellular response towards RDC 41 treatment on 60 cancerous cell lines

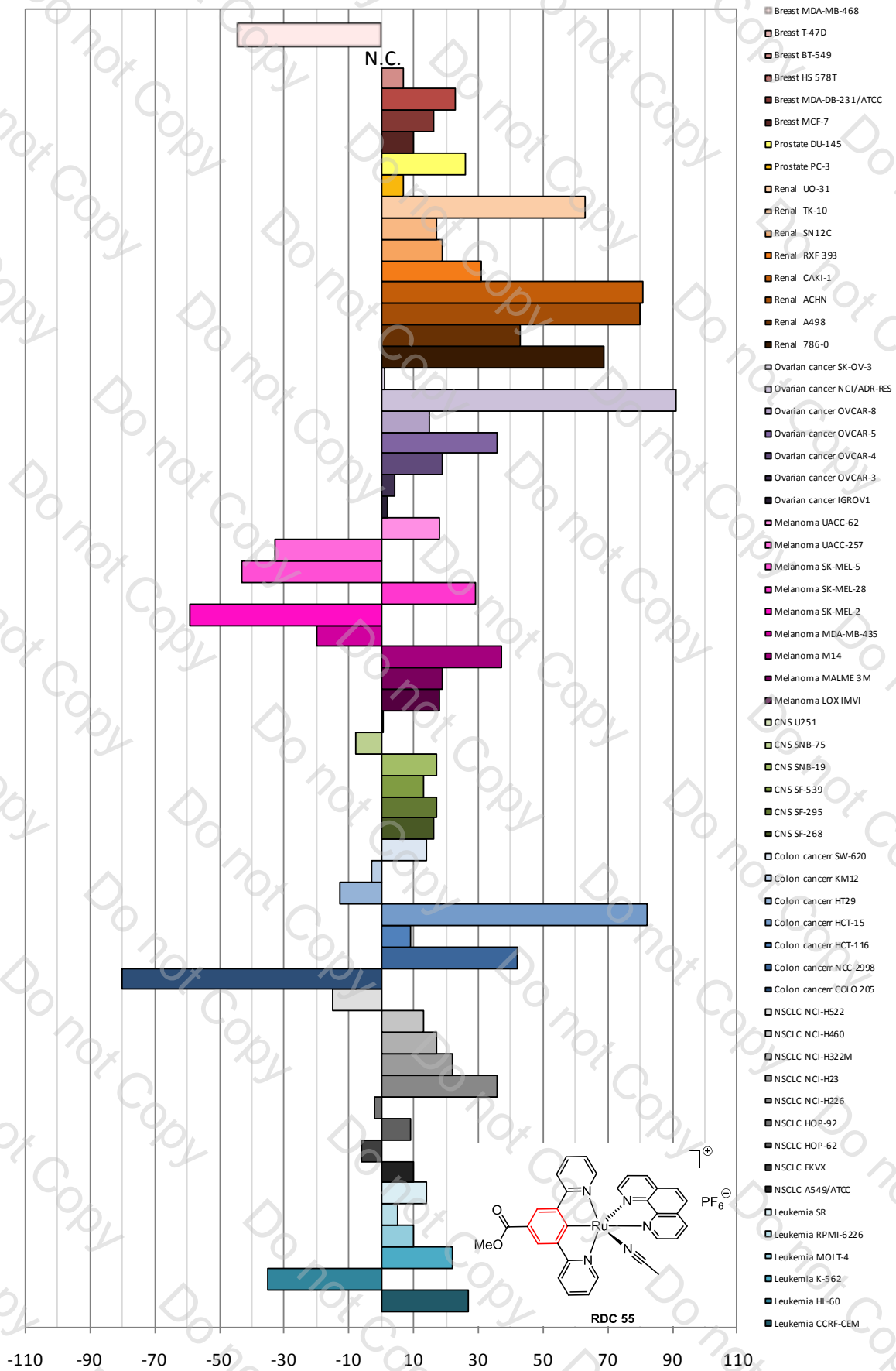


Figure 11: Cellular response towards RDC 55 treatment on 60 cancerous cell lines

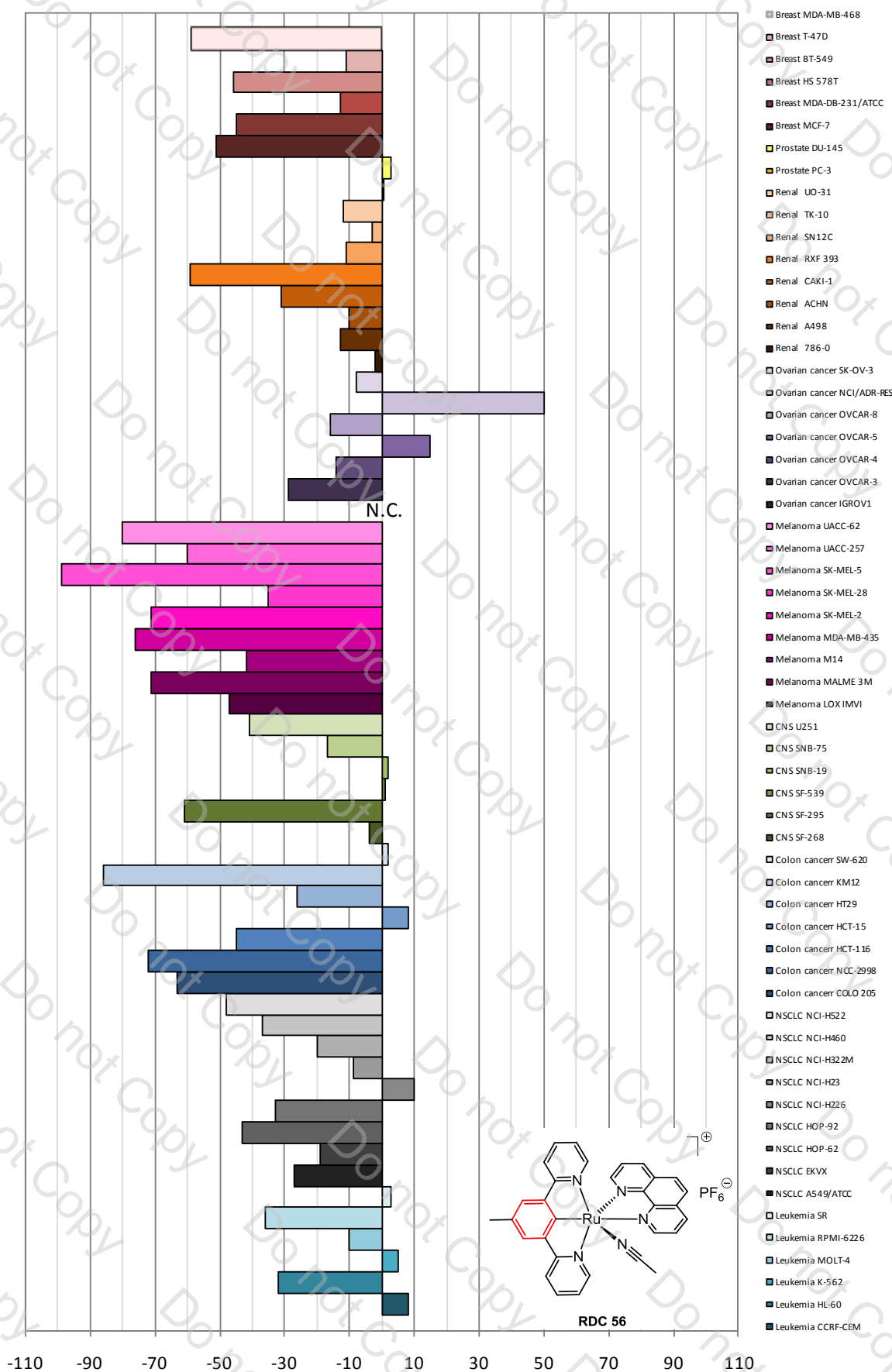


Figure 12: Cellular response towards RDC 56 treatment on 60 cancerous cell lines

2.1.4. Electrochemical properties of first- and second-generation RDCs

From previous chemical library, it was not possible to establish a correlation between the anticancer activities and some physicochemical properties (like stereochemistry or electronic contributions of the ligands) of the ruthenacycles. It was nevertheless concluded that the main factor that contributes to the biological activity is the presence of the ruthenium-carbon bond in the molecular structure. Given that no clear-cut **Structure Activity Relationship (S.A.R)** can be rationalized from the *in vitro* results, we checked whether the red-ox potential could be related to the IC_{50} of a series of first and second generation compounds (**Figure 14**).

The electrochemical properties of these complexes have been studied by cyclic voltammetry in an 0.1M [*n*-Bu₄N][PF₆] electrolyte using a three electrode system consisting of a platinum working electrode, a platinum wire as counter electrode and a silver wire as a pseudo-reference electrode. Electrodes are static and sit in unstirred solutions during cyclic voltammetry. The anodic region of the cyclic volt-amperograms is dominated by reversible waves corresponding to the one-electron oxidation of the Ru^{II} state, while the cathodic region exhibits poorly defined or irreversible waves resulting from the reduction of the ligands. For most complexes, reversible couples Ru^{III/II} describe a hysteresis between **absolute potential** ($E^{\circ}_{1/2}$) located between the **reduction peak** (E_{pc} , cathodic peak potential) and **oxidation peak** (E_{pa} , anodic peak potential) (**Figure 13**).

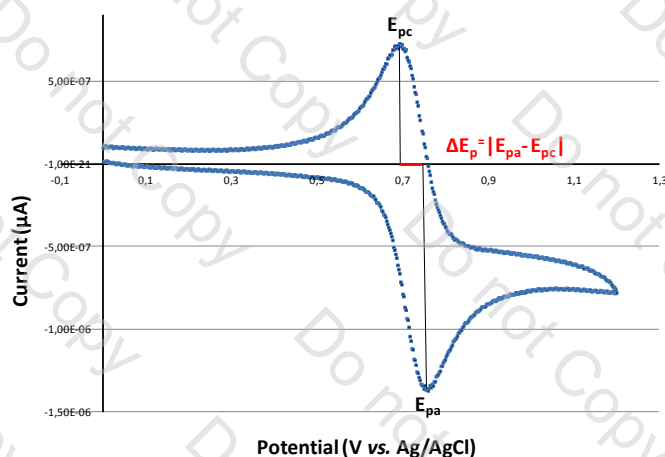


Figure 13: Example of a cyclic volt-ampereogram showing the red-ox process Ru^{III/II}

Notice that in an ideal system, the Butler-Volmer equation and Cottrell equation is simplified to $|E_{pa} - E_{pc}| = 57 \text{ mV}/n$, for an *n* electron process and so, measure of ΔE_p allows to evaluate the reversibility of the system. However, for cyclometalated piano-stool complexes, the waves are non-reversible, perhaps due to a shift in the geometry of the coordination sphere. Hence, it was difficult to determine their thermodynamic $E^{\circ}_{1/2}$ with cyclic voltammetry, even by using higher scan rates and measure of E_{pa} was accepted as an absolute potential.

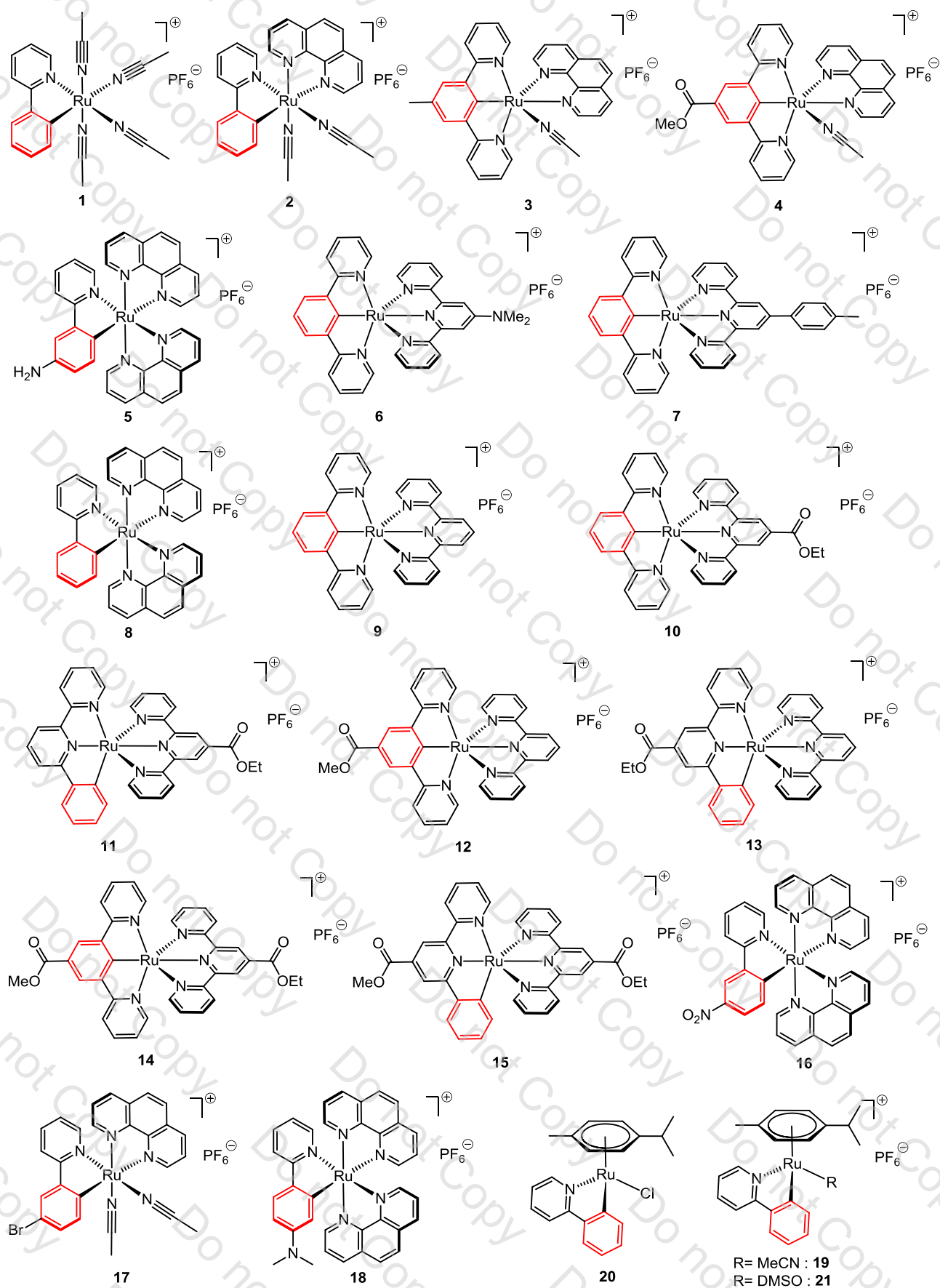


Figure 14: Overall view of first- and second-generation complexes used for the correlation

The electrochemical data for the complexes are presented in **Table 2**. These data clearly show that molecules having a red-ox potential in the range **0.4-0.6V** (vs. SCE) display the lowest IC₅₀ values. Notice also that substitution by an electron-donor like NH₂ in compound **5** induces a cathodic shift of 190mV, whereas substitution by an electron-acceptor like NO₂ in compound **16** induces an anodic shift of 280mV.

Complexes	RDCs equivalent	$E^{\circ}_{1/2} Ru(III/II)$ ($\pm 5mV$)	E_{pa} (mV)	E_{pc} (mV)	ΔE_p	$E^{\circ}_{1/2} R^+/R$ (mV)	IC ₅₀ (μM) A172
1	RDC 8	710	741	679	62	-	>50
2	RDC 11	560	589	531	58	-	3.0 \pm 1.0
3	RDC 56	380	412	348	64	-	0.8 \pm 0.2
4	RDC 55	595	629	561	68	-	1.7 \pm 0.5
5	RDC 41	200	235	265	70	1164 (NH ₂ ⁺ /NH ₂)	5.0 \pm 1.0
6	-	310	337	282	55	885 (NMe ₂ ⁺ /NMe ₂)	3.0 \pm 1.0
7	RDC 47	490	521	459	62	-	0.5 \pm 0.1
8	RDC 34	410	440	380	60	-	0.5 \pm 0.1
9	RDC 51	520	553	487	66	-	0.6 \pm 0.1
10	RDC 53	600	633	568	65	-	0.6 \pm 0.1
11	RDC 58	660	691	629	62	-	1.0 \pm 0.2
12	RDC 54	650	682	618	64	-	1.2 \pm 0.2
13	RDC 59	620	649	591	58	-	1.2 \pm 0.2
14	RDC 52	720	753	688	65	-	1.5 \pm 0.2
15	RDC 57	710	738	681	57	-	0.9 \pm 0.2
16	RDC 40	690	721	569	62	-	0.5 \pm 0.1
17	RDC 32	620	650	590	60	-	1.0 \pm 0.5
18	RDC 36	430	462	398	60	884 (NMe ₂ ⁺ /NMe ₂)	0.5 \pm 0.2
19	RDC 49	1244 ^(a)	1244 ^(a)	-	-	-	14 \pm 1.0
20	RDC 49-Cl	753 ^(a)	753 ^(a)	-	-	-	22 \pm 1.0
21	RDC 49-DMSO	1410 ^(a)	1470 ^(a)	-	-	-	24 \pm 1.0

Table 2: Recapitulative table of red-ox potentials vs. SCE and IC₅₀ on an A172 cell line (a): irreversible wave

$E^{\circ}_{1/2} = (E_{pa} + E_{pc})/2$ vs. FeCp₂ or [Os(tterpy)₂](PF₆)₂, in mV;
Electrolyte: [*n*-Bu₄N][PF₆] 0.1 M; Scan rate: 0.100 V.s⁻¹; 20 °C

Examination of the molecular library constituents led to the conclusion that biological activity will not correlate with the chemical structure, but rather with the physicochemical properties. The red-ox properties of the complexes may be involved in the biological activity given that oxidation states of ruthenium are all accessible under physiological conditions. For that reason we looked for binomial correlation between the anticancer and electrochemical properties (**Figure 15**). Compound **1** was discarded from the correlation because this unstable product can rapidly oxidize and would not have been representative of the initial composition of the solution. The neutral compound **20** was also discarded from the correlation because it does not belong to the same class of compounds bearing a PF₆⁻ as counter ion.

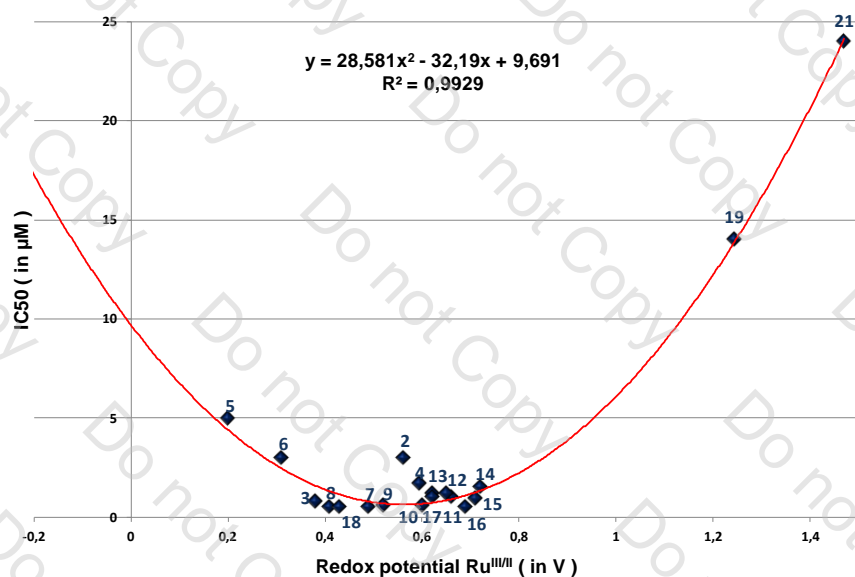


Figure 15 : Binomial correlation between IC_{50} and red-ox potential $E^{\circ}_{1/2}(Ru^{III/II})$

Although the importance of the red-ox potential for ruthenium compounds displaying anticancer properties has been recognized in the late 1970's,²⁷ we did not find many correlations analogous to ours. Fairly good binomial correlation was found between the IC_{50} values and the red-ox potentials of the couple $Ru^{III/II}$. The relative dispersion of the points in the interval **0.4-0.6 V** may reflect the small variations of other parameters like lipophilicity (see Chapter 4, 4.2.) and/or possibly shape.

In 1996, Clarke *et al.* found that the most active ruthenium complexes as metalloimmunosuppressants have reduction potentials between 100 and 400 mV.²⁸ These authors hypothesized that electron transfer could explain their activity and that a likely site of metabolic interference could be the respiratory red-ox pathway producing the ATP essential to cell growth. It is now well accepted that most of the $Ru(III)$ derivatives such as in **NAMI-A** or **KP1019** that display antitumour activities are in fact pro-drugs that are activated by reduction.²⁹ Recently, Keppler *et al.*³⁰ found that the most active compounds in a series of ruthenium indazole (ind) adducts $[Ru^{III}Cl_{(6-n)}(ind)_n]^{(3-n)-}$ were those whose red-ox potential was between $E^{\circ}_{1/2} = 0.1$ and 0.58 V vs. NHE. These compounds (with $n = 3$ and 4) presented IC_{50} just above (2.6 μM , for $n = 3$) or below (0.69 mM, for $n = 4$) the nanomolar range for the inhibition of colon cancer cells (SW480) and ovarian cancer cells (CH1), whereas the compounds with $n = 0$ to 2 , whose $E^{\circ}_{1/2}$ varied from -1.36 to -0.39 V (estimated value),³⁰ had cytotoxicities up to 2 orders of magnitude higher.

Although the relation between the values of red-ox potential and the cytotoxicity of our **RDCs** compounds has not been clarified yet, a reasonable hypothesis however could be that these ruthenium compounds regulate or interfere somehow with some enzymes in the cells.

2.2. Study of the exchange of MeCN vs. DMSO in piano-stool cycloruthenated complexes

2.2.1. Introduction

Since our compounds were synthesized to assess their *in vitro* cytotoxicities towards cancer cell lines, we checked whether their solutions (in neat DMSO diluted with the required amount of cell culture media) were stable at least for two days. All previously synthesized complexes show good stability towards ligand substitution reactions in the absence of light, which was checked either by ^1H NMR or UV-visible spectroscopy (see **Chapter 4, 4.1.**) and hence were considered as good drug candidates.

However, biologists were faced with non-reproducible *in-vivo* and *in vitro* measurements with piano-stool cycloruthenated complexes. For mono acetonitrile type complexes, we found that the MeCN ligand is relatively labile and can exchange with DMSO. This instability was demonstrated by ^1H NMR spectroscopy in DMSO-d^6 , which showed a significant modification of ruthenium arene type complexes after 3 hours. We first discarded these compounds from *in vitro* tests, since collected data were not representative of the initial composition of the compounds.

2.2.2. Synthesis of piano-stool cycloruthenated complexes

The synthesis of piano-stool complexes containing at least one *a priori* labile acetonitrile ligand was achieved by cyclometallation of the dimer starting material bearing an η^6 -arene bind to the ruthenium centre (**Figure 16**).

RDC 49 $[\text{Ru}(\text{o-C}_6\text{H}_4\text{py-}\kappa\text{C,N})(\text{p-cym})(\text{NCMe})]\text{PF}_6$ was obtained by reaction between 2-phenylpyridine and the dimer $[\eta^6\text{-(p-cymene)RuCl}(\mu\text{Cl})_2]$ in the presence of NaOH and KPF_6 in acetonitrile at 45°C for 24h, following a published procedure.³¹ Notice that a similar class of compound closely related to **RDC 49**, in which the acetonitrile ligand was substituted by chloride ion, was reported recently.^{32,33}

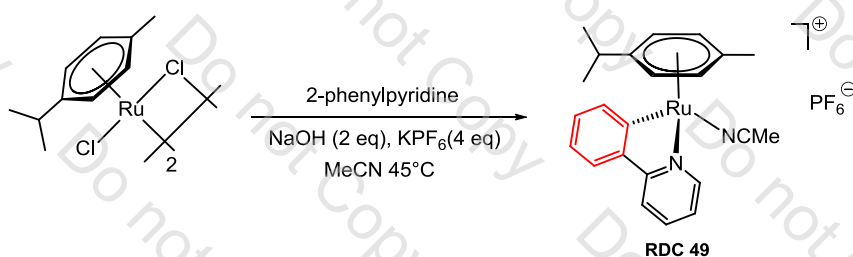


Figure 16: Synthesis of RDC 49

In marked contrast to previous results obtained in the laboratory, when the same reaction was conducted using $[\eta^6-(\text{C}_6\text{H}_6)\text{RuCl}(\mu\text{Cl})]_2$, the η^6 -*p*-cymene unit is not substituted by acetonitrile ligands. In fact, it was found that the η^6 -*p*-cymene was strongly bound to the metal centre, as neither prolonged reflux in acetonitrile (up to 24h), nor use of UV light with prolonged heating led to substitution of the arene unit by MeCN.

This behaviour is in strike contrast to those observed by Berlinguette *et al.*³⁴ who found that the reaction depicted in **Figure 16** using 2-(arene)pyridine ligands substituted at the arene ring by electron-withdrawing substituents, led to a mixture of two compounds: one of them being the tetrakis-acetonitrile cycloruthenated species, the second being closely related to **RDC 49**, but in which two MeCN ligands instead of one were bound to the ruthenium centre.

The formation of this compound is however doubtful, as it would have lead to a 20-electrons complex, unless the arene ligand is not η^6 -coordinated to the ruthenium centre, which is also unlikely. We therefore ascertained the structure of this class of compounds by performing a three-dimensional structure determination by means of an X-ray diffraction study on a single crystal of **RDC 49** (see **Chapter 2, 2.2.4.**).

2.2.3. Preliminary results: kinetic evolution of **RDC 49** in DMSO

First *in vitro* and *in vivo* studies of **RDC 49** were of promising interest. Indeed, this compound displays good antiproliferative properties *in vitro* in HCT116 ($\text{IC}_{50}=10\mu\text{M}$) and in A172 ($\text{IC}_{50}=14\mu\text{M}$) cell lines. Moreover, this compound has demonstrated low toxicity in the first *in vivo* test. However, biologists were rapidly faced with non-reproducible *in vivo* and *in vitro* measurements with **RDC 49**, loosing partially or totally the anticancer activity. This problem was not due to complex instability in the solid state, given that this crystalline powder is stable and does not easily oxidize.

Hence, the problem of non-reproducibility was coming from stock solution in DMSO used by biologists. Samples were either readily prepared in neat DMSO for direct injection in animals or were already prepared, stocked at frozen state and finally left to thaw before use. We note that the lack of reproducibility was not observed in first *in vitro* tests given that solutions in DMSO were directly prepared before cell treatment. It was thus important to follow the evolution of **RDC 49** in DMSO in order to prove the postulate that in this mono acetonitrile type complex, the MeCN ligand is relatively labile and can exchange with DMSO.

In an initial study a sample of **RDC 49** (5.10^{-5}M , in DMSO) was prepared and its kinetic evolution was monitored by UV/vis spectroscopy (**Figure 17**). Notice that in this kinetic model, the concentration of monitored **RDC 49** is not relevant, because this model is 1000 times less concentrated than stock solution used by biologists (50mM). The spectrum showed a rapid evolution in the transition $\pi - \pi^*$ situated in the UV region. However, this spectrum modification did not demonstrate if the evolution of **RDC 49** in DMSO led to a simple degradation of the product or to a new product, imputable to DMSO coordination. That's why further investigations in DMSO- d^6 solution were undergone using ^1H NMR spectroscopy.

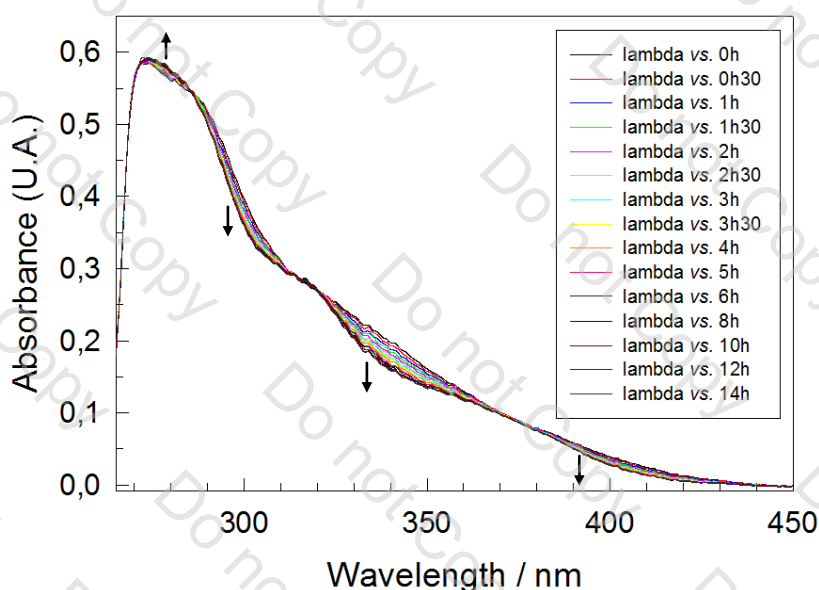


Figure 17: Evolution of **RDC 49** in DMSO monitored by UV/Vis

In a second study a sample of **RDC 49** (10mM, in DMSO- d^6) was prepared and its kinetic evolution was monitored by ^1H NMR spectroscopy (**Figure 18 and Figure 19**). Note again that in this kinetic model, the concentration of **RDC 49** is not relevant, because this model is 5 times less concentrated than stock solution used by biologists (50mM). This concentration was reduced to 10mM because approximately 30mg **RDC 49** would have been necessary to prepare one single NMR tube filled with 1mL DMSO- d^6 at 50mM. Although the model was not perfect, this depicted well the phenomenon.

^1H spectra were recorded at room temperature on a 500MHz spectrometer at regular time intervals ($t= 0, 0.5, 1, 2, 3, 4, 5, 6, 7$ and 9 hours). Evolution of **RDC 49** was quite stricken and exciting, given that no degradation was observed but another air stable compound was formed. **Figure 18** depicted the evolution of 2-phenylpyridine aromatic part, where ^1H signals were either shielded or deshielded, possibly due to substitution of MeCN ligand by DMSO. We will see later on, that this postulate can be easily demonstrated.

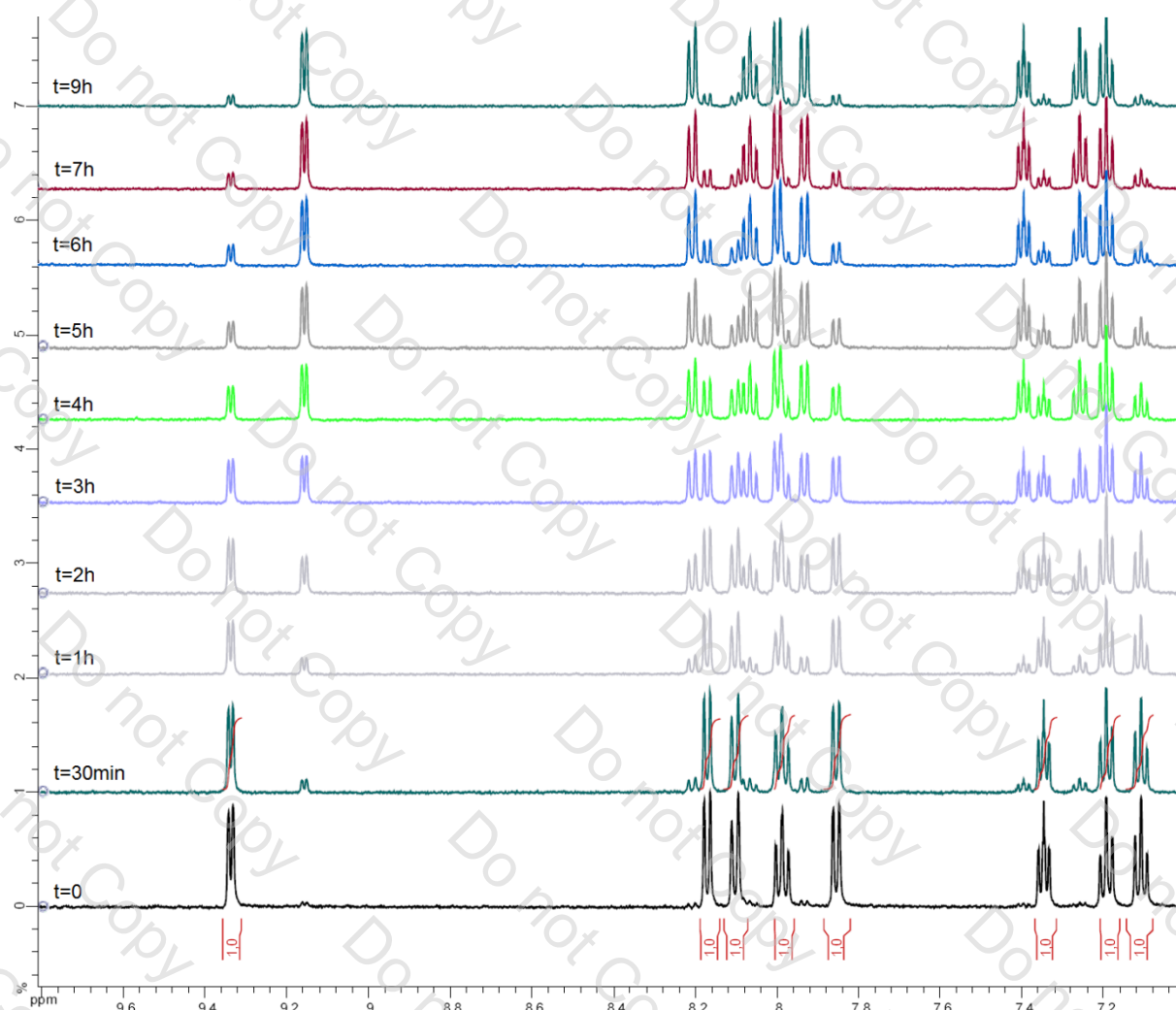


Figure 18: Kinetic of evolution of RDC 49 in DMSO-d⁶ (2-phenylpyridine part)

More interesting is the aliphatic part depicted in **Figure 19**. Modifications of the *isopropyl* Me signals from η^6 -*p*-cymene can be observed leading to a splitting of the signal ($\delta=0.86$ ppm) into two doublets (respectively $\delta=0.95$ and $\delta=0.70$ ppm). Moreover coordinated MeCN ($\delta=1.99$ ppm) **decoordinates**, leading to unligated **MeCN free solvent** ($\delta=2.07$ ppm). Note that Me signals from DMSO cannot be observed because the kinetic study was undertaken in DMSO-d⁶ solvent. However, DMSO is a highly hygroscopic solvent and this experiment does not allow one to be confident if coordinated MeCN is substituted by DMSO or water contained in it. Moreover, during *in vitro* assays, **RDC 49** is diluted in DMSO but is also in contact with a significant amount of water contained in cell culture media.

For this reason, a third experiment, using a standard addition of water, was undertaken in order to see if the addition of a known quantity of water could have an impact on the kinetics. Hence by *reductio ad absurdum*: if water has no impact on the substitution kinetics, it must be DMSO that substitutes the *a priori* labile MeCN.

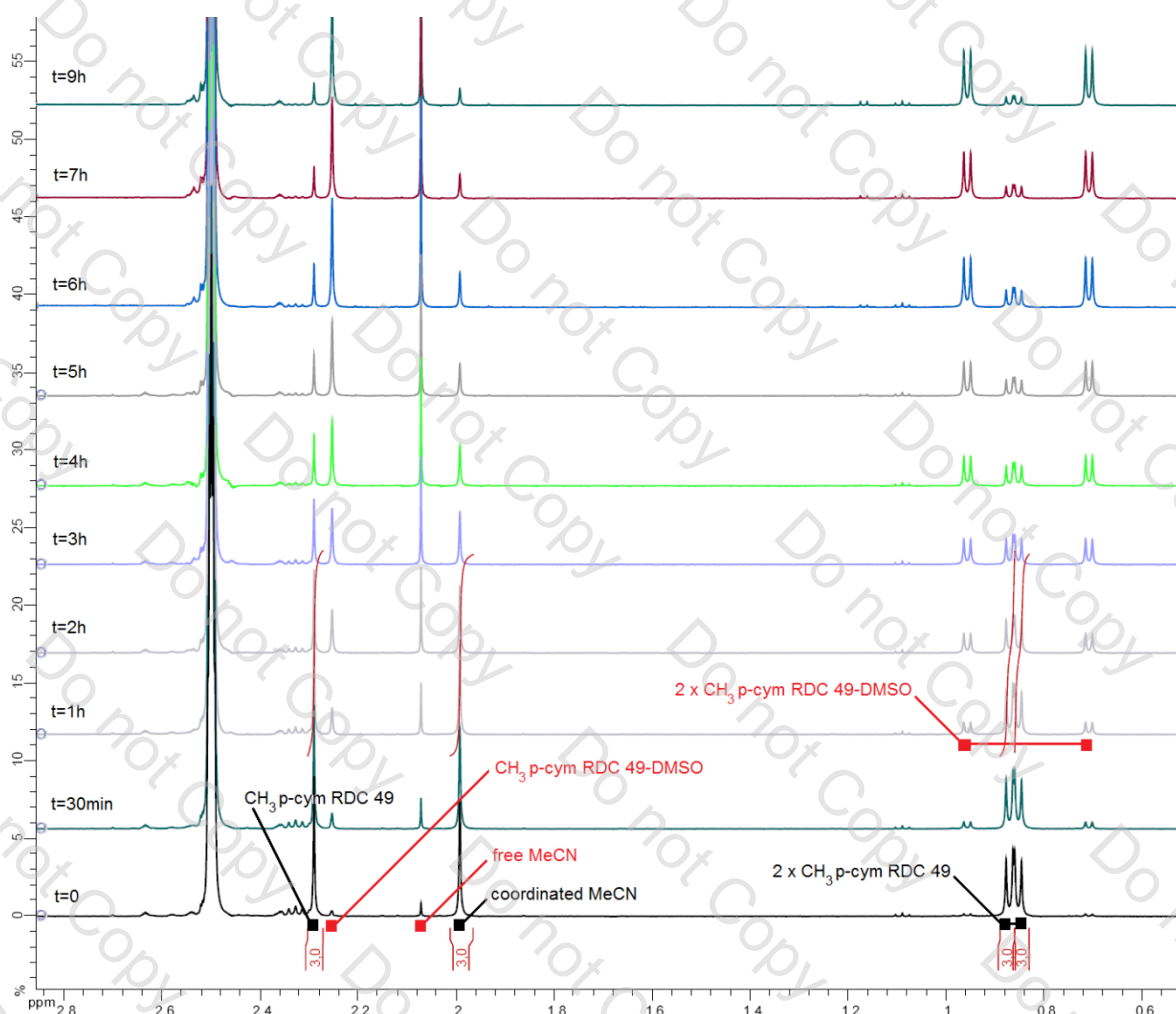


Figure 19: Kinetic study of RDC 49 in DMSO-d⁶ (aliphatic part)

In a third study three samples of **RDC 49** at 10mM in DMSO-d⁶ were prepared and their kinetic evolution was monitored by ¹H NMR spectroscopy. Keeping the whole concentration of **RDC 49** at 10mM, different amounts of water were added to the tubes (0%, 10%, 25% in volume). Notice that addition of 25% is the maximum water that can be added without disrupting the NMR signal. ¹H spectra were recorded at room temperature on a 500MHz spectrometer at regular time intervals (t= 0, 0.5, 1, 2, 3, 4, 5, 6, 7 and 9 hours).

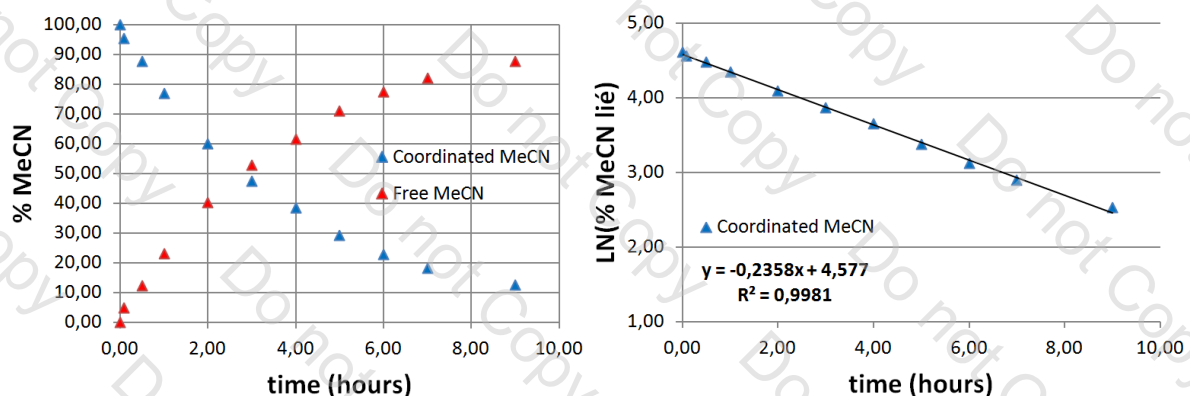


Figure 20: Evolution of RDC 49 in dry DMSO-d⁶ monitored by ¹H NMR spectroscopy at R.T.

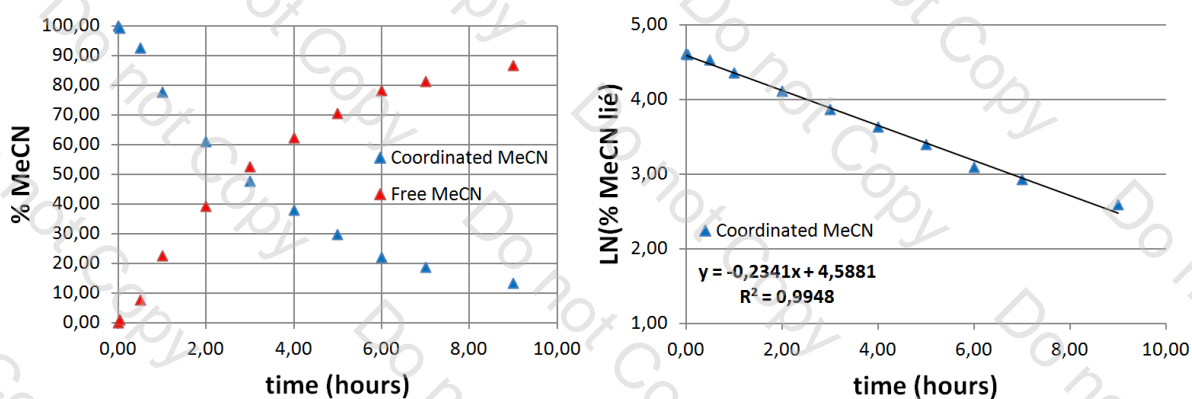


Figure 21: Evolution of RDC 49 in DMSO-d⁶ + 10% H₂O monitored by ¹H NMR spectroscopy at R.T.

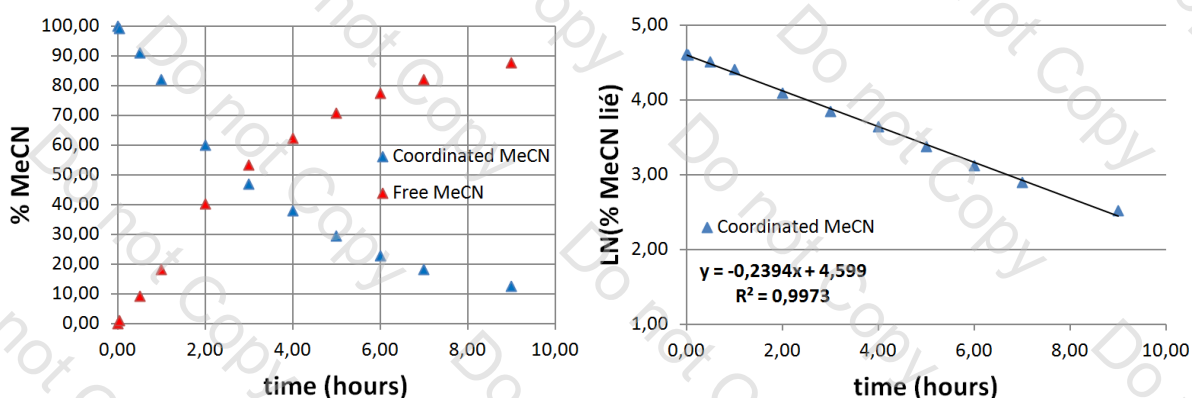


Figure 22: Evolution of RDC 49 in DMSO-d⁶ + 25% H₂O monitored by ¹H NMR spectroscopy at R.T.

The evolution of coordinated MeCN and free MeCN solvent (in relative percentages) is depicted in **Figure 20**, **Figure 21**, and **Figure 22** (left graphs). Obviously, comparison of the different spectra on the same graph (**Figure 23**), allows to see that addition of water (at least 10% and 25%) **does not have any impact on substitution kinetics**.

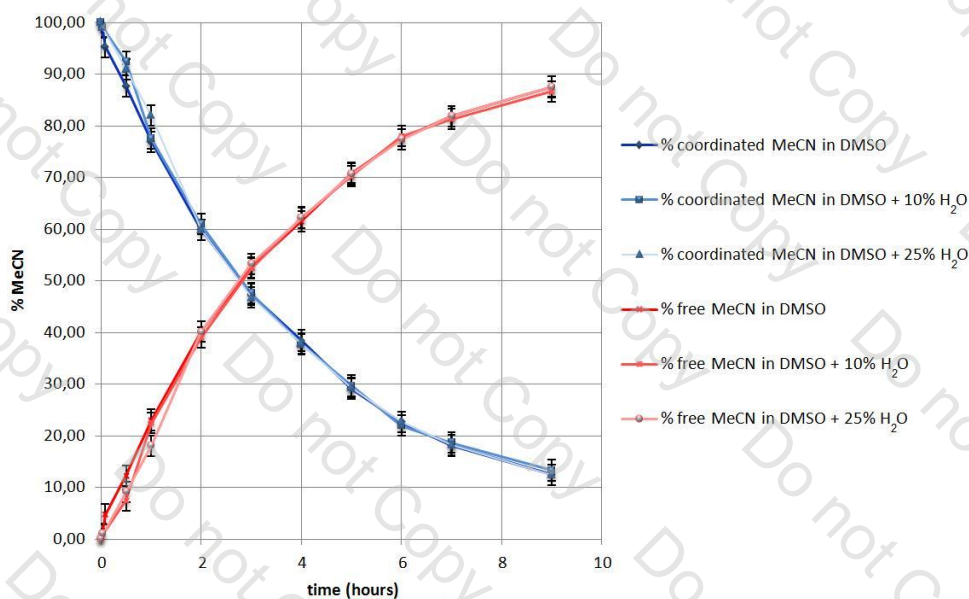


Figure 23: Comparative study on the evolution of RDC 49 at room temperature in the three different conditions

By *reductio ad absurdum*, **DMSO** substitutes the labile MeCN, hence forming a new air stable species **RDC 49-DMSO** (**Figure 24**). However, the coordination mode of DMSO (through the oxygen or sulphur atom) is not determined by this method, and the crystallization in DMSO did not produce single crystals suitable for X-ray diffraction.

The synthesis of this compound by another method (see **Chapter 2, 2.2.4.**) will once again demonstrate that the product **RDC 49-DMSO** is formed by substitution of acetonitrile by DMSO which is coordinated to the metal centre through the sulphur atom.

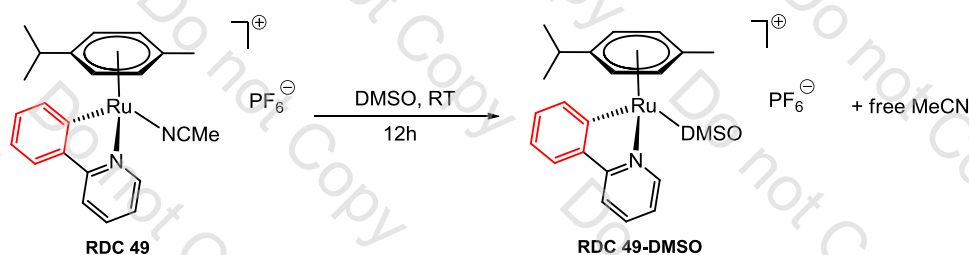
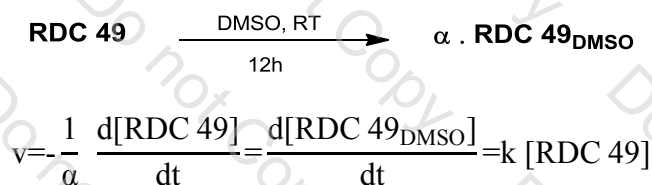


Figure 24: Spontaneous evolution of RDC 49 in DMSO

This kinetic study also enables determination of the kinetic constant at **room temperature** and the half-life of **RDC 49** in DMSO. Based on the general chemical equation, the kinetic law can be written:



Using the mass balance equation and the initial condition, this kinetic law can be easily integrated (supposing a first order reaction).

Mass balance equation:

$$\begin{array}{l} \text{at } t=0 \quad : \quad [\text{RDC 49}] = [\text{RDC 49}]_0 \qquad \qquad \qquad [\text{RDC 49}_{\text{DMSO}}] = 0 \\ \text{at } t \quad \quad : \quad [\text{RDC 49}] = [\text{RDC 49}]_0 - [\text{RDC 49}_{\text{DMSO}}] \end{array}$$

Integration of kinetic law:

$$\int_{t=0}^t \frac{d[\text{RDC 49}]}{[\text{RDC 49}]_0 - \alpha[\text{RDC 49}_{\text{DMSO}}]} = \int_{t=0}^t -\alpha \cdot k \cdot dt$$

$$\ln([\text{RDC 49}]_0 - \alpha[\text{RDC 49}_{\text{DMSO}}]) - \ln([\text{RDC 49}]_0) = -\alpha \cdot k \cdot t$$

$$\ln \frac{[\text{RDC 49}]_0}{[\text{RDC 49}]_0 - \alpha[\text{RDC 49}_{\text{DMSO}}]} = \alpha \cdot k \cdot t$$

The evolution of $\ln([\text{RDC } 49]) = f(t)$ also corresponding to the evolution of $\ln([\text{coordinated MeCN}])=f(t)$ is depicted in **Figure 20**, **Figure 21**, and **Figure 22** (right graphs). If representation of $\ln([\text{RDC } 49]) = f(t)$ is a straight line, this is a **first order reaction**.

In all cases, regression on the data gives a straight line with good correlation factor ($R^2 > 0.99$) Hence, the speed constant can be directly extrapolated from the slope of regression line with $\alpha=1$. At **room temperature**, the mean value of the kinetic constant is approximately:

$$k = 0.237 \pm 0.002 \text{ h}^{-1} = 14.22 \pm 0.12 \text{ min}^{-1}$$

Half-life:

with $\alpha=1$, the value of the half-life **at room temperature** can be directly extrapolated from the diagram (time after which initial concentration of **RDC 49** is divided by two) or precisely calculated:

$$\text{at } t_{1/2} : [\text{RDC } 49] = [\text{RDC } 49]_0 - [\text{RDC } 49]_{\text{DMSO}} = [\text{RDC } 49]_0/2$$

$$\ln \frac{[\text{RDC } 49]_0}{[\text{RDC } 49]_0/2} = \alpha \cdot k \cdot t_{1/2}$$

$$t_{1/2} = \frac{\ln(2)}{\alpha \cdot k}$$

with $\alpha=1$, the value of half-life **at room temperature**:

$$t_{1/2} \text{ at R.T.} = 2.924 \pm 0.020 \text{ h ,}$$

approximately $t_{1/2}$ at R.T. = 2h55min

Notice that $t_{1/2}$ increases when the sample is stored in a cold dark place at -15°C (**Figure 25**):

approximately $t_{1/2}$ at -15°C = 41h45min

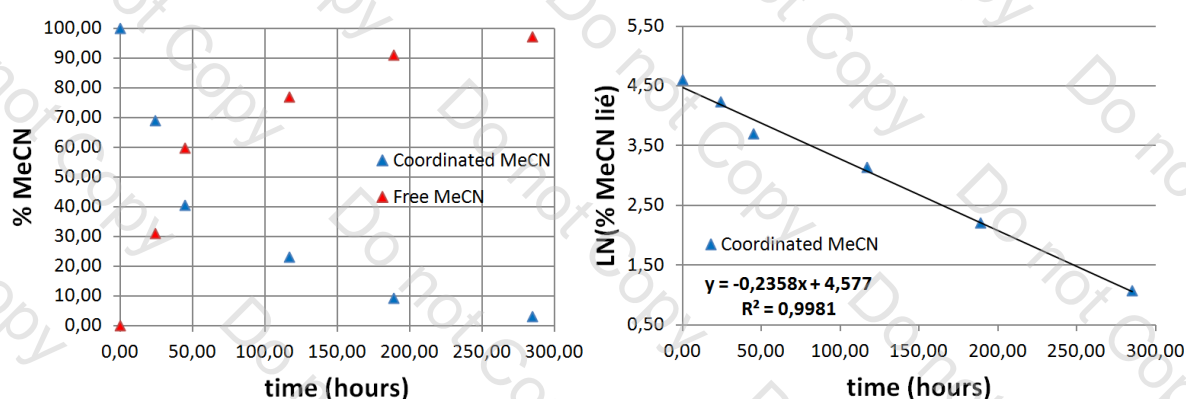


Figure 25: Evolution of RDC 49 in dry DMSO-d⁶ monitored by ¹H NMR spectroscopy at -15°C in a dark place

Thanks to this kinetic study, we found that in mono acetonitrile type complexes, the MeCN ligand is relatively labile and can exchange with DMSO. This study demonstrated by ^1H NMR spectroscopy in DMSO-d^6 , that significant modification of ruthenium arene type complexes could occur after approximately 3 hours at room temperature. Next step is the synthesis and evaluation of the anticancer properties of the newly formed **RDC 49-DMSO** in order to analyze the effect of MeCN substitution by DMSO on *in vitro* cell proliferation.

2.2.4. Synthesis and characterization of RDC 49-DMSO

A similar synthesis of compound closely related to **RDC 49**, in which the acetonitrile ligand was substituted by a chloride ion, was reported recently.^{32,33} This compound **RDC 49-Cl** $[\text{Ru}(o\text{-C}_6\text{H}_4\text{py-}\kappa\text{C,N})(p\text{-cym})(\text{Cl})]$ was obtained by reaction between 2-phenylpyridine and the dimer $[\eta^6\text{-}(p\text{-cymene})\text{RuCl}(\mu\text{Cl})_2]$ in the presence of sodium acetate in dichloromethane at room temperature for 4h (**Figure 26**).

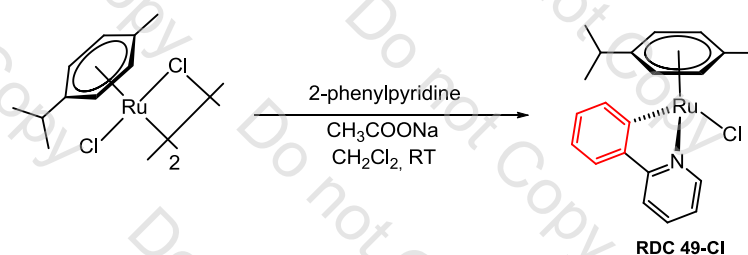


Figure 26: Synthesis of RDC 49-Cl

Silver hexafluorophosphate is a commonly encountered reagent in inorganic and organometallic chemistry which is used to replace halide ligand with the weakly coordinating hexafluorophosphate anion. The abstraction of the halide is driven by the precipitation of the appropriate silver halide. Hence, **RDC 49-DMSO** $[\text{Ru}(o\text{-C}_6\text{H}_4\text{py-}\kappa\text{C,N})(p\text{-cym})(\text{DMSO})]\text{PF}_6$ was obtained through reaction between **RDC 49-Cl** $[\text{Ru}(o\text{-C}_6\text{H}_4\text{py-}\kappa\text{C,N})(p\text{-cym})(\text{Cl})]$ with silver hexafluorophosphate (AgPF_6) in dichloromethane and one equivalent of DMSO (**Figure 27**).

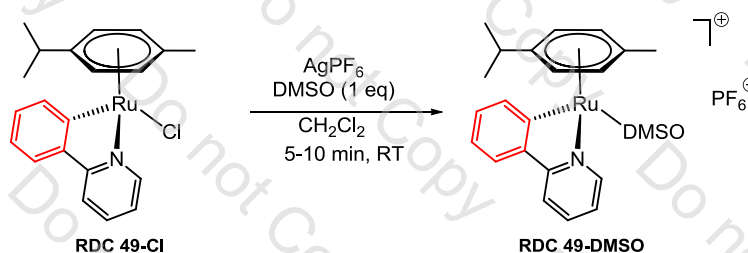


Figure 27: Synthesis of RDC 49-DMSO

The rapid abstraction of halide (5-10min) at room temperature afforded discolouration of the yellow reaction medium yielding to a beige solution and a precipitate of white crystalline AgCl. Filtration over celite, then evaporation followed by recrystallization in dichloromethane/pentane afforded the desired air stable compound.

^1H NMR spectroscopy of the newly synthesized compound was performed in CDCl_3 but also in DMSO-d^6 in order to make a comparison with evolved **RDC 49** in DMSO and its **RDC 49-DMSO** congener (**Figure 28** and **Figure 29**).

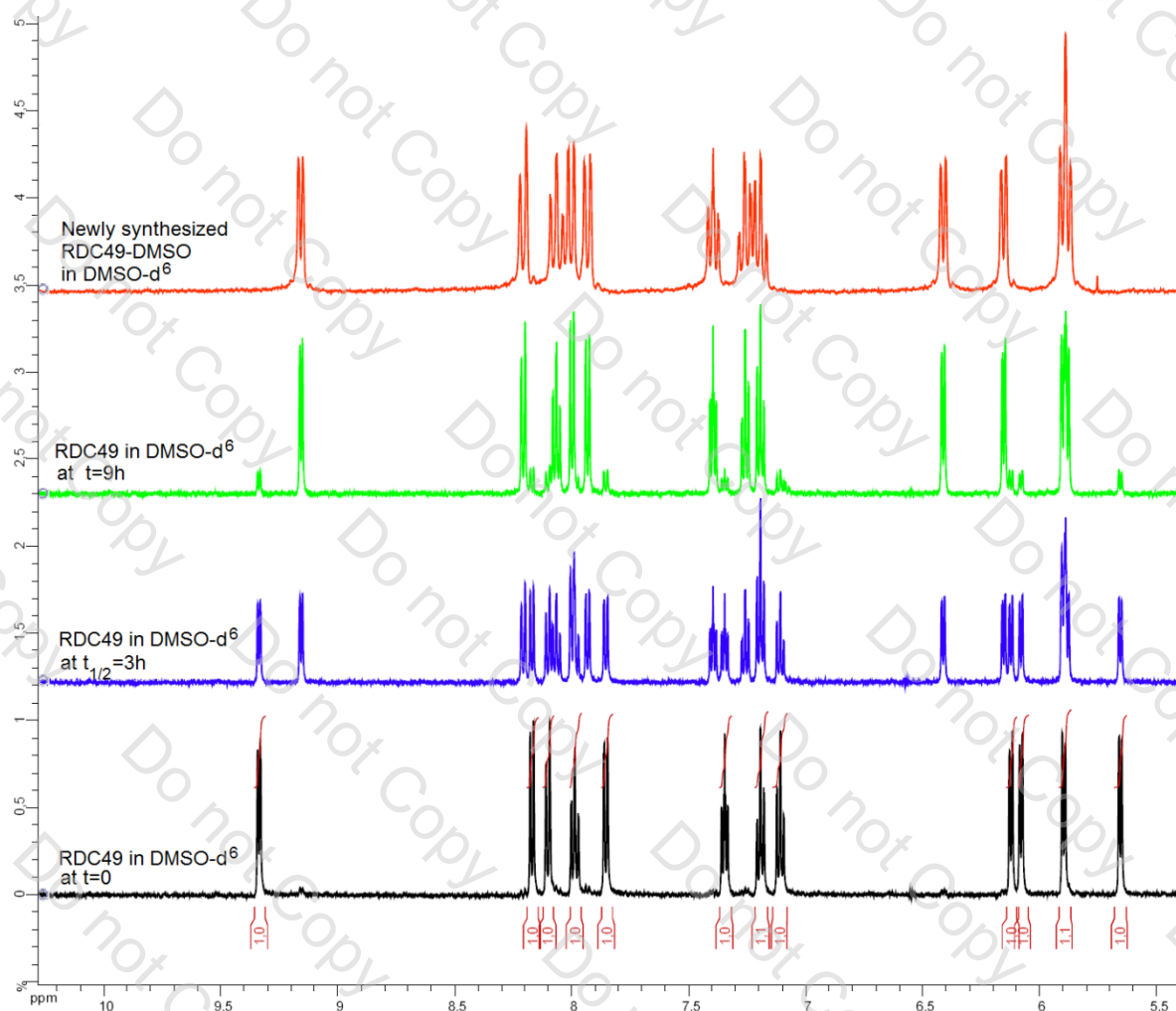


Figure 28: Comparison between **RDC 49-DMSO** and evolved **RDC 49** in DMSO-d^6 (aromatic part)

In these spectra, comparison between **RDC 49** in DMSO-d^6 at time $t=0$, $t_{1/2}=3\text{h}$ and $t=9\text{h}$ and newly synthesized **RDC 49-DMSO** demonstrated again that **DMSO** substitutes the labile MeCN, hence forming a new air stable specie **RDC 49-DMSO**.

The evolution of the 2-phenylpyridine protons ($\delta=7.1\text{-}9.4$ ppm), and of the aromatic part of η^6 -*p*-cymene protons ($\delta=5.6\text{-}6.2$ ppm) fits perfectly with the **RDC 49-DMSO** model (**Figure 28**).

As previously described, important modifications of the methyl (Me) signals from η^6 -*p*-cymene (**Figure 29**) can be observed leading to a splitting of the signal ($\delta=0.86$ ppm) into two doublets (respectively $\delta=0.95$ and $\delta=0.70$ ppm). The proton at $\delta=2.29$ ppm in **RDC 49** shielded to $\delta=2.25$ **RDC 49-DMSO** can be easily attributed to the last Me signal from η^6 -*p*-cymene. Notice that the two methyl groups from coordinated DMSO ($\delta=2.12$ ppm and $\delta=2.75$ ppm) can be now observed in **RDC 49-DMSO**.

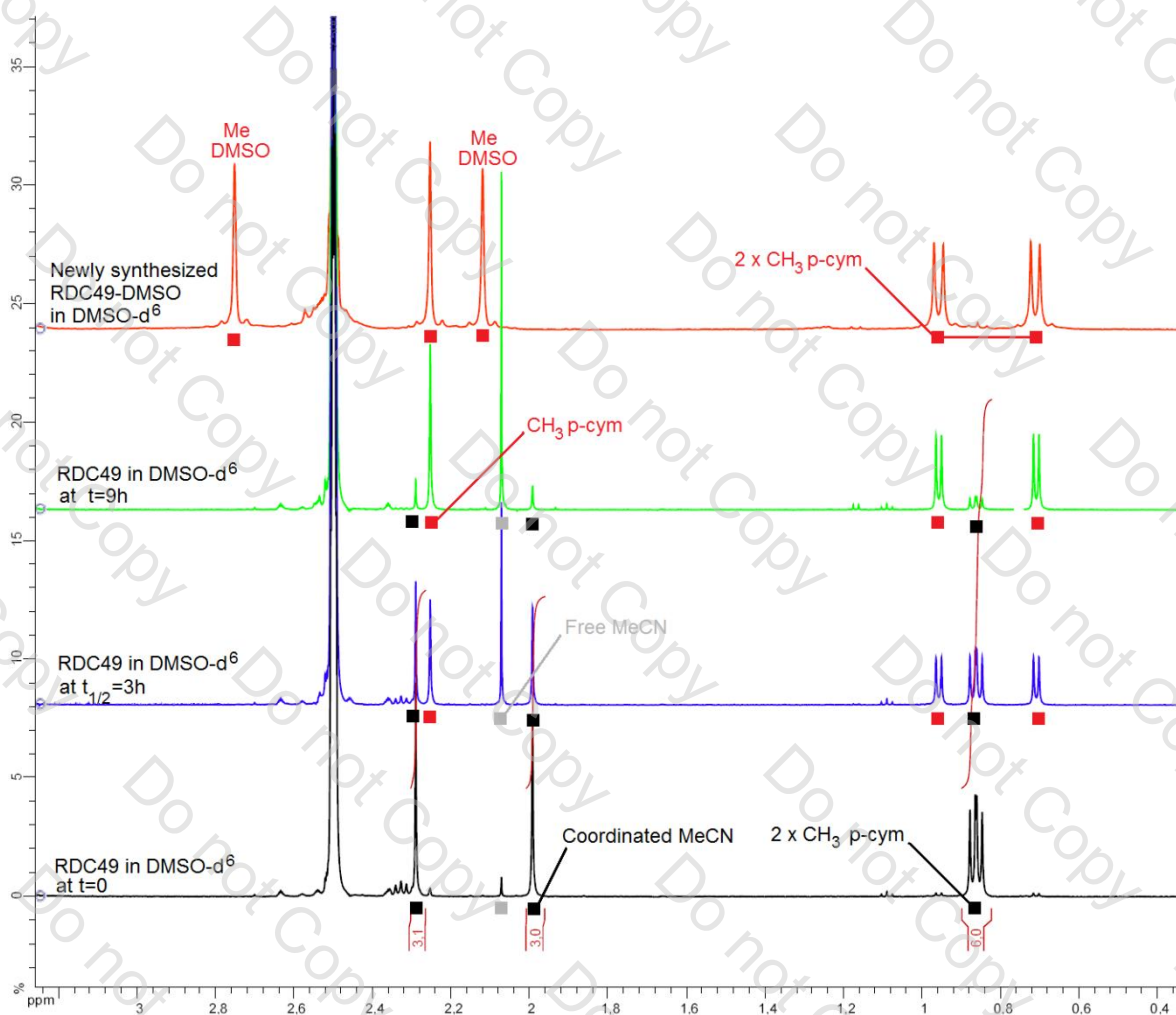


Figure 29: Comparison between RDC 49-DMSO and evolved RDC 49 in DMSO- d^6 (MeCN part)

To complement the study, we therefore ascertained the structure of this class of piano-stool cycloruthenated complexes by performing a three-dimensional structure determination using X-ray diffraction study on single crystals of **RDC 49** and **RDC 49-DMSO**. The results of this study confirm the structure of both complexes (**Figure 30**). Notice that for **RDC 49-DMSO**, DMSO is coordinated to the metal centre through sulphur atom and there are two molecules per asymmetric unit.

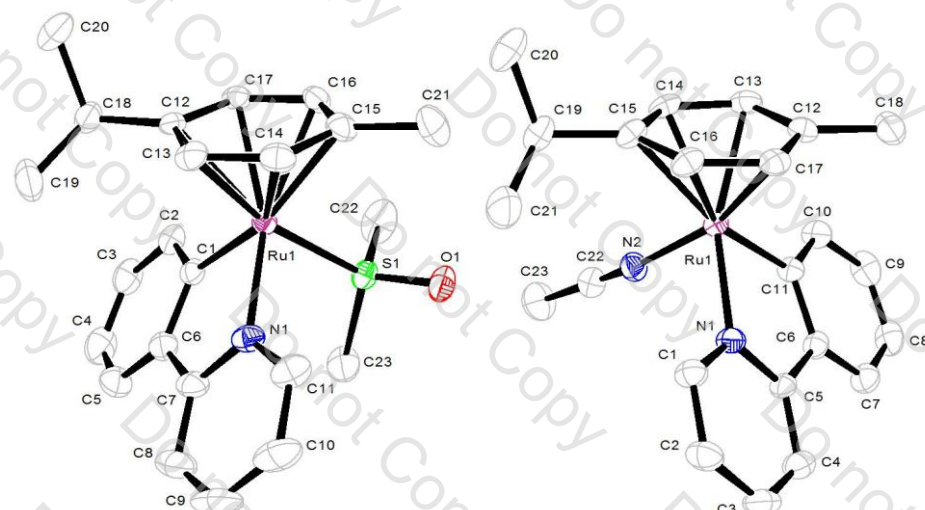


Figure 30: ORTEP diagram of the molecular structure of RDC 49-DMSO (left) and RDC 49 (right). Ellipsoids are drawn at a probability level of 50%. Hydrogen atoms, counter anions and solvent have been omitted for clarity.

	RDC 49-DMSO	RDC 49
Compound reference	RDC 49-DMSO	RDC 49
Chemical formula	$C_{23}H_{28}NORuS \cdot F_6P$	$C_{23}H_{25}N_2Ru \cdot F_6P$
Formula Mass	612.56	575.49
Crystal system	Monoclinic	Monoclinic
$a/\text{\AA}$	8.9594(6)	26.1284(11)
$b/\text{\AA}$	12.4581(9)	10.2866(2)
$c/\text{\AA}$	44.200(3)	9.0901(4)
$\alpha/^\circ$	90.00	90.00
$\beta/^\circ$	90.1900(10)	106.625(2)
$\gamma/^\circ$	90.00	90.00
Unit cell volume/ \AA^3	4933.4(6)	2341.04(15)
Temperature/K	173(2)	173(2)
Space group	$P21/c$	C2
No. of formula units per unit cell, Z	8	4
No. of reflections measured	32709	8662
No. of independent reflections	11770	5089
R_{int}	0.0218	0.0368
Final R_f values ($I > 2\sigma(I)$)	0.0571	0.0259
Final $wR(F^2)$ values ($I > 2\sigma(I)$)	0.1292	0.0710
Final R_f values (all data)	0.0598	0.0289
Final $wR(F^2)$ values (all data)	0.1301	0.0900

Table 3: Details for the X-ray crystal structure determination of RDC 49-DMSO and RDC 49

RDC 49-DMSO		RDC 49	
C1 – Ru1	2.050(4)	C11 – Ru1	2.052(3)
C12 – Ru1	2.260(4)	C12 – Ru1	2.213(4)
C13 – Ru1	2.235(4)	C13 – Ru1	2.191(4)
C14 – Ru1	2.259(5)	C14 – Ru1	2.193(3)
C15 – Ru1	2.318(4)	C15 – Ru1	2.307(3)
C16 – Ru1	2.229(4)	C16 – Ru1	2.269(3)
C17 – Ru1	2.212(4)	C17 – Ru1	2.192(3)
N1 – Ru1	2.074(4)	N1 – Ru1	2.088(3)
S1 – Ru1	2.2743(12)	N2 – Ru1	2.063(3)
C1 – Ru1 – N1	78.49(17)	C11 – Ru1 – N1	78.25(13)
C1 – Ru1 – S1	87.30(13)	C11 – Ru1 – N2	85.06(15)
N1 – Ru1 – S1	86.38(11)	N1 – Ru1 – N2	88.01(13)
Ru1 – C1 – C6	115.2(3)	Ru1 – C11 – C6	115.7(2)
C1 – C6 – C7	115.2(4)	C11 – C6 – C5	115.0(3)
C6 – C7 – N1	113.7(4)	C6 – C5 – N1	113.7(3)
C7 – N1 – Ru1	116.8(3)	C5 – N1 – Ru1	117.2(2)

Table 4: Selected bond length (\AA), angles ($^\circ$) for RDC 49-DMSO and RDC 49

2.2.5. Cytotoxic activity of RDC 49 vs. RDC 49-DMSO

The antitumour potential of **RDC 49**, **RDC 49-Cl**, and **RDC 49-DMSO** has been evaluated by measuring their effects on the cell proliferation of A172 cell line. The cells were treated with different doses of complexes and after 48h the viability of the cells was determined by measuring the mitochondrial succinic hydrogenase activity on the remaining living cells. The IC₅₀ results were compared to those obtained with the previously reported **RDC 11** at 5μM (**Figure 31**).

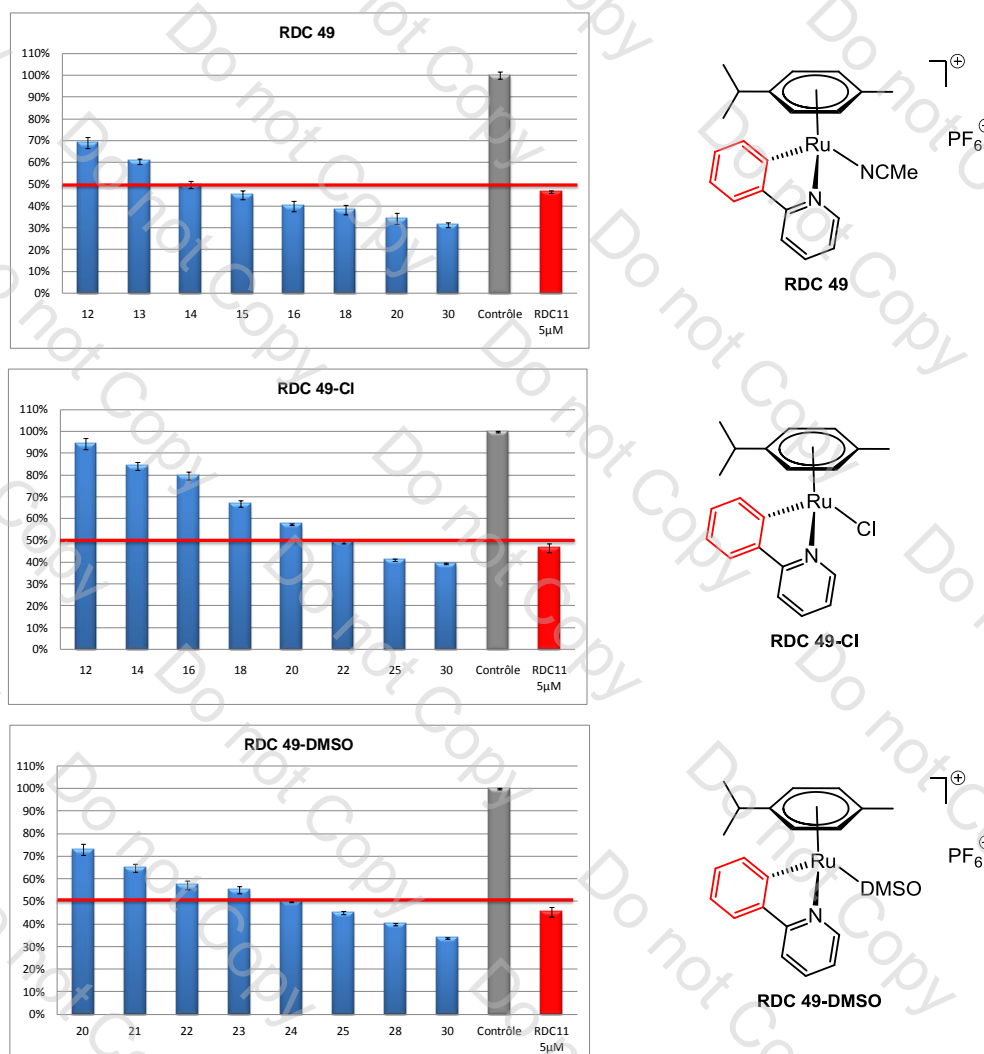


Figure 31: Impact of substitution of MeCN by DMSO on the antiproliferative activity (A172 glioblastoma cell line)

As previously, A172 cells were grown in 96-wells plates. At 70% confluence, cells were treated 48h with **RDC** compounds at the indicated concentrations. The number of cells was assessed by MTT test. Results are presented as percentage compared with the control condition. Graphs represent mean values with standard deviation of eight wells from one experiment out of three independent experiments. The thick red line corresponds to 50% cells viability (IC₅₀).

<i>ODCs compounds</i>	<i>IC₅₀ A172 (μM)</i>
RDC 49	14 ± 1.0
RDC 49-Cl	22 ± 1.0
RDC 49-DMSO	24 ± 1.0

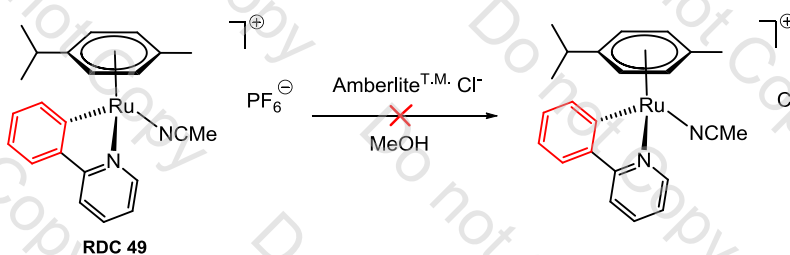
Table 5: Recapitulative table of the IC₅₀ values on an A172 cell line

As expected, **RDC 49-DMSO** displays a lower antiproliferative effect than **RDC 49**. That's why biologists were faced with non-reproducible *in vivo* and *in vitro* measurements with these piano-stool cycloruthenated complexes.

Effect of the lipophilicity and of the red-ox potential will be thoroughly discussed in **Chapter 4**. However, the higher IC₅₀ of **RDC 49-DMSO** compared to the **RDC 49** is no imputable to the lower lipophilicity (which is practically the same), but is possibly due to the increase of **red-ox potential**: E°_{1/2} (**RDC 49**) = 1244mV and E°_{1/2} (**RDC 49-DMSO**) = 1470mV. Moreover, even if **RDC 49-Cl** seems to have a good red-ox potential to interfere with oxidoreductase enzymes, E°_{1/2} (**RDC 49-Cl**) = 753mV, this neutral compound is water soluble and hence does not display enough lipophilicity to cross the membrane of malignant cells.

2.2.6. Exchange of the counter ion PF₆⁻ vs. Cl⁻ in RDC 49

In order to avoid the use of DMSO that rapidly substitutes the weakly bound MeCN ligand, the idea was to exchange the lipophilic PF₆⁻ counter ion for Cl⁻ on an Amberlite^{T.M.} ion exchange resin affording the water soluble compound [Ru(*o*-C₆H₄py-κC,N)(*p*-cym)(MeCN)]Cl (**Figure 32**). Metathesis procedure was recently reported by van Koten *et al.*³⁵ for planar-chiral ruthenium-palladium compounds with pincer ligand.

Figure 32: Supposed anion-exchange (metathesis) of PF₆⁻ for Cl⁻ in RDC 49

However, in the case of **RDC 49**, metathesis of PF₆⁻ for Cl⁻ occurs but substitution of MeCN by Cl (producing the unexpected neutral **RDC 49-Cl**) also takes place, illustrating once again that in the case of mono-acetonitrile complexes, the MeCN is weakly bound to the metal centre (**Figure 33**). Structure elucidation of newly formed product is easily done by comparison of ¹H NMR spectra of **RDC 49** after Amberlite^{T.M.} treatment with the **RDC 49-Cl** (**Figure 34**).

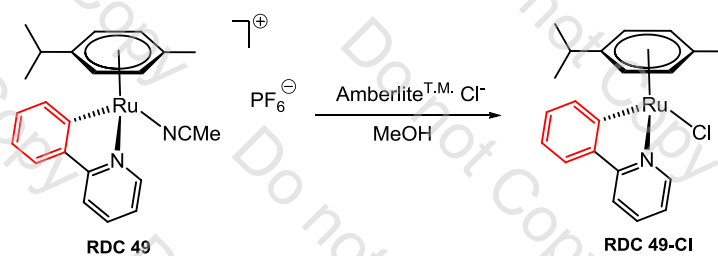


Figure 33: Formation of RDC 49-Cl after Amberlite^{T.M.} treatment

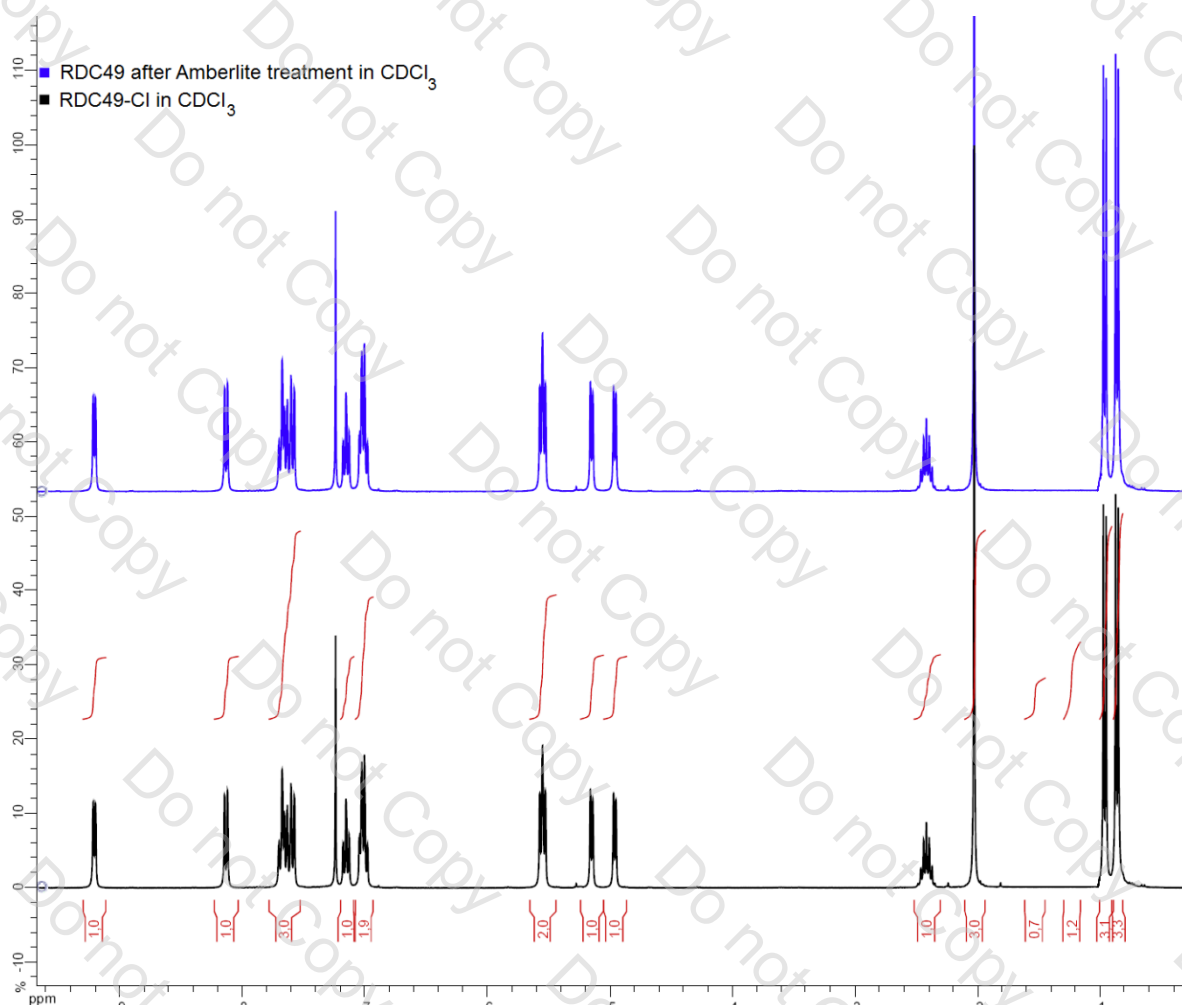


Figure 34: Comparison between RDC 49-Cl and RDC 49 after Amberlite^{T.M.} treatment

2.2.7. Conclusion

Following this study, we have been able to reveal the non-reproducibility of *in vivo* and *in vitro* measurements. Indeed, biologists were either preparing a new solution directly injected into the animal or were using an already prepared stock solution of the compound dissolved in DMSO. Since we are now convinced, that in a relative short time, the MeCN ligand can exchange with DMSO in a stock solution, a new injection protocol and/or formulation must be developed to obtain representative results of the initial composition of the solution.

2.3. Chirality induction in RDC 11 lead compound

2.3.1. Introduction: importance of chirality in everyday science

In the XXth century, stereochemistry has reached a high degree of sophistication, especially in the synthesis of natural compounds, which often comprise a large number of stereogenic centres. In the past 40 years, enantioselective catalysis has been added to the arsenal of methods yielding to many enantiopure compounds, especially those for **pharmaceutical applications**.

The field of chiral drugs has become a multibillion-euro business since the importance of the correct absolute configuration of compounds that interact with the chiral molecular environment in our body, was realized some decades ago. Indeed, many drugs consist of chiral molecules and usually at biological level, two **enantiomers** of a molecule may display different physiological effects, even **antagonistic** ones.

A historic example was the withdrawal of thalidomide from the market because of its unexpected teratogenic side effects.³⁶ Thalidomide was clinically used as a sedative in the late 1950's and it was later demonstrated that one of the enantiomers of thalidomide, exhibited anti-emetic activity while the other one can cause foetal damage.

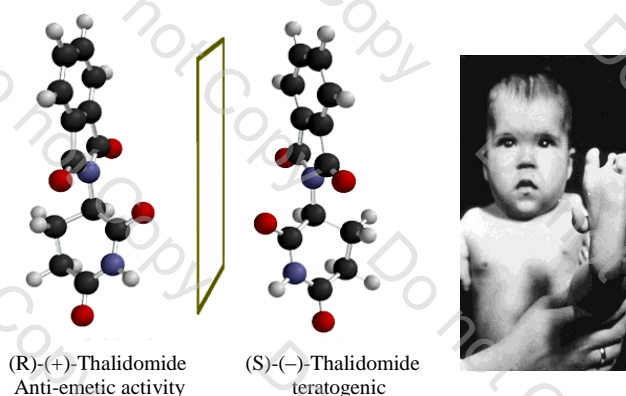


Figure 35: The two enantiomers of Thalidomide

Thus, the US Food and Drug Administration (F.D.A.) recommends that in the case of chiral molecules, the properties – particularly toxicity – of both enantiomers should be studied, which implies the total resolution of the racemates. The lead compound **RDC 11** is chiral and obtained under two non-separable enantiomeric forms **RDC 11 (Δ isomer)** and **RDC 11 (Λ isomer)** (Figure 36). In an attempt to verify the bioactivity of each form in cell lines, and also to verify the toxicity *in vivo*, different strategies using either asymmetric synthesis or chiral resolution were undertaken to separate the two enantiomers of **RDC 11**.

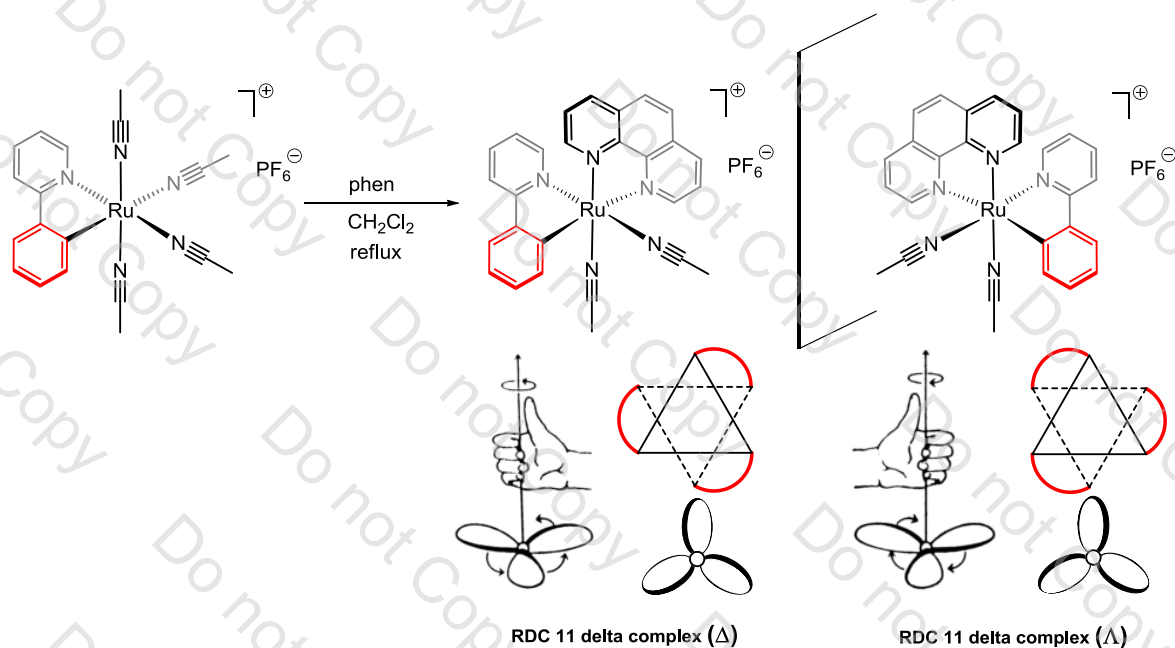


Figure 36: The two enantiomers of RDC 11

2.3.2. Synthesis of RDC 8*

Enantiopure synthesis can be achieved by introducing chirality centers with an α -pinene group in the framework of 2-phenylpyridine. Hence, the pinene-2-phenylpyridine (mppy) is prepared by Krönke-type synthesis depicted in **Figure 37**.

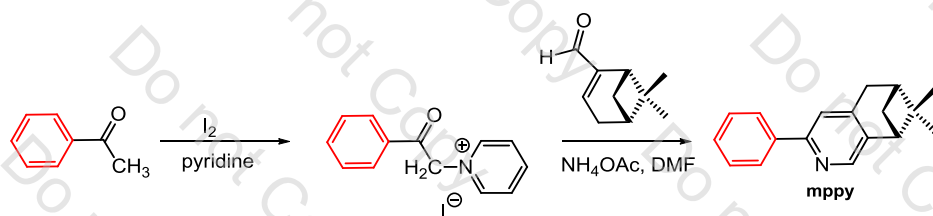


Figure 37: Synthesis of chiral pinene-2-phenylpyridine

The synthesis of **RDC 11*** precursor, was achieved with dimer starting material $[\eta^6\text{-}(\text{C}_6\text{H}_6)\text{RuCl}(\mu\text{Cl})_2]$ in presence of NaOH and KPF_6 . Following a similar procedure,²⁰ lemon yellow **RDC 8*** $[\text{Ru}(\text{pinene-}o\text{-C}_6\text{H}_4\text{py-}\kappa\text{C,N})(\text{NCMe})_4]\text{PF}_6$, unstable in the air (its colour changing gradually yellowish green and then dark green), can be obtained in a good yield. Notice that during the formation of **RDC 8***, a synthetic air stable intermediate $[\text{Ru}(\eta^6\text{-}(\text{C}_6\text{H}_6))(\text{pinene-}o\text{-C}_6\text{H}_4\text{py-}\kappa\text{C,N})(\text{NCMe})]\text{PF}_6$ in which η^6 -benzene unit is not substituted by the MeCN ligand can be easily isolated and identified by ^1H NMR spectroscopy (**Figure 38**). In this case, the η^6 -benzene unit was weakly bound to ruthenium metallic centre, as prolonged reflux up to 48h led to the substitution of arene unit by MeCN.

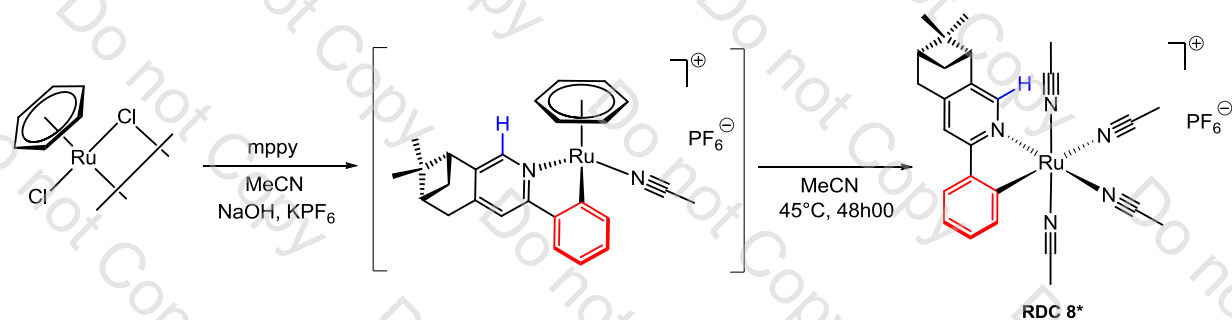


Figure 38: Synthesis of RDC 8* bearing a cyclometalated chiral phenylpyridine

Kinetic study of the reaction allows demonstration of the formation of this synthetic intermediate (η^6 -(C₆H₆))(pinene-*o*-C₆H₄py- κ C,N)(NCMe)]PF₆. The reaction was followed by ¹H NMR spectroscopy, based on the integration of the proton in α position to the nitrogen (depicted in blue, **Figure 38**) for the (η^6 -(C₆H₆))(pinene-*o*-C₆H₄py- κ C,N)(NCMe)]PF₆ (δ =8.75 ppm), the **RDC 8*** (δ =8.39 ppm) and for the free chiral ligand mppy (δ =8.18 ppm).

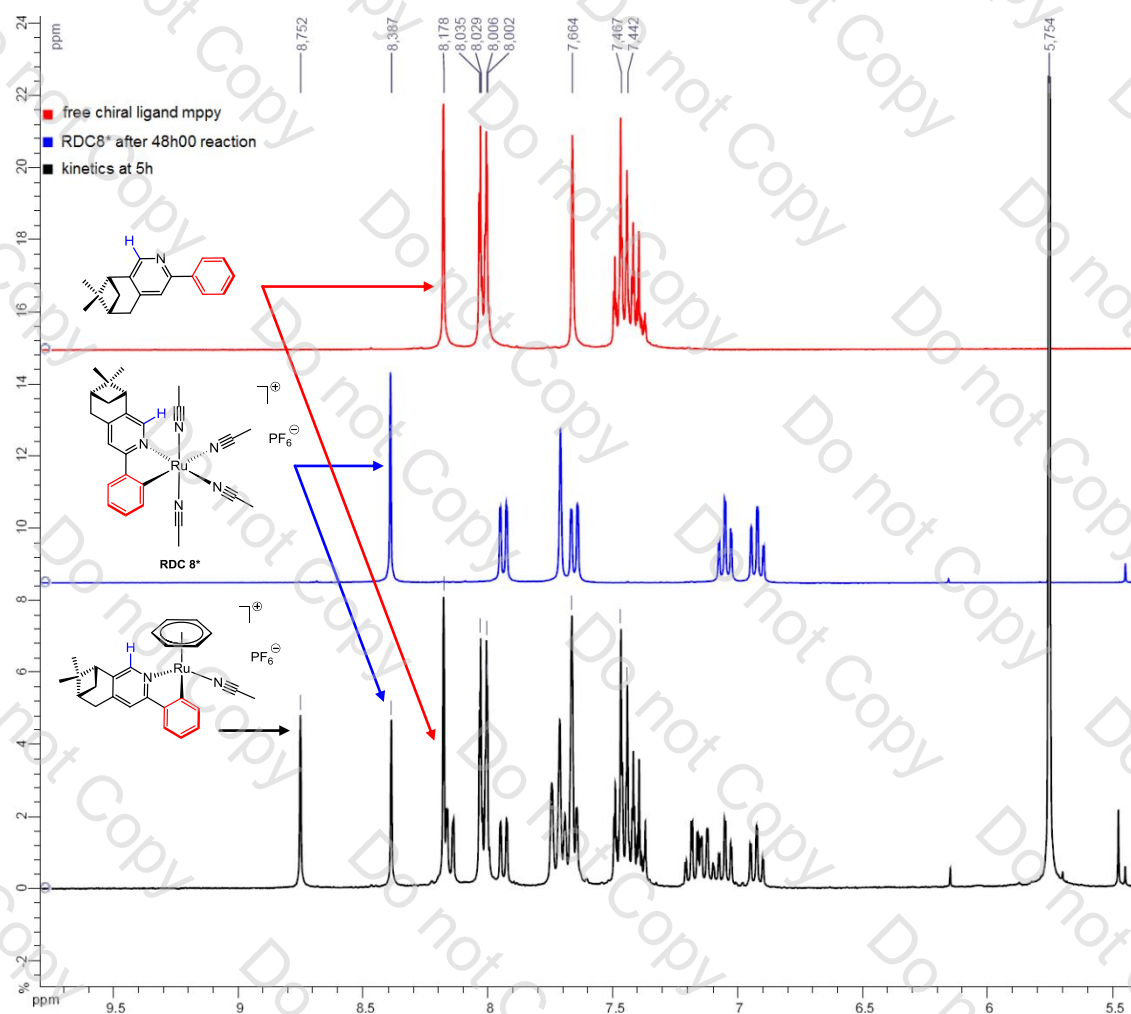


Figure 39: Kinetic evolution of cyclometallation after 5h (black), 48h (blue) and free chiral ligand mppy (red)

^1H spectra were recorded at regular time intervals on a 300MHz spectrometer and the evolution of the different species (% free ligand, % intermediate, % **RDC 8*** and % overall ortho-metalation) in reactive medium is depicted in **Figure 40**. Hence, synthesis of **RDC 8*** compound containing three MeCN ligands was achieved with an optimized reaction time of 48h at 45°C.

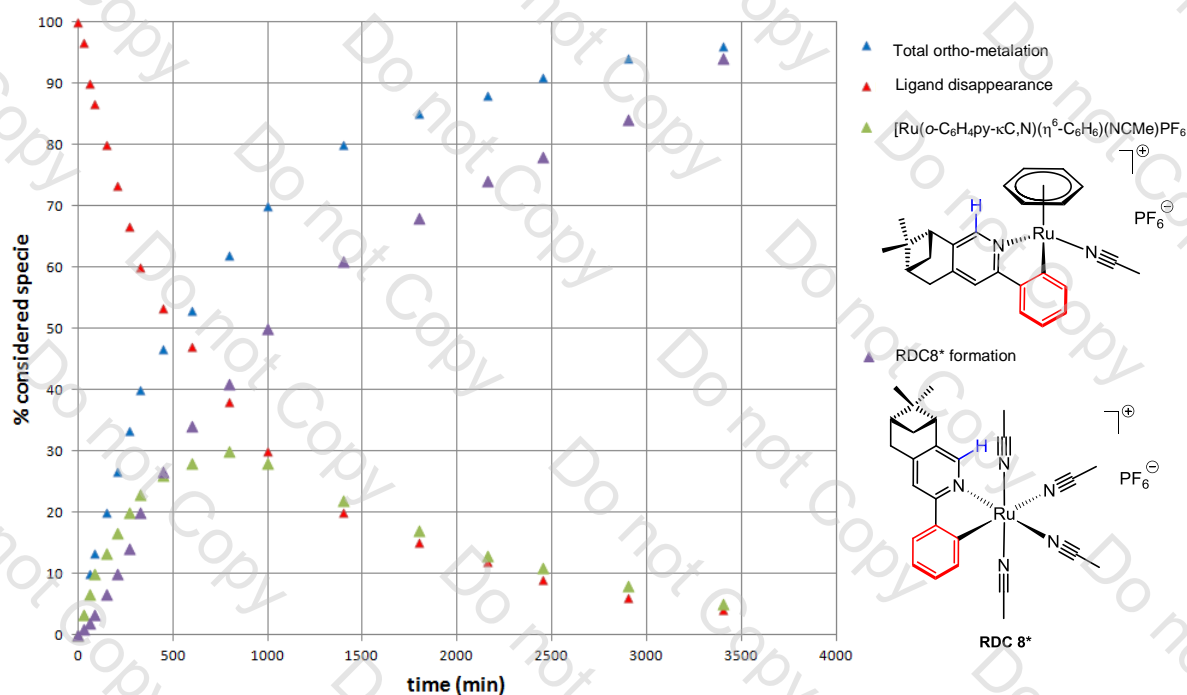


Figure 40: Kinetic study of cyclometallation at 45°C

2.3.3. Synthesis and separation of RDC 11* isomers

Further complexation of **RDC 8*** ligand with 1,10-phenanthroline as bidentate ligand should afford optically pure **RDC 11***. General feature of the **RDC 11*** should be in agreement with X-ray structural characterization on **RDC 11** obtained previously by the laboratory³⁷ *i.e.* a *cis* configuration of the MeCN ligands and the fact that one of the phenanthroline nitrogen is located *trans* to the σ metal-carbon bond.

After 1h, a mixture of *trans* (to the σ metal-carbon bond) isomers was obtained in a 2/3:1/3 ratio due to the presence of α -pinene (**Figure 41**).

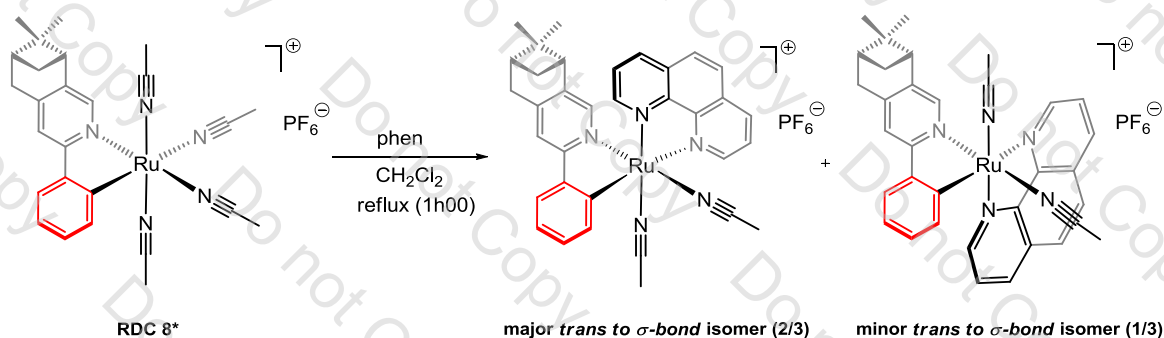


Figure 41: RDC 11* trans diastereomers obtained after 1h reaction

The ratio of *trans* isomers can be easily calculated by direct integration of the methyl groups of the α -pinene unit (**Figure 42**). Repartition of the two isomers is likely due to poor steric hindrance of the α -pinene unit, which is too far from the metallic centre to get one single compound.

Indeed, kinetic studies during the first hour of the reaction demonstrated that the diastereomer ratio (2/3:1/3) of *trans* isomers remains the same, suggesting that these two species are formed at the same time. Moreover, these two species are not in equilibrium given that, neither variable temperature NMR experiments, nor irradiation of methyl group of one diastereomer had an impact on the distribution ratio.

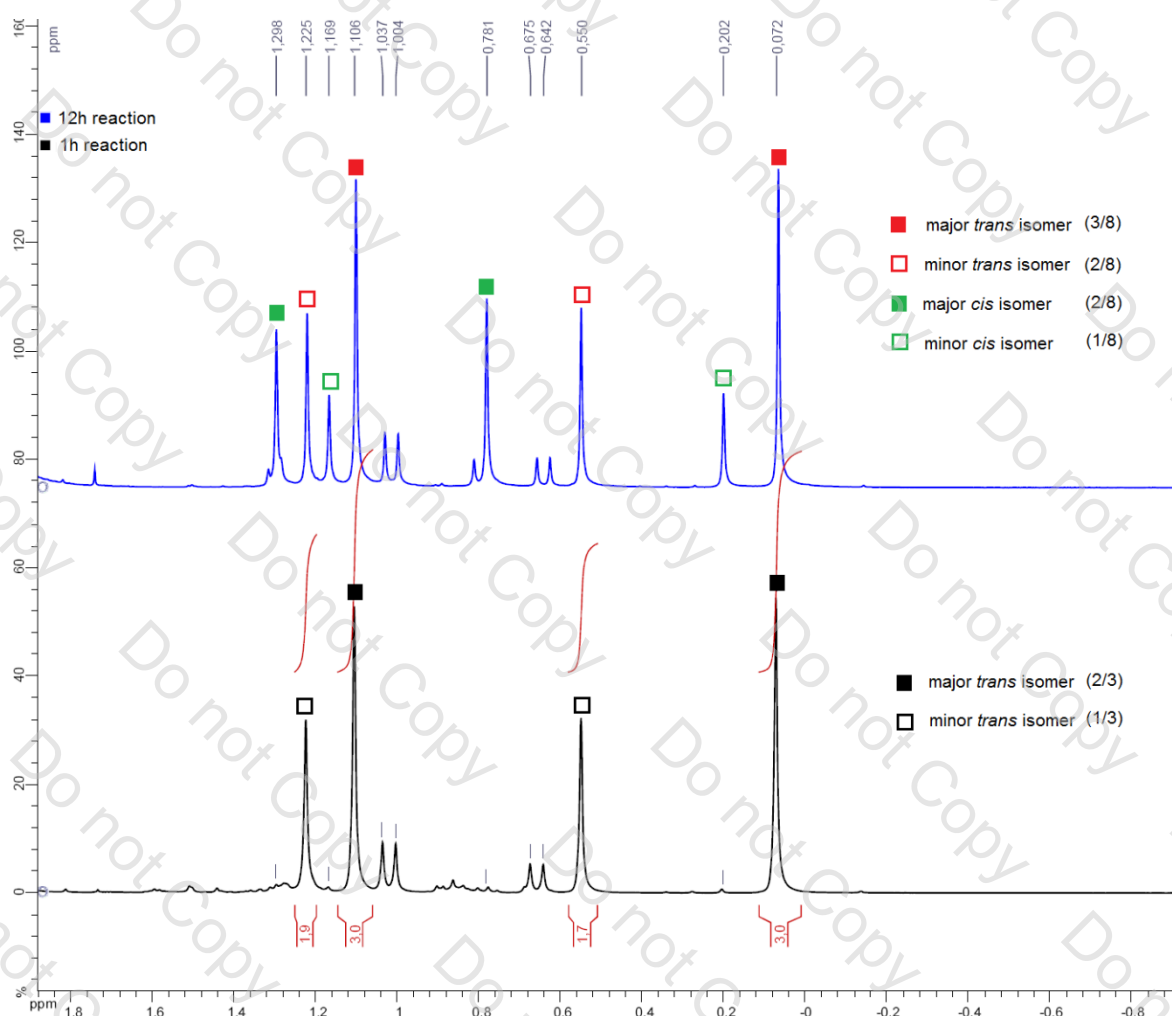


Figure 42: Effect of reaction time on the distribution of isomers (aliphatic part)

After more than 1h, the reactive medium begins to become more complex, leading to a mixture of *trans* and *cis* configuration isomers (**Figure 44**). After 12h, the ratio of *trans* and *cis* isomers can be easily calculated by direct integration of the methyl groups of the α -pinene unit (**Figure 42**). Notice also the appearance of new peaks (highlighted in green, **Figure 43**) in the aromatic part corresponding to the *cis* isomers after 12h.

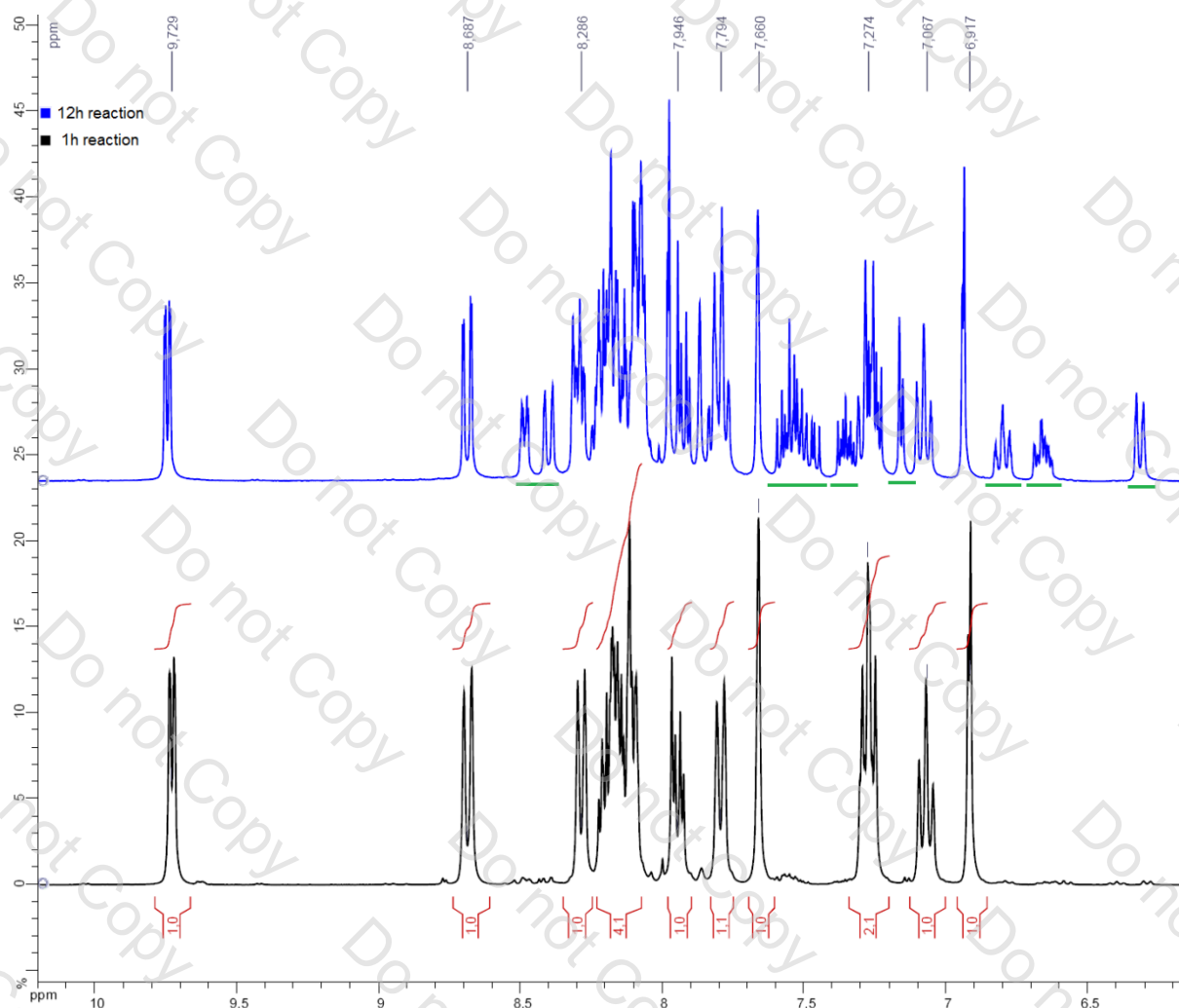
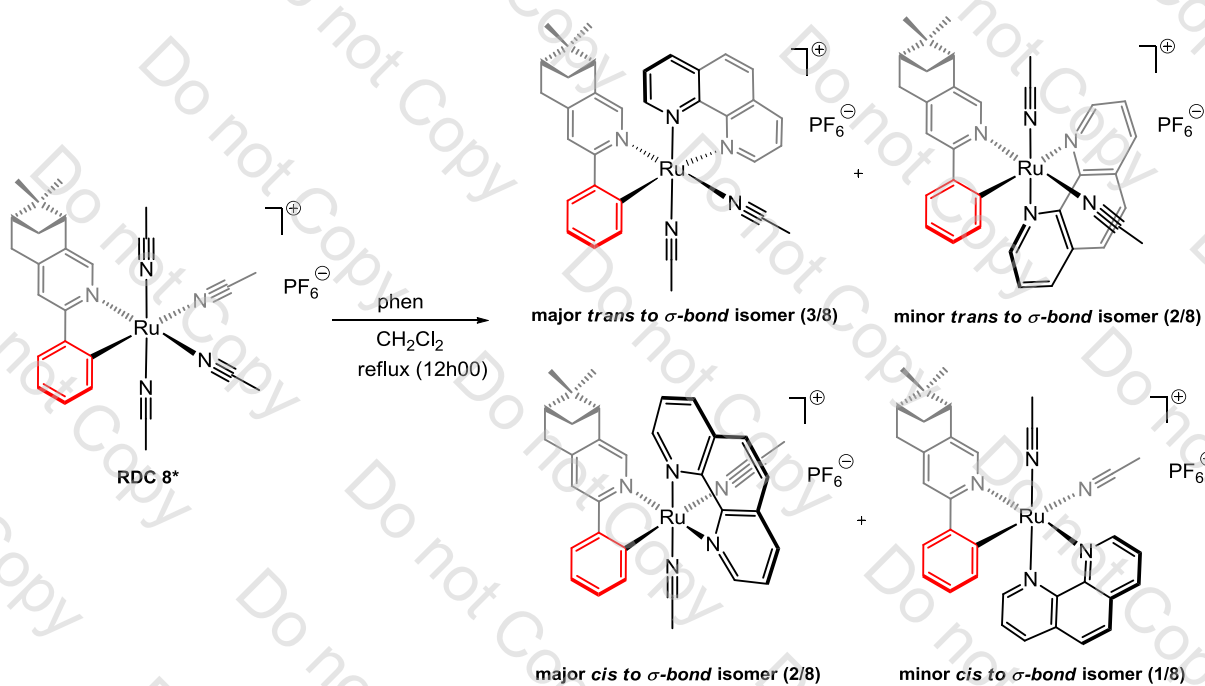


Figure 43: Effect of reaction time on the distribution of isomers (aromatic part)

Figure 44: RDC 11* *cis* and *trans* diastereomers obtained after 12h

In order to avoid formation of *cis* isomers, it was demonstrated that reaction time must be short (up to 1h). However, the *trans* diastereomers thus obtained **cannot be separated** by usual techniques such as chromatography column or recrystallization. That's why the chiral anion approach using (Δ)-Trisphat anion was also used to resolve this chiral organometallic complex.

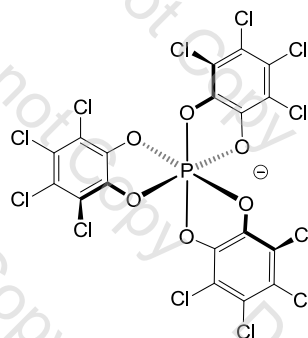


Figure 45: Structure of (Δ)-Trisphat ion

There is chiral recognition when a chiral compound of defined stereochemistry interacts differently with the stereoisomers of another chiral compound. These interactions may result from an association between a cationic complex and a chiral anion forming an ion pair. The latter has been highlighted as the “chiral anion strategy”. This strategy works well with structurally similar ruthenium complex *cis*-[Ru(dmp)₂(CH₃CN)₂][PF₆]₂ (where dmp is 2,9-dimethyl-1,10-phenanthroline).³⁸ Hence, we tried to exchange achiral hexafluorophosphate anion of the **RDC 11** and of the **RDC 11*** with an optically pure chiral anion such as (Δ)-Trisphat. Although metathesis of the anion occurs in both cases, it was not possible to selectively isolate each isomer, associated with (Δ)-Trisphat in the form of the heterochiral pair.

2.3.4. Conclusion

Although the use of the chiral ligand mppy does not allow the synthesis of an optically pure product, this synthesis strategy does not necessarily lead to a deadlock. Indeed, the use of a bulkier group instead of simple α -pinene and/or the synthesis of another chiral ligand where the chiral pool is closer to the metal center could afford diastereospecific synthesis. Total resolution of the racemates has to be fulfilled in order to study the biological activity *in vivo* of these enantiopure compounds, as well as their toxicity, in order to do a step towards drug development and so, fulfill the requirements of the FDA.

2.4. References Chapter 2

- ¹ Gaiddon, C.; Jeannequin, P.; Bischoff, P.; Pfeffer, M.; Sirlin, C.; Loeffler, J. P. *J. Pharmacol. Exp. Ther.*, **2005**, *315*, 1403–1411.
- ² Djukic J.P.; Sortais J.-B.; Barloy L.; Pfeffer M. *Eur. J. Inorg. Chem.* **2009**, *7*, 817–853.
- ³ (a) Ryabov, A. D.; Sukharev, V. S.; Alexandrova, L.; Le Lagadec, R.; Pfeffer, M. *Inorg. Chem.* **2001**, *40*, 6529–6532.
(b) Le Lagadec, R.; Rubio, L.; Alexandrova, L.; Toscano, R. A.; Ivanova, E. V.; Meskys, R.; Laurinavicius, V.; Pfeffer, M.; Ryabov, A. D. *J. Organomet. Chem.* **2004**, *689*, 4820–4832.
(c) Ryabov, A. D.; Le Lagadec, R.; Estevez, H.; Toscano, R. A.; Hernandez, S.; Alexandrova, L.; Kurova, V. S.; Fischer, A.; Sirlin, C.; Pfeffer, M. *Inorg. Chem.* **2005**, *44*, 1626–1634.
(d) Le Lagadec, R.; Alexandrova, L.; Estevez, H.; Pfeffer, M.; Laurinavicius, V.; Razumiene, J.; Ryabov, A. D. *Eur. J. Inorg. Chem.* **2006**, 2735–2738.
(e) Ryabov, A. D.; Kurova, V. S.; Ivanova, E. V.; Le Lagadec, R.; Alexandrova, L. *Anal. Chem.* **2005**, *77*, 1132–1139.
(f) Ivanova, E. V.; Kurnikov, I. V.; Fischer, A.; Alexandrova, L.; Ryabov, A. D. *J. Mol. Catal. B* **2006**, *41*, 110–116.
- ⁴ Meng, X.; Leyva, M. L.; Jenny, M.; Gross, I.; Benosman, S.; Fricker, B.; Harlepp, S.; Hebraud, P.; Boos, A.; Wlosik, P.; Bischoff, P.; Sirlin, C.; Pfeffer, M.; Loeffler, J. P.; Gaiddon, C. *Cancer Res.*, **2009**, *69*, 5458–5466.
- ⁵ Leyva, L.; Sirlin, C.; Rubio, L.; Franco, C.; Le Lagadec, R.; Spencer, J.; Bischoff, P.; Gaiddon, C.; Loeffler, J. P.; Pfeffer, M. *Eur. J. Inorg. Chem.*, **2007**, 3055–3066.
- ⁶ (a) Wadman, S.H.; Lutz, M.; Tooke, S. M.; Spek, A. L.; Hartl, F.; Havenith, R. W. A.; van Klink, G.; van Koten, G. *Inorg. Chem.* **2009**, *48*, 1887–1900.
(b) Wadman, S.H.; Lutz, M.; Tooke, S. M.; Spek, A. L.; Hartl, F.; Havenith, R. W. A.; van Klink, G.; van Koten, G. *Inorg. Chem.* **2009**, *48*, 5685–5696.
(c) Wadman, S.H.; Kroon, J.M.; Bakker, K.; Havenith, R. W. A.; van Klink, G.; van Koten, G. *Organometallics*, **2010**, *29*, 1569–1579.
- ⁷ Sindkhedkar, M.D.; Mulla, H.R.; Wurth, M.A.; Cammers-Goodwin A. *Tetrahedron* **2001**, *57*, 2991–2996.
- ⁸ Jouaiti, A.; Geoffroy, M.; Collin, J.P. *Inorg. Chim. Acta* **1996**, *245*, 69–73.
- ⁹ Sengupta, S.; Sadhukan, S.K.; Singh R.S.; Pal N. *Tetrahedron Lett.* **2002**, *43*, 1117–1121.
- ¹⁰ Neve, F.; Crispini, A.; Di Pietro, C.; Campagna, S. *Organometallics* **2002**, *21*, 3511–3518.
- ¹¹ Williams, J.A.G.; Beeby, A.; Davies, S.; Weinstein, J.; Wilson, C. *Inorg. Chem.* **2003**, *42*, 8609–8611.
- ¹² Kroehnke, F. *Synthesis* **1976**, *1*, 1–24.
- ¹³ Constable, E. C.; Henney, R.; Leese, T. A.; *J. Chem. Soc. Dalton Trans.* **1990**, *2*, 443–449.
- ¹⁴ Lu, W.; Chan, M.C.W.; Zhu, N.; Che, C.-M.; Li, C.; Hui, Z. *J. Am. Chem. Soc.* **2004**, *126*, 7639–7651.
- ¹⁵ Fallahpour, R.A. *Synthesis* **2000**, *8*, 1138–1142.
- ¹⁶ Amb, C.M.; Rasmussen, S.C. *J. Org. Chem.* **2006**, *71*, 4696–4699.
- ¹⁷ Nazeeruddin, M.K.; Péchy, P.; Renouard, T.; Zakeeruddin, S.M.; Humphry-Baker, R.; Comte, P.; Liska, P.; Cevey, L.; Costa, E.; Shklover, V.; Spiccia, L.; Deacon, G.B.; Bignozzi, C.A.; Grätzel, M. *J. Am. Chem. Soc.* **2001**, *123*, 1613–1624.
- ¹⁸ Bhaumik, C.; Das, S.; Saha, D.; Dutta, S.; Baitalik, S. *Inorg. Chem.* **2010**, *49*, 4049–4062.
- ¹⁹ Constable, E.C.; Hannon, M.J. *Inorg. Chem.* **1993**, *32*, 4539–4543.
- ²⁰ Fernandez, S.; Pfeffer, M.; Ritling, V.; Sirlin, C. *Organometallics* **1999**, *18*, 2390–2394.
- ²¹ Wadman, S.H.; Havenith, R.W.A.; Hartl, F.; Lutz, M.; Spek, A.L.; van Klink, G.P.M.; van Koten, G. *Inorg. Chem.* **2009**, *48*, 5685–5696.
- ²² Plitzko, K.M.; Wehrle, G.; Gollas, B.; Rapko, B.; Dannheim, J.; Boekelheide, V. *J. Am. Chem. Soc.* **1990**, *112*, 6556–6564.
- ²³ Morris, R.E.; Sadler, P.J.; Chen, H.; Jodrell, D. *US Patent*, 6979681, **2005**.
- ²⁴ Mosman, T. *J. Immunol. Meth.* **1985**, *65*, 55–63.
- ²⁵ Schatzschneider, U.; Niesel, J.; Ott, I.; Gust, R.; Alborzina H.; Wölfl, S. *ChemMedChem* **2008**, *3*, 1104–1109.
- ²⁶ Shoemaker, R.H. *Nature review Cancer* **2006**, *6*, 813–823.
- ²⁷ Clarke, M.J. *J. Am. Chem. Soc.*, 1978, **100**, 5068–5075.
- ²⁸ Clarke, M. J.; Bailey, V. M.; Doan, P. E.; Hiller, C. D.; LaChance-Galang, K. J.; Daghljan, H.; Mandal, S.; Bastos C. M.; Lang, D. *Inorg. Chem.*, **1996**, *35*, 4896–4903.
- ²⁹ Reisner, E.; Arion, V. B.; Keppler, B. K.; Pombeiro A. J. L. *Inorg. Chim. Acta.* **2008**, *361*, 1569–1583.

- ³⁰ Jakupec, M. A.; Resiner, E.; Eichinger, A.; Pongratz, M.; Arion, V. B.; Galanski, M.; Hartinger, C. G.; Keppler, B. K. *J. Med. Chem.* **2005**, *48*, 2831–2837.
- ³¹ Fernandez, S.; Pfeffer, M.; Ritleng, V.; Sirlin, C. *Organometallics* **1999**, *18*, 2390–2394.
- ³² Boutadla, Y.; Al-Duaij, O.; Davies, D. L.; Griffith G. A.; Singh K. *Organometallics* **2009**, *28*, 433–440.
- ³³ Djukic, J.-P.; Berger, A.; Duquenne, M.; Pfeffer, M.; De Cian, A.; Kyritsakas-Gruber N.; Vachon J.; Lacour J. *Organometallics* **2004**, *23*, 5757–5767.
- ³⁴ Bomben, P.G.; Koivisto B.D. Berlinguette, C.P. *Inorg. Chem.* **2010**, *49*, 4960–4971.
- ³⁵ Bonnet, S.; Li, J.; Siegler, M.A.; von Chrzanowski, L.S.; Spek, A.L.; van Koten, G.; Klein Gebbink, R.J.M. *Chem. Eur. J.* **2009**, *15*, 3340–3343.
- ³⁶ (a) Blaschke, G.; Kraft, H. P.; Fickentscher K.; Kohler, F. *Arzneimittel-Forschung/Drug Res.* **1979**, *29*, 1640–1642.
(b) Gordon J.; Goggin P. *Postgrad. Med. J.* **2003** March; *79*, 127–132
- ³⁷ Ryabov, A.D.; Le Lagadec, R.; Estevez, H.; Toscano, R.A.; Hernandez, S.; Alexandrova, L.; Kurova, V.S.; Fischer, A.; Sirlin, C.; Pfeffer, M. *Inorg. Chem.* **2005**, *44*, 1626–1634.
- ³⁸ (a) Chavarot, M.; Menage, S.; Hamelin, O.; Charnay, F.; Pecaut J.; Fontecave, M. *Inorg. Chem.* **2003**, *42*, 4810–4816.
(b) Bruylants, G.; Bresson, C.; Boisdenghien, A.; Pierard, F.; Kirsch-De Mesmaeker, A.; Lacour J.; Bartik, K. *New J. Chem.* **2003**, *27*, 748–4751.

Chapter 3:

Library of first- and second-generation osmacycles

Cancer comes into life without warning and works its way in. Like a sword of Damocles, it is an unspoken presence in everyday life of cancer patients. That's why research aims at getting tough with fight against cancer by uncovering its secrets. As Bertolt Brecht said "The one who fights can lose, but the one who does not fight has already lost."



Chapter 3: Library of first & second-generation cyclometalated osmium complexes and evaluation of their biological properties as anticancer agents..... 119

3.1. Introduction: Osmium as an alternative to Ruthenium?	121
3.2. Achievement of first-generation piano-stool Os(II) chemical library	122
3.2.1. Synthesis of cyclometalated Os(II) piano-stool complexes	122
3.2.2. Cytotoxic activity of cyclometalated piano-stool osmacycles	126
3.2.3. Study of the exchange of MeCN vs. DMSO in piano-stool ODCs	128
3.3. Completed first-generation Os(II) chemical library	137
3.3.1. Synthesis of other cyclometalated Os(II) complexes	137
3.3.2. Cytotoxic activity of completed first generation Os(II) chemical library	139
3.4. Achievement of second-generation Os(II) chemical library	143
3.4.1. Synthesis of cyclometalated second-generation Os(II) complexes	143
3.4.2. Cytotoxic activity of second generation ODCs.....	147
3.5. Electrochemical properties of first and second generation ODCs.....	154
3.6. References Chapter 3.....	157

Chapter 3: Library of first & second-generation cyclometalated osmium complexes and evaluation of their biological properties as anticancer agents.

3.1. Introduction: Osmium as an alternative to Ruthenium?

The success of ruthenium as an alternative to the existing anticancer treatments has promoted the search of other cytotoxic compounds with enhanced activities. Although osmium belongs to the same group as iron and ruthenium, and should therefore be able to mimic iron, interact with proteins, coenzymes, and nucleic acids, studies on the biological activity of its compounds are still very scarce.

Indeed, osmium complexes have the reputation of being either **highly toxic** (*e.g.* osmium tetroxide OsO₄) or **relatively inert**, which is a common characteristic of low-spin d⁶ metal ions and especially 3rd row transition metals.^{1,2} This may explain why their therapeutic potential has only been scarcely exploited, although osmium and especially OsO₄ are widely used in organic synthesis (*e.g.* to oxidise alkenes to vicinal diols) and in biological or polymer staining (*e.g.* to provide contrast to the image in transmission electron microscopy).

For now, the only **recognised clinical use** of osmium is the local administration of OsO₄ for synovectomy in arthritic patients in Scandinavia.³ The lack of reports of long term side effects suggests that osmium itself can be biocompatible, although this might clearly be dependent on the exact nature of the administered compound.

Since 2006, osmium compounds have thus become a field of growing interest and recent studies made by Keppler *et al.*,⁴ Dyson *et al.*^{1,5} and Sadler *et al.*^{2,6} on osmium complexes demonstrated that this metal can offer an interesting alternative to ruthenium given that heavier osmium congeners can also display *in vitro* antitumour activity, as well as reactivity towards DNA (see also Chapter 1, 1.4.).⁷

All these investigations showed that osmium is another metal that deserves attention for the development of effective antitumour drugs. However, osmium complexes differ from those of ruthenium by their preparation methods, their greater instability in low oxidation states, their stronger π back-bonding and by their kinetics of exchanging ligand that is essential for their application as anticancer agents. Moreover, osmium analogues which are equipotent to their ruthenium congeners have the advantage of being more inert under conditions relevant for drug formulation.^{6c} Hence, the comparison of the osmium chemistry with that of ruthenium

can provide us useful information for the understanding of the **mechanism of action** of ruthenium drugs.

In this context, and in order to enhance the activity and reduce side effects of existing anticancer agents, the Laboratoire de Synthèses Métallo-Induites decided also to focus its studies on osmium derivatives, not only because it complements the **RDC** chemical library, but also because it enables verification of the impact of exchanging the metal. We have been involved in this field since the discovery that some cyclometalated osmium compounds can be good candidates for becoming anticancer drugs.

A new chemical library **ODCs** (**O**smium **D**erived **C**omplexes) of approximately forty compounds in which the carbon-osmium (C-Os) bond is stabilized by one or two intramolecular N-Os bonds was synthesized. Measurements of physico-chemical parameters such as red-ox potential demonstrated that osmium complexes display an interesting Os^{III}/Os^{II} red-ox potential allowing them to interact with enzymes such as oxido-reductase. The antiproliferative properties of these new **ODCs** were also evaluated *in vitro* and compared to their **RDCs** congeners. These complexes are at least as efficient as **RDCs** or even better, some of them attaining an IC₅₀ significantly lower than one micromole, indicating a critical improvement.

3.2. Achievement of first-generation piano-stool Os(II) chemical library

3.2.1. Synthesis of cyclometalated Os(II) piano-stool complexes

Intramolecular cleavage of C(sp²)-H bond by osmium complexes in order to produce cyclometalated compounds is a matter of precedence,⁸ but most of them were synthesized through transmetalation of ortho-mercurated aryl derivatives, thus eliminating the most challenging C(sp²)-H bond activation step. Using the same procedure described by our laboratory⁹ on osmium dimer, Ryabov *et al.*¹⁰ have recently cyclometalated 2-phenylpyridine by C(sp²)-H activation reaction.

Note that cycloruthenation in presence of NaOH involves the dissociation of the η⁶-benzene and the formation of [Ru(N[^]C)(NCMe)₄]PF₆. In marked contrast with ruthenium, the mild electrophilic C(sp²)-H cyclometallation of this species by chloro-bridged osmium(II) dimer [OsCl(μCl)(η⁶-C₆H₆)] in acetonitrile affords pseudotetrahedra piano-stool Os(II) complex [Os(N[^]C)(η⁶-C₆H₆)(NCMe)]PF₆ (**Figure 1**). This suggests that the η⁶-benzene ring is obviously more tightly bound to osmium than to ruthenium given that prolonged refluxing in acetonitrile (up to 48h) does not lead to the substitution of the arene unit by MeCN.¹⁰

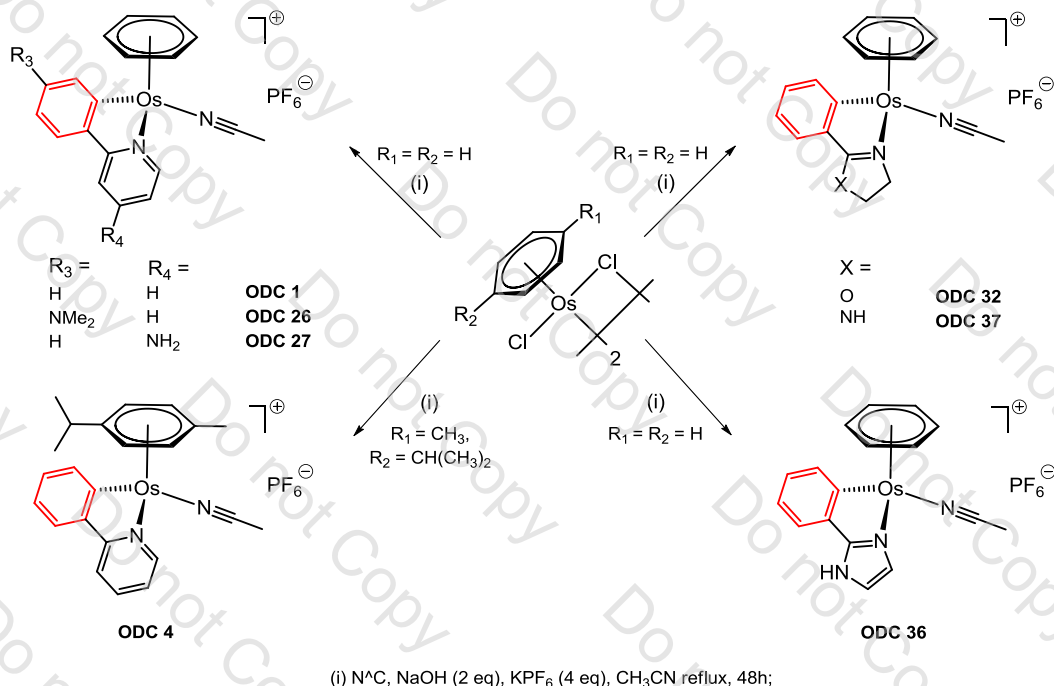


Figure 1: Synthesis of cyclometalated Os(II) piano-stool complexes

In order to develop the variety of cyclometalated piano-stool complexes, but also to verify the impact of red-ox potential on the *in vitro* activities, we decided to synthesize piano-stool complexes using a variety of heterocyclic cyclometalated ligands. As an alternative to 2-phenylpyridine, we studied the case of smaller and more electron-rich ligands.

Using the same procedure, the synthesis of **ODCs** containing one MeCN ligand was achieved with dimer starting material [OsCl(μCl)(η⁶-arene)]₂ having an arene η⁶-bound to the osmium centre (**Figure 1**). A series of piano-stool **ODC** complexes containing cyclometalated ligands such as 2-phenylpyridine, *N,N*-dimethyl-4-(pyridine-2-yl)benzenamine,¹¹ 4-aminophenylpyridine,¹² 2-phenyl-2-oxazoline, 2-phenyl-2-imidazoline, 2-phenylimidazole was synthesized in good to excellent yields. Note that the use of an even more electron-rich 4-phenylpyrimidine led to a complex mixture of unstable and not separable products. Although the exact composition of this mixture still remained unknown, it must likely contain species in which the 4-phenylpyrimidine is bound as monodentate at either 2- or 4-positions of the phenyl ring in addition to the desired cyclometalated product.

To complement the study we ascertained the structure of this class of piano-stool osmium complexes by performing a three-dimensional structure determination using X-ray diffraction on single crystals of **ODC 1**, **ODC 4**, **ODC 32** and **ODC 37** (**Figure 2** and **Figure 3**). The data integration was done using a monoclinic unit cell for **ODC 1** and **ODC 4** and an orthorhombic unit cell for **ODC 32** and **ODC 37**.

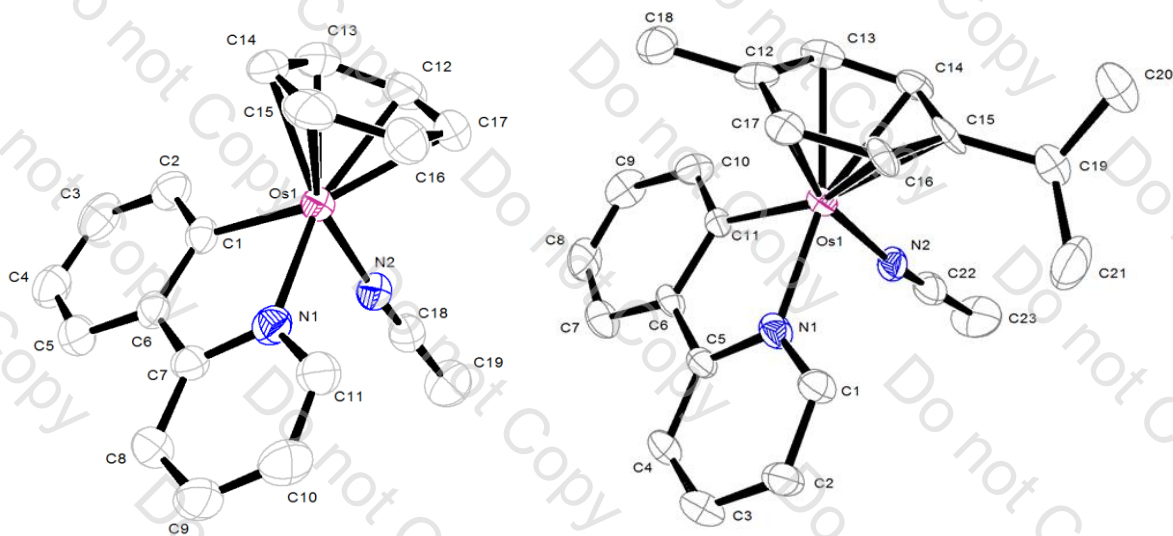


Figure 2: ORTEP diagram of the molecular structure of ODC 1 (left) and ODC 4 (right).

Ellipsoids are drawn at a probability level of 50%.

Hydrogen atoms, counter anions and solvent have been omitted for clarity.

Compound reference	ODC 1	ODC 4
Chemical formula	$C_{19}H_{17}N_2Os \cdot C_3H_6O \cdot F_6P$	$C_{23}H_{25}N_2Os \cdot F_6P$
Formula Mass	666.59	664.62
Crystal system	Monoclinic	Monoclinic
$a/\text{\AA}$	12.8418(4)	26.1320(12)
$b/\text{\AA}$	9.2865(2)	10.2475(3)
$c/\text{\AA}$	21.8939(6)	9.0981(4)
$\alpha/^\circ$	90.00	90.00
$\beta/^\circ$	116.439(2)	106.497(2)
$\gamma/^\circ$	90.00	90.00
Unit cell volume/ \AA^3	2337.88(11)	2336.06(16)
Temperature/K	193(2)	173(2)
Space group	$P2_1/c$	C_2
No. of formula units per unit cell, Z	4	4
No. of reflections measured	17380	11979
No. of independent reflections	5329	5214
R_{int}	0.0498	0.0485
Final R_i values ($I > 2\sigma(I)$)	0.0376	0.0343
Final $wR(F^2)$ values ($I > 2\sigma(I)$)	0.0957	0.0906
Final R_i values (all data)	0.0456	0.0388
Final $wR(F^2)$ values (all data)	0.1143	0.1002

Table 1: Details for the X-ray crystal structure determination of ODC 1 and ODC 4

ODC 1		ODC 4	
C1 – Os1	2.077(5)	C11 – Os1	2.074(6)
C12 – Os1	2.211(5)	C12 – Os1	2.190(11)
C13 – Os1	2.192(5)	C13 – Os1	2.198(11)
C14 – Os1	2.181(5)	C14 – Os1	2.203(8)
C15 – Os1	2.180(5)	C15 – Os1	2.291(8)
C16 – Os1	2.250(5)	C16 – Os1	2.253(8)
C17 – Os1	2.257(5)	C17 – Os1	2.201(8)
N1 – Os1	2.098(5)	N1 – Os1	2.090(8)
N2 – Os1	2.043(4)	N2 – Os1	2.066(7)
C1 – Os1 – N1	77.80(18)	C11 – Os1 – N1	76.9(3)
C1 – Os1 – N2	84.99(15)	C11 – Os1 – N2	84.8(4)
N1 – Os1 – N2	85.16(15)	N1 – Os1 – N2	86.4(3)
Os1 – C1 – C6	116.1(3)	Os1 – C11 – C6	115.8(6)
C1 – C6 – C7	115.5(4)	C11 – C6 – C5	115.0(6)
C6 – C7 – N1	114.0(4)	C6 – C5 – N1	113.1(7)
C7 – N1 – Os1	116.4(3)	C5 – N1 – Os1	118.9(6)

Table 2: Selected bond length (\AA), angles ($^\circ$) for ODC 1 and ODC 4

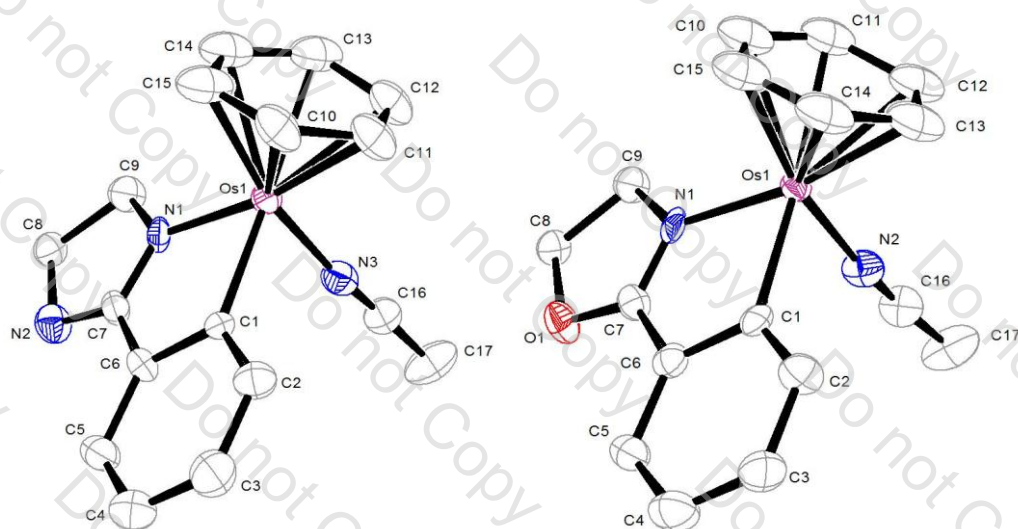


Figure 3: ORTEP diagram of the molecular structure of ODC 37 (left) and ODC 32 (right).

Ellipsoids are drawn at a probability level of 50%.

Hydrogen atoms, counter anions and solvent have been omitted for clarity.

Compound reference	ODC 37	ODC 32
Chemical formula	C ₁₇ H ₁₈ N ₃ Os•F ₆ P	C ₁₇ H ₁₇ N ₂ OOs•F ₆ P
Formula Mass	599.51	600.50
Crystal system	Orthorhombic	Orthorhombic
<i>a</i> /Å	11.7105(2)	11.6190(3)
<i>b</i> /Å	9.8464(2)	9.6830(3)
<i>c</i> /Å	16.3400(4)	16.5337(4)
<i>α</i> /°	90.00	90.00
<i>β</i> /°	90.00	90.00
<i>γ</i> /°	90.00	90.00
Unit cell volume/Å ³	1884.10(7)	1860.15(9)
Temperature/K	173(2)	173(2)
Space group	<i>Pna</i> 2 ₁	<i>Pna</i> 2 ₁
No. of formula units per unit cell, Z	4	4
No. of reflections measured	15483	12323
No. of independent reflections	3834	4141
<i>R</i> _{int}	0.0438	0.0386
Final <i>R</i> _i values (<i>I</i> > 2σ(<i>I</i>))	0.0430	0.0463
Final <i>wR</i> (<i>F</i> ²) values (<i>I</i> > 2σ(<i>I</i>))	0.1248	0.1322
Final <i>R</i> _i values (all data)	0.0470	0.0499
Final <i>wR</i> (<i>F</i> ²) values (all data)	0.1282	0.1355

Table 3: Details for the X-ray crystal structure determination of ODC 37 and ODC 32

ODC 37		ODC 32	
C1 – Os1	2.076(12)	C1 – Os1	2.095(12)
C10 – Os1	2.139(13)	C10 – Os1	2.198(13)
C11 – Os1	2.180(11)	C11 – Os1	2.259(14)
C12 – Os1	2.225(13)	C12 – Os1	2.211(15)
C13 – Os1	2.282(15)	C13 – Os1	2.194(15)
C14 – Os1	2.193(10)	C14 – Os1	2.164(14)
C15 – Os1	2.161(15)	C15 – Os1	2.194(15)
N1 – Os1	2.075(7)	N1 – Os1	2.065(7)
N3 – Os1	2.047(13)	N2 – Os1	2.056(12)
C1 – Os1–N1	76.6(5)	C1 – Os1–N1	75.6(5)
C1 – Os1–N3	85.6(4)	C1 – Os1–N2	85.3(5)
N1 – Os1–N3	84.8(5)	N1 – Os1–N2	87.3(5)
Os1 – C1–C6	115.0(8)	Os1 – C1–C6	114.1(8)
C1 – C6–C7	113.4(9)	C1 – C6–C7	113.6(10)
C6 – C7–N1	115.2(9)	C6 – C7–N1	115.3(10)
C7 – N1–Os1	119.8(9)	C7 – N1–Os1	121.0(9)

Table 4: Selected bond length (Å), angles (°) for ODC 37 and ODC 32

3.2.2. Cytotoxic activity of cyclometalated piano-stool osmacycles

The cytotoxicity of various **ODC** piano-stool complexes have been evaluated by measuring their effects on the cell proliferation in A172 (human glioblastoma) cell line (**Figure 4**). As for **RDCs**, results are presented as percentage compared with the control conditions. Graphs represent mean values with standard deviation of eight wells from one out of three independent experiments. The thick line corresponds to 50% viability (IC_{50}) (**Figure 6**) and results are compared to those obtained with the previously reported **RDC 11** at 5 μ M and are summarized in **Table 5**.

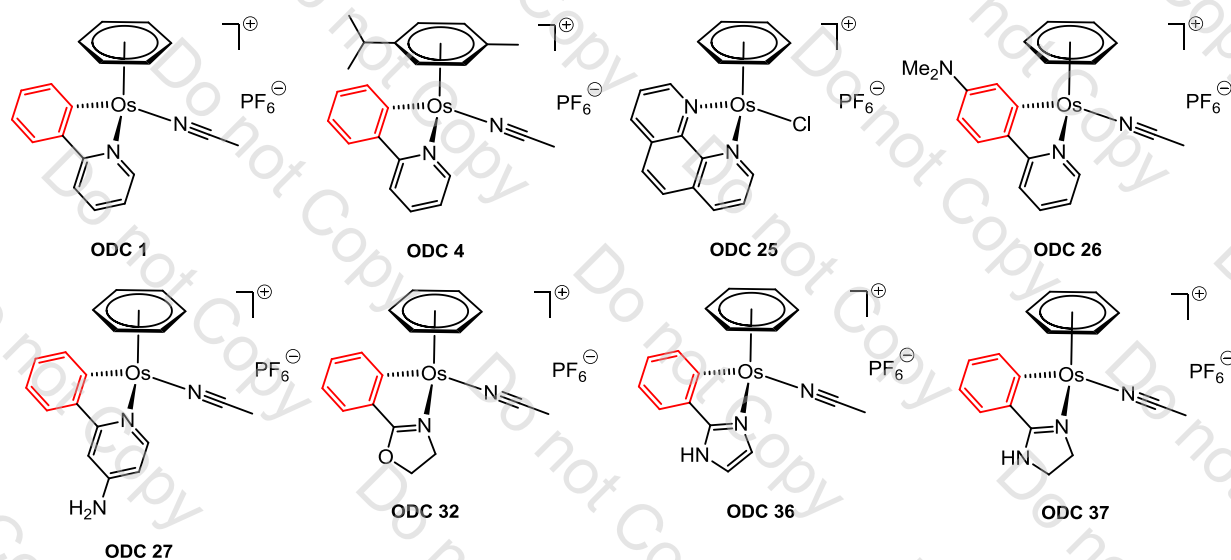


Figure 4: Chemical library of first generation Os(II) piano-stool complexes

In vitro antiproliferative activity of non-cyclometalated **ODC 25** was also determined in order to demonstrate the influence of the metal-carbon bond which appears to be a prerequisite for biological activity in this class of compounds. Note that the **ODC 25** synthesis was achieved using modified procedure of $[RuCl(phen)(\eta^6-C_6H_6)]PF_6$ synthesis¹³ using dimer starting material $[OsCl(\mu Cl)(\eta^6-C_6H_6)]$ instead of ruthenium $[RuCl(\mu Cl)(\eta^6-C_6H_6)]$ (**Figure 5**). To complement the study we ascertained the structure of this complex by performing a three-dimensional structure determination using X-ray diffraction on single crystals of **ODC 25** (see **Appendix, Figure 1**).

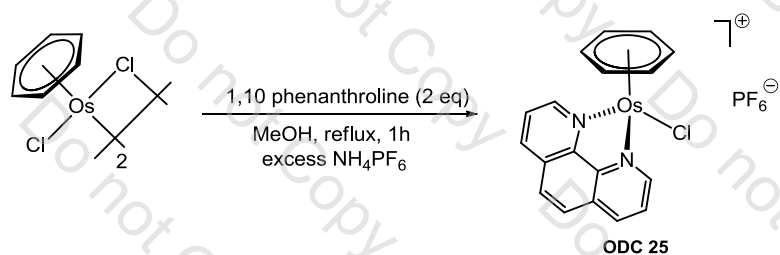


Figure 5: Synthesis of ODC 25 using modified reported procedure¹³



Figure 6: Antiproliferative *in vitro* activity of first generation Os(II) piano-stool complexes

By comparing the IC_{50} of **ODC 1** to its non-cyclometalated analogue **ODC 25**, it appears that the complex without a C-Os bond is non cytotoxic ($IC_{50} > 100\mu M$). However, **ODC 25** should be more lipophilic, and so should cross more easily the membrane of cancer cells than **ODC 1**. Therefore, there is a paradox, but the red-ox potential induced by the carbon-metal bond could easily explain the antiproliferative activity, as it is the case for **RDC** complexes. **ODC 1** and **OCD 4** have similar structures and antiproliferative activities because their red-ox and lipophilicity properties are comparable (see also Chapter 3, 3.5.).

Note that the antiproliferative activity of the **ODC 4** is equivalent to its ruthenium counterpart **RDC 49** ($IC_{50} = 14 \pm 1.0$).

Substitution of 2-phenylpyridine with an electron-donating group (such as NMe_2 in **ODC 26**) or an electron-withdrawing group (such as NH_2 in **ODC 27**) should respectively increase or decrease the lipophilicity but also modify the red-ox potential. However, both of them display a relatively poor antiproliferative activity indicating that both parameters (lipophilicity and red-ox potential) should be taken into account in the drug design.

Replacement of 2-phenylpyridine with smaller and more electron-rich ligands such as 2-phenyl-2-oxazoline, 2-phenyl-2-imidazoline or 2-phenylimidazole, leads to less stable compounds more likely to be oxidized and/or to undergo exchange of the MeCN ligand with DMSO. Although the IC_{50} of **ODC 32**, **ODC 36**, **ODC 37** are quite high, the data obtained for these three compounds may be not representative of the initial composition of the solutions.

<i>ODCs first generation</i>	<i>IC₅₀ (μM)</i>
<i>piano-stool</i>	<i>A172</i>
ODC 1	10 ± 0.5
ODC 4	10 ± 0.5
ODC 25	125 ± 5.0
ODC 26	60 ± 5.0
ODC 27	90 ± 5.0
ODC 32	90 ± 5.0
ODC 36	100 ± 5.0
ODC 37	100 ± 5.0
RDC 11	5 ± 0.5
Cisplatin	5 ± 0.5

Table 5: Recapitulative table of the IC_{50} values on an A172 cell line

3.2.3. Study of the exchange of MeCN vs. DMSO in piano-stool ODCs

3.2.3.1 Introduction

In **Chapter 2**, we demonstrated that in the case of cycloruthenated piano-stool complexes, the MeCN ligand is relatively labile and can exchange significantly with DMSO after approximately 3h at room temperature. In this section, similar studies were undergone on **ODC 1** and **ODC 4** in order to check whether their solutions in DMSO are stable at least for two days to be considered as good drug candidate. This stability was monitored by 1H NMR spectroscopy in $DMSO-d^6$, which showed that despite a slower kinetics, significant modification of osmium arene type complexes could occur after 15h at room temperature.

3.2.3.2. Preliminary results: kinetic evolution of ODC 4 in DMSO

Following the success of first *in vitro* and *in vivo* studies on **RDC 49**, it was a tempting challenge to perform similar studies on its osmium congener **ODC 4**. Indeed, this latter displays similar antiproliferative properties in A172 cell line ($IC_{50} = 10 \pm 0.5 \mu M$). However, biologists rapidly faced similar problems as for its ruthenium congener, losing partially or totally the anticancer properties when old stock solutions of **ODC 4** in DMSO were used. It was again postulated that the MeCN ligand is relatively labile and can exchange with DMSO, as it is the case for **RDC 49**. It was thus important to follow the evolution of **ODC 4** in DMSO in order to prove that a similar phenomenon occurs in osmium piano-stool complexes (**Figure 7**).

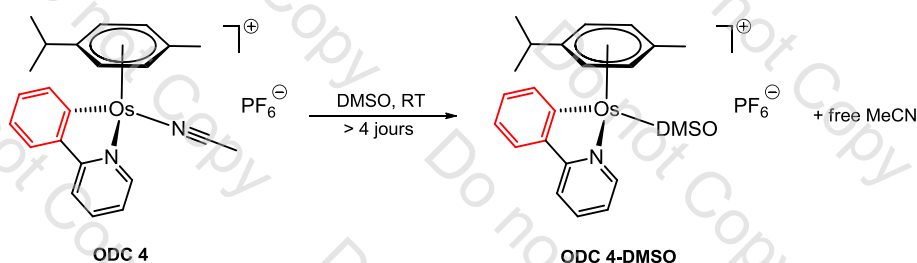


Figure 7: Spontaneous evolution of ODC4 in DMSO

In a first study a sample of **ODC 4** ($5.10^{-5} M$, in DMSO) was prepared and its kinetic evolution was monitored by UV/vis spectroscopy at room temperature (**Figure 8**). Note again that in this kinetic model, the concentration of **ODC 4** is not relevant, because this model is 1000 times less concentrated than stock solution used by biologists (50mM). By comparison with the **RDC 49**, the spectrum shows a **slower evolution** in the $\pi - \pi^*$ transition situated in the UV region.

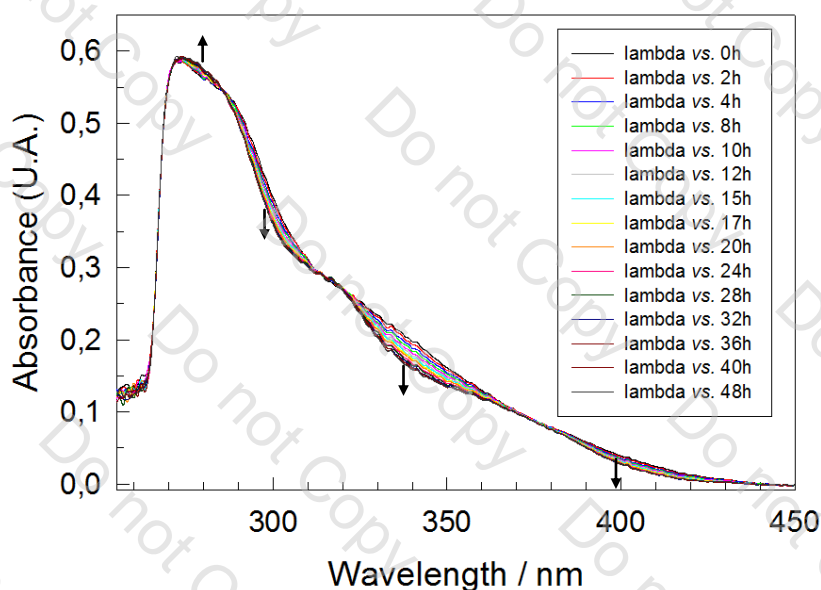


Figure 8: Evolution of ODC 4 in DMSO monitored by UV/Vis at R.T.

Although spectrum modifications do not demonstrate whether the evolution of **ODC 4** in DMSO led to a new product due to DMSO coordination, it must be first admitted that kinetics is much slower than for ruthenium compounds.

In a second study, a sample of **ODC 4** (10mM, in DMSO-d⁶) was prepared and its kinetic evolution was monitored by ¹H NMR spectroscopy (**Figure 9** and **Figure 10**). Notice that in this kinetic model, the concentration of monitored **ODC 4** is still not relevant, because this model is 5 times less concentrated than stock solution used by biologists (50mM). This concentration was reduced to 10mM because approximately 35mg of **ODC 4** would have been necessary to prepare one single NMR tube filled with 1mL DMSO-d⁶ at 50mM. Although the model is not perfect, this depicted well the phenomenon.

¹H spectra were recorded at room temperature on a 500MHz spectrometer at regular time intervals (t= 3, 20, 30, 46, 55, 200, 270 hours). Evolution of **ODC 4** is quite similar to **RDC 49**, given that no degradation is observed but another air stable compound is formed.

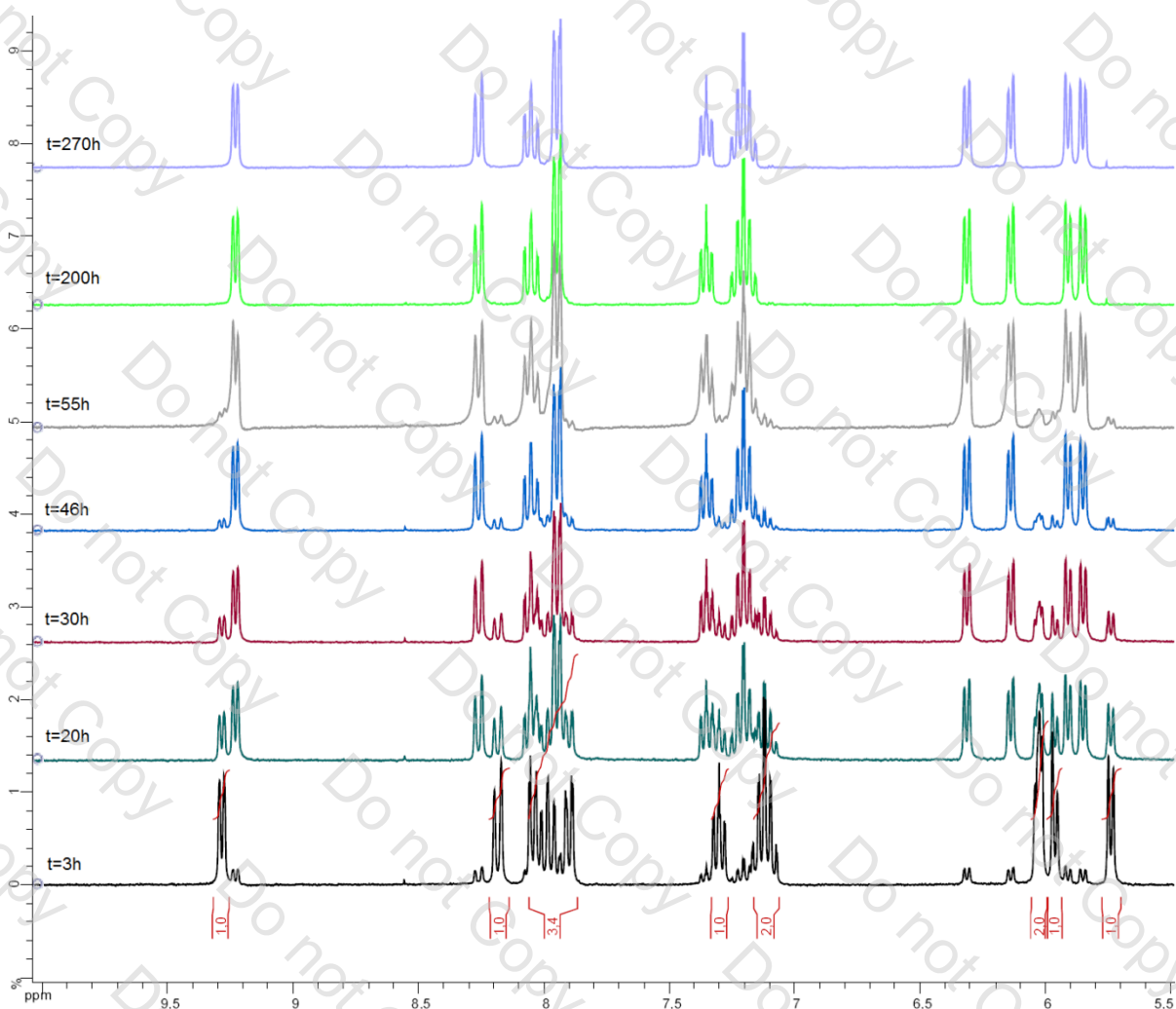


Figure 9: Kinetic of evolution of ODC 4 in DMSO-d⁶ (aromatic part)

Figure 9 depicted the evolution of the 2-phenylpyridine and η^6 -arene aromatic part, where ^1H signals are either shielded or deshielded, due to substitution of MeCN ligand by DMSO. Similar tendency can be observed for **RDC 49**.

More interesting is the aliphatic part depicted in **Figure 10**. Important modifications of the *isopropyl* Me signals of the η^6 -*p*-cymene can be observed leading to a splitting of signal ($\delta=0.84$ ppm) into two doublets (respectively $\delta=0.99$ and $\delta=0.68$ ppm). The other Me group from η^6 -*p*-cymene in **ODC 4** unfortunately merges in solvent peak, but a singlet ($\delta=2.37$ ppm) can be observable when the **ODC 4-DMSO** is formed. Moreover, coordinated MeCN ($\delta=2.16$ ppm) **decoordinates**, leading to unligated MeCN ($\delta=2.07$ ppm). Notice that the Me signals from DMSO cannot be observed because the kinetic study was undertaken in DMSO-d^6 .

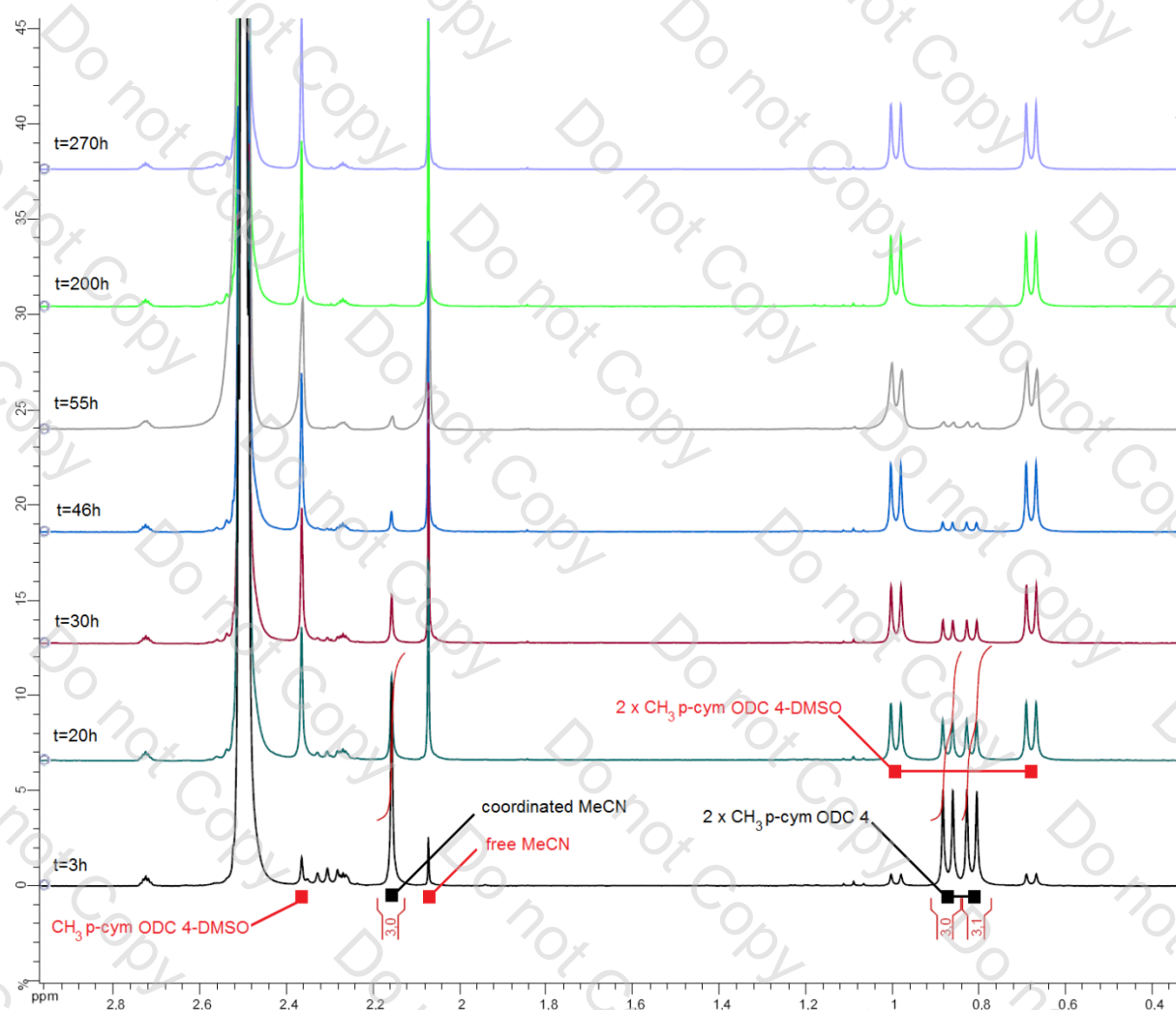


Figure 10: Kinetic study of ODC 4 in DMSO-d^6 (aliphatic part)

The evolution of coordinated MeCN and free MeCN solvent (in relative percentages) is depicted in **Figure 11**. This kinetic study also enables to determine the kinetic constant at **room temperature** and the half-life of **ODC 4** in DMSO.

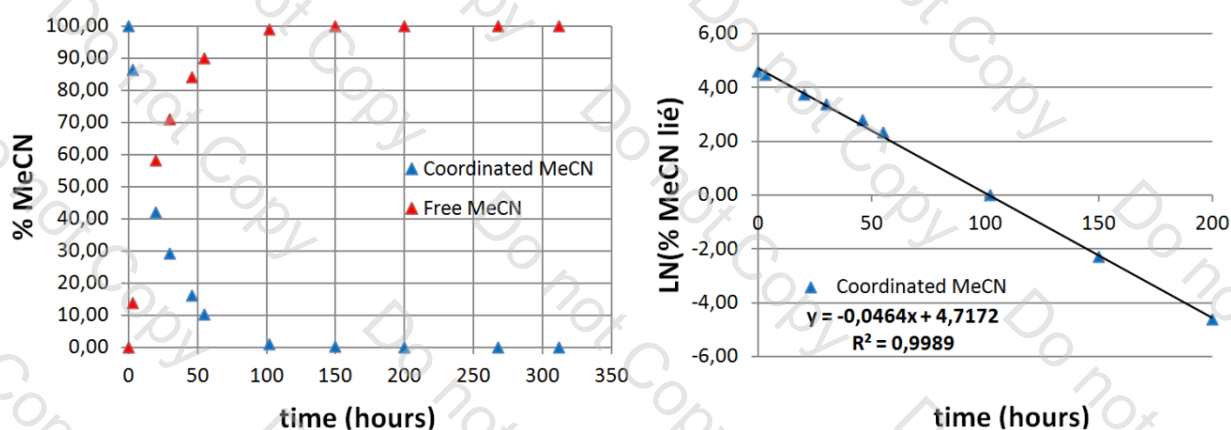
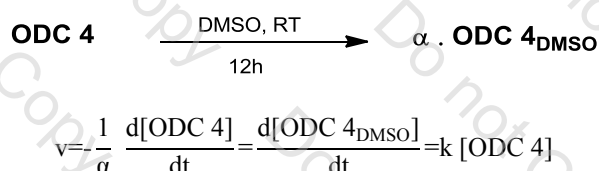


Figure 11: Evolution of ODC 4 in DMSO-d⁶ monitored by ¹H NMR spectroscopy at R.T.

Based on the general chemical equation, the following kinetic law can be written:



Using mass balance equation and the initial condition, this kinetic law can be easily integrated (supposing a first order reaction).

Mass balance equation:

$$\begin{aligned} \text{at } t=0 & : [\text{ODC 4}] = [\text{ODC 4}]_0 & [\text{ODC 4}_{\text{DMSO}}] = 0 \\ \text{at } t & : [\text{ODC 4}] = [\text{ODC 4}]_0 - [\text{ODC 4}_{\text{DMSO}}] \end{aligned}$$

Integration of kinetic law:

$$\int_{t=0}^t \frac{d[\text{ODC 4}]}{[\text{ODC 4}]_0 - \alpha[\text{ODC 4}_{\text{DMSO}}]} = \int_{t=0}^t -\alpha \cdot k \cdot dt$$

$$\ln([\text{ODC 4}]_0 - \alpha[\text{ODC 4}_{\text{DMSO}}]) - \ln([\text{ODC 4}]_0) = -\alpha \cdot k \cdot t$$

$$\ln \frac{[\text{ODC 4}]_0}{[\text{ODC 4}]_0 - \alpha[\text{ODC 4}_{\text{DMSO}}]} = \alpha \cdot k \cdot t$$

The evolution of $\ln([\text{ODC 4}]) = f(t)$ also corresponding to the evolution of $\ln([\text{coordinated MeCN}]) = f(t)$ is depicted in **Figure 11** (right graph). Since the representation of $\ln([\text{ODC 4}]) = f(t)$ is a straight line, this is a **first order reaction**.

Regression on the data gives a straight line (with good correlation factor 0.9989) and hence the speed constant can be directly extrapolated from the slope of regression line with $\alpha=1$. At **room temperature**, the mean value of the kinetic constant is approximately:

$$k = 0.0464 \pm 0.008 \text{ h}^{-1} = 2.78 \pm 0.48 \text{ min}^{-1}$$

Half-life:

with $\alpha=1$, the value of half-life **at room temperature** can be directly extrapolated from the diagram (time after which initial concentration of **ODC 4** is divided by two) or precisely calculated:

$$\text{at } t_{1/2} : [\text{ODC 4}] = [\text{ODC 4}]_0 - [\text{ODC 4}]_{\text{DMSO}} = [\text{ODC 4}]_0/2$$

$$\ln \frac{[\text{ODC 4}]_0}{[\text{ODC 4}]_0/2} = \alpha \cdot k \cdot t_{1/2}$$

$$t_{1/2} = \frac{\ln(2)}{\alpha \cdot k}$$

with $\alpha=1$, the value of half-life **at room temperature**:

$$t_{1/2 \text{ at R.T.}} = 14.94 \pm 0.25 \text{ h ,}$$

approximately $t_{1/2 \text{ at R.T.}} = 14\text{h}56\text{min}$

Notice that $t_{1/2}$ increases when the sample is stored in a cold dark place at -15°C (**Figure 12**):

approximately $t_{1/2 \text{ at } -15^\circ\text{C}} = 433\text{h}15\text{min}$ (extrapolation)

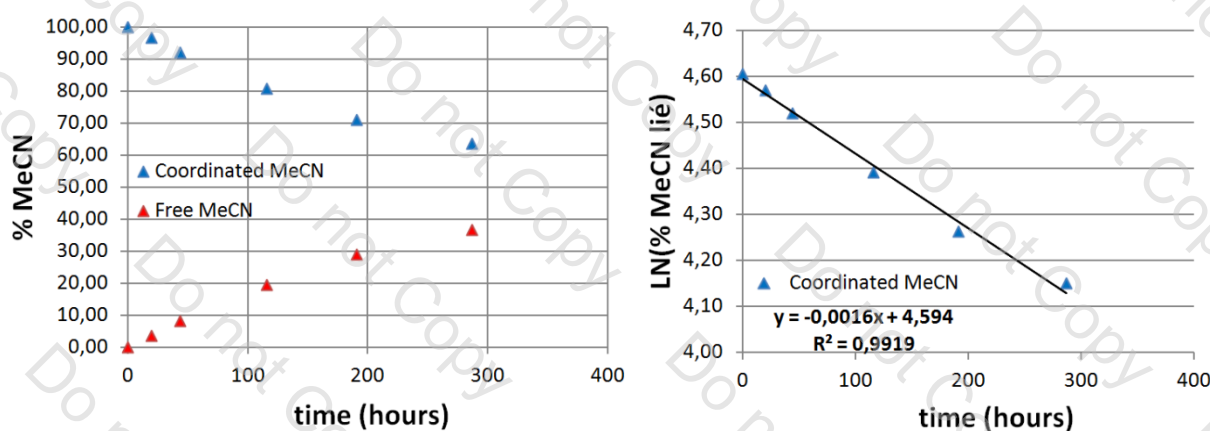


Figure 12: Evolution of ODC 4 in dry DMSO-d⁶ monitored by ¹H NMR spectroscopy at -15°C in a dark place

Based on this kinetic study, we found that the MeCN ligand of osmium piano-complexes is also relatively labile and can exchange with DMSO. However, **slower exchange kinetics** is observed for osmium derivatives **ODC 4** compared to the **RDC 49** ruthenium analogue. ¹H NMR spectroscopy in DMSO-d⁶ demonstrated that significant modification of osmium arene type complexes could occur after approximately **15 hours** (by comparison to 3 hours for **RDC 49**) at room temperature. The evaluation of the anticancer properties of the newly formed DMSO piano-stool **ODCs** remains to be performed in order to confirm the effect of MeCN substitution by DMSO on *in vitro* cell proliferation.

3.2.3.3. Synthesis and characterisation of ODC 39

A similar synthesis of compounds closely related to **ODC 1**, in which the acetonitrile ligand was substituted by a chloride ion, was reported recently by Ryabov *et al.*¹⁰ This compound **ODC 38** [Os(*o*-C₆H₄py- κ C,N)(*p*-cym)(Cl)] was obtained by reaction between excess 2-phenylpyridine and the chloro-bridged osmium(II) dimer [η^6 -(*p*-cymene)OsCl(μ Cl)]₂ in refluxing methanol for 24h (**Figure 13**).

Note that the excess 2-phenylpyridine, which acts as a base, can easily be replaced by sodium acetate. We ascertained the structure of this complex by performing a three-dimensional structure determination using X-ray diffraction on single crystals of **ODC 38** (see **Appendix, Figure 1**).

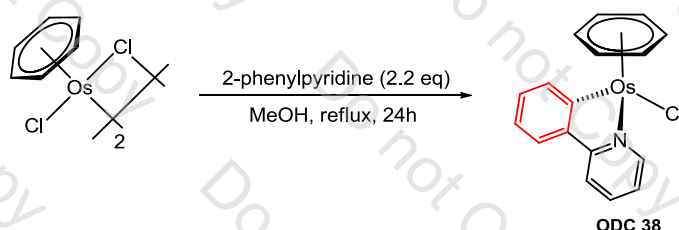


Figure 13: Synthesis of ODC 38

In a similar way as for **RDC 49-DMSO**, we can easily synthesize **ODC 39** [Os(*o*-C₆H₄py- κ C,N)(η^6 -C₆H₆)(DMSO)]PF₆ by reaction of **ODC 38** [Os(*o*-C₆H₄py- κ C,N)(η^6 -C₆H₆)(Cl)] with silver hexafluorophosphate (AgPF₆) in dichloromethane and one equivalent of DMSO (**Figure 14**).

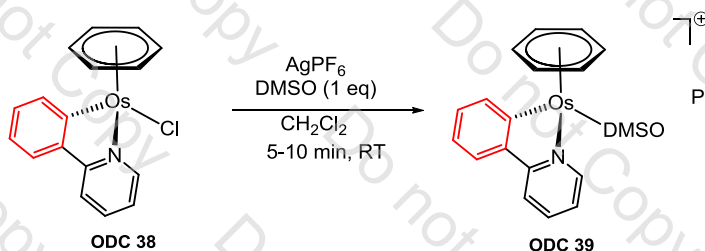


Figure 14: Synthesis of ODC 39

The rapid abstraction of halide (5-10min) at room temperature afforded discolouration of the orange reaction medium yielding a beige solution and a precipitate of white crystalline AgCl. Filtration over celite, evaporation followed by recrystallisation in dichloromethane/pentane afforded the desired air stable compound.

^1H NMR spectroscopy of newly synthesized **ODC 39** was performed in DMSO-d^6 in order to make a comparison with evolved **ODC 1** in DMSO (**Figure 15** and **Figure 16**). In these spectra, comparison between **ODC 1** in DMSO-d^6 at time $t=0$ and $t_{1/2}=15\text{h}$ and newly synthesized **ODC 39** demonstrated that DMSO substitutes the rather labile MeCN ligand in **ODC 1**.

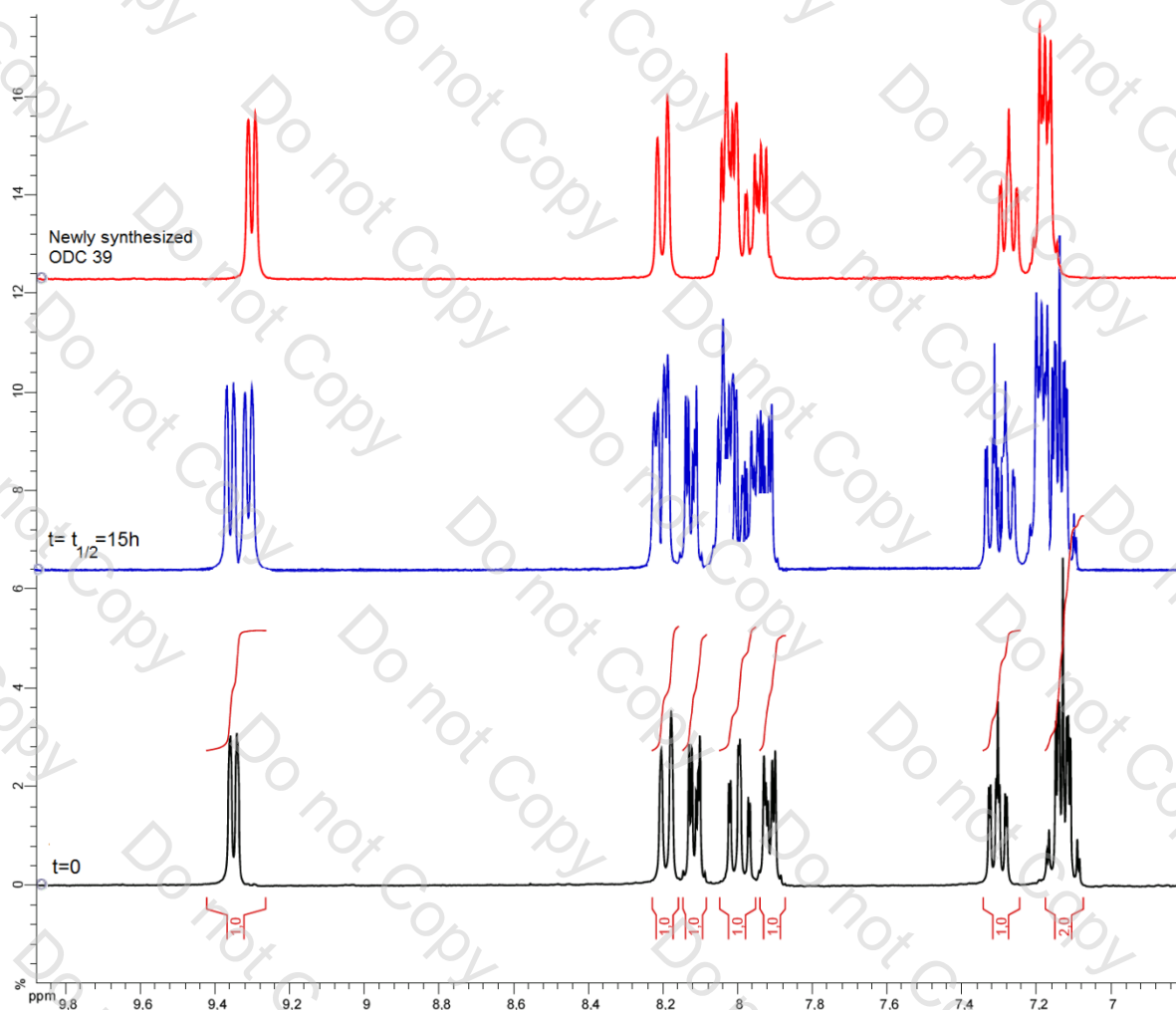


Figure 15: Comparison between ODC 39 and evolved ODC 1 in DMSO-d^6 (2-phenylpyridine part)

With no doubt, the evolution of 2-phenylpyridine protons ($\delta=7.1\text{-}9.4$ ppm) fits perfectly with the **ODC 39** model (**Figure 15**). Moreover, substitution of MeCN by DMSO in **ODC 1** leads to a deshielding of the aromatic protons of the benzene $\eta^6\text{-C}_6\text{H}_6$ ring, ranging from $\delta=5.9$ ppm for **ODC 1** to $\delta=6.1$ ppm for **ODC 39** (**Figure 16**). Note that the two methyl groups from coordinated DMSO ($\delta=3.37$ ppm and $\delta=2.79$ ppm) can now be observed in **ODC 39**.

X-ray structure of **ODC 39** is currently being studied, but similar coordination mode as for **RDC 49** must be observed: *i.e.* coordination of DMSO to the metal centre through sulphur atom.

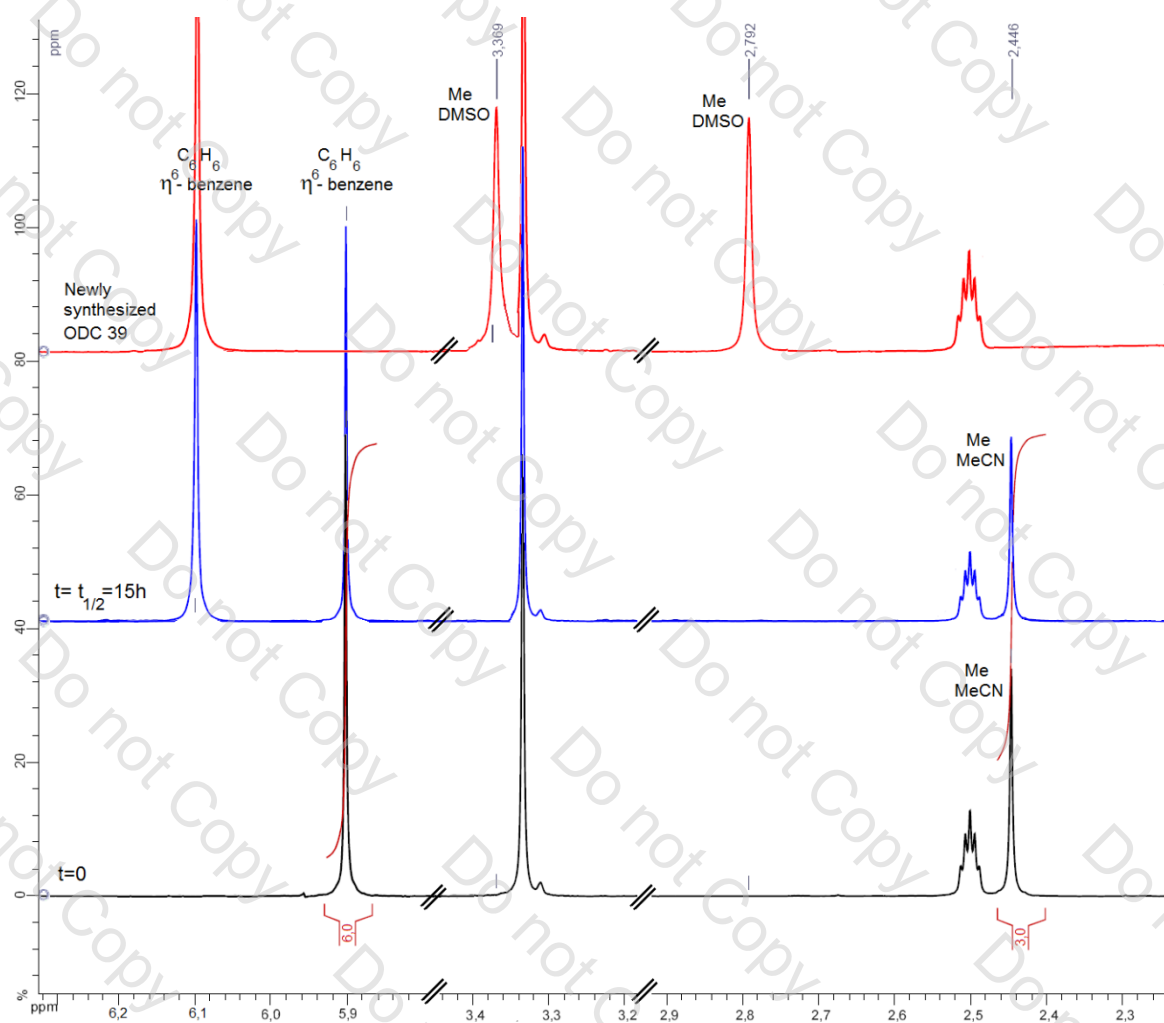


Figure 16: Comparison between ODC 39 and evolved ODC 1 in DMSO- d_6 (η^6 - C_6H_6 and aliphatic part)

3.2.3.4. Cytotoxic activity of ODC 39 vs. ODC 1

The antitumour potential of **ODC 1**, **ODC 38**, and **ODC 39** has been evaluated by measuring their effects on the cell proliferation of A172 cell line. The cells were treated with different doses of complexes and after 48h the viability of the cells was determined by measuring the mitochondrial succinic hydrogenase activity on the remaining living cells. The IC_{50} results are summarized in recapitulative **Table 6** and compared to those obtained with the previously reported **RDC 11** at $5\mu M$ (**Figure 17**).

ODCs compounds	IC_{50} A172 (μM)
ODC 1	10 ± 0.5
ODC 38	22 ± 1.0
ODC 39	300 ± 5.0

Table 6: Recapitulative table of the IC_{50} values on an A172 cell line

As expected, the **ODC 39** displays a lower antiproliferative effect than **ODC 1** explaining the partial or total lost of anticancer properties when old stock of **ODC 1** is used.

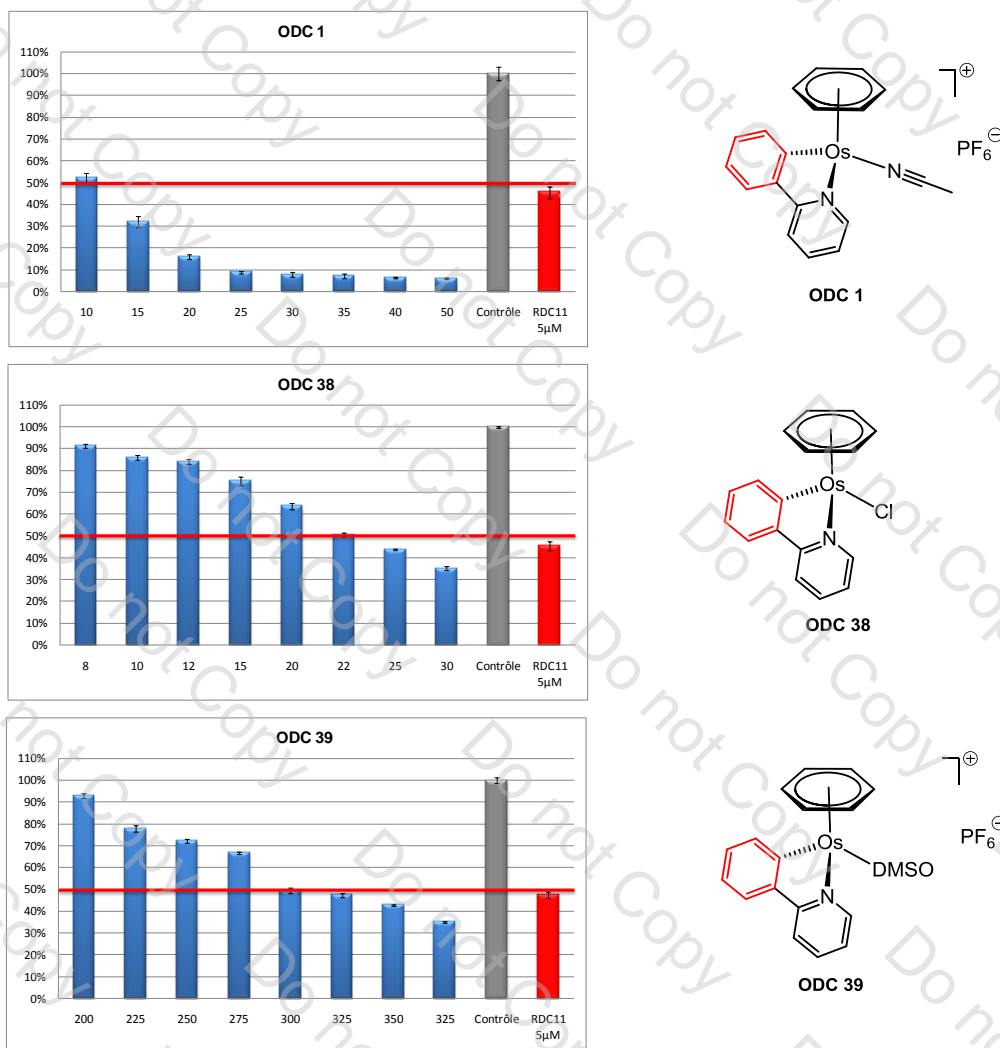


Figure 17: Impact of substitution of MeCN by DMSO on the antiproliferative activity (A172 glioblastoma cell line)

Effect of the lipophilicity and of the red-ox potential will be thoroughly discussed in **Chapter 4**. However, the higher IC_{50} of **ODC 39** compared to **ODC 1** is not imputable to the lower lipophilicity (which is practically the same), but is possibly due to the increase of **red-ox potential**: $E^{\circ}_{1/2}$ (**ODC 1**) = 1250mV and $E^{\circ}_{1/2}$ (**ODC 39**) = 1487mV. Moreover, even if **ODC 38** seems to have quite good red-ox potential to interfere with oxido-reductase enzymes, $E^{\circ}_{1/2}$ (**ODC 38**) = 722mV, this neutral compound is water soluble and hence do not display enough lipophilicity to cross the membrane of malignant cells.

3.3. Completed first-generation Os(II) chemical library

3.3.1. Synthesis of other cyclometalated Os(II) complexes

A series of cyclometalated osmium compounds bearing a bidentate N^C cyclometalated ligand and bidentate N^N or tridentate N^N^N ligand were synthesized and characterized. Some of them (**ODC 2** and **ODC 3**) have been recently published by Ryabov *et al.*¹⁰ using the

same strategy developed by our laboratory⁹ for ruthenium compounds. Further reaction of piano-stool complexes with one or two equivalent of 1,10-phenanthroline or 2,2'-bipyridine (N[^]N) leads to the substitution of the η⁶-bound benzene to produce octahedral species [Os(N[^]C)(N[^]N)(NCMe)₂]PF₆ or [Os(N[^]C)(N[^]N)₂]PF₆ respectively in MeCN or MeOH. Further reaction of piano-stool complexes with one equivalent of tridentate N[^]N[^]N ligand affords for the first time osmium complexes bearing at the same time mono-, bi- and tridentate ligands (**Figure 18** and **Figure 19**).

In stark contrast with results observed by Ryabov *et al.*,¹⁰ we succeeded in coordinating one equivalent of 2,2'-bipyridine forming **ODC 6** in good yield despite coordination of 2,2'-bipyridine is much more difficult than that of 1,10-phenanthroline. Note that lower reactivity of 2,2'-bipyridine compared to 1,10-phenanthroline towards ruthena(II)cycles was already discussed.¹⁴

Further coordination of only one equivalent of 1,10-phenanthroline or 2,2'-bipyridine on substituted piano-stool [Os(R-N[^]C)(η⁶-C₆H₆)(NCMe)]PF₆ (**ODC 26** or **ODC 27**) leads to a mixture of expected mono cycloadducts and unexpected bis cycloadducts (**ODC 28** and **ODC 29** respectively) which are not separable using standard chromatography technique. Despite the effects of dilution, the use of N[^]N in sub-stoichiometry or the drop wise addition of diluted solution of N[^]N over a long period of time, monocycloadducts could not be isolated.

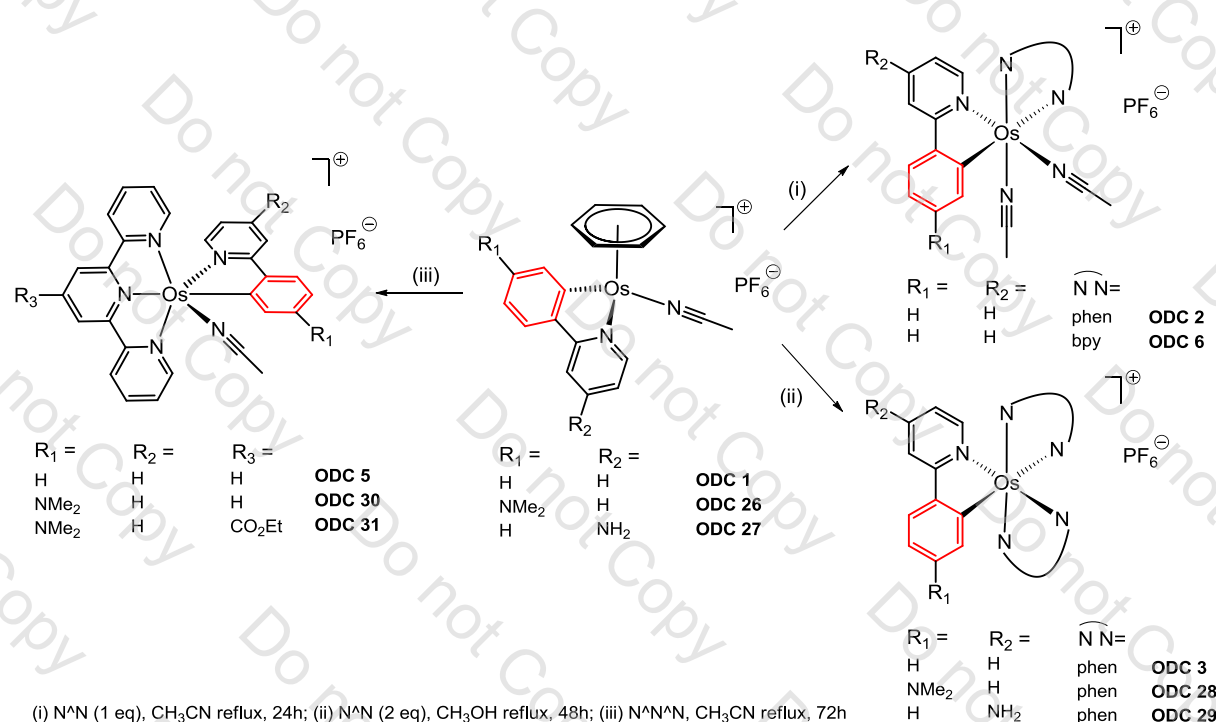


Figure 18: Synthesis of first generation ODCs containing 2-phenylpyridine-type cyclometalated ligand

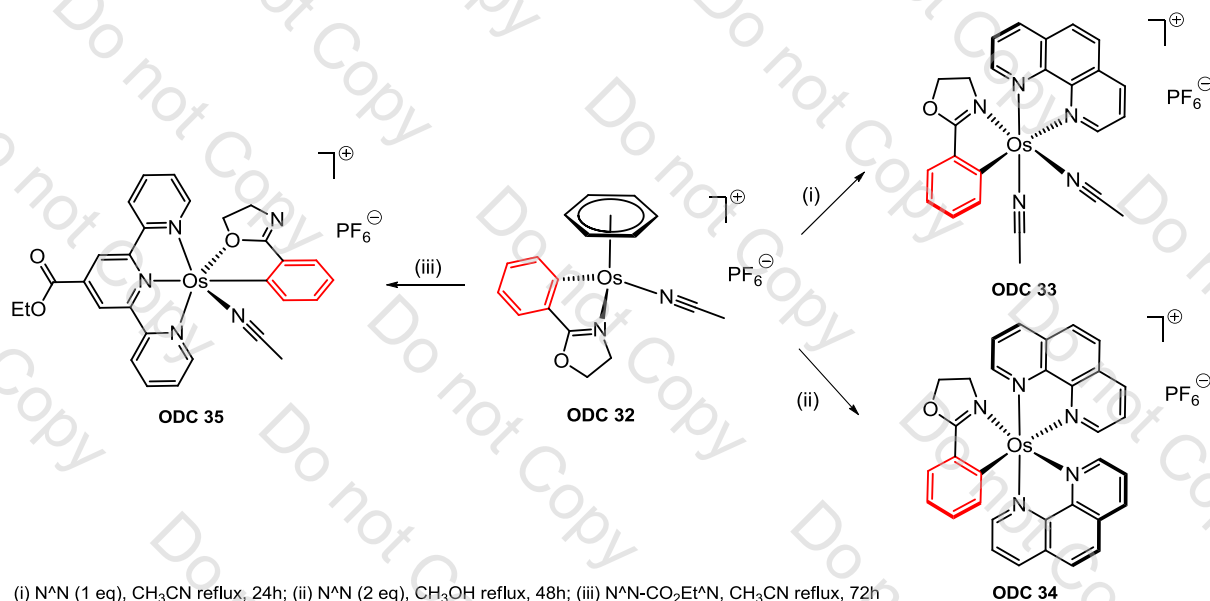


Figure 19: Synthesis of first generation ODCs containing 2-phenyl-2-oxazoline cyclometalated ligand

3.3.2. Cytotoxic activity of completed first generation Os(II) chemical library

3.3.2.1. *In vitro* antiproliferative activity results:

The antitumor potential of these first generation ODCs has been evaluated by measuring their effects on the cell proliferation of A172 (human glioblastoma) in similar way as previously.

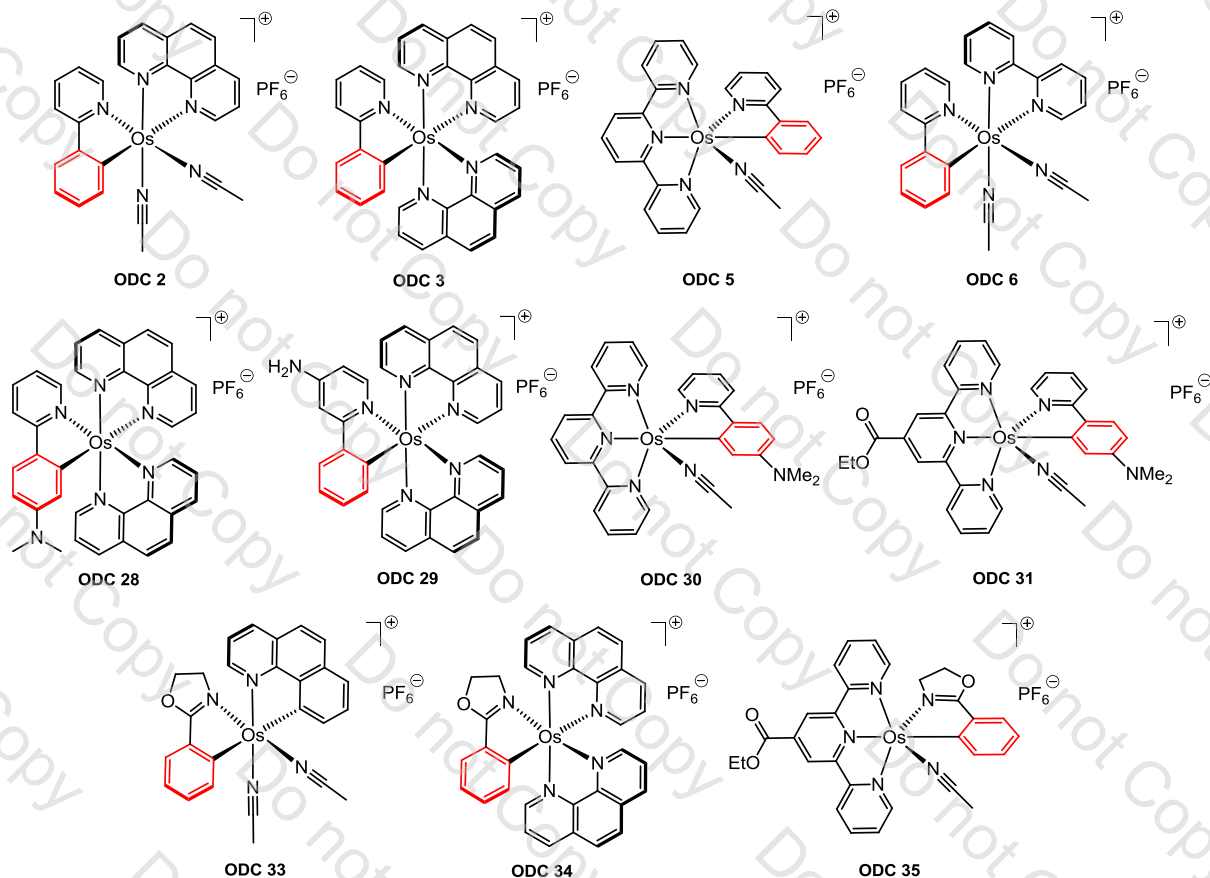
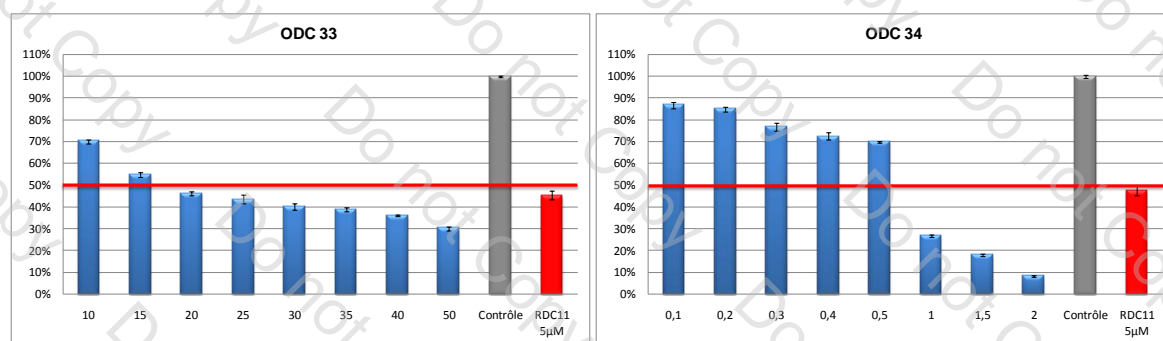


Figure 20: Chemical library of first generation Os(II) complexes



Figure 21: Antiproliferative *in vitro* activity of first generation ODCs containing 2-phenyl-2-oxazoline metalacycle on an A172 cell line



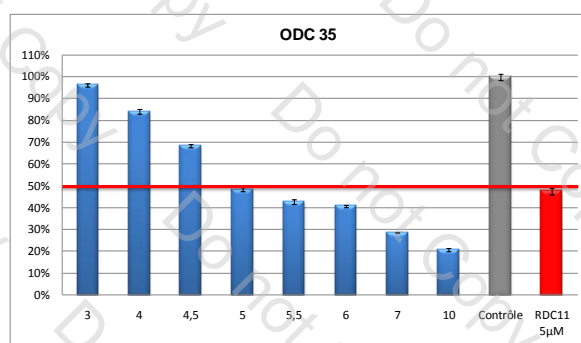


Figure 22: Antiproliferative *in vitro* activity of first generation ODCs containing 2-phenyl-2-oxazoline metalacycle on an A172 cell line

The IC_{50} results are summarised in **Table 7** and compared to those obtained with the previously reported **RDC 11** at $5\mu M$ (**Figure 17**). These compounds show promising effects for their *in vitro* activities comparable to those of ruthenium compounds developed by the laboratory. Indeed, **ODC 2** and **ODC 3** display similar antiproliferative behaviours towards A172 cell line as their corresponding **RDC 11** ($IC_{50} = 5\mu M \pm 0.5$) and **RDC 34** ($IC_{50} = 0.5\mu M \pm 0.1$) ruthenium congeners. However, no clear-cut **Structure Activity Relationship** can be rationalized from these results.

By comparing **ODC 2** and **ODC 33**, these complexes should display similar anticancer behaviour. Indeed, they are quite similar in term of lipophilicity, but the differences can be explained by their different red-ox potential. Substitution of 2-phenylpyridine with an electron-donating group (such as NMe_2 in **ODC 28**) or an electron-withdrawing group (such as NH_2 in **ODC 29**) should respectively increase or decrease the lipophilicity but also modify the red-ox potential. Hence, lipophilicity and red-ox potential should be taken into account in the drug design. For this reason we checked whether the red-ox potential (see **Chapter 3, 3.5.**) and the measurement of lipophilicity (see **Chapter 4, 4.2.**) of our compounds could be correlated with their *in vitro* activity through a rationalized **Property Activity Relationship** (P.A.R.). This class of organometallic osmium complexes has new and unusual features, worthy of further exploration for the design of novel anticancer drugs.

<i>ODCs</i> <i>first generation</i>	IC_{50} (μM) A172	<i>ODCs</i> <i>first generation</i>	IC_{50} (μM) A172
ODC 2	2 ± 0.2	ODC 31	2.25 ± 0.1
ODC 3	0.4 ± 0.2	ODC 33	18 ± 2.0
ODC 5	14 ± 0.5	ODC 34	0.75 ± 0.3
ODC 6	>25	ODC 35	5.0 ± 0.2
ODC 28	1.25 ± 0.1	RDC 11	5 ± 0.5
ODC 29	8.5 ± 0.5	RDC 34	0.5 ± 0.1
ODC 30	3.5 ± 0.5	Cisplatin	5 ± 0.5

Table 7: Recapitulative table of the IC_{50} values on an A172 cell line

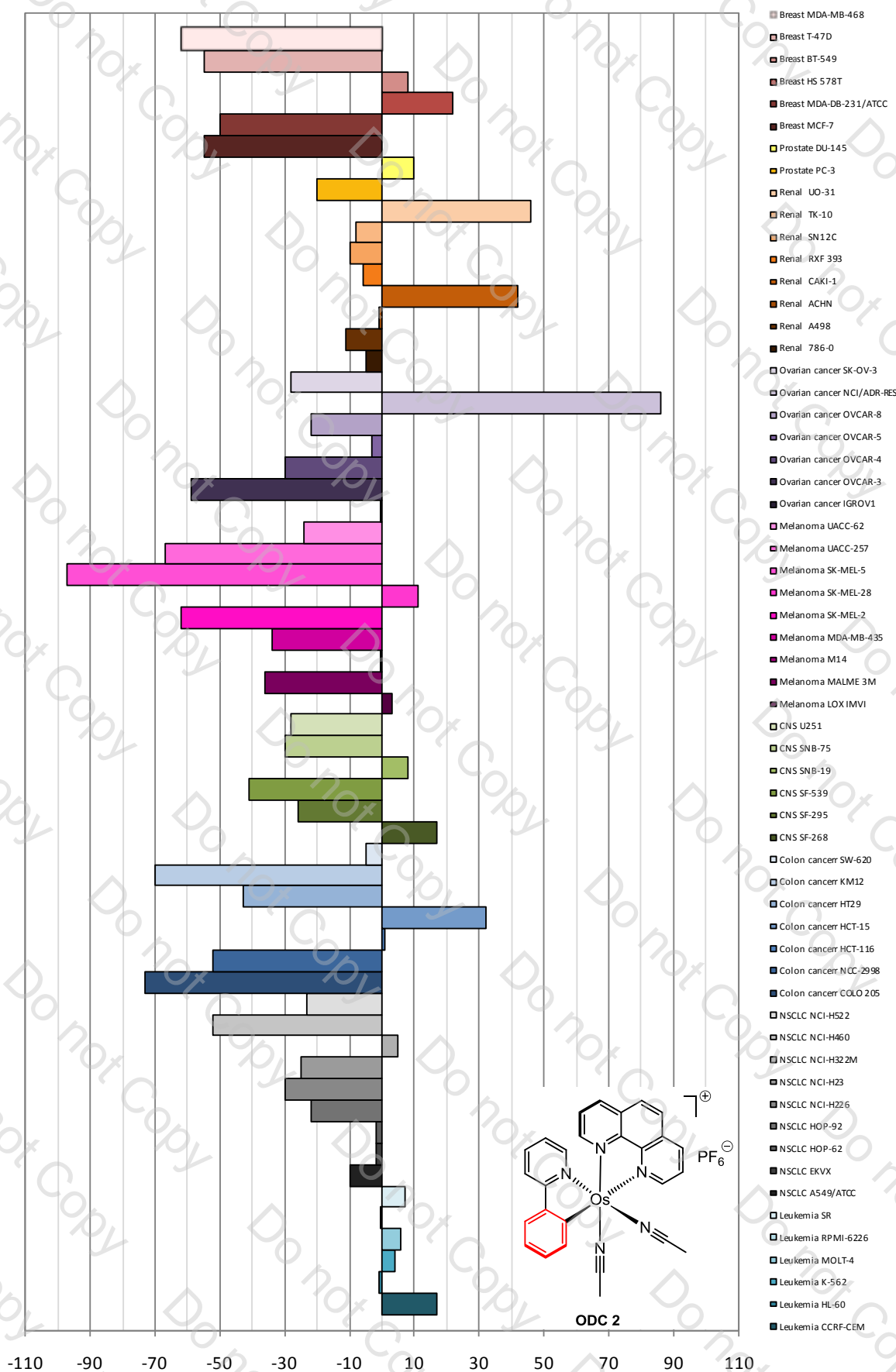


Figure 23: Cellular response towards ODC 2 treatment on 60 cancerous cell lines

3.3.2.2. Results from the National Cancer Institute:

The osmium **ODC 2** (analogue of our lead product **RDC 11**) was also sent to the National Cancer Institute (NCI) to be screened in the 60-cell lines panel, representing nine tumour types (see also Chapter 2, 2.1.3.3.). As expected, **ODC 2** seems to be a good drug candidate, given that it is cytotoxic against several cell lines with different activity potentials. It is particularly active against several breast cancers (MDA-MB-468, T-47D, MDA-D8-231/ATCC, MCF-7), one ovarian cancer (OVCAR-3), several melanomas (UAC-257, SK-MEL-5, SK-MEL-2), several colon cancers (KM 12, COLO 205) and against one non-small-cell lungs carcinoma (NSCL NCI-460) (**Figure 23**). Further extensive *in-vivo* experiments (determining chronic and acute toxicities) should determine if this class of osmium complexes is worthwhile and well tolerated in animal models. Two other samples of first generation **ODC 28** and **ODC 34** were also sent to the NCI and are currently being evaluated.

3.4. Achievement of second-generation Os(II) chemical library

3.4.1. Synthesis of cyclometalated second-generation Os(II) complexes

We demonstrated in Chapter 2 that the other ligands bound to the metal centre also play an important role in the anticancer activity of the complexes. In a similar way, we sought to extend the family of osmium complexes which may exhibit similar antiproliferative behaviour. Therefore, a series of second generation **ODCs** chemical library has been obtained in which the C-Os bond is stabilized by two intramolecular N-Os bonds instead of one in the first generation complexes.

A series of cyclometalated osmium compounds bearing either a tridentate N[^]C[^]N[^]- or N[^]N[^]C[^]- cyclometalated ligand and one bidentate N[^]N or tridentate N[^]N[^]N ligand were synthesized and characterized. All substituted N[^]C(H)[^]N[^] and C(H)[^]N[^]N[^] and substituted terpyridine ligands used in second generation **ODCs** were prepared according to literature procedure (see Chapter 5, Experimental part). Use of substituted N[^]C(H)[^]N[^] and C(H)[^]N[^]N[^] is essential in order to avoid complex mixtures, because in the case of non substituted N[^]C(H)[^]N[^] and C(H)[^]N[^]N[^] cyclometallation can occur either inside or outside the pincer (see discussion Chapter 2, 2.1.2.).

From previous works from Ryabov *et al.*,¹⁰ it is known that the chloro-bridged osmium dimer $[\eta^6-(C_6H_6)OsCl(\mu Cl)]_2$ treated in mild conditions with 2-phenylpyridine in the presence of NaOH and KPF₆ yields the corresponding $[Os(o-C_6H_4py-\kappa C,N)(\eta^6-(C_6H_6))(NCMe)]PF_6$ C,N-cyclometalated complex. A new factor is the stronger binding of the benzene ligand to the

osmium centre. Therefore, intramolecular cleavage of C(sp²)-H bond by osmium complexes to produce cyclometalated N[^]C[^]N[^] or N[^]N[^]^C compounds should be even more difficult. Hence, first attempts to prepare [Os(N[^]C[^]N[^])(NCMe)₃]PF₆ using similar conditions were unsuccessful. In particular, refluxing a solution of dimeric starting material in acetonitrile for 48h or for 72h leads to the quantitative recovery of the dimer. However, by repeating the reaction under photochemical conditions using a 60W lamp (incandescent bulb) **ODC 21-24** are formed in good yields (**Figure 24**).

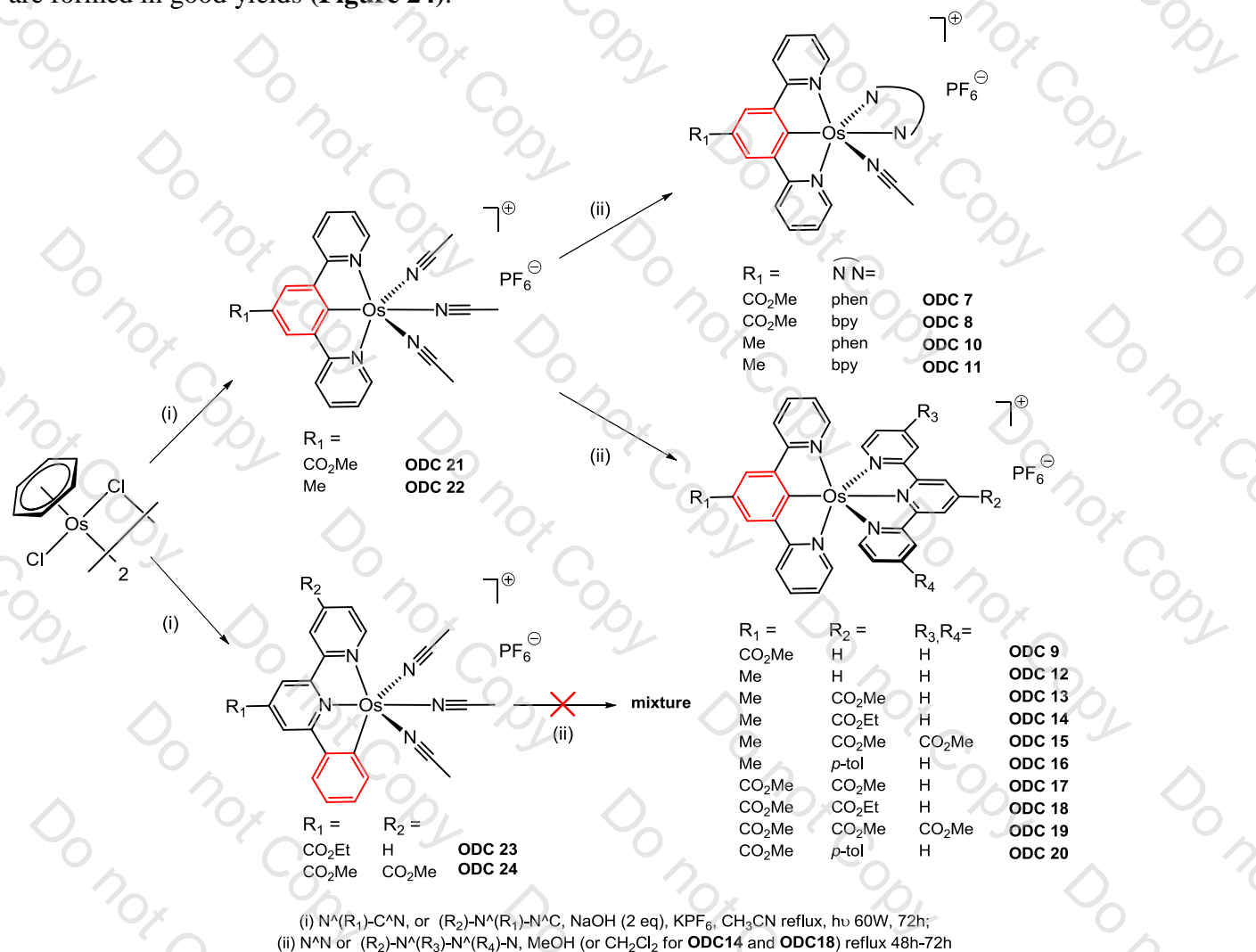


Figure 24: Synthesis of second generation ODCs containing N[^]C[^]N[^] or N[^]N[^]^C pincers

Further reaction of **ODC 21-22** with bidentate 1,10-phenanthroline or 2,2'-bipyridine (N[^]N[^]) or tridentate substituted terpyridine (N[^]N[^]N[^]) affords **ODC 7-20**. Despite many attempts, further reaction of **ODC 23-24** with bidentate or tridentate ligands respectively in dichloromethane (to avoid *trans*-esterification) or methanol led to a complex mixture whose species still remain unknown. To complement the study, we ascertained the structure of this class of compounds by performing a three-dimensional structure determination by means of an X-ray diffraction study on single crystals of **ODC 9**, **ODC 16**, **ODC 12** and **ODC 13**.

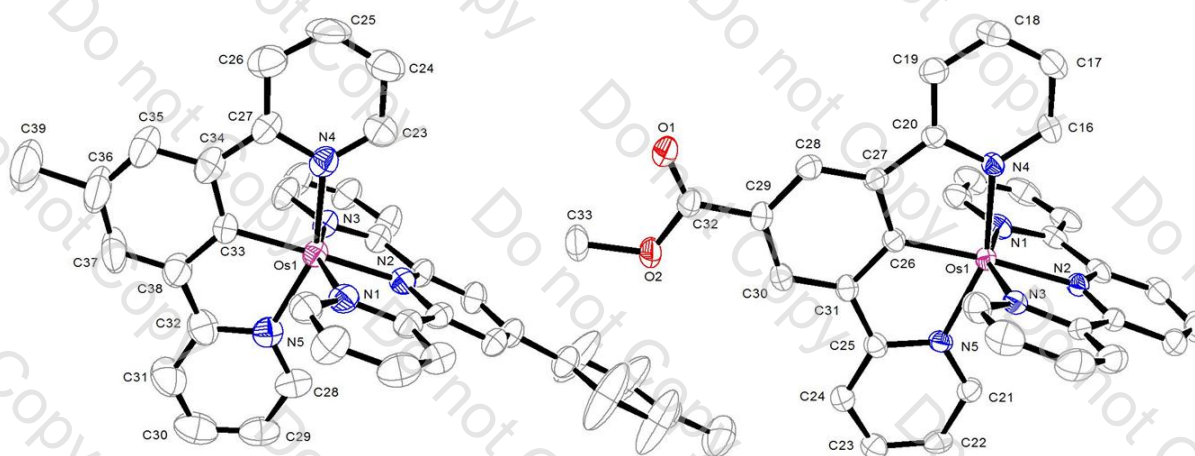


Figure 25: ORTEP diagram of the molecular structure of ODC 16 (left) and ODC 9 (right). Ellipsoids are drawn at a probability level of 50%. Hydrogen atoms, counter anions and solvent have been omitted for clarity.

Compound reference	ODC 16	ODC 9
Chemical formula	$C_{39}H_{30}N_5Os \cdot F_6P$	$C_{33}H_{24}N_5O_2Os \cdot F_6P \cdot CH_2Cl_2$
Formula Mass	903.85	942.67
Crystal system	Monoclinic	Triclinic
$a/\text{\AA}$	20.3616(9)	9.0078(2)
$b/\text{\AA}$	23.1063(10)	13.9936(6)
$c/\text{\AA}$	17.1986(6)	14.0300(5)
$\alpha/^\circ$	90.00	77.509(2)
$\beta/^\circ$	91.309(3)	84.338(2)
$\gamma/^\circ$	90.00	73.697(2)
Unit cell volume/ \AA^3	8089.5(6)	1655.86(10)
Temperature/K	173(2)	173(2)
Space group	$C2/c$	$P-1$
No. of formula units per unit cell, Z	8	2
No. of reflections measured	54318	16533
No. of independent reflections	9215	7549
R_{int}	0.0954	0.0577
Final R_i values ($I > 2\sigma(I)$)	0.0518	0.0393
Final $wR(F^2)$ values ($I > 2\sigma(I)$)	0.1360	0.0956
Final R_i values (all data)	0.0809	0.0489
Final $wR(F^2)$ values (all data)	0.1520	0.1112

Table 8: Details for the X-ray crystal structure determination of ODC 16 and ODC 9

ODC 16		ODC 9	
C33 – Os1	1.982(7)	C26 – Os1	1.971(5)
N1 – Os1	2.053(6)	N1 – Os1	2.068(5)
N2 – Os1	2.018(5)	N2 – Os1	2.038(4)
N3 – Os1	2.055(5)	N3 – Os1	2.053(4)
N4 – Os1	2.076(6)	N4 – Os1	2.084(4)
N5 – Os1	2.080(6)	N5 – Os1	2.085(4)
N1 – Os1 – N2	77.8(2)	N1 – Os1 – N2	77.49(19)
N2 – Os1 – N3	78.0(2)	N2 – Os1 – N3	77.73(18)
N4 – Os1 – C33	77.4(3)	N4 – Os1 – C26	78.37(18)
N5 – Os1 – C33	77.9(3)	N5 – Os1 – C26	78.00(19)
Os1 – C33 – C38	120.1(5)	Os1 – C26 – C31	119.8(4)
C33 – C38 – C32	111.4(6)	C26 – C31 – C25	112.0(4)
C38 – C32 – N5	115.9(6)	C31 – C25 – N5	113.8(4)
C32 – N5 – Os1	114.7(5)	C25 – N5 – Os1	116.2(3)
Os1 – C33 – C34	119.8(5)	Os1 – C26 – C27	119.5(4)
C33 – C34 – C27	112.0(6)	C26 – C27 – C20	111.7(4)
C34 – C27 – N4	114.1(6)	C27 – C20 – N4	114.4(4)
C27 – N4 – Os1	116.4(5)	C20 – N4 – Os1	115.9(3)

Table 9: Selected bond length (Å), angles (°) for ODC 16 and ODC 9

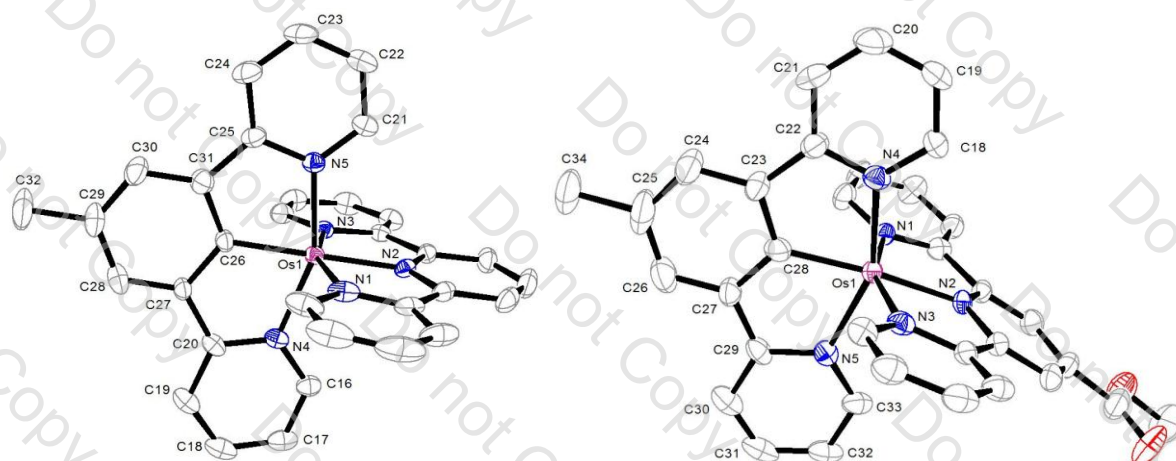


Figure 26: ORTEP diagram of the molecular structure of ODC 12 (left) and ODC 13 (right). Ellipsoids are drawn at a probability level of 50%. Hydrogen atoms, counter anions and solvent have been omitted for clarity.

Compound reference	ODC 12	ODC 13
Chemical formula	$C_{32}H_{24}N_5Os \cdot F_6P \cdot CH_2Cl_2$	$C_{34}H_{26}N_5O_2Os \cdot F_6P$
Formula Mass	898.66	871.77
Crystal system	Monoclinic	Monoclinic
$a/\text{\AA}$	17.4514(7)	19.6684(4)
$b/\text{\AA}$	20.7576(8)	23.1782(3)
$c/\text{\AA}$	24.9930(7)	16.6905(3)
$\alpha/^\circ$	90.00	90.00
$\beta/^\circ$	134.063(2)	90.1190(10)
$\gamma/^\circ$	90.00	90.00
Unit cell volume/ \AA^3	6505.8(4)	7608.8(2)
Temperature/K	173(2)	173(2)
Space group	$P2_1/c$	$P2_1/c$
No. of formula units per unit cell, Z	8	8
No. of reflections measured	105006	51974
No. of independent reflections	19035	17401
R_{int}	0.0289	0.0526
Final R_i values ($I > 2\sigma(I)$)	0.0313	0.0426
Final $wR(F^2)$ values ($I > 2\sigma(I)$)	0.0549	0.1239
Final R_i values (all data)	0.0516	0.0594
Final $wR(F^2)$ values (all data)	0.0659	0.1305

Table 10: Details for the X-ray crystal structure determination of ODC 12 and ODC 13

ODC 12		ODC 13	
C26 – Os1	1.976(3)	C28 – Os1	1.968(5)
N1 – Os1	2.057(3)	N1 – Os1	2.050(4)
N2 – Os1	2.012(3)	N2 – Os1	2.002(4)
N3 – Os1	2.060(3)	N3 – Os1	2.066(4)
N4 – Os1	2.080(3)	N4 – Os1	2.075(4)
N5 – Os1	2.083(3)	N5 – Os1	2.099(4)
N1 – Os1 – N2	78.26(13)	N1 – Os1 – N2	78.39(15)
N2 – Os1 – N3	78.01(11)	N2 – Os1 – N3	77.88(16)
N4 – Os1 – C26	77.67(14)	N4 – Os1 – C28	77.01(18)
N5 – Os1 – C26	78.01(13)	N5 – Os1 – C28	78.17(18)
Os1 – C26 – C27	119.9(3)	Os1 – C28 – C27	119.4(4)
C26 – C27 – C20	112.4(3)	C28 – C27 – C29	112.4(4)
C27 – C20 – N4	113.7(3)	C27 – C29 – N5	114.1(4)
C20 – N4 – Os1	116.2(2)	C29 – N5 – Os1	115.6(3)
Os1 – C26 – C31	120.2(3)	Os1 – C28 – C23	121.0(4)
C26 – C31 – N5	111.9(3)	C28 – C23 – C22	111.4(5)
C31 – C25 – N5	114.3(3)	C23 – C22 – N4	114.0(4)
C25 – N5 – Os1	115.6(2)	C22 – N4 – Os1	116.0(3)

Table 11: Selected bond length (\AA), angles ($^\circ$) for ODC 12 and ODC 13

3.4.2. Cytotoxic activity of second generation ODCs

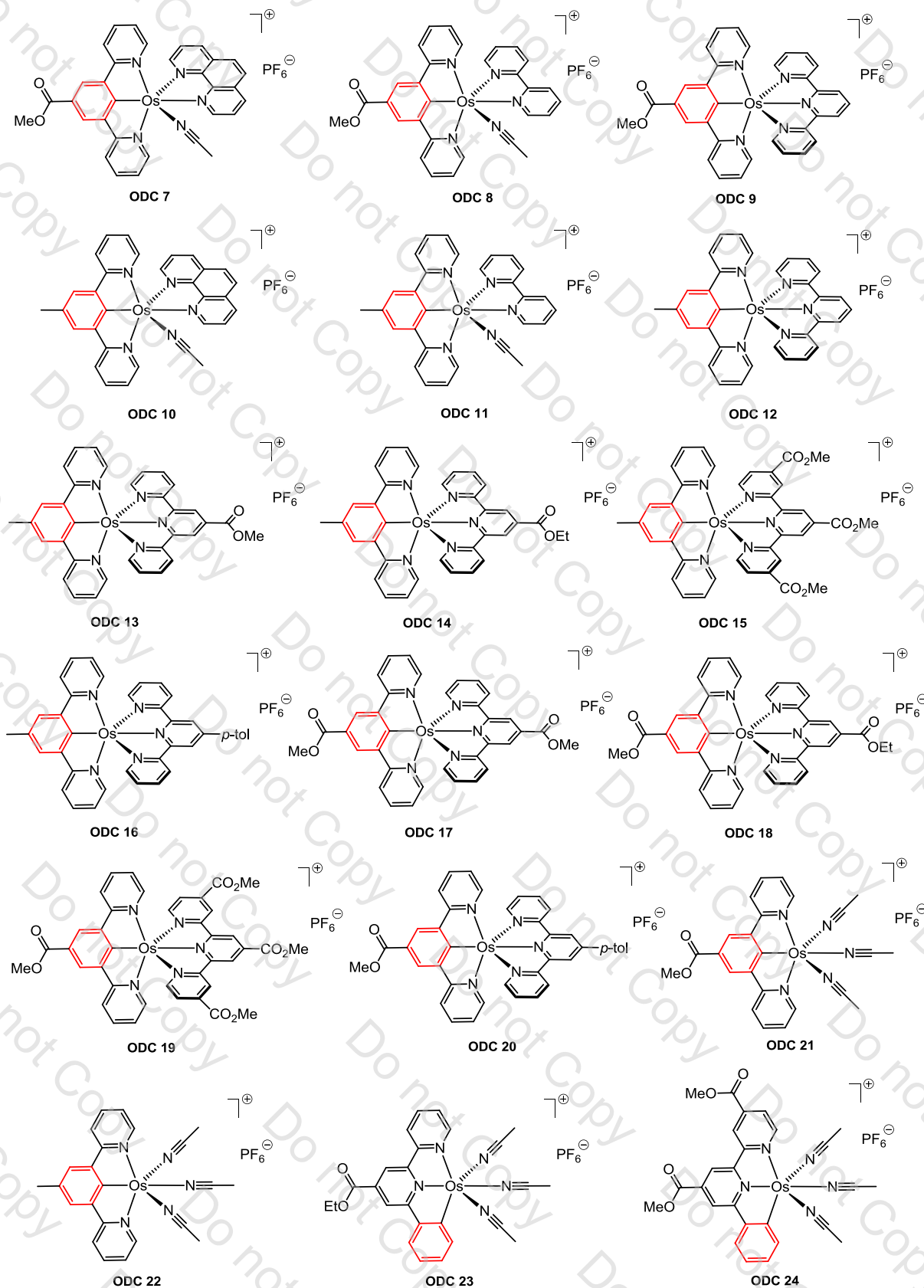
3.4.2.1. *In vitro* antiproliferative activity results:

Figure 27: Chemical library of second generation ODC compounds

The antitumor potential of various second generation ODCs has been evaluated by measuring their effects on the cell proliferation of A172 (human glioblastoma) as previously described. The IC₅₀ results are summarized in recapitulative **Table 12** and compared to those obtained with the previously reported **RDC 11** at 5 μ M (**Figure 28** and **Figure 29**). This new generation of ODC complexes enabled us to diversify and complement the first generation chemical library. We found that these **second generation** compounds display good to very good cytotoxicity passing for nine of them the symbolic barrier of the nanomolar range for their IC₅₀. This indicates a critical improvement comparatively to the **first generation** ODCs.



Figure 28: Antiproliferative *in vitro* activity of second generation ODCs on an A172 cell line



Figure 29: Antiproliferative *in vitro* activity of second generation ODCs on an A172 cell line (continued)

At first sight, it is obvious that all complexes having a genuine N^{^C^N} cyclometalated unit display very good cytotoxicities. Compared to their second generation **RDC** congeners, these **second generation ODCs** display similar antiproliferative effects on the A172 cell line (**Table 12**).

Substitution of the N^{^C^N} cyclometalated ligand had little effect on the cytotoxicity of the molecule. For instance, the exchange of CO₂Me group by methyl group on the cyclometalated ring does not show drastic effects on the activity.

<i>ODCs</i>	<i>IC₅₀ (μM)</i>	<i>ODCs</i>	<i>IC₅₀ (μM)</i>
<i>second generation</i>	<i>A172</i>	<i>second generation</i>	<i>A172</i>
ODC 7	1.6 ± 0.2	ODC 17	0.95 ± 0.1
ODC 8	3.8 ± 0.3	ODC 18	0.95 ± 0.1
ODC 9	0.8 ± 0.1	ODC 19	1.9 ± 0.1
ODC 10	3.6 ± 0.2	ODC 20	0.25 ± 0.1
ODC 11	4.1 ± 0.2	ODC 21	320 ± 5.0
ODC 12	0.3 ± 0.1	ODC 22	375 ± 5.0
ODC 13	0.45 ± 0.1	ODC 23	21 ± 1.0
ODC 14	0.45 ± 0.1	ODC 24	62 ± 1.0
ODC 15	0.85 ± 0.1	RDC 11	5 ± 0.5
ODC 16	0.25 ± 0.1	Cisplatin	5 ± 0.5

Table 12: Recapitulative table of the IC₅₀ values on an A172 cell line

By comparing **ODC 7** with the **ODC 8**, the compounds must display similar red-ox properties because they are structurally similar. But **ODC 7** is more lipophilic than **ODC 8** because of the coordination of 1,10-phenanthroline instead of 2,2'-bipyridine and hence displays better cytotoxic properties. The same trend can be observed with **ODC 10** compared to **ODC 11**.

Paradoxically, by comparing **ODC 13** with the **ODC 15**, **ODC 15** should be more lipophilic, and so more able to cross membrane of tumorous cells than **ODC 13**. However, **ODC 13** displays a better activity than **ODC 15**. The same tendency can be observed for **ODC 16** compared to **ODC 19**. However, the red-ox potential can perhaps explain the antiproliferative activity, as it is the case for **RDC** complexes.

Thus, as we did not find any obvious **Structure Activity Relationship**, we checked whether the red-ox potential (see **Chapter 3, 3.5.**) and the lipophilicities (see **Chapter 4, 4.2.**) could be correlated with their *in vitro* cytotoxicities because these two parameters should be taken into account in drug design.

The precursor **ODC 21-24** are non cytotoxic probably due to their low lipophilicities (**ODC 21** and **ODC 22**) or due to their higher red-ox potential (**ODC 23** and **ODC 24**). But in these complexes, MeCN ligands are relatively labile and solubilization of these latter in DMSO may not represent the initial composition of the compounds. These four compounds were thus discarded from the *in vitro* tests.

We can note that the cellular respon can also be plotted in terms of IC₅₀ as a function of log₁₀([concentration of complex in μM]) to draw sigmoids whose functions can easily be calculated using non-linear regression of the experimental points (**Figure 30**). Fitting of the curves based on a 4-parameter sigmoid function was carried out but no correlation between the IC₅₀ and the slope of the tangent at the inflexion point of the curve can be observed.

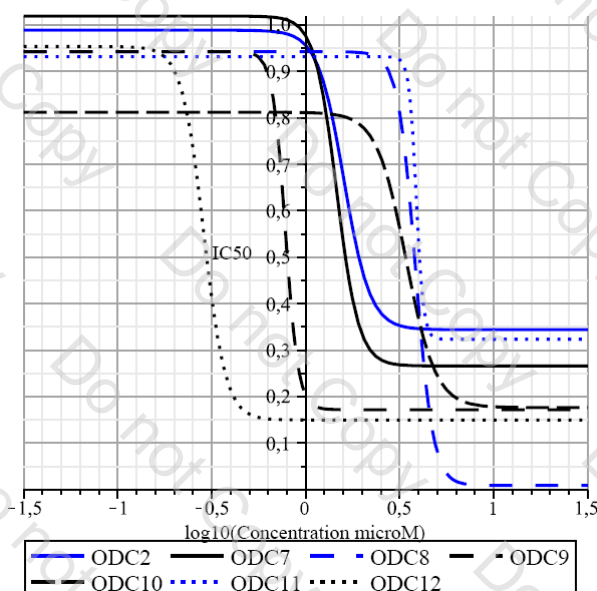


Figure 30: Fittings of the curves were based on a 4-parameter sigmoid function of type $y = y_0 + \frac{a}{1 + e^{-\left(\frac{x-x_0}{b}\right)}}$

3.4.2.2. Results from the National Cancer Institute:

The second generation **ODC 9** and **ODC 12** were sent to the National Cancer Institute (NCI) to be screened in the 60-cell lines panel, representing nine tumour types (see also **Chapter 2, 2.1.3.3.**). As expected, both complexes show antiproliferative properties in practically all cell lines, except leukemia. However, these data must be considered cautiously and be put into perspective. Only further extensive *in-vivo* experiments (determining chronic and acute toxicities) will determine if this class of osmium complexes is worthwhile and well accepted in animal models. Four other samples of second generation **ODC 13, ODC 16, ODC 19** and **ODC 20** were also sent to the NCI and are currently being evaluated.

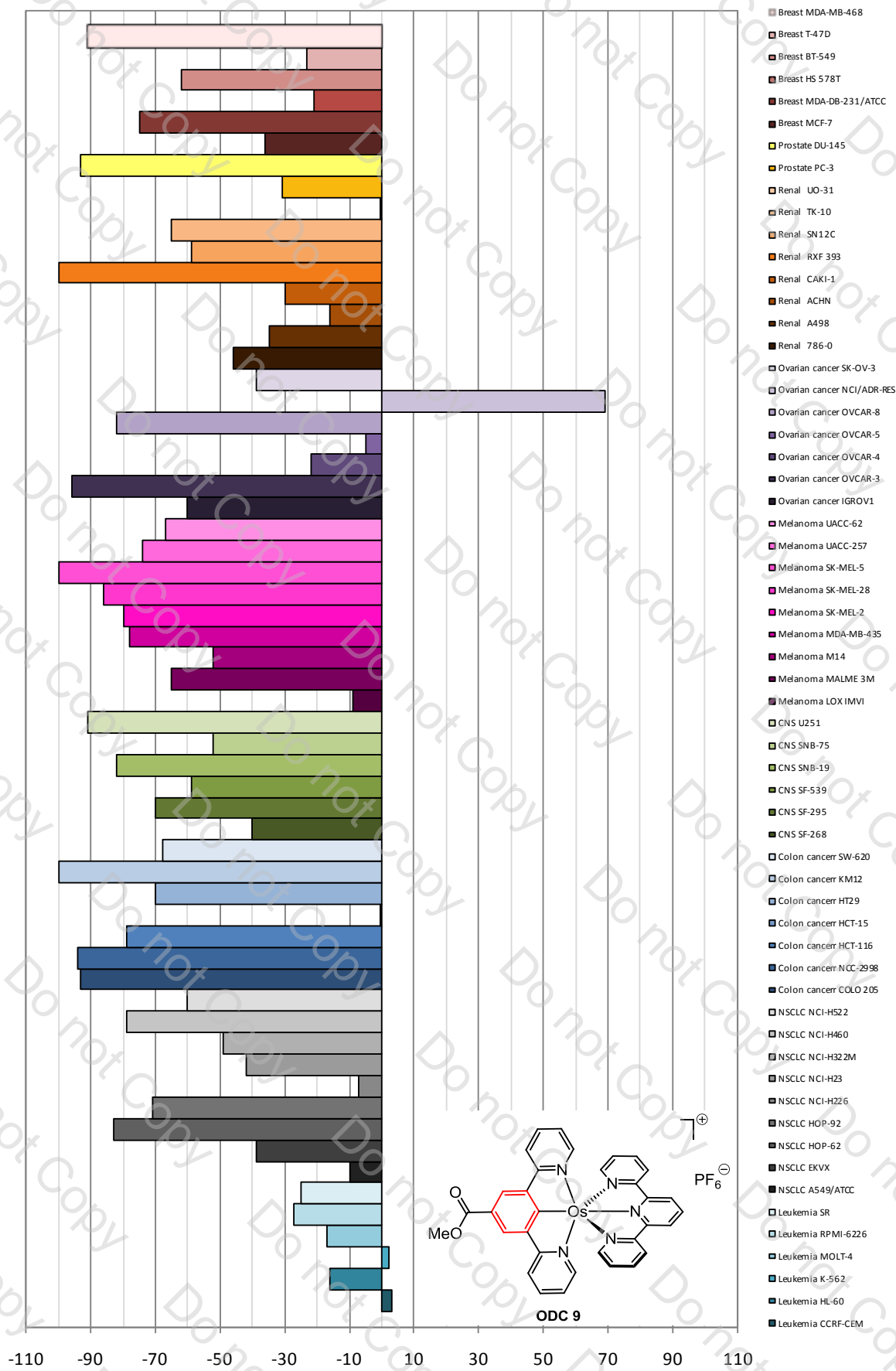


Figure 31: Cellular response towards ODC 9 treatment on 60 cancerous cell lines

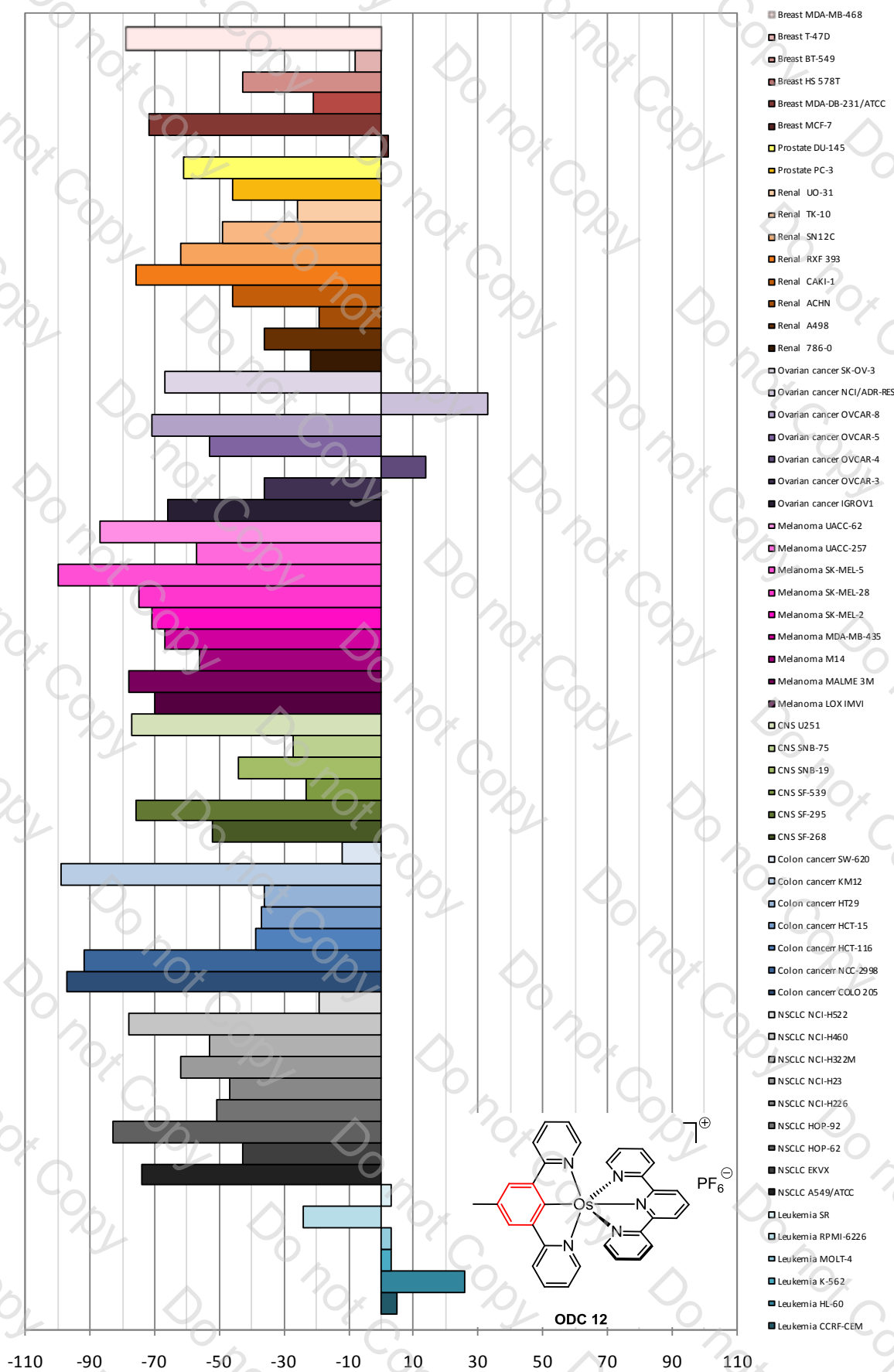


Figure 32: Cellular response towards ODC 12 treatment on 60 cancerous cell lines

3.5. Electrochemical properties of first and second generation ODCs

As already discussed in **Chapter 2, 2.1.4.**, Keppler *et al.*¹⁵ found that the most active compounds in a series of ruthenium indazole (ind) adducts $[\text{Ru}^{\text{III}}\text{Cl}_{(6-n)}(\text{ind})_n]^{(3-n)-}$ were those whose red-ox potential was between 0.1 and 0.58 V vs. NHE. This relation between reduction potentials and cytotoxic activity observed within a homologous series of ruthenium compounds has substantiated the concept of fine tuning biological activity of ruthenium complexes by adjusting their ligand composition to achieve desired red-ox properties.

However, no real correlation between antiproliferative activity and red-ox potential indicates that the main determinant factor for biological activity is the influence of this parameter. In pursuing the long-term goal of elucidating the relationship between $\text{Os}^{\text{III}}/\text{Os}^{\text{II}}$ red-ox potential and cytotoxicity, and hence establishing **Structure Activity Relationship** for osmium congeners, Keppler *et al.* reported also several osmium(III) complexes comprising azole heterocycle.^{16,17} However, for this class of $\text{Os}(\text{III})$ compounds, the authors suggested that there was no evidence of a correlation between antiproliferative activity and red-ox potential.

The Laboratoire de Synthèses Métallo-Induites demonstrated that one of the main factors that contributes to the biological activity is the presence of the genuine **carbon-metal bond** in the molecular structure of our cyclometalated compounds.¹⁸ Given that no clear-cut S.A.R. can be rationalized from *in vitro* results, we demonstrated here that the red-ox potential can be related to the IC_{50} of a series of **ODCs**. For overall view of **first and second generation osmium complexes** see the **Appendix, Figure 2 and Figure 3**.

As previously described for their ruthenium congeners, the electrochemical properties of these **ODCs** have been studied by cyclic voltammetry in an 0.1M $[n\text{-Bu}_4\text{N}][\text{PF}_6]$ electrolyte using a three electrode system (see **Chapter 2, 2.1.4.**). Except for osmium piano-stool complexes which display an irreversible single electron oxidation wave attributed to $\text{Os}^{\text{II}} \rightarrow \text{Os}^{\text{III}}$ process with $E^{\circ}_{1/2}$ potential values between 1.0 and 1.7V (vs. SCE), all the other **ODCs** present a reversible single electron oxidation wave attributed to $\text{Os}^{\text{II}} \rightarrow \text{Os}^{\text{III}}$ process with $E^{\circ}_{1/2}$ potential values between 0.13 and 0.65V (vs. SCE). The electrochemical data for these complexes are summarized in **Table 13**.

With no precedent, a binomial correlation between the red-ox potential and the cytotoxicity of first and second generation **ODCs** has been established (**Figure 33**) with fairly good accuracy ($R^2=0.88$). As discussed previously, compounds **ODC 21-24** were discarded from the correlation because they display labile MeCN ligands and the IC_{50} data would have been not

representative of the initial composition of the tested solutions. **ODC 25** was also discarded from the correlation because it does not contain a carbon-metal bond, and hence do not belong to the same class of compounds. The neutral **ODC 38** does not bear a PF_6^- counterion like its other congeners and was thus also discarded from the correlation. The relative non-cytotoxic compound ($>100\mu\text{M}$) or those which can rapidly substitute MeCN ligand with DMSO were also discarded (**ODC 32, ODC 33, ODC 36, ODC 37, ODC 39**).

Similarly to **RDCs**, these data clearly show that molecules having a red-ox potential in the range **0.3-0.6V** (vs. SCE) display the lowest IC_{50} . We already discussed in previous sections that the biological activity does not seem to correlate with the chemical structure, but rather with the physicochemical properties. Hence, the red-ox properties may again be involved in the biological activity given that oxidation states of osmium are all accessible under physiological conditions.

The rationalization of this correlation is not clear yet, but a reasonable hypothesis could however be that the osmium compounds could alter the behaviour of certain enzymes in a similar manner as their ruthenium congeners. Moreover, the relative dispersion of the points may again reflect small variations of others parameters such as lipophilicity and/or possibly shape. Hence, other key factors influencing the cytotoxicity such as lipophilicity, cellular uptake, and interaction with molecular targets should be taken into account in order to develop and assess a Property-Activity Relationship (P.A.R.) model suitable to predict the cytotoxicity of the future drugs from their bio-physicochemical properties.

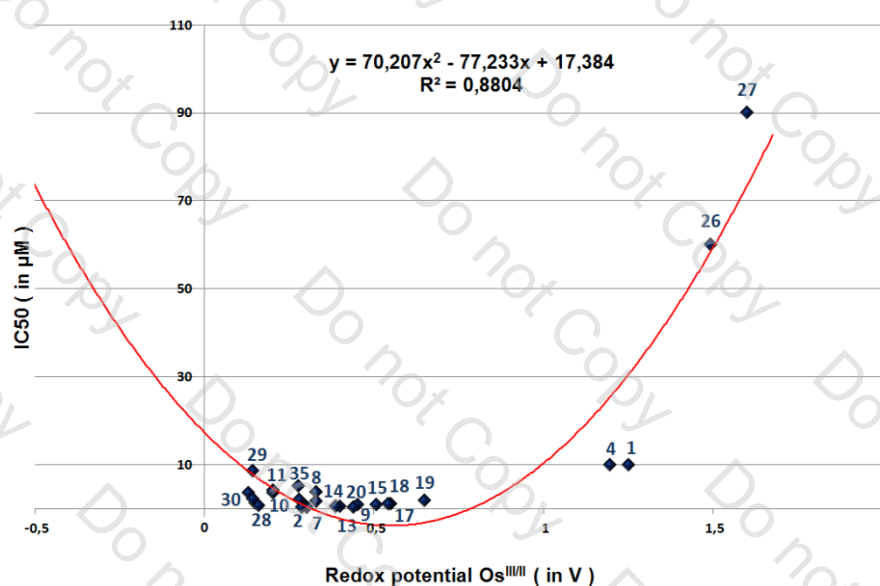


Figure 33: Binomial correlation between IC_{50} and red-ox potential $E^{\circ}_{1/2}(\text{Os}^{\text{III/II}})$

<i>Complexes</i>	<i>ODCs equivalent</i>	$E^{\circ}_{1/2} Os(III/II)$ ($\pm 5mV$)	E_{pa} (<i>mV</i>)	E_{pc} (<i>mV</i>)	ΔE_p	$E^{\circ}_{1/2} R^+/R$ (<i>mV</i>)	IC_{50} (μM) A172
1	ODC 1	1250 ^(a)	1250 ^(a)	-	-	-	10 \pm 0.5
2	ODC 2	280	311	249	62	-	2.0 \pm 0.2
3	ODC 3	300	329	247	58	-	0.4 \pm 0.2
4	ODC 4	1196 ^(a)	1196 ^(a)	-	-	-	10 \pm 0.5
5	ODC 5	195	224	167	57	-	14 \pm 0.5
6	ODC 6	245	289	200	89	-	> 25
7	ODC 7	330	360	300	60	-	1.6 \pm 0.2
8	ODC 8	330	359	302	57	-	3.8 \pm 0.3
9	ODC 9	454	482	425	57	-	0.8 \pm 0.1
10	ODC 10	204	237	171	66	-	3.6 \pm 0.2
11	ODC 11	203	233	172	61	-	4.1 \pm 0.2
12	ODC 12	302	332	272	60	-	0.3 \pm 0.1
13	ODC 13	400	434	366	68	-	0.45 \pm 0.1
14	ODC 14	389	422	357	65	-	0.45 \pm 0.1
15	ODC 15	508	540	476	64	-	0.85 \pm 0.1
16	ODC 16	288	319	256	63	-	0.25 \pm 0.1
17	ODC 17	550	585	516	69	-	0.95 \pm 0.1
18	ODC 18	542	576	508	68	-	0.95 \pm 0.1
19	ODC 19	650	683	618	65	-	1.9 \pm 0.1
20	ODC 20	440	477	404	73	-	0.25 \pm 0.1
21	ODC 21	359	390	328	61	-	320 \pm 0.1
22	ODC 22	213	242	182	60	-	375 \pm 0.1
23	ODC 23	536	569	503	66	-	21 \pm 0.1
24	ODC 24	602	635	569	66	-	62 \pm 0.1
25	ODC 25	1630 ^(a)	1630 ^(a)	-	-	-	125 \pm 5.0
26	ODC 26	1493 ^(a)	1493 ^(a)	-	-	739 (NMe ₂ ⁺ / NMe ₂)	60 \pm 5.0
27	ODC 27	1600 ^(a)	1600 ^(a)	-	-	1164 (NH ₂ ⁺ / NH ₂)	90 \pm 1.0
28	ODC 28	151	184	118	66	885 (NMe ₂ ⁺ / NMe ₂)	1.25 \pm 1.0
29	ODC 29	143	180	107	73	1305 (NH ₂ ⁺ / NH ₂)	8.5 \pm 5.0
30	ODC 30	131	171	91	80	886 (NMe ₂ ⁺ / NMe ₂)	3.5 \pm 5.0
31	ODC 31	143	177	109	68	884(NMe ₂ ⁺ / NMe ₂)	2.25 \pm 0.1
32	ODC 32	1234 ^(a)	1234 ^(a)	-	-	-	90 \pm 5.0
33	ODC 33	176	208	144	64	-	18 \pm 2.0
34	ODC 34	160	193	128	65	-	0.75 \pm 0.3
35	ODC 35	279	311	247	64	-	5.0 \pm 0.2
36	ODC 36	1200 ^(a)	1200 ^(a)	-	-	-	100 \pm 5.0
37	ODC 37	1030 ^(a)	1030 ^(a)	-	-	-	100 \pm 5.0
38	ODC 38	722 ^(a)	722 ^(a)	-	-	-	22 \pm 1.0
39	ODC 39	1487 ^(a)	1487 ^(a)	-	-	-	300 \pm 5.0

Table 13: Recapitulative table of red-ox potentials vs. SCE and IC₅₀ on an A172 cell line
(a): irreversible wave

$E^{\circ}_{1/2} = (E_{pa} + E_{pc})/2$ vs. FeCp₂ or [Os(terpy)₂](PF₆)₂, in mV;
Electrolyte : [*n*-Bu₄N][PF₆] 0.1 M; Scan rate : 0.100 V.s⁻¹; 20 °C

3.6. References Chapter 3

- ¹ Dorcier, A.; Ang, W.H.; Bolano, S.; Gonsalvi, L.; Juillerat-Jeannerat, L.; Laurency, G.; Peruzzini, M.; Phillips, A.D.; Zanobini, F.; Dyson, P.J. *Organometallics* **2006**, *25*, 4090–4096.
- ² Peacock, A.F.A.; Parsons, S.; Sadler, P.J. *J. Am. Chem. Soc.* **2007**, *129*, 3348–3357.
- ³ Ward, D.J.; Sheppard, H. *Rheumatology* **1980**, *19*, 25–29.
- ⁴ (a) Schmid, W. F.; John, R. O.; Arion, V. B.; Jakupec, M. A.; Keppler, B. K. *Organometallics* **2007**, *26*, 6643–6652.
(b) Schmid, W.F.; John, R.O.; Mühlgassner, G.; Heffeter, P.; Jakupec, M.A.; Galanski, M.; Berger, W.; Arion, V.B.; Keppler, B.K. *J. Med. Chem.* **2007**, *50*, 6343–6355.
(c) Schuecker, R.; John, R.O.; Jakupec, M.A.; Arion, V.B.; Keppler, B.K. *Organometallics* **2008**, *27*, 6587–6595.
(d) Stepanenko, I.N.; Krokhin, A.A.; John, R.O.; Roller, A.; Arion, V.B.; Jakupec, M.A.; Keppler, B.K. *Inorg. Chem.* **2008**, *47*, 7338–7347.
(e) Reisner, E.; Arion, V.B.; Keppler, B.K.; Pombeiro A.J.L. *Inorg. Chim. Acta.* **2008**, *361*, 1569–1583.
(f) Buchel, G.E.; Stepanenko, I.N.; Hejl, M.; Jakupec, M.A.; Arion, V.B.; Keppler, B.K., *Inorg. Chem.* **2009**, *48*, 10737–10747
(g) Hanif, M.; Henke, H.; Meier, S.M.; Martic, S.; Labib, M.; Kandioller, W.; Jakupec, M.A.; Arion, V.B.; Kraatz, H.-B.; Keppler, B.K. *Inorg. Chem.* **2010**, *49*, 7953–7963.
(h) Filak, L.K.; Muehlgassner, G.; Bacher, F.; Roller, A.; Galanski, M.; Jakupec, M.A.; Keppler, B.K.; Arion, V.B. *Organometallics* **2011**, *30*, 273–283.
- ⁵ (a) Renfrew, A.K.; Phillips, A.D.; Egger, A.E.; Hartinger, C.G.; Bosquain, S.S.; Nazarov, A.A.; Keppler, B.K.; Gonsalvi, L.; Peruzzini, M.; Dyson, P.J. *Organometallics* **2009**, *28*, 1165–1172.
(b) Barry, N.P.E.; Edate, F.; Dyson, P.J.; Therrien, B. *Dalton Trans.* **2010**, *39*, 2816–2820.
(c) Hanif, M.; Nazarov, A.A.; Hartinger, C.G.; Kandioller, W.; Jakupec, M.A.; Arion, V.B.; Dyson, P.J.; Keppler, B.K. *Dalton Trans.* **2010**, *39*, 7345–7352.
- ⁶ (a) Peacock, A.F.A.; Habtemariam, A.; Fernandez, R.; Walland, V.; Fabbiani, F.P.A.; Parsons, S.; Aird, R. E.; Jodrell, D.I.; Sadler, P. J. *J. Am. Chem. Soc.* **2006**, *128*, 1739–1748.
(b) Peacock, A.F.A.; Melchart, M.; Deeth, R.J.; Habtemariam, A.; Parsons, S.; Sadler, P.J. *Chem. Eur. J.* **2007**, *13*, 2601–2613.
(c) Peacock, A.F.A.; Habtemariam, A.; Moggach, S.A.; Prescimone, A.; Parsons, S.; Sadler, P.J. *Inorg. Chem.* **2007**, *46*, 4049–4059.
(d) Ronconi, L.; Sadler, P.J. *Coord. Chem. Rev.* **2007**, *251*, 1633–1648.
(e) Kostrhunova, H.; Florian, J.; Navakova, O; Prescimone, Peacock, A.F.A.; Sadler, P.J.; Brabec, V. *J. Med. Chem.* **2008**, *51*, 3635–3643.
(f) Sadler, P.J., Peacock, A.F.A.; Van Rijt, S.H.; Habtemariam, A.; *PCT Int. Appl.* **2008**, WO 2008017855 A1 20080214.
(g) Peacock, A.F.A.; Sadler, P.J.; *Chem. Asian J.* **2008**, *3*, 1890–1899.
(h) Van Rijt, S.H.; Peacock, A.F.A.; Johnstone, R.D.L.; Parsons, S.; Sadler, P.J. *Inorg. Chem.* **2009**, *48*, 1753–1752.
(i) Bruijninx, P.C.A.; Sadler, P.J.; *Adv. Inorg. Chem.* **2009**, *61*, 1–62.
(j) Van Rijt, S.H.; Hebden, A.J.; Amaresekera, T.; Deeth, R.J.; Clarkson, G.J.; Parsons, S.; McGowan, P.C.; Sadler, P.J. *J. Med. Chem.* **2009**, *52*, 7753–7764.
(k) Van Rijt, S.H.; Sadler, P.J. *Drug Discovery Today* **2009**, *14*, 1089–1097.
(l) Van Rijt, S.H.; Mukherjee, A.; Pizarro, A.M.; Sadler, P.J. *J. Med. Chem.* **2010**, *53*, 840–849.
(m) Bergamo, A.; Masi, A., Peacock, A.F.A.; Habtemariam, A.; Sadler, P. J.; Sava, G. *J. Inorg. Biochem.* **2010**, *104*, 79–86.
(o) Fu, Y.; Habtemariam, A.; Pizarro, A.M.; Van Rijt, S.H.; Healey, D.J.; Cooper, P.A.; Shnyder, S.D.; Clarkson, G.J.; Sadler, P.J. *J. Med. Chem.* **2010**, *53*, 8192–8196.
(p) Pizarro, A.M.; Habtemariam, A., Sadler, P.J. *Top. Organomet. Chem.* **2010**, *32*, 21–56.
(q) Van Rijt, S.H.; Kostrhunova, H.; Brabec, V.; Sadler, P.J. *Bioconjugate Chem.* **2011**, *22*, 218–226.
- ⁷ (a) Dorcier, A.; Dyson, P.J.; Gossens, C.; Rothlisberger, U.; Scopelliti, R.; Tavernelli, I. *Organometallics* **2005**, *24*, 2114–2123.
(b) Dorcier, A.; Hartinger, C. J.; Scopelliti, R.; Fish, R.H.; Keppler, B.K.; Dyson, P.J. *J. Inorg. Biochem.* **2008**, *102*, 1066–1076.
- ⁸ (a) Ryabov, A. D. *Chem. Rev.* **1990**, *90*, 403–424.

- (b) Mamo, A.; Stefio, I.; Poggi, A.; Tringali, C.; Di Pietro, C.; Campagna, S. *New J. Chem.* **1997**, *21*, 1173–1185.
- (c) Majumder, K.; Peng, S.-M.; Bhattacharya, S. *J. Chem. Soc., Dalton Trans.* **2001**, 284–288.
- (d) Gusev, D. G.; Dolgushin, F. M.; Antipin, M. Y. *Organometallics* **2001**, *20*, 1001–1007.
- (e) Das, A.; Basuli, F.; Falvello, L. R.; Bhattacharya, S. *Inorg. Chem.* **2001**, *40*, 4085–4088.
- (f) Gupta, P.; Butcher, R. J.; Bhattacharya, S. *Inorg. Chem.* **2003**, *42*, 5405–5411.
- (g) Ryabov, A. D.; Soukharev, V.S.; Alexandrova, L.; Le Lagadec, R.; Pfeffer, M. *Inorg. Chem.* **2003**, *42*, 6598–6600.
- ⁹ Fernandez, S.; Pfeffer, M.; Ritleng, V.; Sirlin, C. *Organometallics* **1999**, *18*, 2390–2394.
- ¹⁰ Ceron-Camacho, R.; Morales, D.; Hernandez, S.; Le Lagadec, R.; Ryabov, A. D. *Inorg. Chem.* **2008**, *47*, 4988–4995.
- ¹¹ Gosmini, C.; Bassene-Ernst, C.; Durandetti, M. *Tetrahedron*, **2009**, *65*, 6141–6146
- Gosmini, C.; Lasry, S.; Nedelec, J.-Y.; Perichonn, J. *Tetrahedron*, **1998**, *54*, 1289–1298
- ¹² Streef, J.W.; Den Hertog, H.J. *Tetrahedron Lett.*, **1968**, *57*, 5945–5948
- ¹³ Robertson, D.R.; Robertson, I.W.; Stephenson T.A. *J. Organomet. Chem.* **1980**, *202*, 309–318.
- ¹⁴ Ryabov, A.D.; Le Lagadec, R.; Estevez, H.; Toscano, R.A.; Hernandez, S.; Alexandrova, L.; Kurova, V.S.; Fischer, A.; Sirlin, C.; Pfeffer, M. *Inorg. Chem.* **2005**, *44*, 1626–1634.
- ¹⁵ Jakupec, M. A.; Resiner, E.; Eichinger, A.; Pongratz, M.; Arion, V. B.; Galanski, M.; Hartinger, C. G.; Keppler, B. K. *J. Med. Chem.* **2005**, *48*, 2831–2837.
- ¹⁶ Stepanenko, I.N.; Krokhin, A.A.; John, R.O.; Roller, A.; Arion, V.B.; Jakupec, M.A.; Keppler, B.K. *Inorg. Chem.* **2008**, *47*, 7338–7347.
- ¹⁷ Büchel, G.E.; Stepanenko, I.N.; Hejl, M.; Jakupec, M.A.; Arion, V.B.; Keppler, B.K. *Inorg. Chem.* **2009**, *48*, 10737–10747.
- ¹⁸ Fetzer, L.; Boff, B.; Ali, M.; Xiangjun, M.; Collin, J.-P.; Sirlin, C.; Gaidon, C.; Pfeffer, M. *J. Chem. Soc., Dalton Trans.* **2011**, *40*, 8869–8878.

Chapter 4

Complementary stability studies and evaluation of biophysicochemical properties

Knowing your enemy to better fight against him: a basic principle to wage this awkward war. That's a real problem with cancer, because this daily struggle is not a fight against an external enemy like viruses or bacteria, which colonize patient's body. This is a real battle against the cells of the body itself, which have become deviant and have a lot in common with healthy cells. Although scientists are on the right track, there are still many puzzles to be solved.



Chapter 4: Complementary stability studies and evaluation of bio-physicochemical properties..... 159

4.1. Complementary stability studies	161
4.1.1. Introduction.....	161
4.1.2. UV stability study in different solvent conditions.....	161
4.1.3. Study of the exchange of MeCN vs. DMSO in other complexes	162
4.2. Lipophilicity properties of RDCs and ODCs.....	165
4.2.1. Introduction: Importance of lipophilicity in the drug design	165
4.2.2. Partition coefficient: Definition and techniques.....	166
4.2.3. Correlation between activity, lipophilicity and red-ox potentials: A rational approach in the drug design?.....	168
4.3. Complementary <i>in vitro</i> biological results	174
4.3.1. Direct DNA interaction	174
4.3.2. Detection of Reactive Oxygen Species (ROS).....	175
4.4. Preliminary <i>in vivo</i> biological results	177
4.4.1. <i>In vivo</i> toxicities: Determination of LD ₅₀ and MTD	177
4.4.2. <i>In vivo</i> anticancer activity	179
4.5. References Chapter 4.....	181

Chapter 4: Complementary stability studies and evaluation of bio-physicochemical properties

4.1. Complementary stability studies

4.1.1. Introduction

The stability study of the complexes is crucial because it determines the ability of the future drug to retain its chemical, physical and biopharmaceutical properties. Stability assessments of drug products are mandated by regulatory agencies and are responsible for a number of audit findings. The chemical stability of drugs is of great importance since the product can become less effective when it undergoes degradation. Also, drug decomposition may yield to toxic by-products that can be harmful to the patient. Hence, stability evaluation of drug substance is the cornerstone of drug quality, as it determines how the active ingredient (AI) varies with time under the effect of various environmental factors such as temperature, solvent conditions and light... in order to define the optimal formulation and storage conditions and thus, determine the validity of the product.

Without intending to carry out for the moment an extensive stability study on our compounds, preliminary studies by means of U.V. and NMR spectroscopy helped us to define the stability of various molecules and also to accurately determine, for some of them, the evolution of the product in DMSO (see also Chapter 2, 2.2. and Chapter 3, 3.2.3.). Hence, it was possible to determine the kinetics of appearance of degradation products and also to solve the problems of non-reproducible *in vitro* measurements for the cyclometalated piano-stool complexes. This study has enabled us to meet the needs of biologists and to emphasize the lability of the acetonitrile ligand towards the DMSO resulting in a loss of activity.

4.1.2. UV stability study in different solvent conditions

In order to complement the stability studies, UV spectra of **ODC 2**, **ODC 3**, **ODC 4**, **RDC 55** and **RDC 56** were performed in different conditions by varying environmental factors such as solvent conditions (acetonitrile, DMSO and ethanol), temperature (R.T. or -15°C), or light exposure (see Appendix, Figure 4 to7).

All complexes are stable in acetonitrile at -15°C in the dark (data not shown) but slight modifications of the **LMCT** (Ligand-Metal Charge Transfer, Visible (Vis) or near UV region) and of the **MLCT** (Metal-Ligand Charge Transfer, Vis region) can be observed when the solutions are kept at R.T. and exposed to ambient light (**Appendix, Figure 4**). When

complexes **ODC 2** and **ODC 3** are dissolved into DMSO and kept at -15°C in the dark, they are stable for several months (**Appendix, Figure 5**). However, **ODC 4** and **ODC 56** undergo modifications of the LMCT and MLCT probably due to the exchange of the MeCN ligand with DMSO, as demonstrated for **ODC 4** by ^1H NMR spectroscopy (**Chapter 3, 3.2.3**).



Figure 1: List of complexes studied by UV spectroscopy

All complexes are also relatively stable in EtOH at -15°C in the dark (**Appendix, Figure 6**) but most of the complexes (except **ODC 3** which does not bear MeCN ligand) undergo modifications and/or degradations when the solutions are kept at R.T. exposed to ambient light (**Appendix, Figure 7**). More insight into the stability studies should be undertaken in order to mimic the different conditions under which the future drugs may be exposed and to determine possible metabolites that might be formed.

4.1.3. Study of the exchange of MeCN vs. DMSO in other complexes

Following the same strategy as for the evolution of **RDC 49**, **ODC 1** or **ODC 4**, it was a tempting challenge to perform similar studies on the lead compound **RDC 11** $[\text{Ru}(o\text{-C}_6\text{H}_4\text{py-}\kappa\text{C,N})(\text{phen})(\text{NCMe})_2]\text{PF}_6$, and also on one of the second generation compound **RDC 55** $[\text{Ru}(\text{MeO}_2\text{C-N}^{\wedge}\text{C}(\text{H})^{\wedge}\text{N})(\text{phen})(\text{NCMe})]\text{PF}_6$ bearing one *a priori* weakly bound MeCN.

Previous studies made by the laboratory on **RDC 11** indicated that the two acetonitrile ligands are relatively strongly bound to the metal center given that further complexation with 1,10-phenanthroline in refluxing dichloromethane or methanol does not allow the formation of **RDC 34** $[\text{Ru}(o\text{-C}_6\text{H}_4\text{py-}\kappa\text{C,N})(\text{phen})_2]\text{PF}_6$ (**Figure 2**).

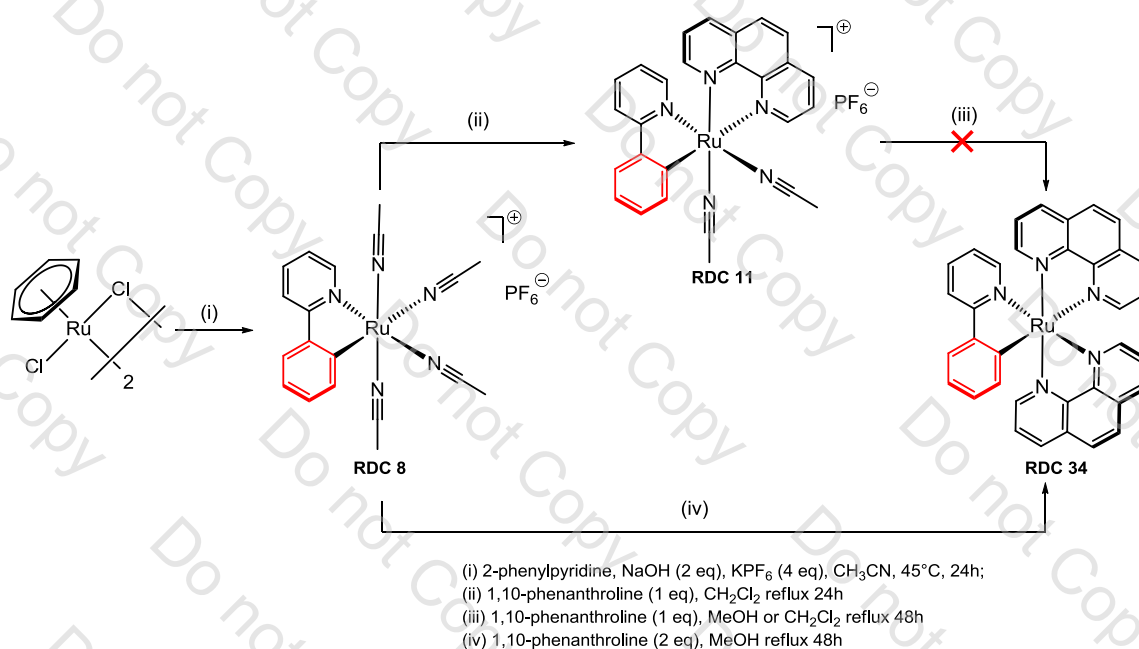
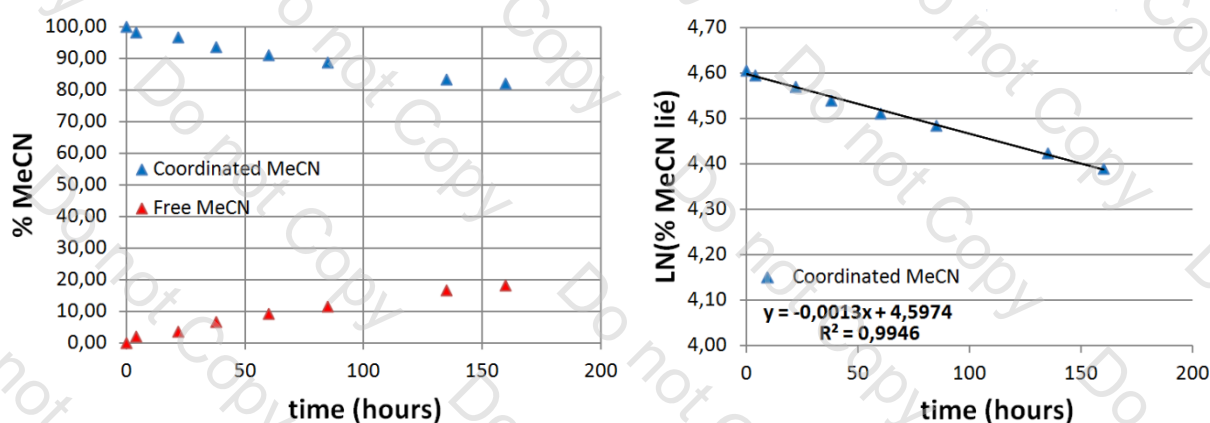


Figure 2: Synthesis of RDC 11 and of RDC 34

Samples of **RDC 11** and **RDC 55** (10mM, in DMSO-d⁶) were prepared and their kinetic evolution was monitored by ¹H NMR spectroscopy at R.T. and at -15°C in the dark. As previously discussed the evolution of **RDC 11** and **RDC 55** can be easily followed by the evolution of coordinated MeCN and free MeCN depicted respectively in **Figure 3** and **Figure 4**. In both cases regression on the data $\ln([\text{coordinated MeCN}])=f(t)$ gives a straight line suggesting a **first order reaction**.

Figure 3: Evolution of RDC 11 in dry DMSO-d⁶ monitored by ¹H NMR spectroscopy at R.T.

In **RDC 11**, the exchange of MeCN by DMSO is relatively slow, hence suggesting that the MeCN ligands are strongly bound to the metal centre (**Figure 3**). At room temperature, the mean value of the kinetic constant is approximately:

$$k = 1.30 \cdot 10^{-3} \pm 0.02 \cdot 10^{-3} \text{ h}^{-1} = 0.78 \pm 0.01 \text{ min}^{-1}$$

The value of half-life at room temperature for **RDC 11** can be calculated with $\alpha=1$:

$$t_{1/2 \text{ at R.T.}} = \frac{\ln(2)}{\alpha.k} = 530.19 \pm 5.07 \text{ h}$$

approximately $t_{1/2 \text{ at R.T.}} = 22 \text{ days}$

Note that the evolution of **RDC 11** in DMSO at -15°C in the dark is not depicted here given that even ^1H spectra after **15 days** do not show any modification, demonstrating again that **RDC 11** is stable in the conditions used by the biologists and hence can be considered as a good drug candidate. Preliminary studies on the heavier osmium congener **ODC 2** demonstrate that the exchange of MeCN with DMSO is even slower than in the case of **RDC 11** (data not shown).

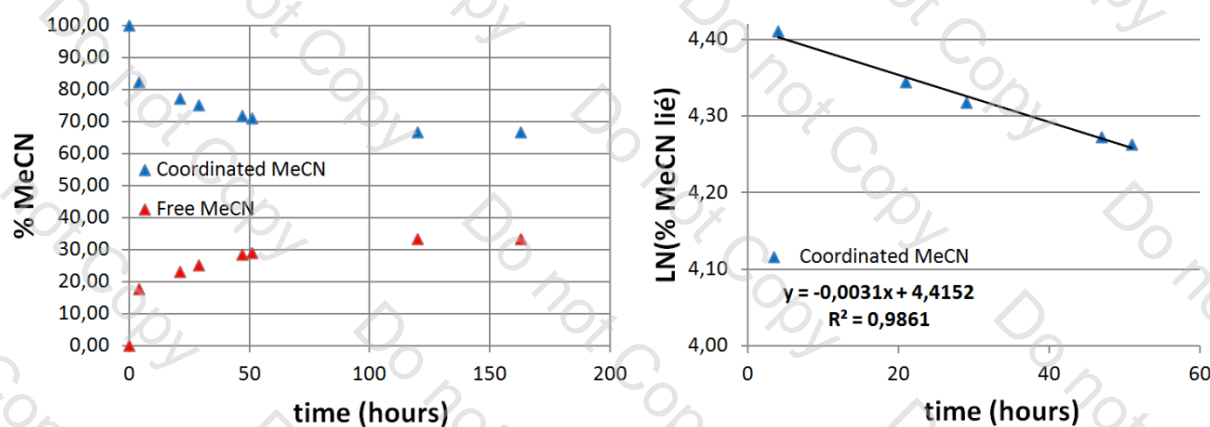


Figure 4: Evolution of **RDC 55** in dry DMSO-d^6 monitored by ^1H NMR spectroscopy at R.T.

In **RDC 55**, the exchange of MeCN by DMSO is slower than for cyclometalated piano-stool complexes, hence suggesting that the MeCN ligand is relatively strongly bound to the metal centre (**Figure 4**). At room temperature, the mean value of the kinetic constant is approximately:

$$k = 3.10 \cdot 10^{-3} \pm 0.05 \cdot 10^{-3} \text{ h}^{-1} = 0.186 \pm 0.001 \text{ min}^{-1}$$

The value of half-life at room temperature for **RDC 55** can be calculated with $\alpha=1$:

$$t_{1/2 \text{ at R.T.}} = \frac{\ln(2)}{\alpha.k} = 223.60 \pm 3.05 \text{ h}$$

approximately $t_{1/2 \text{ at R.T.}} = 9 \text{ days } 19\text{h}$

Note that the evolution of **RDC 55** in DMSO at -15°C in the dark is not depicted here given that even ^1H spectra after **15 days** do not show any modification, demonstrating that **RDC 55** can be considered as a good drug candidate.

4.2. Lipophilicity properties of RDCs and ODCs

4.2.1. Introduction: Importance of lipophilicity in drug design

From a schematic view, the body is composed of a series of membrane barriers dividing aqueous filled compartments. These membranes are principally composed of phospholipid bilayers, which surround cells hence forming intracellular barriers around the organelles (nucleus, mitochondria...) present in the cells. These are formed with the polar ionised head groups of the phospholipid facing towards the aqueous phases and the lipid chains providing a highly hydrophobic inner core. In order to be effective, a molecule must be sufficiently lipophilic to cross membranes and in pharmaceutical science, the measure of the lipophilicity, also known as $\log(P_{o/w})$ allows to estimate the bioavailability of a molecule. Lipophilic drugs (high $\log(P_{o/w})$) are preferentially distributed in the lipophilic compartments such as lipid bilayers while hydrophilic drug (low $\log(P_{o/w})$) are found in the hydrophilic compartments such as blood serum. Hence, measure of lipophilicity found many applications in the **drug design** and especially in pharmacokinetics (*e.g.* ADME properties: Absorption, Distribution, Metabolism and Excretion) and in pharmacodynamics.

The therapeutic effect of anticancer agents is usually explained by the interaction with intracellular targets. However, the limited penetration of cytotoxic drugs into a tumour is believed to be one of the major factors leading to failure of chemotherapy to completely eradicate tumours.¹ Hence, an effective anticancer drug must reach the cells in the tumour but also must be retained in sufficient concentration and on a relevant time scale to inhibit its intracellular target and induce apoptosis. Therefore, anticancer drugs based on transition metals may address the problems associated with platinum drugs currently used in the clinic.

The use of the *n*-octanol/water **partition coefficient (expressed as $\log(P_{o/w})$)** has become the cornerstone of predicting the biological effects of organic and metal based drugs from physical properties. For several classes of metalloanticancer complexes a relation between increased hydrophobicity and increased cytotoxic activity has already been reported.^{2,3,4,5} It was also demonstrated that increased lipophilicity favours uptake by cancer cells, probably through passive diffusion pathways, hence resulting in an increase in anticancer activity.⁶

However, increasing only lipophilicity is not a solution to improve anticancer activity because it can result in difficulties with drug formulation and also lower bioavailability.⁷ Therefore, the ideal lipophilicity for a drug is usually intermediate (not too lipophilic, nor too hydrophilic). Medicinal inorganic chemistry is now focused on this **rational drug design**

aimed at tuning lipophilicity and other physicochemical parameters while maintaining the anticancer activity.

4.2.2. Partition coefficient: Definition and techniques

The inner hydrophobic core of a membrane can be modelled by the use of an organic solvent such as *n*-octanol. Similarly, a water or aqueous buffer can be used to mimic the aqueous filled compartment. If the organic solvent is not miscible with water, then a two phase system (*n*-octanol/water) can be used to study the relative preference of a compound for the aqueous (hydrophilic) or the organic (lipophilic) phase. One of the obvious methods to estimate lipophilicity is to mix the chemical with *n*-octanol and water, shake the biphasic system to assure equilibrium, and measure the concentration of the chemical in the two phases. Lipophilicity can be hence described in terms of its **partition coefficient** $P_{o/w}$ (or more generally $\log(P_{o/w})$) and is defined as the ratio of concentrations of the compound at equilibrium between the organic and aqueous phases (**Figure 5**).⁸

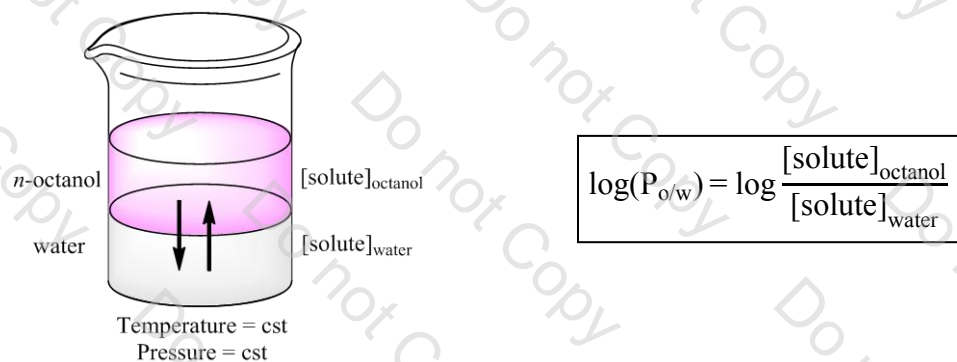


Figure 5: Definition of the partition coefficient factor

Although various methods have been developed for the determination of $\log(P_{o/w})$ including large variety of computation or prediction methods using **Q.S.P.R.** (Quantitative Structure-Property Relationship) algorithms,⁹ the classical *saturation shake-flask* method remained a reference method.¹⁰ Shake-flask technique is based on simple procedures, but it is time-consuming, and requires a lot of manual work. This method can also be laborious because emulsions are formed and analytical methods are needed for each chemical in at least one of the phases. Moreover, there is no accepted standard way to carry out this method,¹¹ and published lipophilicity studies show great differences in separation techniques and in the experimental conditions used, in particular the stirring and the sedimentation times. Indeed, stirring times may vary from 2h to 48h and sedimentation times from 24h to 3 days.¹² In addition, different techniques (sedimentation or centrifugation) can be used for the separation of the two phases.¹³

To avoid the tedious shake-flask method and since the calculation methods give only an approximation of $\log(P_{o/w})$ (the rules cannot take into account the presence of a metal, all functional groups, stereochemistry...) lipophilicity measurements were achieved by a faster method using high performance liquid chromatography. Thanks to the method described by Minick *et al.*¹⁴ and completed by Pomper *et al.*¹⁵ it is now possible to estimate rapidly the octanol/water partition coefficient. Minick's method involves the measurement of the **capacity factor $k'_{(\Phi)}$** for the unknown compounds on a C-8 reversed-phase column at various concentration of methanol ($0.50 \leq \Phi_{\text{methanol}} \leq 0.85$) containing 0.25% octanol and an aqueous phase consisting of 0.15% *n*-decylamine in 0.02M MOPS (3-morpholinopropanesulfonic acid) buffer pH=7.4 (prepared in 1-octanol-saturated water).

Capacity factors $k'_{(\Phi)}$ are given by the relation (eq. 1) where $t_{r(\Phi)}$ is the retention time at a fraction (Φ) of methanol and t_0 is the dead time of the column.

$$k'_{(\Phi)} = \frac{t_{r(\Phi)}}{t_0 - 1} \quad (\text{eq. 1})$$

Note that the column dead time (t_0) can be easily estimated at each eluent composition from the retention time of uracil, which was included as a nonretained internal reference for each injection. Column dead-times estimated by this probe may reflect more precisely the properties of the chromatographic system, which can change when the composition of the eluent is modified. Hence, capacity factors can be written as follows:

$$k'_{(\Phi)} = \frac{t_{r(\Phi)}}{t_{\text{uracil}(\Phi)} - 1} \quad (\text{eq. 2})$$

The logarithm of **capacity factors $\log(k'_{(\Phi)})$** in function of fraction (Φ) of methanol can be drawn (Figure 6). Extrapolation to 100% of aqueous component ($\Phi_{\text{MeOH}}=0$) using linear regression gives $\log(k'_w)$.

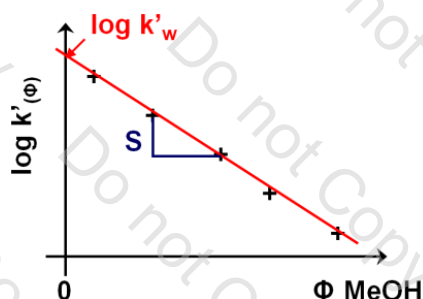


Figure 6: Graphical representation of $\log(k'_{(\Phi)})$ vs. fraction (Φ) MeOH

As documented by Minick *et al.*, this chromatographic system reliably gives a linear relationship between $\log(k'_w)$ and the solvent composition such as:

$$\log(k'_{(\Phi)}) = \log(k'_w) - S \cdot \Phi_{\text{methanol}} \quad (\text{eq. 3})$$

The *n*-octanol/water partition coefficients are then estimated from a standard curve generated from the compounds with experimentally verified partition coefficients. The standard curve is shown in **Figure 7**.

$$\log(P_{o/w}) = a \cdot \log(k'_w) + b = 0.9845 \log(k'_w) + 0.1342 \quad (\text{eq. 4})$$

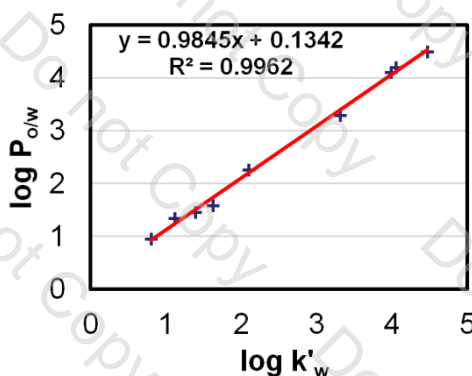


Figure 7: Correlation for standard compounds between $\log(P_{o/w})$ and $\log(k'_w)$ values derived by linear extrapolation on $\log(k'_{(\Phi)})$

Note that the regression line relating to the $\log(k'_w)$ of the standard to their $\log(P_{o/w})$ values shows very high statistical reliability. A correlation such as this is generally considered to indicate that the chromatographic method is accurately reproducing octanol/water partition values that would be measured by the shake-flask method.

4.2.3. Correlation between activity, lipophilicity and red-ox potentials: A rational approach in the drug design?

Preliminary studies have suggested that the lipophilicity of our complexes can have an important impact on the antitumour activity. It was first noticed that minimal lipophilicity is required to achieve a significant biological activity (**Figure 8**). On one hand, **RDC 25** bearing a hydrophilic phosphatriazaadamantane (pta) is non active ($IC_{50} > 50\mu M$) on HCT116 and A172 cell lines, whereas the IC_{50} of **RDC 11** is respectively $3\mu M$ and $1.9\mu M$. On the other hand the **RDC 28** having a rather lipophilic cyclometalating agent benzo[*h*]quinoline is even more active ($IC_{50}=0.5\mu M$ on HCT116) than the **RDC 11**.

In first approximation, this study makes sense since the more a complex is lipophilic, the more easily it will cross the membrane of tumorous cells. But we must also ensure that the lipophilicity of our complexes is not too high in order to avoid difficulties with drug formulation. Therefore, the lipophilicity needs to be precisely evaluated in order to better understand the role of this physicochemical property in the anticancer activity.

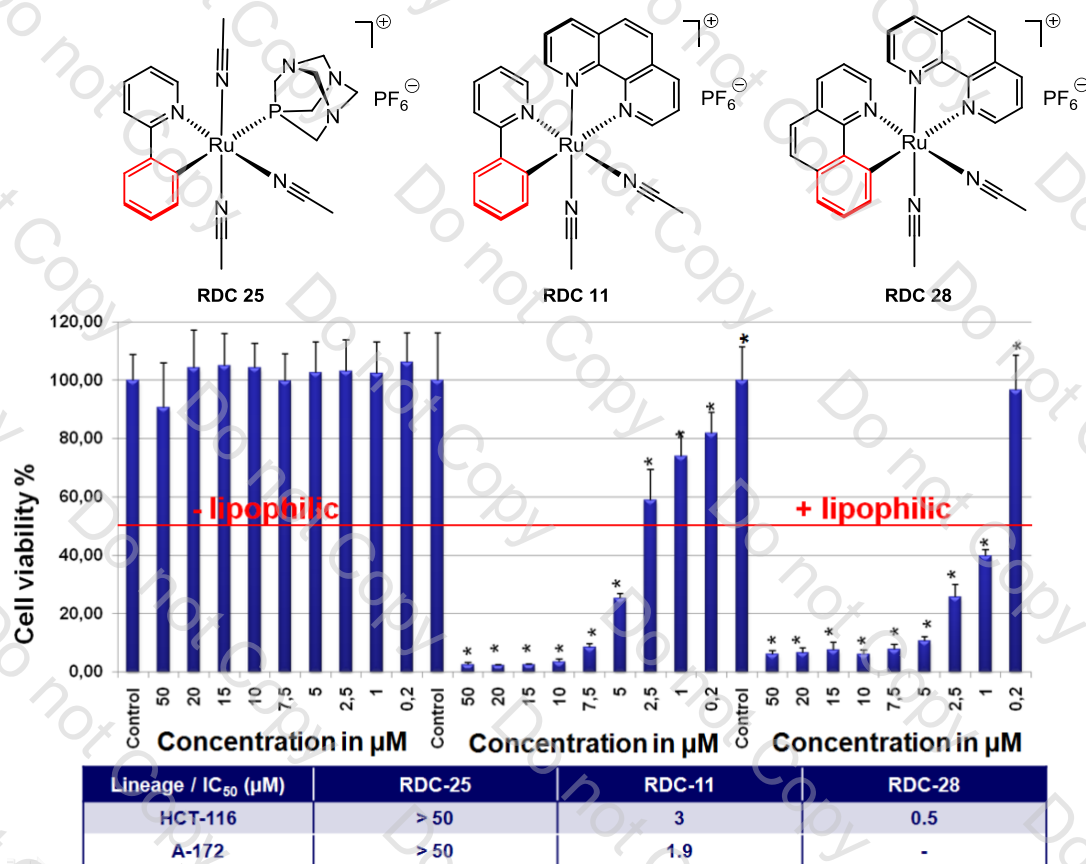


Figure 8: Effect of the lipophilicity on the anticancer activity (preliminary study)

In Chapter 2, 2.1.4. and Chapter 3, 3.5. we demonstrated that despite no clearcut S.A.R., the level of antitumour *in vitro* activity of **RDCs** and **ODCs** can be related to their respectively $\text{Ru}^{\text{III}}/\text{Ru}^{\text{II}}$ and $\text{Os}^{\text{III}}/\text{Os}^{\text{II}}$ red-ox potentials.

In order to see if small variations of other physicochemical parameters can explain the relative dispersion and also to assess a possible **correlation** between the biological activity and the lipophilicity, the partition coefficients $\log(\text{P}_{\text{o/w}})$ of various **RDCs** and **ODCs** were determined by HPLC using *n*-octanol/water partition. The measurements were repeated at least twice and the mean deviation was determined by considering the extreme values found over all experiments.

The partition coefficients $\log(\text{P}_{\text{o/w}})$ which were obtained from $\log(\text{k}'_{\text{w}})$ thanks to (eq. 4), are described in hereafter **Table 1** for **RDCs** and **Table 2** for **ODCs**. By correlating the lipophilicity to the *in vitro* activity of various **RDCs** (**Figure 9**) and **ODCs** (**Figure 10**), we demonstrated that the lipophilicity is an important variable to predict the activity of cyclometalated complexes, since they must display sufficient lipophilicity to cross the membrane of malignant cells.

The data collected for **RDCs** show that most of the complexes having a $\log(P_{o/w})$ above 2.0 display the lowest IC_{50} , *i.e.* in the nanomolar region. The **RDC 41** for example shows some hydrophilic behaviour (due to NH_2 group) with $\log(P_{o/w}) < 1$ and hence displays significantly higher IC_{50} values than the other compounds, regardless of its red-ox potential.

Complexes	RDCs equivalent	$E^*_{1/2 Ru(III/II)}$ ($\pm 5mV$)	IC_{50} (μM) A172	$Log(k'_w)$	$Log(P_{o/w})$
2	RDC 11	560	3.0 ± 1.0	1.10	1.20 ± 0.06
3	RDC 56	380	0.8 ± 0.2	2.30	2.4 ± 0.05
4	RDC 55	595	1.7 ± 0.5	1.65	1.75 ± 0.07
5	RDC 41	200	5.0 ± 1.0	0.80	0.90 ± 0.05
6	-	310	3.0 ± 1.0	2.70	2.80 ± 0.04
7	RDC 47	490	0.5 ± 0.1	3.35	3.45 ± 0.05
8	RDC 34	410	0.5 ± 0.1	2.25	2.35 ± 0.04
9	RDC 51	520	0.6 ± 0.1	2.10	2.20 ± 0.06
10	RDC 53	600	0.6 ± 0.1	2.15	2.25 ± 0.07
11	RDC 58	660	1.0 ± 0.2	2.20	2.30 ± 0.05
12	RDC 54	650	1.2 ± 0.2	1.90	2.00 ± 0.06
13	RDC 59	620	1.2 ± 0.2	2.35	2.45 ± 0.07
14	RDC 52	720	1.5 ± 0.2	1.95	2.05 ± 0.08
15	RDC 57	710	0.9 ± 0.2	2.80	2.90 ± 0.05
16	RDC 40	690	0.5 ± 0.1	1.95	2.05 ± 0.06
17	RDC 32	620	1.0 ± 0.5	1.95	2.05 ± 0.04
18	RDC 36	430	0.5 ± 0.2	2.10	2.20 ± 0.07
19	RDC 49	1244 ^(a)	14 ± 1.0	- ^(a)	-
21	RDC 49-DMSO	1410 ^(a)	24 ± 1.0	- ^(a)	-

Table 1: $\log(P_{o/w})$ obtained $\log(k'_w)$ measured by HPLC method using *n*-octanol/water partition where $\log(P_{o/w}) = 0.098452 \log(k'_w) + 0.13418$

(a): $\log(k'_w)$ non measurable in standard conditions because of too high hydrophilicity

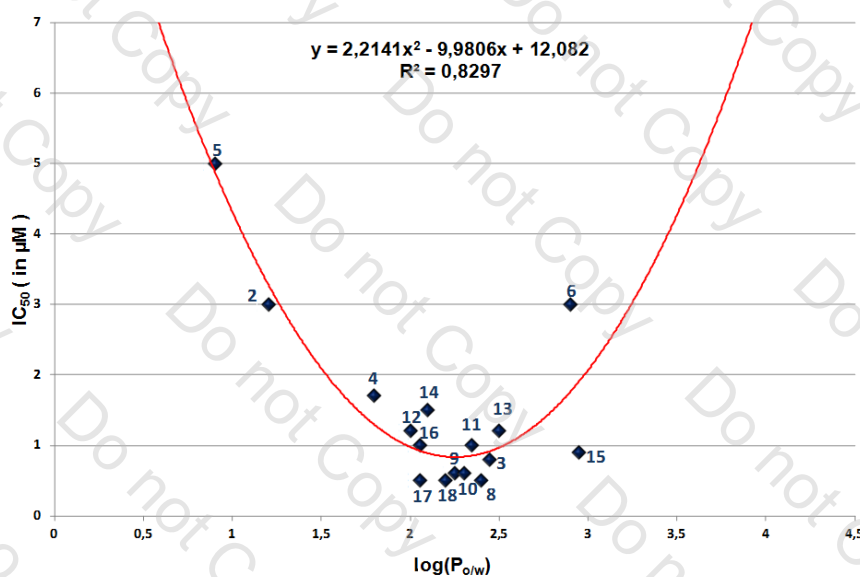


Figure 9: Binomial correlation between IC_{50} and $\log(P_{o/w})$ of several RDCs

<i>Complexes</i>	<i>ODCs equivalent</i>	$E^{\bullet}_{1/2} Ru(III/II)$ ($\pm 5mV$)	IC_{50} (μM) <i>A172</i>	$Log(k'_w)$	$Log(P_{o/w})$
1	ODC 1	1250 ^(a)	10 \pm 0.5	- ^(a)	-
2	ODC 2	280	2.0 \pm 0.2	1.05	1.15 \pm 0.05
3	ODC 3	300	0.4 \pm 0.2	2.33	2.43 \pm 0.04
4	ODC 4	1196 ^(a)	10 \pm 0.5	0.64	0.74 \pm 0.03
5	ODC 5	195	14 \pm 0.5	1.32	1.42 \pm 0.05
6	ODC 6	245	> 25	0.4	0.50 \pm 0.03
7	ODC 7	330	1.6 \pm 0.2	1.67	1.77 \pm 0.05
8	ODC 8	330	3.8 \pm 0.3	1.10	1.20 \pm 0.05
9	ODC 9	454	0.8 \pm 0.1	1.85	1.95 \pm 0.03
10	ODC 10	204	3.6 \pm 0.2	2.38	2.48 \pm 0.04
11	ODC 11	203	4.1 \pm 0.2	2.00	2.10 \pm 0.05
12	ODC 12	302	0.3 \pm 0.1	2.55	2.64 \pm 0.03
13	ODC 13	400	0.45 \pm 0.1	2.35	2.45 \pm 0.05
14	ODC 14	389	0.45 \pm 0.1	2.63	2.72 \pm 0.07
15	ODC 15	508	0.85 \pm 0.1	2.75	2.85 \pm 0.05
16	ODC 16	288	0.25 \pm 0.1	4.20	4.27 \pm 0.08
17	ODC 17	550	0.95 \pm 0.1	1.77	1.88 \pm 0.05
18	ODC 18	542	0.95 \pm 0.1	1.95	2.05 \pm 0.05
19	ODC 19	650	1.9 \pm 0.1	2.17	2.27 \pm 0.07
20	ODC 20	440	0.25 \pm 0.1	3.51	3.59 \pm 0.07
21	ODC 21	359	320 \pm 0.1	0.32	0.45 \pm 0.08
22	ODC 22	213	375 \pm 0.1	0.75	0.85 \pm 0.08
23	ODC 23	536	21 \pm 0.1	1.80	1.91 \pm 0.05
24	ODC 24	602	62 \pm 0.1	2.00	2.10 \pm 0.05
25	ODC 25	1630 ^(a)	125 \pm 5.0	- ^(a)	-
26	ODC 26	1493 ^(a)	60 \pm 5.0	- ^(a)	-
27	ODC 27	1600 ^(a)	90 \pm 1.0	- ^(a)	-
28	ODC 28	151	1.25 \pm 1.0	2.54	2.64 \pm 0.05
29	ODC 29	143	8.5 \pm 5.0	0.70	0.80 \pm 0.05
30	ODC 30	131	3.5 \pm 5.0	1.68	1.78 \pm 0.05
31	ODC 31	143	2.25 \pm 0.1	2.13	2.23 \pm 0.06
32	ODC 32	1234 ^(a)	90 \pm 5.0	^(a)	-
33	ODC 33	176	18 \pm 2.0	1.02	1.13 \pm 0.07
34	ODC 34	160	0.75 \pm 0.3	2.41	2.50 \pm 0.06
35	ODC 35	279	5.0 \pm 0.2	1.41	1.52 \pm 0.06
36	ODC 36	1200 ^(a)	100 \pm 5.0	- ^(a)	-
37	ODC 37	1030 ^(a)	100 \pm 5.0	- ^(a)	-
38	ODC 38	722 ^(a)	22 \pm 1.0	- ^(a)	-
39	ODC 39	1487 ^(a)	300 \pm 5.0	- ^(a)	-

Table 2: $\log(P_{o/w})$ obtained $\log(k'_w)$ measured by HPLC method using *n*-octanol/water partition where $\log(P_{o/w})=0.098452 \log(k'_w) + 0.13418$

(a): $\log(k'_w)$ non measurable in standard conditions because of too high hydrophilicity

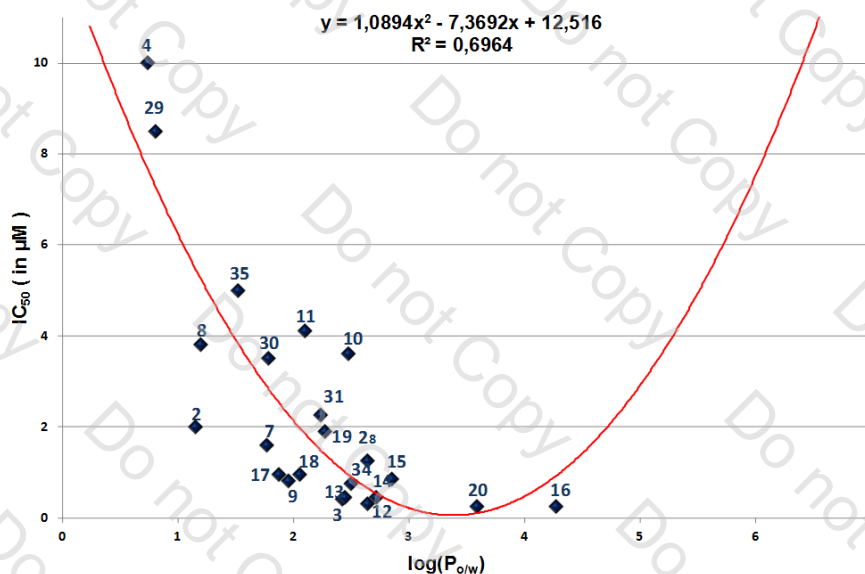


Figure 10: Binomial correlation between IC_{50} and $\log(P_{o/w})$ of several ODCs

Similarly to **RDCs**, the data collected for **ODCs** show that most of the complexes having a $\log(P_{o/w})$ above 2.0-2.5 display the lowest IC_{50} , *i.e.* in the nanomolar region. The **ODC 4** and **ODC 29** (bearing NH_2 group) show some hydrophilic behaviour with $\log(P_{o/w}) < 1$ and hence display significantly higher IC_{50} values than the other compounds.

However, in both cases, the correlation of the activity with the lipophilicity tends to be less accurate ($R^2=0.8297$ for **RDCs**, $R^2=0.6964$ for **ODCs**) by comparison with the correlation with the red-ox potential ($R^2=0.9929$ for **RDCs**, $R^2=0.8809$ for **ODCs**). This suggests that, even if lipophilicity should play a role in the activity of the complexes, the role of the red-ox potential induced by the genuine carbon-metal bond should be preponderant.

In order to better understand if these two parameters (red-ox potential and lipophilicity) can be linked and explain together the anticancer *in vitro* activity, three-dimensional correlations for **RDCs** (Figure 11) and **ODCs** (Figure 12) were determined with Maple technical computing software. Programming details of the 3D non-linear regression using matrix are displayed in **Appendix**. After having verified that the optimization problem admits a unique solution (determinant of the matrix must be non-zero, **Appendix, eq. 2.1**), the polynomial defining the surface is:

For RDCs	$IC_{50} = 10.72 - 32.92 E^{\circ}_{1/2} (Ru^{III/II}) - 0.53 \log(P_{o/w}) + 45.85 E^{\circ}_{1/2}{}^2 (Ru^{III/II}) + 0.51 \log(P_{o/w})^2 - 5.93 E^{\circ}_{1/2} (Ru^{III/II}) \cdot \log(P_{o/w})$ <p>3D Correlation factor $R^2= 0.89$</p>
-----------------	---

For ODCs	$IC_{50} = 16.35 - 33.91 E^{\circ}_{1/2} (Os^{III/II}) - 6.32 \log(P_{o/w}) + 23.24 E^{\circ}_{1/2}{}^2 (Os^{III/II}) + 0.61 \log(P_{o/w})^2 + 5.96 E^{\circ}_{1/2} (Os^{III/II}) \cdot \log(P_{o/w})$ <p>3D Correlation factor $R^2= 0.87$</p>
-----------------	---

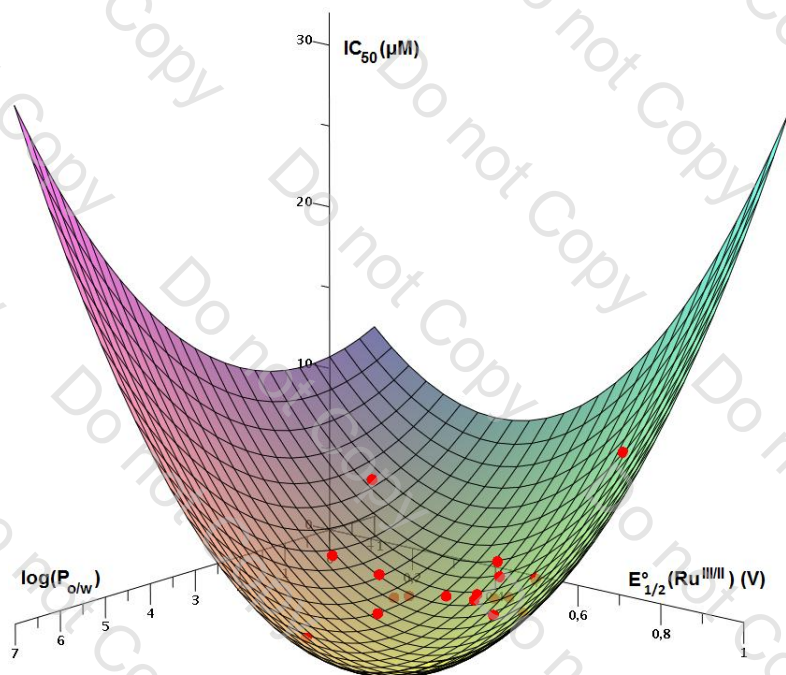


Figure 11: Three-dimensional representation of the correlation between IC_{50} , the red-ox potential $E^{\circ}_{1/2}(Ru^{III/II})$ and the lipophilicity $\log(P_{o/w})$ of RDCs.
 $R^2=0.89$

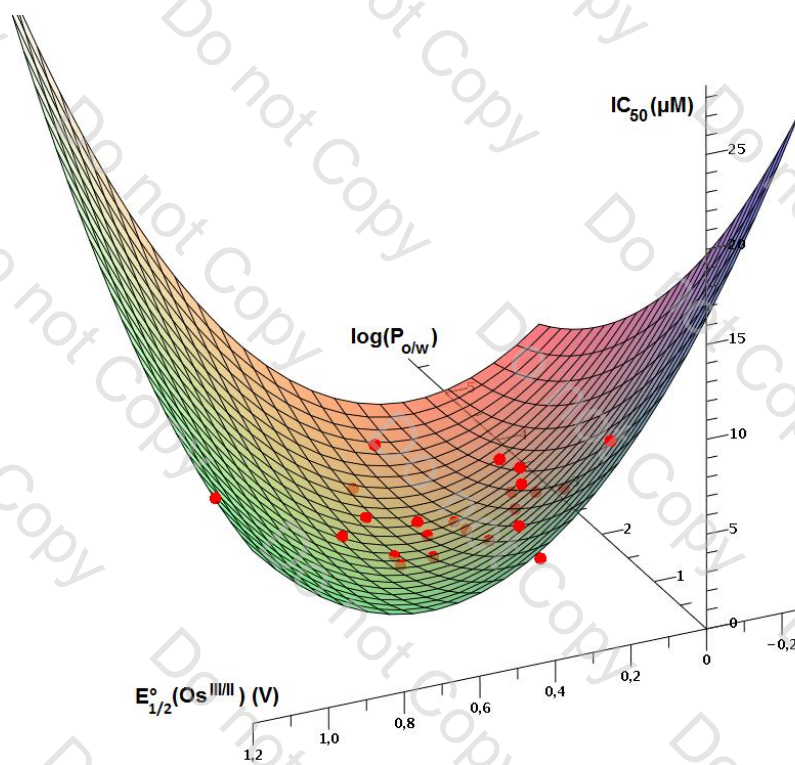


Figure 12: Three-dimensional representation of the correlation between IC_{50} , the red-ox potential $E^{\circ}_{1/2}(Os^{III/II})$ and the lipophilicity $\log(P_{o/w})$ of ODCs.
 $R^2=0.87$

A binomial relation has been established between the red-ox potential values, the lipophilicity and the cytotoxicity of several **RDCs** and **ODCs** with good non-linear correlation coefficients. From a statistical approach of the problem, could these models allow a rational conception in the drug design? Is it a step towards a possible Property-Activity Relationship? These questions remained largely opened given that only a few complexes were studied. Indeed, the point here is not to define a physico-chemical law for the cyclometalated complexes, but it cannot be denied that the activity of these complexes is somehow related to these two intrinsic parameters. However, we are far from being able to give a rational explanation about the exact role of the red-ox potential and of the lipophilicity. To better understand the role of these two parameters, further biological studies will be necessary to propose a satisfactory mode of action.

4.3. Complementary *in vitro* biological results

In order to complement preliminary *in vitro* results, biologists decided to study more precisely the mechanism of action of several **RDCs** and several **ODCs** by analysing the effects of these compounds on the induction of DNA damage and of oxidative stress.

4.3.1. Direct DNA interaction

Many anticancer drugs, known as alkylating agents induce apoptosis by binding and causing damage to DNA. Previous studies demonstrated that **RDC 11** interacts with DNA and triggers a cellular response normally induced by DNA damage.¹⁶ The interaction of molecules with DNA can be observed by agarose gel electrophoresis. Increasing amounts of test compounds are mixed with fixed amounts of supercoiled DNA (10 base pairs (bp)) and then loaded onto an agarose matrix. In the presence of interactions with the molecules, the migration front can display a reduced intensity or can be slowed down. This migration front can also be modified due to DNA uncoiling or to damages induced in the double helix.

The results presented in **Figure 13** indicate that, compared with the profile obtained with the **RDC 11**, the **RDC 40** and **RDC 41** seem to interact more significantly with DNA. Indeed, from a ratio of 5 molecules/10 bp, these two compounds induce more important slowdown in migration by comparison with **RDC 11** under the same conditions. For **RDC 40**, the absence of migration observed for 5 and 20 molecules/10 bp suggests that the affinity of the compound for DNA is large enough to neutralize the charges carried by DNA. However, the affinity of **RDC 34** with DNA is not greater than the **RDC 11**, while its cytotoxicity is much higher. The results obtained with **ODCs** show that **ODC 2** affects more significantly the

migration and at lower doses compared to **ODC 3**. This again shows a lack of strict correlation between cytotoxicity and the ability to interact with DNA, since **ODC 3** is more cytotoxic than the **ODC 2**.

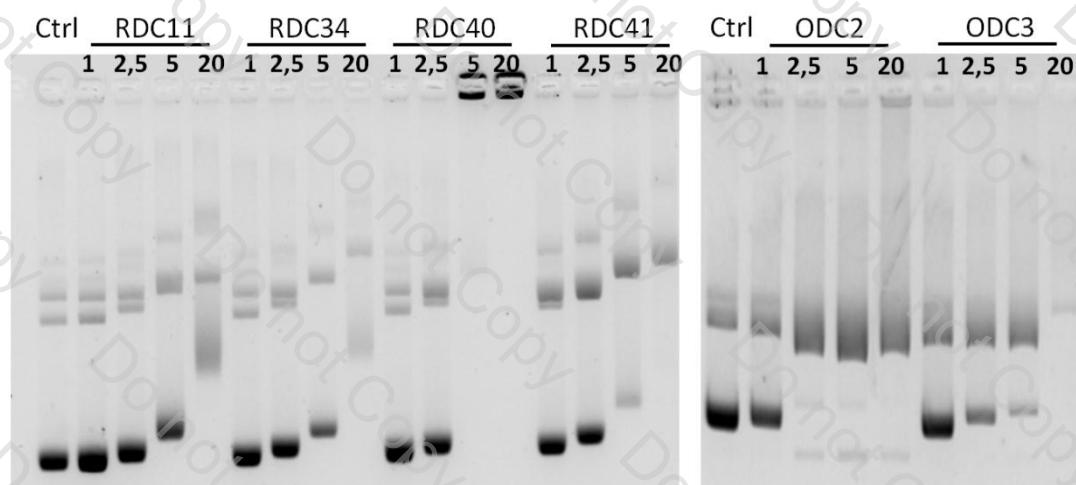


Figure 13: Direct interaction of RDCs and ODCs with DNA

4.3.2. Detection of Reactive Oxygen Species (ROS)

Given that our compounds seem to affect the oxido-reductase enzymes, we hypothesized that the latter could alter the cycle of production and detoxification of oxygen radicals in the cell.¹⁷ Biologists recently evidenced that the activity of **RDCs** in tumour cells induced some oxidative stress with various degrees. Another aspect of the endoplasmic reticulum stress is the induction of **reactive oxygen species (ROS)** resulting from oxidative stress. The synthesis of **ROS** can be induced by various factors such as pollution, ionizing waves, metabolism, inflammation or UV. Normally, the cell is able to regulate the rate of **ROS** by means of antioxidants involved in reducing the number of ROS. However, in the presence of an excessive number of **ROS**, the cell induces signaling pathways leading to apoptosis.¹⁸

The intracellular **ROS** level was detected by using 5-(and-6)-carboxy-2',7'-dichlorodihydrofluorescein diacetate (carboxy-H₂DCFDA). Carboxy-H₂DCFDA is a cell-permeable indicator for **ROS** that is nonfluorescent until the acetate groups are removed by intracellular esterases and oxidation occurs within the cell (**Figure 14**). When oxidized by various active oxygen species, the probe is irreversibly converted to the fluorescent form, DCF. This reduced dye is therefore very useful for the detection of oxidative activities in viable cells, including superoxide generation in mitochondria. Therefore elevated fluorescence in cells treated with **RDCs** or **ODCs** is an indication of **ROS** production. Using this tool, biologists performed comparative studies on relative **ROS** production between ruthenium- and osmium-derived compounds.

Figure 15 shows the rate of fluorescence (RFU) detected in cells treated with the compounds at different concentrations and durations of treatment. The rate of fluorescence obtained with **RDCs** and **ODCs** showed that all of them induce a fluorescent signal, and therefore produce ROS, at least similarly to the positive control menadione (MND). It is interesting to note that **RDC 34** and osmium analogue **ODC 3** particularly stimulate the production of ROS leading to significant cytotoxicity observed in cell lines. But how exactly the intrinsic red-ox properties of these **RDCs** and **ODCs** are responsible for the cellular oxidative stress is still under investigation.

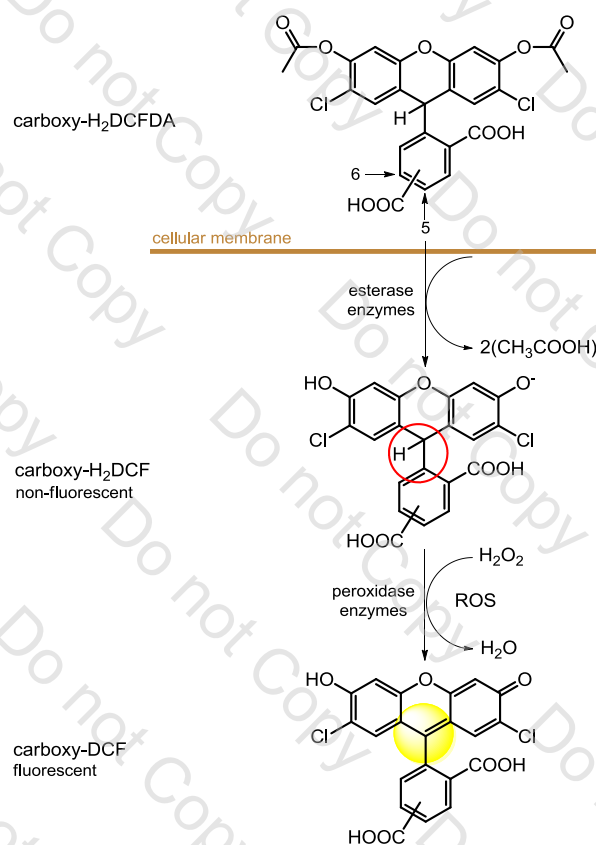


Figure 14: Mechanism of action of the molecular probe carboxy-H₂DCFDA

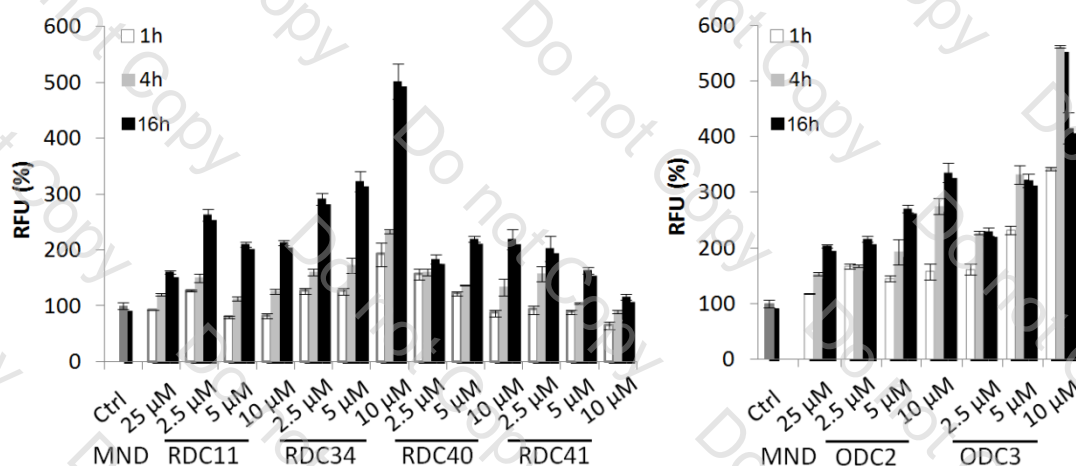


Figure 15: *In vitro* detection of ROS. Menadione (MND) is used as positive control.

4.4. Preliminary *in vivo* biological results

On the basis of the IC_{50} obtained in experiments conducted *in vitro*, several compounds were selected for *in vivo* studies. The *in vivo* toxicity and the activity of two new RDCs and three ODCs on an implanted Lewis lung (3LL) tumour model were evaluated. It was particularly interesting to compare the *in vivo* activity of structurally identical compounds which only differ by the metal.

4.4.1. *In vivo* toxicities: Determination of LD_{50} and MTD

The toxicity studies allow evaluation of the LD_{50} (Dose inducing 50% lethality) and the MTD (Maximum Tolerated Dose which does not induce more than 20% weight loss) in order to determine the maximum concentration of product that can be tolerated by the animal during chronic treatment. The **Figure 16** represents the evolution of C57/Black6 mice survival in function of the concentration of administered **ODC 3** drug. Four different doses (between 5 to $30\mu\text{mole/kg}$) were administered to groups of four mice by **intraperitoneal injection (IP)**. The days of IP injection are indicated by an asterisk. In chronic treatment conditions, the **ODC 3** dose inducing 50% lethality is $LD_{50}=7.5\mu\text{M/kg}$. During this experiment, healthy mice (without grafted tumour) tolerated a dose of $5\mu\text{mole/kg}$ almost for one month treatment. Note that the first 2 injections are spaced 7 days to assess any possible acute toxicity and to adjust concentrations if necessary. Before each injection, mice were observed and weighed. During the studies, if the body weight loss was $\geq 20\%$ or if obvious signs of pain or suffering were observed, mice were sacrificed.

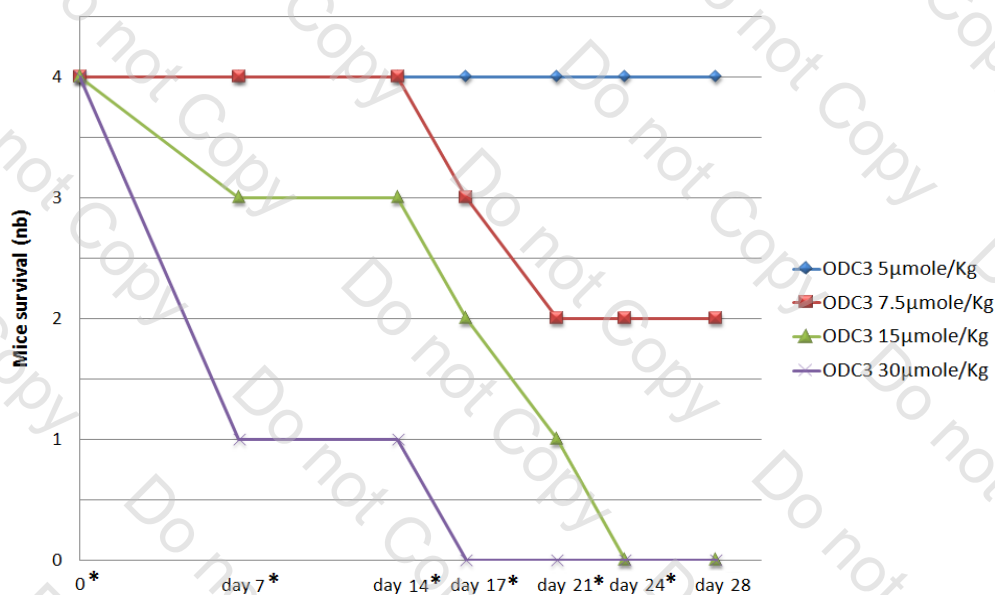


Figure 16: *In vivo* chronic toxicity of ODC 3
N=4 mice /group

Using the same method, the **LD₅₀** and the **MTD** of several complexes were evaluated and summarized in **Table 3**. These results were also used to conduct the *in vivo* activity study considering the MTD concentration as maximal dose affording the lowest toxicity.

<i>Compounds</i>	<i>LD₅₀</i> ($\mu\text{M.kg}^{-1}$)	<i>MTD</i> ($\mu\text{M.kg}^{-1}$)
Cisplatin	56	26
RDC 11	56	26
RDC 34	6	2
RDC 41	30	15
RDC 55	30	7.5
RDC 56	15	7.5
ODC 2	15	7.5
ODC 3	7.5	5
ODC 4	n.d.	80

Table 3: *In vivo* toxicities (**LD₅₀** and **MTD**) of some complexes

The toxicity data (**LD₅₀** and **MTD**) evidence variable degrees of toxicity depending on the compounds. These data show greater toxicity of **RDC 34** vs. **RDC 11** and of **ODC 3** vs. **ODC 2** that can be related to increased cytotoxicity observed *in vitro*. Hence, the presence of a second 2-phenanthroline ligand induces a higher toxicity to the molecule. However, **ODC 3** seems to be slightly better tolerated than its **RDC 34** ruthenium analogue. On the contrary, this is not the case for **ODC 2** which is practically 4 times more toxic than its **RDC 11** ruthenium analogue.

ODC 4 is particularly well tolerated by mice, since the injection can be done up to 80 $\mu\text{mol/kg}$ before detecting any toxicity. Nevertheless, this result should be qualified, because of the possible exchange of MeCN ligand in stock solution (see **Chapter 3, 3.2.3.**).

Although second generation ruthenium compounds **RDC 55** and **RDC 56** display the same MTD of 7.5 $\mu\text{mol/kg}$, they differ by their **LD₅₀**, the **RDC 56** being more toxic than the **RDC 55**. Hence, these two compounds have a toxicity comprised between that of **RDC 11** and that of **RDC 34**. Paradoxically, first generation **RDC 41** seems to be more toxic than **RDC 11** while its *in vitro* cytotoxic activity was lower. This could be explained by metabolization of the compound into particularly toxic metabolites and/or by an accumulation of the compound in sensitive organs such as kidneys or liver.

Complementary toxicity studies related to extensive *in vivo* activity will enable us to determine which of the ruthenium or osmium derivative compounds is the most suitable in terms of therapeutic index.

4.4.2. *In vivo* anticancer activity

In order to assess the anti-cancer activity of several compounds, biologists measured the evolution of tumour growth in syngeneic tumours implanted *in vivo*. 3LL murine cancer cells were subcutaneously injected to 8 week-old C57/Black6 male mice. When the tumour size reached 80mm³ the mice were treated twice a week with different compounds at the concentration identified by previous chronic toxicity studies. The growth of the tumour was followed over 3 weeks. **Figure 17** represents the evaluation of the anticancer activity (3LL tumour model) of **RDC 56** (12µmole/kg) and of **ODC 4** (30µmole/kg) on day 21. In this experiment 8 C57/Black6 mice were used for each condition. Each point represents the volume of a tumour 21 days after initiation of treatment and bars represent the means volume of tumour and standard errors.

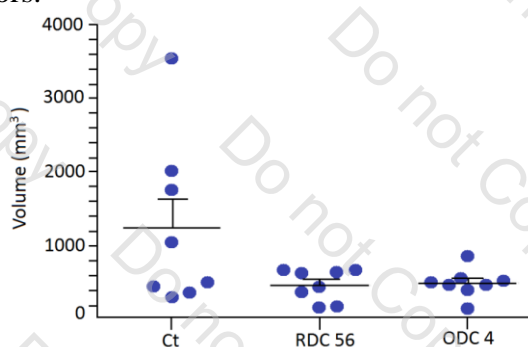


Figure 17: Evaluation of the anticancer activity of RDC 56 and ODC 4 on Lewis Lung 3LL tumour model (day 21); Ct: Non-treated group

Tumour growth curves of **RDC 34** (**Figure 18**) seem to show a slowing down of tumour growth in the 3LL model. Although the last points of “control mice group” and of treated group at 2µM/kg twice a week are not significant (n= 1 mouse), the graph suggests that the protocol of administration 2µM/kg twice a week (red line) seems to be more effective than the treatment with 1µM/kg twice a week (green curve). Nevertheless, since this study includes preliminary data, the number of mice per group is quite low and does not allow one to carry out statistical analysis.

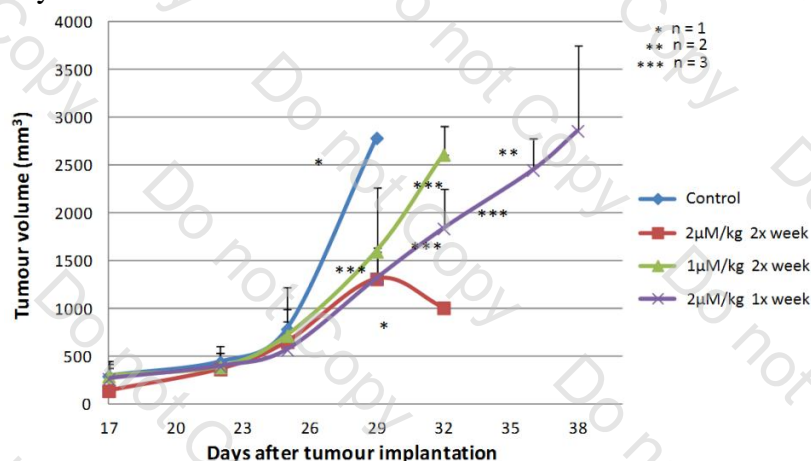


Figure 18: In vivo anticancer activity of RDC 34 on Lewis Lung 3LL tumour model

The values of the ratios T/C (Percentage of tumour volume in treated condition (T) compared to the control condition (C)) obtained for the different compounds are summarized in **Table 4**. The asterisk indicates experiment where only one administration protocol has been tested and where the toxicity of the product was too high, inducing abnormal mortality.

<i>Compounds</i>	<i>Concentration ($\mu\text{M.kg}^{-1}$)</i>	<i>T/C ratio</i>
Cisplatin	13	60
RDC 11	13	60
RDC 34	2.5	58.7
RDC 41	7.5	56.9
RDC 55	30	66
RDC 56	12	48
ODC 2	5	52.7 *
ODC 3	5	89.2 *
ODC 4	30	47

Table 4: *In vivo* anticancer activity of some complexes

At this stage, the ratios T/C suggest that most of the tested compounds display anticancer properties similar to **RDC 11**. However, second generation **RDC 56** (12 $\mu\text{mole/kg}$) and **ODC 4** (30 $\mu\text{mole/kg}$) seem to be more active. It should be noted that these studies are preliminary and need to be repeated on larger group of animals. Concentration and/or administration frequencies of osmium derivatives (especially **ODC 2** and **ODC 3**) should be optimized in order to maintain a survival rate of animals consistent with the observation of antitumour effect. Thus, these changes in protocol will enable us to determine the optimum conditions to get the maximum of activity.

Note also that some compounds that have demonstrated high cytotoxic properties *in vitro* may have limited anticancer activity *in vivo*. This may be related to metabolization process of the product into weakly active metabolite, but also to poor biodistribution or to low stability of the compounds in physiological condition (related to pH for example). The study of these different aspects should also be taken into account when the anticancer activity of the compounds will be better characterized. Hence, the study of the biological activity of these compounds *in vivo* as well as their toxicity studies on normal cells is therefore worthwhile and will be actively pursued in the future.

4.5. References Chapter 4

- ¹ Tredan, O.; Galmarini, C. M.; Patel, K.; Tannock, I. F. *J. Natl. Cancer Inst.* **2007**, *99*, 1441–1454.
- ² Loh, S. Y.; Mistry, P.; Kelland, L. R.; Abel, G.; Harrap, K. R. *Br. J. Cancer* **1992**, *66*, 1109–1115.
- ³ Barbieri, R. *Inorg. Chim. Acta* **1992**, *191*, 253–259.
- ⁴ Mendoza-Ferri, M.-G.; Hartinger, C. G.; Eichinger, R. E.; Stolyarova, N.; Severin, K.; Jakupec, M. A.; Nazarov, A. A.; Keppler, B. K. *Organometallics* **2008**, *27*, 2405–2407.
- ⁵ Song, R.; Park, S. Y.; Kim, Y.-S.; Kim, Y.; Kim, S.-J.; Ahn, B. T.; Sohn, Y. S. *J. Inorg. Biochem.* **2003**, *96*, 339–345.
- ⁶ Van Rijt, S.H.; Mukherjee, A.; Pizarro, A.M.; Sadler, P.J. *J. Med. Chem.* **2010**, *53*, 840–849.
- ⁷ Veber, D.F.; Johnson, S.R.; Cheng, H.-Y.; Smith, B.R.; Ward, K.W.; Kopple, K.D. *J. Med. Chem.* **2002**, *45*, 2615–2623.
- ⁸ Leo, A.; Hansch, C.; Elkins, D. *Chem. Rev.* **1971**, *71*, 525–616.
- ⁹ Lyman, W. J.; Reehl, W. F.; Rosenblatt, D. H.; Handbook of Chemical Property Estimation Methods, McGraw-Hill, New-York **1983**.
- ¹⁰ Sangster, J. *Octanol-water partition coefficients: Fundamentals and physical chemistry*, vol. 2 of Wiley series in solution chemistry **1997**.
- ¹¹ Box, K.J.; Völgyi, G.; Baka, E.; Stuart, M.; Takács-Novák, K.; Comer, J.E.A. *J. Pharm. Sci.* **2006**, *95*, 1298–1307.
- ¹² (a) Lipinski, C.A.; Lombardo, F.; Dominy, B.W.; Feeney, P.J. *Adv. Drug Deliv. Rev.* **2001**, 3–26.
(b) Etzweiler, F.; Senn, E.; Schmidt, H.W.H. *Anal. Chem.* **1995**, *67*, 655–658.
(c) Mora, C.P.; Martínez, F. *Fluid Phase Equilib.* **2007**, *255*, 70–77.
- ¹³ Yalkowsky, S.H.; Banerjee, S. *Aqueous Solubility Methods of Estimation for Organic Compounds*, Dekker, New York, **1992**.
- ¹⁴ Minick, D.J.; Frenz, J.H.; Patrick, M.A.; Brent, D.A. *J. Med. Chem.* **1988**, *31*, 1923–1933.
- ¹⁵ Pomper, M.J.; Vanbrocklin, H.; Thieme, A.M.; Thomas, R.D.; Katzenellengogen, J.A. *J. Med. Chem. Soc.* **1990**, *33*, 3143–31550.
- ¹⁶ Meng, X.; Leyva, M. L.; Jenny, M.; Gross, I.; Benosman, S.; Fricker, B.; Harlepp, S.; Hebraud, P.; Boos, A.; Wlosik, P.; Bischoff, P.; Sirlin, C.; Pfeffer, M.; Loeffler, J. P.; Gaiddon, C. *Cancer Res.*, **2009**, *69*, 5458–5466.
- ¹⁷ Ryabov, A. D.; Sukharev, V. S.; Alexandrova, L.; Le Lagadec, R.; Pfeffer, M. *Inorg. Chem.* **2001**, *40*, 6529–6532.
- ¹⁸ Bras, M.; Queenan, B.; Susin, S.A. *Biochemistry* **2005**, *70*, 213–239.

Conclusion and perspectives:

The goal of developing superior therapies that have a meaningful impact on the live of cancer patients is seen with optimism by considering the huge number of molecules in preclinical or clinical testings. Although actual treatments accepted by public health agencies are heavy and long, they have the virtue of giving a glimmer of hope to the patients.



This thesis is part of medicinal inorganic chemistry and comes in the line of previous works made by the laboratory since the discovery that cycloruthenated complexes can display anticancer properties. In the essential aim of increasing the activity and reducing the side effects of anticancer agents, this thesis presented the recent advances of the laboratory in this field and the development of a second generation **RDC** chemical library in which the cyclometallating ligand is stabilized by two N-Ru bond. At the same time, we decided to focus our study on osmium heavier congener **ODCs**, not only to complete the existing **RDC** chemical library, but also to verify the impact of exchanging the metal.

The study of the biological activity of the several second generation **RDCs** confirmed that organometallic ruthenium having a genuine carbon-metal bond stabilized by two intramolecular N-Ru bonds display important cytotoxicity against cancer cell lines. The *in vitro* evaluation of osmium derivatives **ODCs** showed that osmium is another metal that must deserve attention for the development of new effective antitumour drugs. Thus, several **RDCs** and **ODCs** reached an IC_{50} in the order or significantly lower than one micromole, indicating a critical improvement. Introduction of bioisosterism into the design could lead in the future to the discovery of compounds with different pharmaceutical properties.

As we did not find any obvious relationship between the activity of the compounds and their structures, we demonstrated that the activity can be related to the red-ox potential $E^{\circ}_{1/2}(\text{Ru}^{\text{III/II}})$ and $E^{\circ}_{1/2}(\text{Os}^{\text{III/II}})$. Measurement of the lipophilicity correlated to the values of red-ox potential and biological *in vitro* activity allowed me to established a three dimensional correlation for both chemical library. Through this possible property activity relationship, it was demonstrated for the first time that both $E^{\circ}_{1/2}(\text{Ru}^{\text{III/II}})$ and $E^{\circ}_{1/2}(\text{Os}^{\text{III/II}})$ red-ox potentials (that allow possibly complexes to efficiently interfere with oxido-reductase enzymes), and good **lipophilicities** (that allow their entries into the cells) are somehow closely related, even if this rationalization is not clear yet.

Stability studies demonstrated that in piano-stool complexes, the MeCN ligand is relatively labile and can be easily replaced by DMSO. Thanks to this study, we have been able to reveal the non-reproducibility of *in vivo* and *in vitro* measurements made by the biologists on complexes bearing one *a priori* labile MeCN ligand. Indeed, the exchange of the MeCN ligand by DMSO modifies significantly the red-ox potential and hence, leading to a product displaying practically no *in vitro* activity against cancer cells.

These stability studies also confirmed that in **RDCs** and **ODCs** bearing two or no MeCN ligands, the coordination sphere around the metal centre is stable, since a substitution reaction of a N-ligand at the metal centre cannot easily take place (at least in the absence of light for acetonitrile containing compounds). Hence, if exchange of electrons between biological macromolecules (such as oxido-reductase enzymes for example) and the organo-ruthenium or osmium cations are taking place within the cells, it should occur through an outer-sphere mechanism.

Complementary *in vitro* tests demonstrated that the **RDCs** and **ODCs** can induce DNA-dependent mechanisms of action but also mechanisms of action targeting reticulum stress pathway and synthesis of ROS. However, the identification of a direct biological target which is essential for the development of therapeutic molecules has not been clearly determined. More insight into the role of the red-ox potential and of the lipophilicity will probably become clearer as we progress into the mechanism of action of these promising species.

At the same time, biologists study some **RDCs** and **ODCs** compounds *in vivo* in order to characterize the acute toxicity and the antiproliferative properties. Preliminary tests on animal models demonstrated that osmium compounds do not lead consistently to high toxicity *in vivo*. As expected from three-dimensional correlation, biologists also evidenced that even minor structural and/or metal related modification can drastically modify physico-chemical properties and thus, modify the *in vivo* cytotoxicity. Hence, *in vivo* studies as well as toxicity studies on normal cells are therefore worthwhile and will be actively pursued in the future. But for now, there is no clear information on the mechanism of action and on the main molecular target responsible for the antitumour activity. This naturally leads to serious limitation to the development of these drugs.

As a conclusion, we can never be sure that these compounds will become a drug one day. But the discovery of the mode of action which seems to be significantly different from the existing compounds, will allow to progress in the design of new cytotoxic compounds.

List of communications:**Oral communications:**

- 20-21/05/2010: **Congrès SFC Grand-Est** (Illkirch-Graffenstaden, France):
«Ruthénium Derivatives Compounds: Corrélation entre propriétés anticancéreuses et physicochimiques de composés organométalliques»
Boff, B.; Collin, J.-P.; Sirlin, C.; Gaiddon, C. Loeffler, J. P.; Pfeffer, M.
- 10/11/2010: **Journée des doctorants en chimie** (Strasbourg, France) :
«Ruthénium Derivatives Compounds: Extension de la chimiothèque et Etudes physico-chimique de composé antitumoraux du Ruthénium (II)»
Boff, B.; Collin, J.-P.; Sirlin, C.; Gaiddon, C.; Pfeffer, M.
- 3-7/04/2011: **13th International Seminar of PhD Students on Organometallic and Coordination Chemistry** (Liblice, République Tchèque):
«Ruthenium Derivative Compounds: Correlation between anticancer and physicochemical properties of Organo-Ruthenium (II) compounds»
Boff, B.; Collin, J.-P.; Sirlin, C.; Gaiddon, C.; Pfeffer, M.
- 30/08-01/09/2011: **Summer School «Biology up to the frontiers with Chemistry and Physics»** (Strasbourg, France)
«Bio-physicochemical properties of ruthenium(II) anticancer agents: a possible step forward property-activity relationship»
Boff, B.; Collin, J.-P.; Sirlin, C.; Gaiddon, C.; Pfeffer, M.

Poster communications:

- 1-2-/07/2010: Congrès «**La chimie aux frontières de la biologie et de la physique**» (Strasbourg, France)
Boff, B.; Collin, J.-P.; Sirlin, C.; Gaiddon, C. Loeffler, J. P.; Pfeffer, M.
- 15-20/05/2011: **GECOM CONCOORD** (Merlimont, France):
« Ruthenium Derivatives Compounds: Corrélation entre propriétés physicochimiques et activités biologiques de ruthénacycles »
Boff, B.; Collin, J.-P.; Sirlin, C.; Gaiddon, C. ; Pfeffer, M.

Publication:

- “Library of Second Generation Cycloruthenated Compounds and Evaluation of their Biological Properties as Potential Anticancer Drugs: Passing the nanomolar barrier”
Fetzer, L.; Boff, B.; Ali, M.; Xiangjun, M.; Collin, J.-P.; Sirlin, C.; Gaiddon, C. ; Pfeffer, M.
J. Chem. Soc., Dalton Trans. **2011**, 40, 8869–8878.

Chapter 5

Experimental part

The experimentation looks like a discovery trail, full of sudden revival and peripeteia. It is only at the end of the way that one must meet the solution of the secrets, which promotes scientific thought and kindle the spirit of inquiry. Therefore, the experimental approach inspires scientists who are eager to know the ultimate cause of the phenomena.



Chapter 5: Experimental part..... 189

5.1. General remarks191

5.1.1. Generalities191

5.1.2. Analytical instruments192

5.1.3. Electrochemical measurements192

5.1.4. Hydrophobic properties measurement192

5.1.5. Biological assays193

5.2. Synthesis protocols.....194

5.3. References Chapter 5.....211

Chapter 5: Experimental part

5.1. General remarks

5.1.1. Generalities

Experiments were carried out under an argon atmosphere using a vacuum line. Diethyl ether and pentane were distilled over sodium/benzophenone, dichloromethane and acetonitrile over calcium hydride and methanol and ethanol over magnesium under argon immediately before use. Chromatography columns were carried out on Merk aluminium oxide 90 standardized.

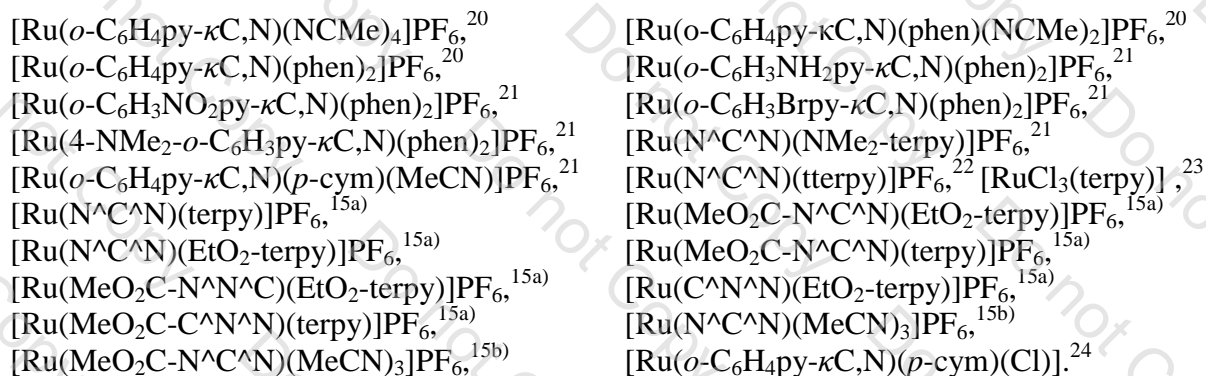
The following reagents were used as received. Aldrich: 1,3-cyclohexadiene, α -phellandren, 2-phenylpyridine, 2-tri-*n*-butylstannylpyridine, *bis*-(triphenylphosphine)palladiumdichloride, 2,2'-bipyridine, phenyllithium, *tert*-butyllithium; Strem: ruthenium trichloride, osmium trichloride, 2,2':6',2''-terpyridine; Alfa Aesar : 1,10-phenanthroline, lithium chloride, zincdichloride, 1,3-dibromobenzene, methyl 3,5-dibromobenzoate; Lancaster: potassium hexafluorophosphate.

The dimeric complexes $[(\eta^6\text{-bz})\text{RuCl}_2]_2$,¹ $[(p\text{-cym})\text{RuCl}_2]_2$,² $[(\eta^6\text{-bz})\text{OsCl}_2]_2$ ³ and $[(p\text{-cym})\text{OsCl}_2]_2$ ⁴ were synthesized according to reported procedure.

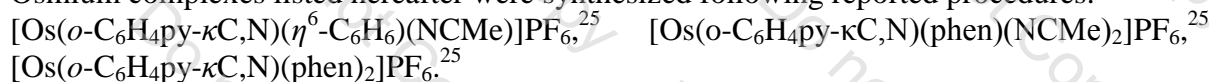
The ligands listed hereafter were synthesized following reported procedures:

N,N-dimethyl-4-(pyridin-2-yl)benzenamine,⁵ 4-amino-2-phenylpyridine,⁶ 1,3-di(pyridin-2-yl)benzene ($\text{N}^{\wedge}\text{C}(\text{H})^{\wedge}\text{N}$),^{7,8} Methyl-3,5-di(2-pyridyl)benzoate ($\text{MeO}_2\text{C}-\text{N}^{\wedge}\text{C}(\text{H})^{\wedge}\text{N}$),^{9,10,11} 3,5-di(2-pyridyl)toluene ($\text{Me}-\text{N}^{\wedge}\text{C}(\text{H})^{\wedge}\text{N}$),¹¹ 6-phenyl-2,2'-bipyridine ($\text{C}(\text{H})^{\wedge}\text{N}^{\wedge}\text{N}$),^{12,13} 4-ethoxycarbonyl-6-phenyl-2,2'-bipyridine ($\text{EtO}_2\text{C}-\text{C}(\text{H})^{\wedge}\text{N}^{\wedge}\text{N}$),^{14,15c} 4,4'-di(methoxycarbonyl)-6-phenyl-2,2'-bipyridine ($\text{MeO}_2\text{C})_2-\text{C}(\text{H})^{\wedge}\text{N}^{\wedge}\text{N}$),^{15c} 4'-ethoxycarbonyl-2,2':6',2''-terpyridine ($\text{EtO}_2\text{C}-\text{terpy}$),^{15c,16,17} trimethyl 2,2':6',2''-terpyridine-4-4'-4'' tricarboxylate ($(\text{MeO}_2\text{C})_3-\text{terpy}$),¹⁸ 4'-(4-methylphenyl)-2,2':6',2''-terpyridine ($\text{MePh}-\text{terpy}$).¹⁹ 4'-methoxycarbonyl-2,2':6',2''-terpyridine ($\text{MeO}_2\text{C}-\text{terpy}$) was synthesized using same method as for 4'-ethoxycarbonyl-2,2':6',2''-terpyridine ($\text{EtO}_2\text{C}-\text{terpy}$)^{15c} using methanol instead of ethanol for final esterification. Moreover a new synthetic route for ligand $\text{C}(\text{H})^{\wedge}\text{N}^{\wedge}\text{N}$ and more simple than the existing procedure was discovered.

Ruthenium complexes listed hereafter were synthesized following reported procedures:



Osmium complexes listed hereafter were synthesized following reported procedures:



5.1.2. Analytical instruments

The NMR spectra were obtained at room temperature on Bruker spectrometers. ^1H NMR spectra were recorded at 300.13 MHz (AC-300) or 400.13 MHz (AM-400) and referenced to SiMe_4 . $^{13}\text{C}\{^1\text{H}\}$ NMR spectra were recorded at 75.48 MHz (AC-300) or 100.62 MHz (AC-400) and referenced to SiMe_4 . The NMR assignments were supported by COSY spectra for ^1H NMR. The chemical shifts are referenced to the residual solvent peak. Chemical shifts (δ) and coupling constants (J) are expressed in ppm and Hz respectively. Multiplicity: s = singlet, d = doublet, t = triplet, q = quadruplet, sept = septuplet, m = multiplet. Adopted numeration for the assignment of NMR spectra is depicted in **Appendix, Figure 2** and **Figure 3**.

The infra-red spectra were recorded on an alpha ATR spectrometer from Bruker Optics and analysed with OPUS software. UV/Vis spectra (absorption spectroscopy) were recorded with a Kontron Instruments UVIKON 860 spectrometer at RT

ES-MS spectra and elemental analyses were carried out by the corresponding facilities at the Institut de chimie, Université de Strasbourg and at the Service Central d'Analyse du CNRS, Vernaison.

5.1.3. Electrochemical measurements

Electrochemical experiments were performed with a three-electrode system consisting of a platinum working electrode, a platinum wire counter electrode, and a silver wire as a pseudo-reference electrode. The potentials were referenced to SCE using ferrocene FeCp_2 or $[\text{Os}(\text{ttrpy})_2](\text{PF}_6)_2$ as an internal reference. The measurements were carried out under argon, in degassed CH_3CN at 298 K (scan rate: $0.100 \text{ V}\cdot\text{s}^{-1}$) using 0.1 M $[(n\text{Bu})_4\text{N}](\text{PF}_6)$ as the supporting electrolyte. An EG&G Princeton Applied Research Model 273A potentiostat connected to a computer was used for the cyclic voltammetry experiments.

5.1.4. Hydrophobic properties measurement

Hydrophobic properties measurements were performed by determining the octanol/water partition $\log(P_{o/w})$. Thanks to the method described by Minick *et al.*²⁶ and completed by Pomper *et al.*,²⁷ it is now possible to carry out the measurement by HPLC, thus avoiding the tedious "shake-flask" method of measurement.

5.1.4.1. Preparation of the mobile phases

The aqueous portion of the mobile phase was prepared by first dissolving the buffer agent 4-morpholinepropanesulfonic acid MOPS (0.02M) and *n*-decylamine amino modifier (0.15%, v/v) in deionized 1-octanol saturated water and then adjusting the pH of this solution to 7.4. The organic portion was prepared by diluting 1-octanol (0.20%, v/v) into analytical grade methanol. All mobile-phase solvents were filter through $0.45\mu\text{m}$ filters before use and degassed continuously during the experiment.

5.1.4.2. Measurements

Measurements were performed on a Varian prostar 210 HPLC equipped with a Prostar 335 photodiode array detector and a Prostar 410 autosampler. The stationary phase was a 250mm x 4.6mm column packed with 10\AA Kromasil C-8. The different compounds were dissolved into methanol ($5\cdot 10^{-5} \text{ M}$) and then injected onto the column ($5\mu\text{L}$). Column void volume was estimated from the retention time of uracil, which was included as a nonretained internal

reference for each injection.²⁸ The $\log(k'_w)$ was determined by linear extrapolation of $\log(k'_\phi)$ vs. Φ_{methanol} data acquired in the region $0.50 \leq \Phi_{\text{methanol}} \leq 0.85$. The measurements were repeated at least twice and the mean deviation was determined by considering the extreme values found over all experiments.

5.1.5. Biological assays

5.1.5.1. Cell proliferation assays

A172 cells were obtained from American Type Cell Culture Collection and maintained in culture as described by the provider. The cells were routinely grown in DMEM medium containing 10% foetal calf serum (FCS) and PS antibiotics at 37°C and 5% CO₂. Cells were seeded in 96-wells plates (25000 cells per well) and treated at 70% confluence.

Complex samples for *in vitro* tests were obtained from 50 mM solutions of the ruthenium or osmium complexes in neat DMSO. The mother solutions were then sequentially diluted with the required amount of cell culture media in order to obtain the studied solutions whose concentration varies from 0.2 to 200 μM .

After 48h treatment, the medium was removed and MTT (3-(4,5-dimethylthiazol-2-yl)-2,5-diphenyltetrazolium bromide) (0.5mg/mL) in DMEM was added for 1h. The medium was removed again and 0.04% HCl in isopropanol was added to dissolve the violet crystals of formazan. Optical density was quantified using a multiwell Elisa plate reader (Metertech USA) at 490-650 nm. The percentage of surviving cells was calculated from the ratio of absorbance of treated to untreated cells. The experiments were repeated at least 3 times and the mean deviation was determined by considering the extreme values found over all experiments.

5.1.5.2. DNA direct interaction study by agarose gel electrophoresis

Increasing amounts of tested compounds are incubated with supercoiled plasmid DNA for 16h. The ratios used are: 1, 2.5, 5 and 20 molecules/10 base pairs. The samples are loaded onto a 1% agarose gel, TAE 20 mM Tris acetate, 1 mM EDTA pH 8.0 in H₂O. The migration takes place under constant voltage 100V in a TAE buffer. After migration, the gel is incubated in a solution TAE - Ethidium bromide (0.5%) for 25 min before revealing it under UV.

5.1.5.3. Detection of Reactive Oxygen Species (ROS)

A172 cells were seeded in 96-wells black plates (20000 cells per well) and treated with the different compounds at 70% confluence for 1h, 4h and 16h at indicated concentration (2.5 μM , 5 μM and 10 μM). Menadione which generate ROS through red-ox cycling is using as positive control. After treatment, the medium was removed and the molecular probe H2DCF-DA (25mM diluted in PBS) was added for 1h. The medium was removed again, cells were washed twice, and 100 μL of PBS 1X was added to the wells. Fluorescence was measured by a plate reader with an excitation wavelength of 485 nm and an emission wavelength of 538 nm. Intensity of fluorescence is directly proportional to the quantity of ROS in the cells.

5.1.5.4. *In vivo* chronic toxicity

8 weeks old C57/Black6 male mice were treated by intraperitoneal injection of 200 μL of test compounds on day 0, 7, 10, 13, 17, 21, and on day 24. The first 2 injections are spaced 7 days to assess any possible acute toxicity and to adjust concentrations if necessary. Before each

injection, mice were observed and their weight was measured. For each compound, 4 groups of 4 mice are made to test the following concentration ranges:

- 2; 4; 6 and 8 $\mu\text{M}\cdot\text{kg}^{-1}$ for compounds with *in vitro* $\text{IC}_{50} < 1\text{mM}$
- 1; 2.5; 4 and 10 $\mu\text{M}\cdot\text{kg}^{-1}$ for compounds with *in vitro* $1\text{mM} < \text{IC}_{50} < 10\text{mM}$

During the studies, if the animal had a weight loss $\geq 20\%$ or if their pain or suffering fell into certain categories regarded as unacceptable (cachexia, prostration...) they were euthanized.

5.1.5.5. *In vivo* anticancer activity

These studies evaluated the evolution of tumour growth in syngeneic tumours implanted *in vivo*. 3LL murine cancer cells (600,000 cells/mL) were subcutaneously injected to 8 week old C57/Black6 male mice. After 15 days, tumours were measured with a calliper. When tumours reached 80mm^3 , compounds are injected twice a week (for 6 to 7 weeks) at concentration identified by previous chronic toxicity studies. Volume of the tumours and weight of the animals were measured before each injection. When the volume of the tumour exceeds 2500mm^3 the animal were euthanized.

5.2. Synthesis protocols

6-phenyl-2,2'-bipyridine

(C(H)^N^N)

A three-neck round bottom flask containing a magnetic stirring bar fitted with a thermometer, a reflux condenser and a side arm capped with a rubber septum was charged with 2,2'-bipyridine (1.0g, 6.4 mmol) and freshly distilled toluene (15 mL). The flask was then cooled to 0°C and phenyllithium (4.5 mL, 1.66M, 7.68 mmol) is slowly added *via* a canula. Rate of addition is such that the temperature should not exceed 30°C .

After one night under agitation at room temperature, the reaction mixture was then cooled to 0°C and slowly hydrolyzed with water (20 mL). Aqueous layer was extracted with dichloromethane (3 x 40 mL). 50-70g of MnO_2 were finally added to the yellow organic layer and the medium was vigorously agitated for 30min. The organic layer faded gradually from yellow to colorless. The organic layer was then dried over MgSO_4 and filtrated. Solid residues were washed twice with 40 mL of dichloromethane and then solvent was removed. Purification was accomplished by chromatography column using silica gel (eluant: CH_2Cl_2 : hexane; 50:50). The pure product was isolated as a white solid (750mg, 50%).

$^1\text{H NMR}$ (300.13 MHz, CDCl_3 , 300K): 8.70 (d, 1H, $^2J_{\text{HH}}=4.8$), 8.65 (d, 1H, $^2J_{\text{HH}}=8.1$), 8.38 (dd, 1H, $^2J_{\text{HH}}=8.1$, $^3J_{\text{HH}}=8.1$), 8.13 (m, 2H), 7.89 (t, 1H, $^3J_{\text{HH}}=7.7$), 7.85 (td, 1H, $^3J_{\text{HH}}=7.9$, $^4J=1.8$), 7.77 (dd, 1H, $^2J_{\text{HH}}=7.9$, $^3J_{\text{HH}}=0.9$), 7.41-7.55 (m, 3H), 7.30-7.35 (m, 1H).

[Ru(MeO₂C-N^C^N)(phen)(NCMe)]PF₆

(RDC 55)

A solution of [Ru(MeO₂C-N^C^N)(NCMe)₃]PF₆ (18 mg, 0.027) with 1,10-phenanthroline (5.4 mg, 0.027 mmol) in methanol (2 mL) was refluxed for 12h. The solvent was evaporated under vacuum, and the dark brown residue was dissolved in 5 mL of MeCN and filtered through Al_2O_3 using NCMe as eluent. The purple fraction was collected and evaporated to dryness under vacuum. Crystallization from CH_2Cl_2 /pentane or acetone/pentane (slow diffusion) gave dark purple crystals, which were washed with diethyl ether and dried under vacuum (18 mg, 88%).

Anal. calcd. for $\text{C}_{32}\text{H}_{24}\text{F}_6\text{N}_5\text{O}_2\text{PRu}$:

C, 50.80; H, 3.20; N, 9.26. Found: C, 50.55; H, 3.25; N, 9.26%.

MS (ES, m/z): Calcd. for $\text{C}_{32}\text{H}_{24}\text{N}_5\text{O}_2^{102}\text{Ru}$: 612.0974 (M); Found: 612.095

IR (cm⁻¹): 2264 (medium, $\nu\text{N}\equiv\text{C}$), 1690 (strong, $\nu\text{C}=\text{O}$), 840 (strong, νPF)

¹H NMR (400.13 MHz, CD₃CN, 300K): 10.02 (dd, 1H, ³J_{HH}=5.1, ⁴J_{HH}=1.5, H_o), 8.81 (dd, 1H, ³J_{HH}=7.5, ⁴J_{HH}=1.5, H_p), 8.62 (s, 2H, H₅), 8.35 (dd, 1H, ³J_{HH}=7.5, ³J_{HH}=5.1, H_m), 8.21 (d, 1H, ³J_{HH}=8.8, H_{phen}), 8.20 (d, 2H, ³J_{HH}=8.0, H_l), 8.06 (dd, 1H, ³J_{HH}=8.3, ⁴J_{HH}=1.5, H_o), 7.99 (d, 1H, ³J_{HH}=8.8, H_{phen}), 7.70 (td, 2H, ³J_{HH}=7.5, ⁴J_{HH}=1.5, H₂), 7.57 (d, 2H, ³J_{HH}=7.5, H₄), 7.32 (dd, 1H, ³J_{HH}=5.1, ⁴J_{HH}=1.5, H_p), 7.11 (dd, 1H, ³J_{HH}=8.3, ³J_{HH}=5.1, H_m), 6.81 (td, 2H, ³J_{HH}=7.5, ³J_{HH}=1.5, H₃), 4.05 (s, 3H, CH₃), 2.10 (s, 3H, NCCH₃).

¹³C NMR (100.62 MHz, CD₃CN, 300K): 230.9, 169.1, 168.5, 155.3, 153.8, 151.2, 150.0, 146.2, 145.4, 137.2, 136.1, 134.8, 131.7, 131.1, 128.8, 128.4, 127.0, 126.4, 125.2, 124.4, 123.4, 122.8, 120.7, 50.6, 4.43

[Ru(Me-N[^]C[^]N)(phen)(NCMe)]PF₆ (RDC 56)

A solution of [Ru(Me-N[^]C[^]N)(NCMe)₃]PF₆ (20 mg, 0.033) with 1,10-phenanthroline (6.5 mg, 0.033 mmol) in methanol (2 mL) was refluxed for 12h. The solvent was evaporated under vacuum, and the dark brown residue was dissolved in 5 mL of MeCN and filtered through Al₂O₃ using NCMe as eluent. The purple fraction was collected and evaporated to dryness under vacuum. Crystallization from CH₂Cl₂/pentane or acetone/pentane (slow diffusion) gave dark purple crystals, which were washed with diethyl ether and dried under vacuum (20 mg, 85%).

Anal. calcd. for C₃₁H₂₄F₆N₅PRu:

C, 52.25; H, 3.39; N, 9.83. Found: C, 52.18; H, 3.35; N, 9.78%.

HRMS (ES, m/z): Calcd. for C₃₁H₂₄N₅¹⁰²Ru: 568.10752 (M); Found: 568.107

IR (cm⁻¹): 2265 (medium, νN≡C), 841 (strong, νPF)

¹H NMR (400.13 MHz, CD₃CN, 300K): 10.01 (dd, 1H, ³J_{HH}=5.4, ⁴J_{HH}=1.5, H_o), 8.76 (dd, 1H, ³J_{HH}=8.1, ⁴J_{HH}=1.5, H_p), 8.31 (dd, 1H, ³J_{HH}=8.1, ³J_{HH}=5.4, H_m), (d, 1H, ³J_{HH}=8.8, H_{phen}) 7.99-8.04 (m, 3H, H_o+ H_l+ H_{phen}), 7.97 (s, 2H, H₅), 7.65 (td, 2H, ³J_{HH}=7.7, ⁴J_{HH}=1.5, H₂), (d, 2H, ³J_{HH}=7.7, H₄), 7.37 (dd, 1H, ³J_{HH}=5.4, ⁴J_{HH}=1.5, H_p), 7.14 (dd, 2H, ³J_{HH}=6.2, ³J_{HH}=5.4, H_m), 6.73 (td, 2H, ³J_{HH}=7.7, ⁴J_{HH}=1.5, H₃), 2.66 (s, 3H, CH₃), 2.09 (s, 3H, NCCH₃)

¹³C NMR (100.62 MHz, CD₃CN, 300K): 214.4, 169.7, 155.7, 154.1, 154.1, 151.4, 146.9, 145.3, 137.1, 135.7, 134.3, 131.9, 131.3, 130.4, 129.0, 128.7, 127.3, 126.4, 125.9, 125.2, 122.9, 120.4, 22.4, 4.7

Ru(*o*-C₆H₄py-κC,N)(*p*-cym)(dmsO)] PF₆ (RDC 49-DMSO)

To a suspension of [Ru(*o*-C₆H₄py-κC,N)(*p*-cym)(Cl)] (50 mg, 0.12 mmol), AgPF₆ (30 mg, 0.12 mmol) in 5 mL of dichloromethane was added dimethyl sulfoxide (10 μL, 0.12 mmol). The mixture was stirred at RT for 15 min and then filtered over celite. The light yellow fraction was collected and concentrated to about 5 mL. Addition of 50 mL of pentane causes precipitation of a beige solid (65 mg, 88%) which was washed with diethyl ether and dried under vacuum.

Anal. calcd. for C₂₃H₂₈F₆NOPS Ru:

C, 45.10; H, 4.61; N, 2.29. Found: C, 45.28; H, 4.68; N, 2.31

MS (ES, m/z): Calcd. for C₂₃H₂₈NOS¹⁰²Ru: 467.6095 (M); Found: 467.609

IR (cm⁻¹): 838 (strong, νPF), 562 (strong, νPF)

¹H NMR (300 MHz, CDCl₃, 300K): 9.16 (d, 1H, ³J_{HH}=5.6, H₁₂), 7.83-7.96 (m, 3H, H₈ + H₉ + H₁₀), 7.70 (d, 1H, ³J_{HH}=7.6, H₅), 7.38 (dd, 1H, ³J_{HH}=7.4, H₆), 7.17-7.30 (m, 2H, H₇ + H₁₁), 6.31 (d, 1H, ³J_{HH}=6.4, H_{arom}), 5.95 (d, 1H, ³J_{HH}=6.4, H_{arom}), 5.75 (d, 1H, ³J_{HH}=6.4, H_{arom}), 5.58 (d, 1H, ³J_{HH}=6.4, H_{p-cym}), 2.50 (q, ³J_{HH}=6.9, 1H, H₁₄), 2.43 (s, 1H, CH₃ DMSO), 2.31 (s, 1H, CH₃ DMSO), 2.29 (s, 3H, H₁₃), 0.97 (s, 3H, H₁₅ ou H₁₆), 0.81 (s, 3H, H₁₅ ou H₁₆)

¹³C {¹H} NMR (78 MHz, CDCl₃, 300K): 172.1, 165.7, 156.9, 144.6, 141.1, 139.6, 131.3, 125.2, 124.4, 120.1, 115.5, 111.5, 97.1, 92.9, 91.6, 90.1, 77.4, 46.2, 45.7, 31.2, 22.6, 21.7, 19.0

[Os(*o*-C₆H₄py-κC,N)(η⁶-C₆H₆)(NCMe)]PF₆ (ODC 1)

The [Os(*o*-C₆H₄py-κC,N)(η⁶-C₆H₆)(NCMe)]PF₆ was synthesised according to reference 25.

Anal. calcd. for C₁₉H₁₇F₆N₂POs · 0.5 CH₂Cl₂:

C, 35.98; H, 2.79; N, 4.30. Found: C, 36.15; H, 2.85; N, 4.38

MS (ES, m/z): Calcd. for $C_{19}H_{17}N_2^{192}Os$: 465.1007 (M); Found: 465.101

IR (cm⁻¹): 2287 (weak, $\nu N\equiv C$), 837 (strong, νPF), 551 (medium, νPF)

¹H NMR (300 MHz, CD₃CN, 300K): 9.20 (dd, 1H, ³J_{HH}=5.7, ⁴J_{HH}=0.8, H₁₂), 8.09 (dd, 1H, ³J_{HH}=6.3, ⁴J_{HH}=0.8, H₉), 8.03 (dd, 1H, ³J_{HH}=8.3, ⁴J_{HH}=0.8, H₅), 7.93 (td, 1H, ³J_{HH}=8.3, ⁴J_{HH}=1.7, H₁₁), 7.84 (dd, 1H, ³J_{HH}=7.2, ⁴J_{HH}=1.7, H₈), 7.25-7.13 (m, 3H, H₆ + H₇ + H₁₀), 5.79 (s, 6H, C₆H₆), 2.23 (s, 3H, NCMe)

¹³C {¹H} NMR (78 MHz, CD₃CN, 300K): 167.0, 157.0, 156.4, 145.3, 139.7, 138.9, 130.5, 124.4, 123.8, 123.4, 119.5, 117.4, 80.1

[Os(o-C₆H₄py- κ C,N)(phen)(NCMe)₂]PF₆ (ODC 2)

The [Os(o-C₆H₄py- κ C,N)(phen)(NCMe)₂]PF₆ was synthesised according to reference 25.

Anal. calcd. for C₂₇H₂₂F₆N₅OsP · 0.5 CH₂Cl₂:

C, 41.59; H, 2.92; N, 8.82. Found: C, 41.69; H, 2.91; N, 8.64

MS (ES, m/z): Calcd. for C₂₇H₂₂N₅¹⁹²Os: 608.1490 (M); Found: 608.149

IR (cm⁻¹): 2265 (medium, $\nu N\equiv C$), 841 (strong, νPF), 560 (medium, νPF)

¹H NMR (300 MHz, CD₃CN, 300K): 9.57 (dd, 1H, ³J_{HH}=5.2, ⁴J_{HH}=1.1, H_o), 8.48 (dd, 1H, ³J_{HH}=8.1, ⁴J_{HH}=1.1, H_p), 8.21 (dd, 1H, ³J_{HH}=7.5, ⁴J_{HH}=1.1, H₁₂), 8.17 (d, 1H, ³J_{HH}=9.0, H_{phen}), 8.09-8.15 (m, 1H, H_m), 8.07 (d, 1H, ³J_{HH}=9.0, H_{phen}), 7.99-8.05 (m, 2H, H_o + H_m ou H_p), 7.83-7.89 (m, 2H, H₅ et H₉), 7.30-7.39 (m, 2H, H₆ + H_m ou H_p), 7.25 (td, 1H, ³J_{HH}=7.2, ⁴J_{HH}=1.3, H₁₁), 7.19 (d, 1H, ³J_{HH}=6.2, H₈), 6.98 (t, 1H, ³J_{HH}=7.5, H₁₀), 6.51 (td, 1H, ³J_{HH}=6.2, ⁴J_{HH}=1.3, H₇), 2.64 (s, 3H, NCCH₃), 2.32 (s, 3H, NCCH₃)

¹³C {¹H} NMR (78 MHz, CD₃CN, 300K): 191.7, 155.2, 151.1, 150.1, 145.9, 138.1, 135.6, 135.5, 134.1, 130.1, 128.3, 127.5, 127.4, 125.9, 124.2, 123.8, 121.0, 120.5

[Os(o-C₆H₄py- κ C,N)(phen)₂]PF₆ (ODC 3)

The [Os(o-C₆H₄py- κ C,N)(phen)₂]PF₆ was synthesised according to reference 25.

Anal. calcd. for C₃₅H₂₄F₆N₅OsP · CH₂Cl₂:

C, 46.26; H, 2.80; N, 7.49. Found: C, 46.36; H, 3.22; N, 7.69

MS (ES, m/z): Calcd. for C₃₅H₂₄N₅¹⁹²Os: 706.1647 (M); Found: 706.165

IR (cm⁻¹): 843 (strong, νPF), 565 (medium, νPF)

¹H NMR (300 MHz, CD₃CN, 300K): 8.41 (dd, 1H, ³J_{HH}=5.5, ⁴J_{HH}=1.2, H_o), 8.34 (dd, 1H, ³J_{HH}=5.5, ⁴J_{HH}=1.2, H_o), 8.24 (dd, 1H, ³J_{HH}=8.1, ⁴J_{HH}=1.2, H_p), 8.1-7.99 (m, 8H), 7.95-7.88 (m, 2H), 7.81 (d, 1H, ³J_{HH}=8.1, ⁴J_{HH}=1.2, H_p), 7.55 (dd, 1H, ³J_{HH}=8.1, ³J_{HH}=5.5, H_m), 7.48 (m, 3H), 7.38 (d, 1H, ³J_{HH}=5.5), 7.25 (dd, 1H, ³J_{HH}=8.1, ³J_{HH}=5.5, H_m), 7.80-7.72 (m, 2H), 6.65 (td, 1H, ³J_{HH}=7.4, ⁴J_{HH}=1.3), 6.08 (dd, 1H, ³J_{HH}=7.4, ⁴J_{HH}=0.9)

¹³C {¹H} NMR (78 MHz, CD₃CN, 300K): 155.2, 150.4, 150.2, 150.1, 149.7, 136.0, 135.1, 134.2, 133.6, 132.4, 132.3, 129.3, 128.0, 127.8, 127.7, 126.1, 125.8, 125.7, 124.5, 122.7, 120.9, 118.7

[Os(o-C₆H₄py- κ C,N)(p-cym)(NCMe)]PF₆ (ODC 4)

To a suspension of [OsCl(μ -Cl)(p-cym)]₂ (795 mg, 1.0 mmol), NaOH (80 mg, 2.0 mmol) and KPF₆ (369 mg, 4.0 mmol) in 120 mL of acetonitrile was added 2-phenylpyridine (311 mg, 2.0 mmol). The mixture was stirred at 40 °C for 48 h. The solvent was evaporated under vacuum, and the dark residue was dissolved in 20 mL of CH₂Cl₂. The solution was filtered through Al₂O₃, using a 10:1 CH₂Cl₂/NCMe mixture as eluent. The bright yellow fraction was collected and concentrated to about 5 mL. Addition of 50 mL of diethyl ether caused precipitation of a yellow solid (962 mg, 75%).

Anal. calcd. for C₂₃H₂₅F₆N₂POs:

C, 41.56; H, 3.79; N, 4.21. Found: C, 41.64; H, 3.85; N, 4.21

MS (ES, m/z): Calcd. for C₂₃H₂₅N₂¹⁹²Os: 521.1633 (M); Found: 521.164

IR (cm⁻¹): 2287 (weak, $\nu N\equiv C$), 837 (strong, νPF), 575 (medium, νPF)

¹H NMR (300 MHz, CD₃CN, 300K): 9.13 (dd, 1H, ³J_{HH}=5.7, ⁴J_{HH}=1.2, H₁₂), 8.03-8.98 (m, 2H, H₉ + H₅), 7.90 (td, 1H, ³J_{HH}=7.3, ⁴J_{HH}=1.5, H₁₁), 7.84 (dd, 1H, ³J_{HH}=7.3, ⁴J_{HH}=1.8, H₈), 7.24-7.10 (m, 3H, H₆ + H₇ + H₁₀), 5.86 (d, 1H, ³J_{HH}=5.7, H_{arom}), 5.83 (d, 1H, ³J_{HH}=5.7, H_{arom}), 5.73 (d, 1H, ³J_{HH}=5.7, H_{arom}), 5.51 (d, 1H, ³J_{HH}=5.7, H_{arom}), 2.32 (q, 1H, ³J_{HH}=6.9, H₁₄), 2.23 (s, 3H, NCMe), 2.16 (s, 3H, H₁₃), 0.92 (d, 3H, ³J_{HH}=6.9, H₁₅ ou H₁₆), 0.86 (d, 3H, ³J_{HH}=6.9, H₁₅ ou H₁₆)

^{13}C { ^1H } NMR (78 MHz, CD_3CN , 300K): 156.2, 139.7, 138.9, 130.5, 124.3, 123.6, 123.4, 119.4, 83.2, 79.8, 74.8, 30.8

[Os(*o*- $\text{C}_6\text{H}_4\text{py-}\kappa\text{C,N}$)(terpy)(NCMe)]PF₆ (ODC 5)

A solution of [Os(*o*- $\text{C}_6\text{H}_4\text{py-}\kappa\text{C,N}$)($\eta^6\text{-C}_6\text{H}_6$)(NCMe)]PF₆ (20 mg, 0.033 mmol) with 2,2',6',2''-terpyridine (7.28 mg, 0.031 mmol) in acetonitrile (5 mL) was refluxed for 24 h. The solvent was evaporated under vacuum, and the dark residue was dissolved in 10 mL of CH_2Cl_2 . The solution was filtered through Al_2O_3 using a 90:10 $\text{CH}_2\text{Cl}_2/\text{NCMe}$ mixture as eluent. The dark purple fraction was collected and evaporated to dryness under vacuum. Crystallization from acetone/pentane or dichloromethane/pentane (slow diffusion) gave dark purple microcrystals (20 mg, 80%), which were washed with pentane and dried under vacuum.

Anal. calcd. for $\text{C}_{28}\text{H}_{22}\text{F}_6\text{N}_5\text{Os}$:

C, 44.04; H, 2.90; N, 9.17. Found: C, 43.81; H, 2.89; N, 8.97

MS (ES, m/z): Calcd. for $\text{C}_{28}\text{H}_{22}\text{N}_5^{192}\text{Os}$: 620.1490 (M); Found: 620.154

IR (cm⁻¹): 2287 (weak, $\nu\text{N}\equiv\text{C}$), 830 (strong, νPF), 562 (medium, νPF)

^1H NMR (400 MHz, CD_3CN , 300K): 8.44 (d, 2H, $^3J_{\text{HH}}=8.1$, H_c), 8.28 (d, 2H, $^3J_{\text{HH}}=8.2$, H_a), 8.24 (d, 1H, $^3J_{\text{HH}}=7.5$, H₁₂), 7.98 (d, 1H, $^3J_{\text{HH}}=7.5$, H₉), 7.82-7.87 (m, 3H, H_d + H₈ ou H₅), 7.68 (td, 2H, $^3J_{\text{HH}}=8.2$, $^4J_{\text{HH}}=1.4$, H_b), 7.6 (dd, 1H, $^3J_{\text{HH}}=8.1$, H_f), 7.35 (td, 1H, $^3J_{\text{HH}}=7.5$, $^4J_{\text{HH}}=1.2$, H₁₁), 7.24 (td, 1H, $^3J_{\text{HH}}=7.5$, $^4J_{\text{HH}}=1.5$, H₇ or H₆), 7.15 (td, 2H, $^3J_{\text{HH}}=8.2$, $^4J_{\text{HH}}=1.5$, H_c), 6.96 (td, 1H, $^3J_{\text{HH}}=7.5$, $^4J_{\text{HH}}=1.5$, H₁₀), 6.63 (d, 1H, $^3J_{\text{HH}}=7.5$, H₈ or H₅), 6.42 (td, 1H, $^3J_{\text{HH}}=7.5$, $^4J_{\text{HH}}=1.5$, H₇ ou H₆), 2.11 (s, 3H, NCMe)

^{13}C { ^1H } NMR (100.62 MHz, CD_3CN , 300K): 156.2, 149.0, 135.5, 135.2, 135.0, 132.8, 129.4, 128.5, 123.6, 120.8, 120.7, 119.9

[Os(*o*- $\text{C}_6\text{H}_4\text{py-}\kappa\text{C,N}$)(bpy)(NCMe)₂]PF₆ (ODC 6)

A solution of [Os(*o*- $\text{C}_6\text{H}_4\text{py-}\kappa\text{C,N}$)($\eta^6\text{-C}_6\text{H}_6$)(NCMe)]PF₆ (20 mg, 0.033 mmol) with 2,2'-bipyridine (4.88 mg, 0.031 mmol) in acetonitrile (5 mL) was refluxed for 24 h. The solvent was evaporated under vacuum, and the dark residue was dissolved in 10 mL of CH_2Cl_2 . The solution was filtered through Al_2O_3 using a 90:10 $\text{CH}_2\text{Cl}_2/\text{NCMe}$ mixture as eluent. The dark purple fraction was collected and evaporated to dryness under vacuum. Crystallization from acetone/pentane or dichloromethane/pentane (slow diffusion) gave dark purple microcrystals (18 mg, 80%), which were washed with pentane and dried under vacuum.

Anal. calcd. for $\text{C}_{25}\text{H}_{22}\text{F}_6\text{N}_5\text{Os}$:

C, 41.26; H, 3.05; N, 9.62. Found: C, 41.05; H, 2.95; N, 9.52

MS (ES, m/z): Calcd. for $\text{C}_{25}\text{H}_{22}\text{N}_5^{192}\text{Os}$: 584.1490 (M); Found: 584.158

IR (cm⁻¹): 2287 (weak, $\nu\text{N}\equiv\text{C}$), 830 (strong, νPF), 570 (medium, νPF)

^1H NMR (400 MHz, CD_3CN , 300K): 9.23 (d, 1H, $^3J_{\text{HH}}=5.4$, H_a), 8.39 (d, 1H, $^3J_{\text{HH}}=8.2$, H_d), 8.20 (d, 1H, $^3J_{\text{HH}}=8.0$, H_a), 7.92-8.00 (m, 3H, H₁₂, H_b, H_d), 7.85 (d, 1H, $^3J_{\text{HH}}=8.6$, H₅ ou H₈), 7.81 (d, 1H, $^3J_{\text{HH}}=7.2$, H₉), 7.71 (td, 1H, $^3J_{\text{HH}}=6.7$, $^4J_{\text{HH}}=1.3$, H_c), 7.50 (td, 1H, $^3J_{\text{HH}}=7.9$, $^4J_{\text{HH}}=1.4$, H_b), 7.41 (td, 1H, $^3J_{\text{HH}}=7.8$, $^4J_{\text{HH}}=1.5$, H₆ ou H₇), 7.32 (d, 1H, $^3J_{\text{HH}}=5.7$, H₅ ou H₈), 7.18 (td, 1H, $^3J_{\text{HH}}=7.3$, $^4J_{\text{HH}}=1.3$, H₁₁), 6.90-6.99 (m, 2H, H_c + H₁₀), 6.67 (td, 1H, $^3J_{\text{HH}}=6.7$, $^4J_{\text{HH}}=1.3$, H₆ ou H₇), 2.54 (s, 3H, NCMe), 2.43 (s, 3H, NCMe)

^{13}C { ^1H } NMR (100.62 MHz, CD_3CN , 300K): 154.8, 150.4, 149.0, 136.0, 135.8, 135.3, 133.9, 129.5, 127.7, 126.2, 124.4, 123.2, 123.0, 121.4, 120.0

[Os(MeO₂C-N[^]C[^]N)(phen)(NCMe)]PF₆ (ODC 7)

A solution of [Os(MeO₂C-N[^]C[^]N)(NCMe)₃]PF₆ (57 mg, 0.076 mmol) with 1,10-phenanthroline (15 mg, 0.076 mmol) in methanol (5 mL) was refluxed for 48 h. The solvent was evaporated under vacuum, and the dark brown residue was dissolved in 10 mL of CH_2Cl_2 and filtered through Al_2O_3 using a 10:0.5 $\text{CH}_2\text{Cl}_2/\text{NCMe}$ mixture as eluent. The purple fraction was collected and evaporated to dryness under vacuum. Crystallization from

CH₂Cl₂/pentane or acetone/pentane (slow diffusion) gave dark purple crystals, which were washed with diethyl ether and dried under vacuum (43 mg, 68%).

Remark. One pot coordination can be done directly from [Os(MeO₂C-N[^]C[^]N)(NCMe)₃]PF₆ in acetonitrile without further purification.

Anal. calcd. for C₃₂H₂₄F₆N₅O₂POs:

C, 45.44; H, 2.86; N, 8.28. Found: C, 45.25; H, 2.91; N, 8.18

MS (ES, m/z): Calcd. for C₃₂H₂₄N₅O₂¹⁹²Os: 702.1545 (M); Found: 702.159

IR (cm⁻¹): 2249 (weak, νN≡C), 1688 (medium νC=O), 831 (strong, νPF), 565 (medium, νPF)

¹H NMR (300 MHz, CD₃CN, 300K): 9.83 (dd, 1H, ³J_{HH}=5.5, ⁴J_{HH}=1.1, H_o), 8.69 (s, 2H, H₅), 8.50 (dd, 1H, ³J_{HH}=8.1, ⁴J_{HH}=1.1, H_p), 8.21-8.26 (m, 4H, H_m+H_{phen}+H₁), 8.00 (d, 1H, ³J_{HH}=9.0, H_{phen}), 7.85 (dd, 1H, ³J_{HH}=8.1, ⁴J_{HH}=1.1, H_o), 7.63 (td, 2H, ³J_{HH}=5.9, ⁴J_{HH}=1.5, H₂), 7.57 (d, 2H, ³J_{HH}=5.9, H₄), 7.21 (dd, 1H, ³J_{HH}=5.5, ⁴J_{HH}=1.1, H_p), 7.07 (dd, 1H, ³J_{HH}=8.1, ³J_{HH}=5.5, H_m), 6.78 (td, 2H, ³J_{HH}=5.9, ⁴J_{HH}=1.5, H₃), 4.00 (s, 3H, CH₃), 2.34 (s, 3H, NCCH₃)

¹³C {¹H} NMR (78 MHz, CD₃CN, 300K): 171.4, 169.0, 155.9, 154.3, 149.6, 144.1, 137.0, 134.5, 133.9, 132.0, 131.3, 128.9, 128.6, 127.3, 125.0, 123.8, 121.5, 120.8, 120.0, 51.5

[Os(MeO₂C-N[^]C[^]N)(bpy)(NCMe)]PF₆ (ODC 8)

A solution of [Os(MeO₂C-N[^]C[^]N)(NCMe)₃]PF₆ (55 mg, 0.074 mmol) with 2,2'-bipyridine (11.5 mg, 0.074 mmol) in methanol (5 mL) was refluxed for 48 h. The solvent was evaporated under vacuum, and the dark brown residue was dissolved in 10 mL of CH₂Cl₂ and filtered through Al₂O₃ using a 10:0.5 CH₂Cl₂/NCMe mixture as eluent. The purple fraction was collected and evaporated to dryness under vacuum. Crystallization from CH₂Cl₂/pentane or acetone/pentane (slow diffusion) gave dark purple crystals, which were washed with diethyl ether and dried under vacuum (39 mg, 65%).

Remark. One pot coordination can be done directly from [Os(MeO₂C-N[^]C[^]N)(NCMe)₃]PF₆ in acetonitrile without further purification.

Anal. calcd. for C₃₀H₂₄F₆N₅O₂POs :

C, 43.85; H, 2.94; N, 8.52. Found: C, 43.55; H, 2.91; N, 8.39

MS (ES, m/z): Calcd. for C₃₀H₂₄N₅O₂¹⁹²Os: 678.1545 (M); Found: 678.150

IR (cm⁻¹): 2251 (weak, νN≡C), 1696 (medium νC=O), 834 (strong, νPF), 565 (medium, νPF)

¹H NMR (300 MHz, CD₃CN, 300K): 9.51 (d, 1H, ³J_{HH}=5.7, H_a), 8.64 (s, 2H, H₅), 8.52 (d, 1H, ³J_{HH}=7.5, H_a), 8.19-8.26 (m, 3H, H_d+H₁), 7.95 (td, 1H, ³J_{HH}=7.5, ⁴J_{HH}=1.3, H_b), 7.80 (dd, 1H, ³J_{HH}=5.7, ⁴J_{HH}=1.3, H_b), 7.63-7.70 (m, 4H, H₂+H₄), 7.33 (dd, 1H, ³J_{HH}=7.5, ⁴J_{HH}=1.3, H_c), 6.88-6.95 (m, 3H, H_d+H₃), 6.67 (dd, 1H, ³J_{HH}=5.5, ⁴J_{HH}=1.3, H_c), 3.98 (s, 3H, OCH₃), 2.26 (s, 3H, NCCH₃)

¹³C {¹H} NMR (78 MHz, CD₃CN, 300K): 153.8, 153.0, 147.8, 142.9, 136.0, 133.9, 133.1, 127.6, 125.9, 124.0, 123.5, 122.9, 119.8, 51.5

[Os(MeO₂C-N[^]C[^]N)(terpy)]PF₆ (ODC 9)

A solution of [Os(MeO₂C-N[^]C[^]N)(NCMe)₃]PF₆ (55 mg, 0.074 mmol) with 2,2';6',2''-terpyridine (17.0 mg, 0.074 mmol) in methanol (5 mL) was refluxed for 48 h. The solvent was evaporated under vacuum, and the dark brown residue was dissolved in 10 mL of CH₂Cl₂ and filtered through Al₂O₃ using a 10:0.5 CH₂Cl₂/NCMe mixture as eluent. The purple fraction was collected and evaporated to dryness under vacuum. Crystallization from CH₂Cl₂/pentane or acetone/pentane (slow diffusion) gave dark purple crystals, which were washed with diethyl ether and dried under vacuum (39 mg, 65%).

Remark. One pot coordination can be done directly from [Os(MeO₂C-N[^]C[^]N)(NCMe)₃]PF₆ in acetonitrile without further purification.

Anal. calcd. for $C_{33}H_{24}F_6N_5O_2POs$:

C, 46.21; H, 2.82; N, 8.16. Found: C, 46.05; H, 2.83; N, 8.06

MS (ES, m/z): Calcd. for $C_{33}H_{24}N_5O_2^{192}Os$: 714.1545 (M); Found: 714.155

IR (cm⁻¹): 1698 (medium $\nu_{C=O}$), 834 (strong, ν_{PF}), 565 (medium, ν_{PF})

¹H NMR (300 MHz, CD₃CN, 300K): 8.91 (s, 2H, H₅), 8.73 (d, 2H, ³J_{HH}=8.1, H_c), 8.42 (d, 2H, ³J_{HH}=8.1, H_a), 8.30 (d, 2H, ³J_{HH}=8.1, H_d), 7.81 (t, 1H, ³J_{HH}=8.1, H_f), 7.50-7.59 (m, 4H, H_b + H_c), 7.06 (d, 2H, ³J_{HH}=5.9, H_l), 6.91 (d, 2H, ³J_{HH}=5.9, H₄), 6.85 (td, 2H, ³J_{HH}=5.9, ⁴J_{HH}=1.5, H₂), 6.64 (td, 2H, ³J_{HH}=5.9, ⁴J_{HH}=1.5, H₃), 4.04 (s, 3H, OCH₃)

¹³C {¹H} NMR (78 MHz, CD₃CN, 300K): 155.4, 151.9, 135.3, 134.7, 131.0, 127.1, 124.3, 123.7, 122.1, 120.9, 120.1, 51.5

[Os(Me-N[^]C[^]N)(phen)(NCMe)]PF₆ (ODC 10)

A solution of [Os(Me-N[^]C[^]N)(NCMe)₃]PF₆ (65 mg, 0.092 mmol) with 1,10-phenanthroline (18.3 mg, 0.092 mmol) in methanol (5 mL) was refluxed for 48 h. The solvent was evaporated under vacuum, and the dark brown residue was dissolved in 10 mL of CH₂Cl₂ and filtered through Al₂O₃ using a 10:0.5 CH₂Cl₂/NCMe mixture as eluent. The purple fraction was collected and evaporated to dryness under vacuum. Crystallization from CH₂Cl₂/pentane or acetone/pentane (slow diffusion) gave dark purple crystals, which were washed with diethyl ether and dried under vacuum (50 mg, 68%).

Remark. One pot coordination can be done directly from [Os(Me-N[^]C[^]N)(NCMe)₃]PF₆ in acetonitrile without further purification.

Anal. calcd. for $C_{31}H_{24}F_6N_5POs$:

C, 46.44; H, 3.01; N, 8.74. Found: C, 46.25; H, 3.02; N, 8.65

MS (ES, m/z): Calcd. for $C_{31}H_{24}N_5^{192}Os$: 658.1647 (M); Found: 658.165

IR (cm⁻¹): 2248 (weak, $\nu_{N\equiv C}$), 835 (strong, ν_{PF}), 575 (medium, ν_{PF})

¹H NMR (300 MHz, CD₃CN, 300K): 9.85 (dd, 1H, ³J_{HH}=5.5, ⁴J_{HH}=1.1, H_o), 8.40 (dd, 1H, ³J_{HH}=8.1, ⁴J_{HH}=1.1, H_p), 8.20 (d, 1H, ³J_{HH}=8.8, H_{phen}), 8.17 (dd, 1H, ³J_{HH}=8.1, ³J_{HH}=5.5, H_m), 8.07 (d, 2H, ³J_{HH}=7.5, H_l), 7.98 (d, 1H, ³J_{HH}=8.8, H_{phen}), 7.97 (s, 2H, H₅), 7.79 (dd, 1H, ³J_{HH}=8.1, ⁴J_{HH}=1.1, H_o), 7.56 (td, 2H, ³J_{HH}=7.5, ⁴J_{HH}=1.5, H₂), 7.48 (d, 2H, ³J_{HH}=7.5, ⁴J_{HH}=1.1, H₄), 7.28 (dd, 1H, ³J_{HH}=5.5, ⁴J_{HH}=1.1, H_p), 7.08 (dd, 1H, ³J_{HH}=8.1, ⁴J_{HH}=5.5, H_m), 6.68 (td, 2H, ³J_{HH}=7.3, ⁴J_{HH}=2.1, H₃), 2.73 (s, 3H, CH₃), 2.39 (s, 3H, NCCH₃)

¹³C {¹H} NMR (78 MHz, CD₃CN, 300K): 171.2, 155.3, 153.1, 148.05, 142.7, 135.5, 132.5, 132.0, 131.1, 130.2, 128.7, 127.8, 127.5, 126.3, 124.3, 122.0, 119.2, 21.0, 3.58

[Os(Me-N[^]C[^]N)(bpy)(NCMe)]PF₆ (ODC 11)

A solution of [Os(Me-N[^]C[^]N)(NCMe)₃]PF₆ (65 mg, 0.092 mmol) with 2,2'-bipyridine (14.42 mg, 0.092 mmol) in methanol (5 mL) was refluxed for 48 h. The solvent was evaporated under vacuum, and the dark brown residue was dissolved in 10 mL of CH₂Cl₂ and filtered through Al₂O₃ using a 10:0.5 CH₂Cl₂/NCMe mixture as eluent. The purple fraction was collected and evaporated to dryness under vacuum. Crystallization from CH₂Cl₂/pentane or acetone/pentane (slow diffusion) gave dark purple crystals, which were washed with diethyl ether and dried under vacuum (46 mg, 65%).

Remark. One pot coordination can be done directly from [Os(Me-N[^]C[^]N)(NCMe)₃]PF₆ in acetonitrile without further purification.

Anal. calcd. for $C_{29}H_{24}F_6N_5POs$:

C, 44.79; H, 3.11; N, 9.00. Found: C, 44.45; H, 3.08; N, 8.95

MS (ES, m/z): Calcd. for $C_{29}H_{24}N_5^{192}Os$: 634.1647 (M); Found: 634.166

IR (cm⁻¹): 2244 (weak, $\nu_{N\equiv C}$), 830 (strong, ν_{PF}), 575 (medium, ν_{PF})

¹H NMR (300 MHz, CD₃CN, 300K): 9.53 (d, 1H, ³J_{HH}=5.7, H_a), 8.48 (d, 1H, ³J_{HH}=8.2, H_a), 8.20 (d, 1H, ³J_{HH}=8.2, H_d), 8.07 (dd, 2H, ³J_{HH}=8.4, ⁴J_{HH}=1.6, H_l), 7.95 (s, 2H, H₅), 7.87 (td, 1H, ³J_{HH}=8.2, ⁴J_{HH}=1.5, H_b), 7.76 (td, 1H, ³J_{HH}=5.7, ⁴J_{HH}=1.5, H_b), 7.57-7.64 (m, 4H, H₂ + H₄), 7.30 (dd, 1H, ³J_{HH}=8.2, ⁴J_{HH}=1.5, H_c), 6.99 (d, 1H, ³J_{HH}=5.7, H_d), 6.83 (td, 2H, ³J_{HH}=8.4, ⁴J_{HH}=1.5, H₃), 6.68 (td, 1H, ³J_{HH}=5.7, ⁴J_{HH}=1.5, H_c), 2.69 (s, 3H, CH₃), 2.31 (s, 3H, NCCH₃)

^{13}C { ^1H } NMR (78 MHz, CD_3CN , 300K): 153.8, 152.9, 147.6, 142.7, 135.6, 132.8, 132.2, 127.5, 125.6, 124.3, 123.5, 122.7, 122.2, 119.3, 21.0, 3.51

[Os(Me-N $^{\wedge}$ C $^{\wedge}$ N)(terpy)]PF $_6$ (ODC 12)

A solution of [Os(Me-N $^{\wedge}$ C $^{\wedge}$ N)(NCMe) $_3$]PF $_6$ (65 mg, 0.092 mmol) with 2,2';6',2''-terpyridine (21.5 mg, 0.092 mmol) in methanol (5 mL) was refluxed for 48 h. The solvent was evaporated under vacuum, and the dark brown residue was dissolved in 10 mL of CH_2Cl_2 and filtered through Al_2O_3 using a 10:0.5 CH_2Cl_2 /NCMe mixture as eluent. The purple fraction was collected and evaporated to dryness under vacuum. Crystallization from CH_2Cl_2 /pentane or acetone/pentane (slow diffusion) gave dark purple crystals, which were washed with diethyl ether and dried under vacuum (49 mg, 65%).

Remark. One pot coordination can be done directly from [Os(Me-N $^{\wedge}$ C $^{\wedge}$ N)(NCMe) $_3$]PF $_6$ in acetonitrile without further purification.

Anal. calcd. for $\text{C}_{32}\text{H}_{24}\text{F}_6\text{N}_5\text{Os}$:

C, 47.23; H, 2.97; N, 8.61. Found: C, 46.93; H, 2.98; N, 8.61

MS (ES, m/z): Calcd. for $\text{C}_{32}\text{H}_{24}\text{N}_5^{192}\text{Os}$: 670.1647 (M); Found: 670.163

IR (cm $^{-1}$): 836 (strong, νPF), 560 (medium, νPF)

^1H NMR (300 MHz, CD_3CN , 300K): 8.70 (d, 2H, $^3J_{\text{HH}}=8.0$, H $_e$), 8.41 (d, 2H, $^3J_{\text{HH}}=8.2$, H $_a$), 8.22 (s, 2H, H $_5$), 8.12 (d, 2H, $^3J_{\text{HH}}=8.2$, H $_d$), 7.70 (t, 1H, $^3J_{\text{HH}}=8.0$, H $_f$), 7.55 (td, 2H, $^3J_{\text{HH}}=8.5$, $^4J_{\text{HH}}=1.5$, H $_b$), 7.45 (td, 2H, $^3J_{\text{HH}}=8.5$, $^4J_{\text{HH}}=1.5$, H $_c$), 7.55 (d, 2H, $^3J_{\text{HH}}=5.5$, H $_1$), 6.88 (td, 2H, $^3J_{\text{HH}}=5.5$, $^4J_{\text{HH}}=1.5$, H $_2$), 6.76 (d, 2H, $^3J_{\text{HH}}=5.5$, H $_4$), 6.51 (td, 2H, $^3J_{\text{HH}}=5.5$, $^4J_{\text{HH}}=1.5$, H $_2$), 2.90 (s, 3H, CH $_3$)

^{13}C { ^1H } NMR (78 MHz, CD_3CN , 300K): 170.8, 160.7, 155.3, 152.7, 151.8, 139.8, 134.9, 133.9, 129.5, 127.0, 124.3, 123.5, 121.3, 120.7, 119.6, 20.8

[Os(Me-N $^{\wedge}$ C $^{\wedge}$ N)(4'-methoxycarbonyl-2,2':6',2''-terpy)]PF $_6$ (ODC 13)

A solution of [Os(Me-N $^{\wedge}$ C $^{\wedge}$ N)(NCMe) $_3$]PF $_6$ (80.0 mg, 0.114 mmol) with methyl 4'-methoxycarbonyl-2,2':6',2''-terpyridine (31.8 mg, 0.136 mmol) in methanol (5 mL) was refluxed for 72 h. The solvent was evaporated under vacuum, and the dark brown residue was dissolved in 10 mL of CH_2Cl_2 and filtered through Al_2O_3 using a 10:1 CH_2Cl_2 /NCMe mixture as eluent. The purple fraction was collected and evaporated to dryness under vacuum. Crystallization from CH_2Cl_2 /pentane or acetone/pentane (slow diffusion) gave dark purple crystals, which were washed with diethyl ether and dried under vacuum (54 mg, 45%).

Anal. calcd. for $\text{C}_{34}\text{H}_{26}\text{F}_6\text{N}_5\text{O}_2\text{Os}$:

C, 46.84; H, 3.01; N, 8.03. Found: C, 46.78; H, 3.01; N, 8.05

MS (ES, m/z): Calcd. for $\text{C}_{34}\text{H}_{26}\text{N}_5\text{O}_2^{192}\text{Os}$: 728.1701 (M); Found: 728.163

IR (cm $^{-1}$): 1700 (medium $\nu\text{C}=\text{O}$), 836 (strong, νPF), 570 (medium, νPF)

^1H NMR (300 MHz, CD_3CN , 300K): 9.10 (s, 2H, H $_e$), 8.59 (d, 2H, $^3J_{\text{HH}}=8.1$, H $_a$), 8.25 (s, 2H, H $_5$), 8.13 (d, 2H, $^3J_{\text{HH}}=8.1$, H $_d$), 7.61 (td, 2H, $^3J_{\text{HH}}=8.1$, $^4J_{\text{HH}}=1.4$, H $_b$), 7.45 (td, 2H, $^3J_{\text{HH}}=8.1$, $^4J_{\text{HH}}=1.4$, H $_c$), 7.18 (d, 2H, $^3J_{\text{HH}}=5.5$, H $_1$), 6.98 (td, 2H, $^3J_{\text{HH}}=5.5$, $^4J_{\text{HH}}=1.3$, H $_2$), 6.69 (d, 2H, $^3J_{\text{HH}}=5.5$, H $_4$), 6.49 (td, 2H, $^3J_{\text{HH}}=5.5$, $^4J_{\text{HH}}=1.3$, H $_3$), 4.13 (s, 3H, OCH $_3$), 2.90 (s, 3H, CH $_3$)

^{13}C { ^1H } NMR (78 MHz, CD_3CN , 300K): 171.7, 162.0, 157.0, 153.5, 153.0, 140.6, 138.2, 136.9, 136.0, 131.9, 128.6, 128.4, 125.9, 125.0, 122.9, 122.7, 121.2, 54.0, 22.0, 15.2

[Os(Me-N $^{\wedge}$ C $^{\wedge}$ N)(4'-ethoxycarbonyl-2,2':6',2''-terpy)]PF $_6$ (ODC 14)

A solution of [Os(Me-N $^{\wedge}$ C $^{\wedge}$ N)(NCMe) $_3$]PF $_6$ (80.0 mg, 0.114 mmol) with 4'-ethoxycarbonyl-2,2':6',2''-terpyridine (31.8 mg, 0.136 mmol) in CH_2Cl_2 (5 mL) was refluxed for 72 h. The solvent was evaporated under vacuum, and the dark brown residue was dissolved in 10 mL of CH_2Cl_2 and filtered through Al_2O_3 using a 10:1 CH_2Cl_2 /NCMe mixture as eluent. The purple fraction was collected and evaporated to dryness under vacuum. Crystallization from

CH₂Cl₂/pentane or acetone/pentane (slow diffusion) gave dark purple crystals, which were washed with diethyl ether and dried under vacuum (60 mg, 50%).

Anal. calcd. for C₃₅H₂₈F₆N₅O₂POs:

C, 47.46; H, 3.19; N, 7.91. Found: C, 47.35; H, 3.33; N, 7.97

MS (ES, m/z): Calcd. for C₃₅H₂₈N₅O₂¹⁹²Os: 742.1858 (M); Found: 743.187

IR (cm⁻¹): 1695 (medium νC=O), 834 (strong, νPF), 572 (medium, νPF)

¹H NMR (300 MHz, CD₃CN, 300K): 9.10 (s, 2H, H_c), 8.60 (d, 2H, ³J_{HH}=8.2, H_a), 8.25 (s, 2H, H₅), 8.13 (d, 2H, ³J_{HH}=8.2, H_d), 7.61 (td, 2H, ³J_{HH}=8.2, ⁴J_{HH}=1.5, H_b), 7.45 (td, 2H, ³J_{HH}=8.2, ⁴J_{HH}=1.5, H_c), 7.18 (d, 2H, ³J_{HH}=5.9, H₁), 6.99 (td, 2H, ³J_{HH}=5.9, ⁴J_{HH}=1.5, H₂), 6.69 (d, 2H, ³J_{HH}=5.9, H₄), 6.49 (td, 2H, ³J_{HH}=5.9, ⁴J_{HH}=1.5, H₂ ou H₃), 4.59 (q, ³J_{HH}=7.1, OCH₂), 2.92 (s, 3H, CH₃), 1.56 (3H, t, ³J_{HH}=7.1, OCH₂CH₃)

¹³C {¹H} NMR (78 MHz, CD₃CN, 300K): 171.8, 166.4, 163.2, 157.0, 153.5, 143.9, 141.8, 136.9, 136.0, 130.7, 128.9, 128.5, 125.9, 125.0, 122.9, 122.8, 121.2, 63.3, 32.9, 22.0, 15.2

[Os(Me-N[^]C[^]N)(trimethyl 2,2':6'2''-terpy-4-4'-4''-tricarboxylate)]PF₆ (ODC 15)

A solution of [Os(Me-N[^]C[^]N)(NCMe)₃]PF₆ (172 mg, 0.245 mmol) with trimethyl 2,2':6'2''-terpyridine-4-4'-4''-tricarboxylate (100 mg, 0.245 mmol) in methanol (10 mL) was refluxed for 72 h. The solvent was evaporated under vacuum, and the dark brown residue was dissolved in 10 mL of CH₂Cl₂ and filtered through Al₂O₃ using a 10:1 CH₂Cl₂/NCMe mixture as eluent. The purple fraction was collected and evaporated to dryness under vacuum. Crystallization from CH₂Cl₂/pentane or acetone/pentane (slow diffusion) gave dark purple crystals, which were washed with diethyl ether and dried under vacuum (60 mg, 25%).

Anal. calcd. for C₃₈H₃₀F₆N₅O₆POs:

C, 46.20; H, 3.06; N, 7.09. Found: C, 46.10; H, 3.08; N, 7.12

MS (ES, m/z): Calcd. for C₃₈H₃₀N₅O₆¹⁹²Os: 844.1811 (M); Found: 844.184

IR (cm⁻¹): 1695 (medium νC=O), 828 (strong, νPF), 565 (medium, νPF)

¹H NMR (300 MHz, CD₃CN, 300K): 9.35 (s, 2H, H_d), 9.07 (s, 2H, H_c), 8.26 (s, 2H, H₅), 8.12 (d, 2H, ³J_{HH}=8.1, H_a ou H_b), 7.61 (td, 2H, ³J_{HH}=7.1, ⁴J_{HH}=1.6, H₂), 7.45 (d, 2H, ³J_{HH}=8.1, H_a ou H_b), 7.38 (dd, 2H, ³J_{HH}=7.1, ⁴J_{HH}=1.6, H₁), 6.54 (d, 2H, ³J_{HH}=7.1, H₄), 6.46 (d td, 2H, ³J_{HH}=7.1, ⁴J_{HH}=1.6, H₃), 4.16 (s, 3H, OCH₃), 3.91 (s, 6H, OCH₃), 2.97 (s, 3H, CH₃)

¹³C {¹H} NMR (78 MHz, CD₃CN, 300K): 178.6, 166.4, 163.2, 157.0, 153.5, 145.4, 141.8, 136.9, 132.0, 130.7, 128.9, 128.5, 125.9, 125.0, 122.9, 122.8, 121.2, 99.4, 63.3, 56.4, 46.5, 32.9, 22.0, 15.2

[Os(Me-N[^]C[^]N)(4'-(4-methylphenyl)-2,2':6'2''-terpy)]PF₆ (ODC 16)

A solution of [Os(Me-N[^]C[^]N)(NCMe)₃]PF₆ (80.0 mg, 0.113 mmol) with 4'-(4-methylphenyl)-2,2':6'2''-terpyridine (36.8 mg, 0.113 mmol) in methanol (5 mL) was refluxed for 72 h. The solvent was evaporated under vacuum, and the dark brown residue was dissolved in 10 mL of CH₂Cl₂ and filtered through Al₂O₃ using a 10:1 CH₂Cl₂/NCMe mixture as eluent. The purple fraction was collected and evaporated to dryness under vacuum. Crystallization from CH₂Cl₂/pentane or acetone/pentane (slow diffusion) gave dark purple crystals, which were washed with diethyl ether and dried under vacuum (62 mg, 60%).

Anal. calcd. for C₃₉H₃₀F₆N₅POs:

C, 51.82; H, 3.35; N, 7.75. Found: C, 51.57; H, 3.34; N, 7.80

MS (ES, m/z): Calcd. for C₃₉H₃₀N₅¹⁹²Os: 760.2116 (M); Found: 760.212

IR (cm⁻¹): 837 (strong, νPF), 575 (medium, νPF)

¹H NMR (300 MHz, CD₃CN, 300K): 8.98 (s, 2H, H_c), 8.56 (d, 2H, ³J_{HH}=8.2, H_a), 8.24 (s, 2H, H₅), 8.14 (d, 2H, ³J_{HH}=8.2, H_d), 8.07 (d, 2H, ³J_{HH}=8.1, H₁), 7.58 (td, 2H, ³J_{HH}=8.1, ⁴J_{HH}=1.3, H_b ou H_c), 7.53 (d, 2H, ³J_{HH}=8.1, H₄), 7.46 (td, 2H, ³J_{HH}=8.1, ⁴J_{HH}=1.3, H_b ou H_c), 7.10 (d, 2H, ³J_{HH}=5.6, H_{phenyl}), 6.89 (td, 2H, ³J_{HH}=8.1, ⁴J_{HH}=1.3, H₂ ou H₃), 6.84 (d, 2H, ³J_{HH}=5.6, H_{phenyl}), 6.52 (td, 2H, ³J_{HH}=8.1, ⁴J_{HH}=1.3, H₂ ou H₃), 2.92 (s, 3H, CH₃ NCN), 2.53 (s, 3H, CH₃ NNN)

¹³C {¹H} NMR (78 MHz, CD₃CN, 300K): 171.6, 161.7, 155.6, 151.8, 134.9, 133.9, 129.9, 127.7, 127.0, 124.1, 123.6, 121.3, 119.7, 118.3, 117.3, 63.7, 59.8, 20.7, 20.3

[Os(MeO₂C-N[^]C[^]N)(4'-methoxycarbonyl-2,2':6',2''-terpy)]PF₆ (ODC 17)

A solution of [Os(MeO₂C-N[^]C[^]N)(NCMe)₃]PF₆ (80.0 mg, 0.107 mmol) with 4'-methoxycarbonyl-2,2':6',2''-terpyridine (25 mg, 0.107 mmol) in methanol (5 mL) was refluxed for 72 h. The solvent was evaporated under vacuum, and the dark brown residue was dissolved in 10 mL of CH₂Cl₂ and filtered through Al₂O₃ using a 10:1 CH₂Cl₂/NCMe mixture as eluent. The purple fraction was collected and evaporated to dryness under vacuum. Crystallization from CH₂Cl₂/pentane or acetone/pentane (slow diffusion) gave dark purple crystals, which were washed with diethyl ether and dried under vacuum (54 mg, 45%).

Anal. calcd. for C₃₅H₂₆F₆N₅O₄POs:

C, 45.90; H, 2.86; N, 7.65. Found: C, 45.56; H, 2.91; N, 7.69

MS (ES, m/z): Calcd. for C₃₅H₂₆N₅O₄¹⁹²Os: 772.1600 (M); Found: 772.157

IR (cm⁻¹): 1705 (medium νC=O), 835 (strong, νPF), 565 (medium, νPF)

¹H NMR (300 MHz, CD₃CN, 300K): 9.14 (s, 2H, H_c), 8.93 (s, 2H, H₅), 8.59 (d, 2H, ³J_{HH}=8.1, H_a), 8.29 (d, 2H, ³J_{HH}=8.1, H_d), 7.61 (td, 2H, ³J_{HH}=8.1, ⁴J_{HH}=1.4, H_b), 7.52 (td, 2H, ³J_{HH}=8.1, ⁴J_{HH}=1.4, H_e), 7.16 (d, 2H, ³J_{HH}=5.5, H₁), 6.95 (td, 2H, ³J_{HH}=5.5, ⁴J_{HH}=1.3, H₂), 6.82 (d, 2H, ³J_{HH}=5.5, H₄), 6.61 (td, 2H, ³J_{HH}=5.5, ⁴J_{HH}=1.3, H₃), 4.14 (s, 3H, OCH₃), 4.05 (s, 3H, OCH₃)

¹³C {¹H} NMR (78 MHz, CD₃CN, 300K): 169.6, 163.2, 159.9, 155.7, 152.1, 151.3, 135.9, 135.2, 127.2, 124.5, 123.9, 122.2, 121.5, 120.3, 54.3, 51.6, 48.9

[Os(MeO₂C-N[^]C[^]N)(4'-ethoxycarbonyl-2,2':6',2''-terpy)]PF₆ (ODC 18)

A solution of [Os(MeO₂C-N[^]C[^]N)(NCMe)₃]PF₆ (50.0 mg, 0.067 mmol) with 4'-ethoxycarbonyl-2,2':6',2''-terpyridine (15 mg, 0.067 mmol) in CH₂Cl₂ (5 mL) was refluxed for 72 h. The dark brown solution was filtered through Al₂O₃ using a 10:1 CH₂Cl₂/NCMe mixture as eluent. The purple fraction was collected and evaporated to dryness under vacuum. Crystallization from CH₂Cl₂/pentane or acetone/pentane (slow diffusion) gave dark purple crystals, which were washed with diethyl ether and dried under vacuum (7 mg, 10%).

Anal. calcd. for C₃₆H₂₈F₆N₅O₄POs:

C, 46.50; H, 3.04; N, 7.53. Found: C, 46.40; H, 3.07; N, 7.58

MS (ES, m/z): Calcd. for C₃₆H₂₈N₅O₄¹⁹²Os: 786.1756 (M); Found: 786.174

IR (cm⁻¹): 1698 (medium νC=O), 836 (strong, νPF), 575 (medium, νPF)

¹H NMR (300 MHz, CD₃CN, 300K): 9.14 (s, 2H, H_c), 8.93 (s, 2H, H₅), 8.61 (d, 2H, ³J_{HH}=8.2, H_a), 8.30 (d, 2H, ³J_{HH}=8.2, H_d), 7.62 (td, 2H, ³J_{HH}=8.2, ⁴J_{HH}=1.5, H_b), 7.53 (td, 2H, ³J_{HH}=8.2, ⁴J_{HH}=1.5, H_e), 7.16 (d, 2H, ³J_{HH}=5.5, H₁), 6.95 (td, 2H, ³J_{HH}=5.5, ⁴J_{HH}=1.5, H₂), 6.83 (d, 2H, ³J_{HH}=5.5, H₄), 6.61 (td, 2H, ³J_{HH}=5.5, ⁴J_{HH}=1.5, H₃), 4.61 (q, ³J_{HH}=7.1, OCH₂), 4.05 (s, 3H, OCH₃), 1.56 (3H, t, ³J_{HH}=7.1, OCH₂CH₃)

¹³C {¹H} NMR (78 MHz, CD₃CN, 300K): 171.8, 166.4, 163.2, 158.7, 155.7, 152.2, 137.9, 138.8, 135.8, 135.1, 136.0, 130.7, 128.9, 127.1, 124.7, 124.4, 123.9, 122.1, 121.4, 120.3, 106.4, 62.1, 51.5, 19.9

[Os(MeO₂C-N[^]C[^]N)(trimethyl 2,2':6'2''-terpy-4-4'-4''-tricarboxylate)]PF₆ (ODC 19)

A solution of [Os(MeO₂C-N[^]C[^]N)(NCMe)₃]PF₆ (80 mg, 0.107 mmol) with trimethyl 2,2':6',2''-terpyridine-4-4'-4''-tricarboxylate (44 mg, 0.107 mmol) in methanol (10 mL) was refluxed for 72 h. The solvent was evaporated under vacuum, and the dark brown residue was dissolved in 10 mL of CH₂Cl₂ and filtered through Al₂O₃ using a 10:1 CH₂Cl₂/NCMe mixture as eluent. The purple fraction was collected and evaporated to dryness under vacuum. Crystallization from CH₂Cl₂/pentane or acetone/pentane (slow diffusion) gave dark purple crystals, which were washed with diethyl ether and dried under vacuum (60 mg, 58%).

Anal. calcd. for C₃₉H₃₀F₆N₅O₈POs:

C, 45.39; H, 2.93; N, 6.79. Found: C, 45.76; H, 3.31; N, 6.88

MS (ES, m/z): Calcd. for C₃₉H₃₀N₅O₈¹⁹²Os: 888.1709 (M); Found: 888.167

IR (cm⁻¹): 1695 (medium νC=O), 834 (strong, νPF), 565 (medium, νPF)

¹H NMR (300 MHz, CD₃CN, 300K): 9.37 (s, 2H, H_d), 9.07 (s, 2H, H_c), 9.06 (s, 2H, H_e), 8.95 (s, 2H, H₅), 8.29 (d, 2H, ³J_{HH}=8.1, H_a ou H_b), 7.55 (td, 2H, ³J_{HH}=7.3, ⁴J_{HH}=1.6, H₂), 7.42 (d, 2H, ³J_{HH}=8.1, H_a ou H_b), 7.33 (dd,

2H, $^3J_{\text{HH}}=7.3$, $^4J_{\text{HH}}=1.6$, H₁), 6.69(d, 2H, $^3J_{\text{HH}}=7.3$, H₄), 6.59 (d td, 2H, $^3J_{\text{HH}}=7.3$, $^4J_{\text{HH}}=1.6$, H₃), 4.17 (s, 3H, OCH₃), 4.05 (s, 3H, OCH₃), 3.91 (s, 6H, OCH₃)
 ^{13}C { ^1H } NMR (78 MHz, CD₃CN, 300K): 181.7, 167.4, 162.5, 157.5, 153.9, 141.0, 138.0, 128.2, 127.1, 124.5, 123.8, 123.0, 121.9, 120.6, 115.5, 54.2, 54.0, 53.0, 15.8

[Os(MeO₂C-N[^]C[^]N)(4'-(4-methylphenyl)-2,2':6',2''-terpy)PF₆ (ODC 20)

A solution of [Os(MeO₂C-N[^]C[^]N)(NCMe)₃]PF₆ (100 mg, 0.133 mmol) with 4'-(4-methylphenyl)-2,2':6',2''-terpyridine (43 mg, 0.133 mmol) in methanol (5 mL) was refluxed for 72 h. The solvent was evaporated under vacuum, and the dark brown residue was dissolved in 10 mL of CH₂Cl₂ and filtered through Al₂O₃ using a 10:1 CH₂Cl₂/NCMe mixture as eluent. The purple fraction was collected and evaporated to dryness under vacuum. Crystallization from CH₂Cl₂/pentane or acetone/pentane (slow diffusion) gave dark purple crystals, which were washed with diethyl ether and dried under vacuum (82 mg, 65%).

Anal. calcd. for C₄₀H₃₀F₆N₅O₂POs:

C, 50.68; H, 3.19; N, 7.39. Found: C, 50.19; H, 3.25; N, 7.50

MS (ES, m/z): Calcd. for C₄₀H₃₀N₅O₂¹⁹²Os: 804.2014 (M); Found: 804.199

IR (cm⁻¹): 835 (strong, νPF), 572 (medium, νPF)

^1H NMR (300 MHz, CD₃CN, 300K): 8.99 (s, 2H, H_c), 8.91 (s, 2H, H₅), 8.57 (d, 2H, $^3J_{\text{HH}}=8.2$, H_a), 8.31 (d, 2H, $^3J_{\text{HH}}=8.2$, H_d), 8.06 (d, 2H, $^3J_{\text{HH}}=8.1$, H₁), 7.59 (td, 2H, $^3J_{\text{HH}}=8.1$, $^4J_{\text{HH}}=1.3$, H_b ou H_c), 7.55 (d, 2H, $^3J_{\text{HH}}=8.1$, H₄), 7.53 (td, 2H, $^3J_{\text{HH}}=8.1$, $^4J_{\text{HH}}=1.3$, H_b ou H_c), 7.07 (d, 2H, $^3J_{\text{HH}}=5.6$, H_{phenyl}), 6.99 (d, 2H, $^3J_{\text{HH}}=5.6$, H_{phenyl}), 6.86 (td, 2H, $^3J_{\text{HH}}=8.1$, $^4J_{\text{HH}}=1.3$, H₂ ou H₃), 6.66 (td, 2H, $^3J_{\text{HH}}=8.1$, $^4J_{\text{HH}}=1.3$, H₂ ou H₃), 4.04 (s, 3H, OCH₃), 2.54 (s, 3H, CH₃)

^{13}C { ^1H } NMR (78 MHz, CD₃CN, 300K): 171.6, 161.7, 156.9, 153.7, 153.3, 141.2, 136.7, 136.0, 131.4, 129.1, 128.4, 125.7, 125.2, 123.5, 121.5, 119.9, 51.5, 41.0

[Os(MeO₂C-N[^]C[^]N)(NCMe)₃]PF₆ (ODC 21)

To a suspension of [OsCl(μ-Cl)(η⁶-C₆H₆)₂] (100 mg, 0.147 mmol), NaOH (12 mg, 0.294 mmol) and KPF₆ (91 mg, 0.588 mmol) in 10 mL of acetonitrile was added methyl-3,5-(2-pyridyl)benzoate (85 mg, 0.294 mmol). The mixture was refluxed for 72 h under an incandescent lamp irradiation (60W). The solvent was evaporated under vacuum, and the dark residue was dissolved in 10 mL of CH₂Cl₂. The solution was filtered through Al₂O₃, using a 10:1 CH₂Cl₂/NCMe mixture as eluent. The dark yellow fraction was collected and concentrated to about 1 mL. Addition of 10 mL of diethyl ether caused precipitation of a dark yellow solid (164 mg, 75%).

Anal. calcd. for C₂₄H₂₂F₆N₅O₂POs:

C, 38.55; H, 2.97; N, 9.37. Found: C, 38.54; H, 3.01; N, 9.43

MS (ES, m/z): Calcd. for C₂₄H₂₂N₅O₂¹⁹²Os: 604.1388 (M); Found: 604.143

IR (cm⁻¹): 2258 (medium, νN≡C), 1686 (medium, νC=O), 830 (strong, νPF), 565 (medium, νPF)

^1H NMR (300 MHz, CD₃CN, 300K): 8.98 (d, 2H, $^3J_{\text{HH}}=5.5$, H₁), 8.43 (s, 2H, H₅), 8.19 (d, 2H, $^3J_{\text{HH}}=8.0$, H₄), 7.84 (td, 2H, $^3J_{\text{HH}}=8.0$, $^4J_{\text{HH}}=1.5$, H₃), 7.33 (td, 2H, $^3J_{\text{HH}}=5.5$, $^4J_{\text{HH}}=1.5$, H₂), 3.93 (s, 3H, OMe), 1.98 (s, 3H, NCMe), 1.97 (s, 6H, NCMe)

^{13}C { ^1H } NMR (78 MHz, CD₃CN, 300K): 226.2, 168.9, 168.3, 154.7, 146.6, 137.5, 123.7, 123.6, 122.7, 120.3, 52.4, 3.27

[Os(Me-N[^]C[^]N)(NCMe)₃]PF₆ (ODC 22)

To a suspension of [OsCl(μ-Cl)(η⁶-C₆H₆)₂] (100 mg, 0.147 mmol), NaOH (12 mg, 0.294 mmol) and KPF₆ (91 mg, 0.588 mmol) in 10 mL of acetonitrile was added 3,5-di(2-pyridyl)toluene (73 mg, 0.294 mmol). The mixture was refluxed for 72 h under an incandescent lamp irradiation (60W). The solvent was evaporated under vacuum, and the dark residue was dissolved in 10 mL of CH₂Cl₂. The solution was filtered through Al₂O₃, using a 10:1 CH₂Cl₂/NCMe mixture as eluent. The dark yellow fraction was collected and

concentrated to about 1 mL. Addition of 10 mL of diethyl ether caused precipitation of a dark yellow solid (151 mg, 73%).

Anal. calcd. for $C_{23}H_{22}F_6N_5PO_5$:

C, 39.26; H, 3.15; N, 9.95. Found: C, 39.16; H, 2.35; N, 9.86

MS (ES, m/z): Calcd. for $C_{23}H_{22}N_5^{192}Os$: 560.1490 (M); Found: 560.153

IR (cm⁻¹): 2240 (medium, $\nu N\equiv C$), 827 (strong, νPF_6), 565 (medium, νPF_6)

¹H NMR (300 MHz, CD₃CN, 300K): 8.99 (d, 2H, $^3J_{HH}=5.5$, H₁), 8.00 (d, 2H, $^3J_{HH}=8.2$, H₄), 7.76 (td, 2H, $^3J_{HH}=8.0$, $^4J_{HH}=1.5$, H₃), 7.74 (s, 2H, H₅), 7.24 (td, 2H, $^3J_{HH}=5.5$, $^4J_{HH}=1.5$, H₂), 2.59 (s, 3H, Me), 2.00 (s, 3H, NCMe), 1.96 (s, 6H, NCMe)

¹³C {¹H} NMR (78 MHz, CD₃CN, 300K): 171.2, 155.3, 151.9, 145.6, 140.0, 135.8, 128.7, 123.4, 122.7, 120.0, 118.7, 112.2, 20.8, 2.61

[Os(N[^]N-(EtO₂C)[^]C)(NCMe)₃]PF₆ (ODC 23)

To a suspension of $[OsCl(\mu-Cl)(\eta^6-C_6H_6)]_2$ (200 mg, 0.294 mmol), NaOH (24 mg, 0.588 mmol) and KPF₆ (108 mg, 0.588 mmol) in 10 mL of acetonitrile was added 4-ethoxycarbonyl-6-phenyl-2,2'-bipyridine (179 mg, 0.588 mmol). The mixture was refluxed for 72 h under an incandescent lamp irradiation (60W). The solvent was evaporated under vacuum, and the dark residue was dissolved in 10 mL of CH₂Cl₂. The solution was filtered through Al₂O₃, using a 10:1 CH₂Cl₂/NCMe mixture as eluent. The dark orange/brown fraction was collected and concentrated to about 1 mL. Addition of 10 mL of diethyl ether caused precipitation of a brown solid (110 mg, 25%).

Anal. calcd. for $C_{25}H_{24}F_6N_5O_2PO_5$:

C, 39.42; H, 3.18; N, 9.19. Found: C, 39.56; H, 3.38; N, 9.09

MS (ES, m/z): Calcd. for $C_{25}H_{24}N_5O_2^{192}Os$: 618.1545 (M); Found: 618.154

IR (cm⁻¹): 1700 (medium $\nu C=O$), 2238 (medium, $\nu N\equiv C$), 828 (strong, νPF_6), 570 (medium, νPF_6)

¹H NMR (300 MHz, CD₃CN, 300K): 8.89 (d, 1H, $^3J_{HH}=5.5$, H₁), 8.41 (d, 1H, $^3J_{HH}=8.1$, H₄), 8.18 (m, 2H, H₅ + H₆), 7.79 (td, 1H, $^3J_{HH}=8.1$, $^4J_{HH}=1.5$, H₃), 7.46-7.51 (m, 3H, H₂ + H₇ + H₁₀), 7.39 (td, 1H, $^3J_{HH}=6.1$, $^4J_{HH}=1.5$, H₈ ou H₉), 7.30 (td, 1H, $^3J_{HH}=6.1$, $^4J_{HH}=1.5$, H₈ ou H₉), 4.35 (q, 2H, $^3J_{HH}=7.1$, OCH₂), 2.75 (s, 3H, NCMe), 2.29 (s, 6H, NCMe), 1.37 (t, 3H, $^3J_{HH}=7.1$, OCH₂CH₃)

¹³C {¹H} NMR (78 MHz, CD₃CN, 300K): 153.5, 141.0, 138.0, 130.1, 129.4, 127.0, 125.2, 122.1, 61.8, 15.2, 5.1, 4.2

[Os((MeO₂C)[^]N-(MeO₂C)[^]N[^]C)(NCMe)₃]PF₆ (ODC 24)

To a suspension of $[OsCl(\mu-Cl)(\eta^6-C_6H_6)]_2$ (200 mg, 0.294 mmol), NaOH (24 mg, 0.588 mmol) and KPF₆ (108 mg, 0.588 mmol) in 10 mL of acetonitrile was added 4,4'-di(methoxycarbonyl)-6-phenyl-2,2'-bipyridine (204 mg, 0.588 mmol). The mixture was refluxed for 72 h under an incandescent lamp irradiation (60W). The solvent was evaporated under vacuum, and the dark residue was dissolved in 10 mL of CH₂Cl₂. The solution was filtered through Al₂O₃, using a 10:1 CH₂Cl₂/NCMe mixture as eluent. The dark orange/brown fraction was collected and concentrated to about 1 mL. Addition of 10 mL of diethyl ether caused precipitation of a brown solid (118 mg, 25%).

Anal. calcd. for $C_{26}H_{24}F_6N_5O_4PO_5$:

C, 38.76; H, 3.00; N, 8.69. Found: C, 38.96; H, 3.10; N, 8.75

MS (ES, m/z): Calcd. for $C_{26}H_{24}N_5O_4^{192}Os$: 662.1443 (M); Found: 662.144

IR (cm⁻¹): 2240 (medium, $\nu N\equiv C$), 1700 (medium $\nu C=O$), 827 (strong, νPF_6), 565 (medium, νPF_6)

¹H NMR (300 MHz, CD₃CN, 300K): 9.08 (d, 1H, $^3J_{HH}=5.9$, H₁), 8.75 (d, 1H, $^3J_{HH}=2.0$, H₄), 8.17 (m, 2H, H₅ + H₆), 7.67 (dd, 1H, $^3J_{HH}=5.9$, $^3J_{HH}=2.0$, H₂), 7.48-7.56 (m, 3H, H₇ + H₈ ou H₉ + H₁₀), 7.41 (td, 1H, $^3J_{HH}=7.1$, $^4J_{HH}=1.5$, H₈ ou H₉), 4.0 (s, 3H, OCH₃), 3.9 (s, 3H, OCH₃), 2.79 (s, 3H, NCMe), 2.28 (s, 6H, NCMe)

¹³C {¹H} NMR (78 MHz, CD₃CN, 300K): 155.8, 142.5, 139.0, 128.2, 129.5, 126.0, 124.8, 121.2, 68.5, 62.3, 15.8, 18.4, 5.3, 4.5

[Os(phen)(η^6 -C₆H₆)(Cl)]PF₆ (ODC 25)

[OsCl(μ -Cl)(η^6 -C₆H₆)]₂ (65 mg, 0.096 mmol) was stirred with 1,10-phenanthroline (37.9 mg, 0.119 mmol) in 5 mL of methanol for ca. 1h. The reaction mixture was then filtered and addition of an excess of NH₄PF₆ (65 mg, 0.400 mmol) to the yellow filtrate precipitated the product as a yellow solid, which was filtered off and washed thoroughly with water, methanol and diethylether.

Anal. calcd. for C₁₈H₁₄ClF₆N₂POs:

C, 34.37; H, 2.24; N, 4.45. Found: C, 34.45; H, 2.26; N, 4.55

MS (ES, m/z): Calcd. for C₁₈H₁₄ClN₂¹⁹²Os: 485.0460 (M); Found: 485.047

IR (cm⁻¹): 825 (strong, ν PF), 560 (medium, ν PF), 305 (weak, ν Cl)

¹H NMR (300 MHz, CD₃CN, 300K): 9.68 (dd, 2H, ³J_{HH}=5.4, ⁴J_{HH}=1.2, H_o), 8.75 (dd, 2H, ³J_{HH}=8.2, ⁴J_{HH}=1.2, H_p), 8.20 (s, 2H, H_{phen}), 8.00 (dd, 2H, ³J_{HH}=8.2, ³J_{HH}=5.4, H_m), 6.24 (s, 6H, C₆H₆)

¹³C {¹H} NMR (78 MHz, CD₃CN, 300K): 156.7, 148.2, 140.5, 132.2, 129.13, 128.1, 79.0

[Os(*o*-C₆H₃NMe₂py- κ C,N)(η^6 -C₆H₆)(NCMe)]PF₆ (ODC 26)

To a suspension of [OsCl(μ -Cl)(η^6 -C₆H₆)]₂ (343 mg, 0.504 mmol), NaOH (40 mg, 1.010 mmol) and KPF₆ (371 mg, 2.010 mmol) in 50 mL of acetonitrile was added *N,N*-dimethyl-4-(pyridin-2-yl)benzenamine (200 mg, 1.010 mmol). The mixture was stirred at 40 °C for 48 h. The solvent was evaporated under vacuum, and the dark residue was dissolved in 20 mL of CH₂Cl₂. The solution was filtered through Al₂O₃, using a 10:1 CH₂Cl₂/NCMe mixture as eluent. The bright yellow fraction was collected and concentrated to about 5 mL. Addition of 50 mL of diethyl ether caused precipitation of a yellow solid (489 mg, 75%).

Anal. calcd. for C₂₁H₂₂F₆N₃POs:

C, 38.71; H, 3.40; N, 6.45. Found: C, 38.60; H, 3.42; N, 6.40

MS (ES, m/z): Calcd. for C₂₁H₂₂N₃¹⁹²Os: 508.1429 (M); Found: 508.145

IR (cm⁻¹): 2289 (weak, ν N \equiv C), 836 (strong, ν PF), 562 (medium, ν PF)

¹H NMR (300 MHz, CD₃CN, 300K): 9.01 (d, 1H, ³J_{HH}=5.9, H₁₂), 7.69-7.78 (m, 2H, H_o + H₁₁), 7.61 (d, 1H, ³J_{HH}=8.8, H₈), 7.35 (d, 1H, ³J_{HH}=2.6, H₅), 6.97 (td, 1H, ³J_{HH}=6.2, ⁴J_{HH}=2.4, H₁₀), 6.51 (dd, 1H, ³J_{HH}=8.8, ³J_{HH}=2.6, H₇), 5.73 (s, 6H, C₆H₆), 3.07 (s, 6H, NMe₂), 2.22 (s, 3H, NCMe)

¹³C {¹H} NMR (78 MHz, CD₃CN, 300K): 168.8, 160.8, 157.0, 153.4, 139.5, 134.7, 127.0, 122.9, 121.8, 120.4, 119.2, 109.5, 81.1, 40.9

[Os(4-amino-*o*-C₆H₄py- κ C,N)(η^6 -C₆H₆)(NCMe)]PF₆ (ODC 27)

To a suspension of [OsCl(μ -Cl)(η^6 -C₆H₆)]₂ (599 mg, 0.881 mmol), NaOH (70 mg, 1.762 mmol) and KPF₆ (649 mg, 3.525 mmol) in 50 mL of acetonitrile was added 4-amino-phenylpyridine (300 mg, 1.762 mmol). The mixture was stirred at 40 °C for 48 h. The solvent was evaporated under vacuum, and the dark residue was dissolved in 20 mL of CH₂Cl₂. The solution was filtered through Al₂O₃, using a 10:1 CH₂Cl₂/NCMe mixture as eluent. The bright yellow fraction was collected and concentrated to about 5 mL. Addition of 50 mL of diethyl ether caused precipitation of a yellow solid (768 mg, 70%).

Anal. calcd. for C₁₉H₁₈F₆N₃POs:

C, 36.60; H, 2.91; N, 6.74. Found: C, 36.32; H, 2.87; N, 6.69

MS (ES, m/z): Calcd. for C₁₉H₁₈N₃¹⁹²Os: 480.1116 (M); Found: 480.110

IR (cm⁻¹): 2289 (weak, ν N \equiv C), 836 (strong, ν PF), 565 (medium, ν PF)

¹H NMR (300 MHz, CD₃CN, 300K): 8.58 (d, 1H, ³J_{HH}=6.6, H₁₂), 8.01 (d, 1H, ³J_{HH}=8.8, ⁴J_{HH}=2.0, H₅ ou H₈), 7.60 (d, 1H, ³J_{HH}=8.8, ⁴J_{HH}=2.0, H₅ ou H₈), 7.04-7.14 (m, 3H, H₆ + H₇ + H₉), 6.43 (dd, 1H, ³J_{HH}=6.6, ³J_{HH}=2.0, H₁₁), 5.67 (s, 6H, C₆H₆), 5.45 (s, 6H, NH₂), 2.22 (s, 3H, NCMe)

¹³C {¹H} NMR (78 MHz, CD₃CN, 300K): 167.4, 158.3, 157.3, 156.9, 147.3, 140.9, 131.2, 124.9, 124.7, 110.3, 104.5, 80.6

[Os(*o*-C₆H₃NMe₂py-κC,N)(phen)₂]PF₆**(ODC 28)**

A solution of [Os(*o*-C₆H₃NMe₂py-κC,N)(η⁶-C₆H₆)(NCMe)]PF₆ (100 mg, 0.153 mmol) with 1,10-phenanthroline (61 mg, 0.307 mmol) in methanol (10 mL) was refluxed for 48 h. The solvent was evaporated under vacuum, and the dark brown residue was dissolved in 10 mL of CH₂Cl₂ and filtered through Al₂O₃ using a 10:0.5 CH₂Cl₂/NCMe mixture as eluent. The purple fraction was collected and evaporated to dryness under vacuum. Crystallization from CH₂Cl₂/pentane or acetone/pentane (slow diffusion) gave dark purple crystals, which were washed with diethyl ether and dried under vacuum (87 mg, 65%).

Anal. calcd. for C₃₇H₂₆F₆N₆POs:

C, 49.77; H, 3.27; N, 9.41. Found: C, 49.53; H, 3.31; N, 9.41

MS (ES, m/z): Calcd. for C₃₇H₂₆N₆¹⁹²Os: 749.2069 (M); Found: 749.207

IR (cm⁻¹): 836 (strong, νPF), 562 (medium, νPF)

¹H NMR (300 MHz, CD₃CN, 300K): 8.54 (d, 1H, ³J_{HH}=5.2, H_o), 8.38 (d, 1H, ³J_{HH}=5.2, H_o), 8.23 (d, 1H, ³J_{HH}=8.1, H_p), 8.09 (d, 2H, ³J_{HH}=20.0, H_{phen}), 8.01 (d, 2H, ³J_{HH}=20.0, H_{phen}), 9.91-8.14 (m, 5H, 2 x H_o, 3 x H_p), 7.75 (dd, 1H, ³J_{HH}=8.6, ⁴J_{HH}=1.4, H₁₂), 7.62 (d, 1H, ³J_{HH}=8.6, H₈), 7.58 (dd, 1H, ³J_{HH}=5.2, ³J_{HH}=8.1, H_m), 7.49 (dd, 1H, ³J_{HH}=5.2, ³J_{HH}=8.1, H_m), 7.48 (dd, 1H, ³J_{HH}=5.2, ³J_{HH}=8.1, H_m), 7.36 (dd, 1H, ³J_{HH}=8.6, ³J_{HH}=1.4, H₁₁), 7.22 (dd, 1H, ³J_{HH}=5.2, ³J_{HH}=8.1, H_m), 7.19 (dd, 1H, ³J_{HH}=8.6, ³J_{HH}=1.4, H₉), 6.54 (dd, 1H, ³J_{HH}=8.6, ⁴J_{HH}=1.4, H₁₀), 6.19 (dd, 1H, ³J_{HH}=8.6, ³J_{HH}=2.4, H₇), 5.26 (d, 1H, ³J_{HH}=2.4, H₅), 2.51 (s, 1H, NMe₂)

¹³C {¹H} NMR (78 MHz, CD₃CN, 300K): 156.3, 153.4, 153.3, 153.1, 152.7, 152.4, 151.9, 151.5, 151.3, 150.8, 145.4, 136.9, 136.6, 134.7, 133.6, 133.4, 133.3, 133.2, 132.4, 132.3, 132.2, 132.1, 132.0, 130.1, 129.9, 129.8, 129.7, 129.6, 129.4, 129.1, 129.0, 128.1, 128.0, 127.5, 121.4, 40.2, 31.2

[Os(4-amino-*o*-C₆H₄py-κC,N)(phen)₂]PF₆**(ODC 29)**

A solution of [Os(4-amino-*o*-C₆H₄py-κC,N)(η⁶-C₆H₆)(NCMe)]PF₆ (100 mg, 0.160 mmol) with 1,10-phenanthroline (63 mg, 0.320) in methanol (10 mL) was refluxed for 48 h. The solvent was evaporated under vacuum, and the dark brown residue was dissolved in 10 mL of CH₂Cl₂ and filtered through Al₂O₃ using a 10:0.5 CH₂Cl₂/NCMe mixture as eluent. The purple fraction was collected and evaporated to dryness under vacuum. Crystallization from CH₂Cl₂/pentane or acetone/pentane (slow diffusion) gave dark purple crystals, which were washed with diethyl ether and dried under vacuum (91 mg, 66%).

Anal. calcd. for C₃₅H₂₅F₆N₆POs:

C, 48.61; H, 2.91; N, 9.72. Found: C, 48.53; H, 3.04; N, 10.12

MS (ES, m/z): Calcd. for C₃₅H₂₅N₆¹⁹²Os: 721.1756 (M); Found: 721.176

IR (cm⁻¹): 836 (strong, νPF), 568 (medium, νPF)

¹H NMR (300 MHz, CD₃CN, 300K): 8.43 (d, 1H, ³J_{HH}=5.5, H_o), 8.38 (d, 1H, ³J_{HH}=5.5, H_o), 8.19 (d, 1H, ³J_{HH}=7.9, H_p), 8.38 (d, 1H, ³J_{HH}=5.5, H_o), 8.07 (d, 4H, ³J_{HH}=19.6, 2 x H_{phen}), 7.97 (d, 1H, ³J_{HH}=7.9, H_p), 7.94 (d, 2H, ³J_{HH}=7.9, 2 x H_p), 7.88 (d, 1H, ³J_{HH}=5.5, H_o), 8.85 (d, 1H, ³J_{HH}=5.5, H_o), 7.66 (m, 1H, H₅), 7.53 (dd, 1H, ³J_{HH}=5.5, ³J_{HH}=7.9, H_m), 7.52 (dd, 1H, ³J_{HH}=5.5, ³J_{HH}=7.9, H_m), 7.43 (dd, 1H, ³J_{HH}=5.5, ³J_{HH}=7.9, H_m), 7.21 (d, 1H, ³J_{HH}=2.1, H₉), 7.17 (dd, 1H, ³J_{HH}=5.5, ³J_{HH}=7.9, H_m), 6.72 (dd, 1H, ³J_{HH}=6.4, ³J_{HH}=2.1, H₁₁), 6.65 (m, 2H, H₆ + H₇), 6.06 (dd, 1H, ³J_{HH}=6.4, ⁴J_{HH}=2.1, H₁₂), 5.84 (m, 1H, H₈)

¹³C {¹H} NMR (78 MHz, CD₃CN, 300K): 169.8, 167.3, 156.1, 155.7, 154.0, 152.9, 152.6, 152.4, 151.8, 151.3, 150.9, 150.7, 150.3, 147.6, 141.3, 136.2, 134.1, 133.4, 133.2, 132.4, 132.3, 132.1, 132.0, 129.9, 129.8, 129.4, 129.2, 129.0, 127.3, 127.1, 127.0, 124.6, 122.7, 110.1, 104.9

[Os(*o*-C₆H₃NMe₂py-κC,N)(terpy)(NCMe)]PF₆**(ODC 30)**

A solution of [Os(*o*-C₆H₃NMe₂py-κC,N)(η⁶-C₆H₆)(NCMe)]PF₆ (100 mg, 0.153 mmol) with 2,2',6',2''-terpyridine (25 mg, 0.153) in acetonitrile (10 mL) was refluxed for 72 h. The solvent was evaporated under vacuum, and the dark brown residue was dissolved in 10 mL of CH₂Cl₂ and filtered through Al₂O₃ using a 10:0.5 CH₂Cl₂/NCMe mixture as eluent. The purple fraction was collected and evaporated to dryness under vacuum. Crystallization from

CH₂Cl₂/pentane gave dark red crystals, which were washed with diethyl ether and dried under vacuum (74 mg, 60%).

Anal. calcd. for C₃₀H₂₇F₆N₆POs:

C, 44.66; H, 3.37; N, 10.42. Found: C, 44.63; H, 3.40; N, 10.43

MS (ES, m/z): Calcd. for C₃₀H₂₇N₆¹⁹²Os: 663.1912 (M); Found: 663.192

IR (cm⁻¹): 836 (strong, νPF), 565 (medium, νPF)

¹H NMR (300 MHz, CD₃CN, 300K): 8.43 (d, 2H, ³J_{HH}=8.1, H_e), 8.28 (d, 2H, ³J_{HH}=8.1, H_a), 8.00 (d, 2H, ³J_{HH}=5.3, H_d), 7.86 (d, 1H, ³J_{HH}=8.8, H₁₂), 7.68 (dd, 2H, ³J_{HH}=8.1, ³J_{HH}=5.6, H_b), 7.51-7.58 (m, 2H, H₉ + H_f), 7.35 (m, 1H, H₅), 7.22 (dd, 2H, ³J_{HH}=5.6, H_c), 7.10 (t, 1H, ³J_{HH}=8.8, H₁₁), 6.40 (d, 1H, ³J_{HH}=5.8, H₈), 6.33 (m, 1H, H₇), 7.10 (t, 1H, ³J_{HH}=6.3, H₁₀), 3.16 (s, 6H, NMe₂), 2.12 (s, 3H, NCMe)

¹³C {¹H} NMR (78 MHz, CD₃CN, 300K): 163.6, 159.6, 149.5, 136.7, 135.8, 133.7, 130.1, 124.8, 121.9, 119.7, 117.6, 41.0, 4.2

[Os(*o*-C₆H₃NMe₂py-κC,N)(4'-ethoxycarbonyl-2,2':6',2''-terpy)(NCMe)]PF₆ (ODC 31)

A solution of [Os(*o*-C₆H₃NMe₂py-κC,N)(η⁶-C₆H₆)(NCMe)]PF₆ (100 mg, 0.153 mmol) with 4'-ethoxycarbonyl-2,2':6',2''-terpyridine (47 mg, 0.153) in acetonitrile (10 mL) was refluxed for 72 h. The solvent was evaporated under vacuum, and the dark brown residue was dissolved in 10 mL of CH₂Cl₂ and filtered through Al₂O₃ using a 10:0.5 CH₂Cl₂/NCMe mixture as eluent. The purple fraction was collected and evaporated to dryness under vacuum. Crystallization from CH₂Cl₂/pentane gave dark red crystals, which were washed with diethyl ether and dried under vacuum (74 mg, 55%).

Anal. calcd. for C₃₃H₃₁F₆N₆POs:

C, 45.10; H, 3.56; N, 9.56. Found: C, 45.08; H, 3.65; N, 9.34

MS (ES, m/z): Calcd. for C₃₃H₃₁N₆¹⁹²Os: 735.2123 (M); Found: 735.211

IR (cm⁻¹): 2260 (weak, νN≡C), 1702 (medium, νC=O), 838 (strong, νPF), 555 (medium, νPF)

¹H NMR (300 MHz, CD₃CN, 300K): 8.81 (s, 2H, H_e), 8.47 (d, 2H, ³J_{HH}=8.1, H_a), 7.99 (d, 2H, ³J_{HH}=5.1, H_d), 7.88 (d, 1H, ³J_{HH}=8.8, H₁₂), 7.74 (dd, 2H, ³J_{HH}=8.1, ³J_{HH}=5.1, H_b), 7.57 (d, 1H, ³J_{HH}=7.9, H₉), 7.38 (m, 1H, H₅), 7.29 (dd, 2H, ³J_{HH}=5.1, ³J_{HH}=8.1, H_c), 7.10 (dd, 1H, ³J_{HH}=8.8, ³J_{HH}=7.9, H₁₁), 6.45 (m, 1H, H₇), 6.30 (d, 1H, ³J_{HH}=5.3, H₈), 7.10 (dd, 1H, ³J_{HH}=7.9, ³J_{HH}=8.8, H₁₀), 4.55 (q, 2H, ³J_{HH}=7.1, OCH₂), 3.17 (s, 6H, NMe₂), 2.11 (s, 3H, NCMe), 1.52 (t, 3H, ³J_{HH}=7.1, OCH₂CH₃)

¹³C {¹H} NMR (78 MHz, CD₃CN, 300K): 163.2, 159.5, 158.0, 149.7, 137.3, 136.3, 132.3, 130.2, 125.1, 122.2, 119.7, 63.4, 41.0, 15.1, 4.2

[Os(C₆H₄-oxazoline-κC,N)(η⁶-C₆H₆)(NCMe)]PF₆ (ODC 32)

To a suspension of [OsCl(μ-Cl)(*p*-cym)]₂ (900 mg, 1.32 mmol), NaOH (105 mg, 2.64 mmol) and KPF₆ (974 mg, 5.29 mmol) in 120 mL of acetonitrile was added 2-phenyl-2-oxazoline (389 mg, 2.6 mmol). The mixture was stirred at 40 °C for 48 h. The solvent was evaporated under vacuum, and the dark residue was dissolved in 20 mL of CH₂Cl₂. The solution was filtered through Al₂O₃, using a 10:1 CH₂Cl₂/NCMe mixture as eluent. The bright yellow fraction was collected and concentrated to about 5 mL. Addition of 50 mL of diethyl ether caused precipitation of a yellow brown solid (1144 mg, 72%).

Anal. calcd. for C₁₇H₁₇F₆N₂OPOs:

C, 34.00; H, 2.85; N, 4.66. Found: C, 34.24; H, 2.88; N, 4.82

MS (ES, m/z): Calcd. for C₁₇H₁₇N₂O¹⁹²Os: 457.0956 (M); Found: 457.094

IR (cm⁻¹): 2258 (weak, νN≡C), 1686 (medium, νC=O), 836 (strong, νPF), 560 (medium, νPF)

¹H NMR (300 MHz, CD₃CN, 300K): 8.05 (d, 1H, ³J_{HH}=7.5, H₅), 7.42 (d, 1H, ³J_{HH}=7.5, H₈), 7.22 (dd, 1H, ³J_{HH}=7.5, H₈ ou H₇), 7.09 (dd, 1H, ³J_{HH}=7.5, H₈ ou H₇), 5.71 (s, 6H, C₆H₆), 4.83-4.91 (m, 2H, H₁₀ ou H₁₁), 4.83-4.91 (m, 2H, H₁₀ ou H₁₁), 4.12-4.22 (m, 1H, H₁₀ ou H₁₁), 3.93-4.03 (m, 1H, H₁₀ ou H₁₁)

¹³C {¹H} NMR (78 MHz, CD₃CN, 300K): 187.4, 181.5, 173.8, 160.4, 141.1, 133.4, 132.6, 127.8, 124.8, 120.8, 80.0, 73.9, 56.7

[Os(C₆H₄-oxazoline-κC,N)(phen)(NCMe)₂]PF₆ (ODC 33)

A solution of [Os(C₆H₄-oxazoline-κC,N)(η⁶-C₆H₆)(NCMe)]PF₆ (80 mg, 0.133 mmol) with 1,10-phenanthroline (26.5 mg, 0.133) in acetonitrile (10 mL) was refluxed for 72 h. The solvent was evaporated under vacuum, and the dark brown residue was dissolved in 10 mL of CH₂Cl₂ and filtered through Al₂O₃ using a 10:1 CH₂Cl₂/NCMe mixture as eluent. The purple fraction was collected and evaporated to dryness under vacuum. Crystallization from CH₂Cl₂/pentane gave dark red crystals, which were washed with diethyl ether and dried under vacuum (63 mg, 64%).

Anal. calcd. for C₂₅H₂₂F₆N₅OPOs:

C, 40.38; H, 2.98; N, 9.42. Found: C, 40.48; H, 3.20; N, 9.35

MS (ES, m/z): Calcd. for C₂₅H₂₂N₅O¹⁹²Os: 600.1439 (M); Found: 600.144

IR (cm⁻¹): 2258 (weak, νN≡C), 840 (strong, νPF), 560 (medium, νPF)

¹H NMR (300 MHz, CD₃CN, 300K): 9.50 (d, 1H, ³J_{HH}=5.1, H_o), 8.39 (dd, 1H, ³J_{HH}=8.1, ⁴J_{HH}=1.1, H_p), 8.25 (d, 1H, ³J_{HH}=5.1, H_o), 8.11 (d, 1H, ³J_{HH}=8.8, H_{phen}), 8.04 (d, 1H, ³J_{HH}=8.8, H_{phen}), 8.03 (dd, 1H, ³J_{HH}=8.1, ⁴J_{HH}=1.1, H_p), 7.96 (dd, 2H, ³J_{HH}=8.1, ³J_{HH}=5.1, 2 x H_m), 7.37-7.42 (m, 2H, H₅ + H₈), 7.24 (dd, 1H, ³J_{HH}=7.5, H₆), 7.24 (dd, 1H, ³J_{HH}=7.5, H₆), 6.89 (dd, 1H, ³J_{HH}=7.5, H₇), 4.49-4.58 (m, 1H, H₁₀ ou H₁₁), 4.18-4.28 (m, 1H, H₁₀ ou H₁₁), 4.12-4.23 (m, 1H, H₁₀ ou H₁₁), 2.82 (s, 1H, NCMe), 2.38 (s, 1H, NCMe), 2.22-2.38 (m, 1H, H₁₀ ou H₁₁)

¹³C {¹H} NMR (78 MHz, CD₃CN, 300K): 183.5, 157.7, 154.6, 151.5, 150.8, 138.3, 135.7, 134.5, 132.1, 131.7, 131.5, 128.8, 128.7, 127.4, 127.0, 126.3, 71.8, 51.3, 5.0, 4.4

[Os(C₆H₄-oxazoline-κC,N)(phen)₂]PF₆ (ODC 34)

A solution of [Os(C₆H₄-oxazoline-κC,N)(η⁶-C₆H₆)(NCMe)]PF₆ (80 mg, 0.133 mmol) with 1,10-phenanthroline (54 mg, 0.268) in methanol (10 mL) was refluxed for 72 h. The solvent was evaporated under vacuum, and the dark brown residue was dissolved in 10 mL of CH₂Cl₂ and filtered through Al₂O₃ using a 10:1 CH₂Cl₂/NCMe mixture as eluent. The purple fraction was collected and evaporated to dryness under vacuum. Crystallization from CH₂Cl₂/pentane gave dark red crystals, which were washed with diethyl ether and dried under vacuum (94 mg, 84%).

Anal. calcd. for C₃₃H₂₄F₆N₅OPOs:

C, 47.09; H, 2.87; N, 8.32. Found: C, 47.33; H, 3.13; N, 8.08

MS (ES, m/z): Calcd. for C₃₃H₂₄N₅O¹⁹²Os: 698.1596 (M); Found: 698.160

IR (cm⁻¹): 836 (strong, νPF), 560 (medium, νPF)

¹H NMR (300 MHz, CD₃CN, 300K): 9.50 (d, 1H, ³J_{HH}=5.5, H_o), 8.47 (d, 1H, ³J_{HH}=5.5, H_o), 8.18 (d, 1H, ³J_{HH}=8.1, H_p), 8.01-8.16 (m, 7H, H_o + 2 x H_p + 4 x H_{phen}), 7.99 (d, 1H, ³J_{HH}=5.5, H_o), 7.95 (d, 1H, ³J_{HH}=8.1, H_p), 7.70 (dd, 1H, ³J_{HH}=8.1, ³J_{HH}=5.5, H_m), 7.64 (dd, 1H, ³J_{HH}=8.1, ³J_{HH}=5.5, H_m), 7.41 (dd, 1H, ³J_{HH}=8.1, ³J_{HH}=5.5, H_m), 7.35 (dd, 1H, ³J_{HH}=6.8, ⁴J_{HH}=2.2, H₅), 7.22 (dd, 1H, ³J_{HH}=8.1, ³J_{HH}=5.5, H_m), 6.63-6.71 (m, 2H, H₇ + H₆), 6.03 (dd, 1H, ³J_{HH}=6.8, ⁴J_{HH}=2.2, H₈), 4.81-4.90 (m, 1H, H₁₀ ou H₁₁), 4.44-4.53 (m, 1H, H₁₀ ou H₁₁), 3.59-3.69 (m, 1H, H₁₀ ou H₁₁), 2.49-2.59 (m, 1H, H₁₀ ou H₁₁)

¹³C {¹H} NMR (78 MHz, CD₃CN, 300K): 182.3, 146.9, 154.3, 153.8, 153.1, 152.5, 152.3, 151.5, 151.4, 150.8, 150.7, 136.0, 135.8, 134.9, 134.3, 133.6, 132.9, 132.5, 132.2, 132.1, 132.0, 131.9, 129.2, 129.1, 129.0, 129.9, 127.9, 127.3, 127.2, 127.1, 126.8, 121.8, 72.4

[Os(C₆H₄-oxazoline-κC,N)(4'-ethoxycarbonyl-2,2':6',2''-terpy)(NCMe)]PF₆ (ODC 35)

A solution of [Os(C₆H₄-oxazoline-κC,N)(η⁶-C₆H₆)(NCMe)]PF₆ (80 mg, 0.133 mmol) with 4'-ethoxycarbonyl-2,2':6',2''-terpyridine (41 mg, 0.133) in acetonitrile (10 mL) was refluxed for 72 h. The solvent was evaporated under vacuum, and the dark brown residue was dissolved in 10 mL of CH₂Cl₂ and filtered through Al₂O₃ using a 10:1 CH₂Cl₂/NCMe mixture as eluent. The purple fraction was collected and evaporated to dryness under vacuum. Crystallization from CH₂Cl₂/pentane gave dark red crystals, which were washed with diethyl ether and dried under vacuum (66 mg, 60%).

Anal. calcd. for $C_{29}H_{26}F_6N_5O_3PO_3$:

C, 42.08; H, 3.17; N, 8.46. Found: C, 42.24; H, 3.21; N, 8.54

MS (ES, m/z): Calcd. for $C_{29}H_{26}N_5O_3^{192}Os$: 684.1650 (M); Found: 684.164

IR (cm⁻¹): 2250 (weak, $\nu N\equiv C$), 1685 (medium, $\nu C=O$), 836 (strong, νPF_6), 560 (medium, νPF_6)

¹H NMR (300 MHz, CD₃CN, 300K): 8.75 (s, 2H, H₉), 8.44 (d, 2H, $^3J_{HH}=8.2$, H_a), 8.17 (d, 1H, $^3J_{HH}=7.5$, H₅), 7.97 (d, 2H, $^3J_{HH}=5.9$, H_d), 7.76 (dd, 2H, $^3J_{HH}=8.2$, $^3J_{HH}=5.9$, H_b), 7.52 (d, 1H, $^3J_{HH}=7.7$, H₈), 7.44 (dd, 1H, $^3J_{HH}=7.5$, $^3J_{HH}=7.7$, H₆), 7.35 (dd, 2H, $^3J_{HH}=8.2$, $^3J_{HH}=5.9$, H_c), 6.89 (dd, 1H, $^3J_{HH}=7.5$, $^3J_{HH}=7.7$, H₇), 4.52 (q, 2H, $^3J_{HH}=7.1$, OCH₂), 4.21 (t, 2H, $^3J_{HH}=9.3$, H₁₀ ou H₁₁), 2.17 (t, 2H, $^3J_{HH}=9.3$, H₁₀ ou H₁₁), 2.11 (s, 3H, NCMe), 1.50 (t, 3H, $^3J_{HH}=7.1$, OCH₂CH₃)

¹³C {¹H} NMR (78 MHz, CD₃CN, 300K): 182.8, 181.7, 165.5, 163.3, 159.2, 158.4, 137.1, 136.6, 132.7, 131.7, 130.5, 130.1, 127.7, 124.4, 121.9, 121.7, 71.7, 63.3, 48.4, 15.0, 4.2

[Os(C₆H₄-imidazole- κ C,N)(η^6 -C₆H₆)(NCMe)]PF₆ (ODC 36)

To a suspension of [OsCl(μ -Cl)(*p*-cym)]₂ (900 mg, 1.32 mmol), NaOH (105 mg, 2.64 mmol) and KPF₆ (974 mg, 5.29 mmol) in 120 mL of acetonitrile was added 2-phenylimidazole (382 mg, 2.6 mmol). The mixture was stirred at 40 °C for 48 h. The solvent was evaporated under vacuum, and the dark residue was dissolved in 20 mL of CH₂Cl₂. The solution was filtered through Al₂O₃, using a 10:1 CH₂Cl₂/NCMe mixture as eluent. The bright yellow fraction was collected and concentrated to about 5 mL. Addition of 50 mL of diethyl ether caused precipitation of a yellow brown solid (640 mg, 45%).

Anal. calcd. for $C_{17}H_{16}F_6N_3PO_3$:

C, 34.17; H, 2.70; N, 7.03. Found: C, 34.12; H, 2.71; N, 7.05

MS (ES, m/z): Calcd. for $C_{17}H_{16}N_3^{192}Os$: 454.0959 (M); Found: 454.098

IR (cm⁻¹): 2258 (weak, $\nu N\equiv C$), 835 (strong, νPF_6), 565 (strong, νPF_6)

¹H NMR (300 MHz, CD₃CN, 300K): 8.03-8.05 (m, 1H, H₅), 7.52-7.55 (m, 1H, H₈), 7.36 (d, 1H, $^3J_{HH}=1.7$, H₁₀ ou H₁₁), 7.15 (d, 1H, $^3J_{HH}=1.7$, H₁₀ ou H₁₁), 7.08-7.11 (m, 2H, H₆ + H₇), 5.70 (s, 6H, C₆H₆), 2.18 (m, 1H, NH), 1.96 (s, 3H, NCMe)

¹³C {¹H} NMR (78 MHz, CD₃CN, 300K): 159.9, 156.1, 141.3, 136.8, 131.7, 130.4, 125.0, 123.1, 119.0, 79.9

[Os(C₆H₄-imidazoline- κ C,N)(η^6 -C₆H₆)(NCMe)]PF₆ (ODC 37)

To a suspension of [OsCl(μ -Cl)(*p*-cym)]₂ (900 mg, 1.32 mmol), NaOH (105 mg, 2.64 mmol) and KPF₆ (974 mg, 5.29 mmol) in 120 mL of acetonitrile was added 2-phenyl-2-imidazoline (387 mg, 2.6 mmol). The mixture was stirred at 40 °C for 48 h. The solvent was evaporated under vacuum, and the dark residue was dissolved in 20 mL of CH₂Cl₂. The solution was filtered through Al₂O₃, using a 10:1 CH₂Cl₂/NCMe mixture as eluent. The bright yellow fraction was collected and concentrated to about 5 mL. Addition of 50 mL of diethyl ether caused precipitation of a yellow brown solid (1031 mg, 65%).

Anal. calcd. for $C_{17}H_{18}F_6N_3PO_3$:

C, 34.06; H, 3.03; N, 7.01. Found: C, 34.16; H, 3.02; N, 7.07

MS (ES, m/z): Calcd. for $C_{17}H_{18}N_3^{192}Os$: 456.1116 (M); Found: 456.109

IR (cm⁻¹): 2259 (weak, $\nu N\equiv C$), 838 (strong, νPF_6), 565 (strong, νPF_6)

¹H NMR (300 MHz, CD₃CN, 300K): 8.02 (d, 1H, $^3J_{HH}=7.3$, H₅), 7.35 (d, 1H, $^3J_{HH}=7.3$, H₈), 7.16 (dd, 1H, $^3J_{HH}=7.3$, H₆), 7.06 (dd, 1H, $^3J_{HH}=7.3$, H₇), 6.45 (m, 1H, NH), 5.63 (s, 6H, C₆H₆), 3.79-4.12 (m, 4H, H₁₀ + H₁₁), 1.96 (s, 3H, NCMe)

¹³C {¹H} NMR (78 MHz, CD₃CN, 300K): 178.6, 161.0, 141.1, 136.6, 132.3, 126.5, 124.5, 79.6, 57.7, 47.1, 2.1

[Os(*o*-C₆H₄py- κ C,N)(η^6 -C₆H₆)(Cl)] (ODC 38)

The [Os(*o*-C₆H₄py- κ C,N)(phen)₂](PF₆)₂ was synthesised according to reference 25. A new method was also developed:

A mixture of [OsCl(μ -Cl)(η^6 -C₆H₆)]₂ (200 mg, 294 mmol), 2-phenylpyridine (100.3 mg, 646 mmol) and sodium acetate (60 mg, 740 mmol) in 10 mL of CH₂Cl₂ was refluxed for 6h. The

solution was filtered through Celite and rotary evaporated to dryness. The product was crystallized from CH₂Cl₂/pentane to give yellow crystals (190 mg, 70%) which were washed with ether and dried under vacuum.

Anal. calcd. for C₁₇H₁₄CINO:

C, 44.58; H, 3.08; N, 3.06. Found: C, 44.46; H, 3.07; N, 3.13

MS (ES, m/z): Calcd. for C₁₇H₁₄CIN¹⁹²Os: 459.0430 (M); Found: 459.040

¹H NMR (300 MHz, CDCl₃, 300K): 9.20 (d, 1H, ³J_{HH}=5.2, H₁₂), 8.10 (d, 1H, ³J_{HH}=7.4, H₅), 7.79 (d, 1H, ³J_{HH}=8.1, H₉), 7.61-7.70 (m, 2H, H₈ + H₁₀), 7.14 (dd, 1H, ³J_{HH}=8.1, H₆), 6.98-7.06 (m, 2H, H₇ + H₁₁), 5.54 (s, 6H, C₆H₆)

¹³C {¹H} NMR (78 MHz, CD₃CN, 300K): 166.9, 165.7, 155.3, 144.4, 139.2, 137.3, 130.7, 124.4, 123.1, 122.5, 119.2, 77.6

[Os(*o*-C₆H₄py- κ C,N)(η^6 -C₆H₆)(DMSO)] PF₆ (ODC 39)

To a suspension of [Os(*o*-C₆H₄py- κ C,N)(η^6 -C₆H₆)(Cl)] (100 mg, 0.22 mmol), AgPF₆ (56 mg, 0.22 mmol) in 5 mL of dichloromethane was added dimethyl sulfoxide (20 μ L, 0.22 mmol). The mixture was stirred at RT for 15 min and then filtered over celite. The light yellow fraction was collected and concentrated to about 5 mL. Addition of 50 mL of pentane causes precipitation of a beige solid (128 mg, 90%) which was washed with ether and dried under vacuum.

Anal. calcd. for C₁₉H₂₀F₆NOPSO:

C, 35.35; H, 3.12; N, 2.17. Found: C, 35.30; H, 3.01; N, 2.12

MS (ES, m/z): Calcd. for C₁₉H₂₀NOS¹⁹²Os: 502.0880 (M); Found: 502.089

IR (cm⁻¹): 838 (strong, ν PF), 562 (strong, ν PF)

¹H NMR (300 MHz, DMSO, 300K): 9.30 (d, 1H, ³J_{HH}=5.4, H₁₂), 8.10 (d, 1H, ³J_{HH}=7.4, H₅), 7.92-8.04 (m, 3H, H₈ + H₉ + H₁₀), 7.29 (dd, 1H, ³J_{HH}=7.9, H₆), 7.14-7.20 (m, 2H, H₇ + H₁₁), 6.14 (s, 6H, C₆H₆), 3.37 (s, 3H, CH₃_{DMSO}), 2.80 (s, 3H, CH₃_{DMSO})

¹³C {¹H} NMR (78 MHz, DMSO, 300K): 167.0, 156.9, 154.4, 145.9, 140.2, 139.3, 130.3, 125.0, 123.8, 123.5, 120.1, 50.5, 45.9

5.3. References Chapter 5

- ¹ Zelonka, R. A.; Baird, M. C. *Can. J. Chem.* **1972**, *50*, 3063–72.
- ² Bennett, M. A.; Smith, A. K. *J. Chem. Soc., Dalton Trans.* **1974**, 233–241.
- ³ Peacock, A. F.; Habtemariam, A.; Fernandez, R.; Walland, V.; Fabbiani, F.B.A.; Parsons, S.; Aird, R.E.; Jodrell, I.; Sadler, P.J. *J. Am. Chem. Soc.* **2006**, *128*, 1739–1748.
- ⁴ Werner, H.; Zenkert, K. *J. Organomet. Chem.* **1988**, *345*, 151–166.
- ⁵ Gosmini, C.; Bassene-Ernst, C.; Durandetti, M. *Tetrahedron*, **2009**, *65*, 6141–6146.
- Gosmini, C.; Lasry, S.; Nedelec, J.-Y.; Perichonn, J. *Tetrahedron*, **1998**, *54*, 1289–1298.
- ⁶ Streef, J.W.; Den Hertog, H.J. *Tetrahedron Lett.*, **1968**, *57*, 5945–5948.
- ⁷ Sindkhedkar, M.D.; Mulla, H.R.; Wurth, M.A.; Cammers-Goodwin A. *Tetrahedron* **2001**, *57*, 2991–2996.
- ⁸ Jouaiti, A.; Geoffroy, M.; Collin, J.P. *Inorg. Chim. Acta* **1996**, *245*, 69–73.
- ⁹ Sengupta, S.; Sadhukan, S.K.; Singh R.S.; Pal N. *Tetrahedron Lett.* **2002**, *43*, 1117–1121.
- ¹⁰ Neve, F.; Crispini, A.; Di Pietro, C.; Campagna, S. *Organometallics* **2002**, *21*, 3511–3518.
- ¹¹ Williams, J.A.G.; Beeby, A.; Davies, S.; Weinstein, J.; Wilson, C. *Inorg. Chem.* **2003**, *42*, 8609–8611.
- ¹² Kröhnke, F. *Synthesis* **1976**, *1*, 1–24.
- ¹³ Constable, E. C.; Henney, R.; Leese, T. A.; *J. Chem. Soc. Dalton Trans.* **1990**, *2*, 443–449.
- ¹⁴ Lu, W.; Chan, M.C.W.; Zhu, N.; Che, C.-M.; Li, C.; Hui, Z. *J. Am. Chem. Soc.* **2004**, *126*, 7639–7651.
- ¹⁵ a) Wadman, S.H.; Lutz, M.; Tooke, S. M.; Spek, A. L.; Hartl, F.; Havenith, R. W. A.; van Klink, G.; van Koten, G. *Inorg. Chem.* **2009**, *48*, 1887–1900.
b) Wadman, S.H.; Lutz, M.; Tooke, S. M.; Spek, A. L.; Hartl, F.; Havenith, R. W. A.; van Klink, G.; van Koten, G. *Inorg. Chem.* **2009**, *48*, 5685–5696.
c) Wadman, S.H.; Kroon, J.M.; Bakker, K.; Havenith R. W. A.; van Klink G.; van Koten G. *Organometallics* **2010**, *29*, 1569–1579.
- ¹⁶ Fallahpour, R.A. *Synthesis* **2000**, *8*, 1138–1142.
- ¹⁷ Amb, C.M.; Rasmussen, S.C. *J. Org. Chem.* **2006**, *71*, 4696–4699.
- ¹⁸ Nazeeruddin, M.K.; Péchy, P.; Renouard, T.; Zakeeruddin, S.M.; Humphry-Baker, R.; Comte, P.; Liska, P.; Cevey, L.; Costa, E.; Shklover, V.; Spiccia, L.; Deacon, G.B.; Bignozzi, C.A.; Grätzel, M. *J. Am. Chem. Soc.* **2001**, *123*, 1613–1624.
- ¹⁹ Bhaumik, C.; Das, S.; Saha, D.; Dutta, S.; Baitalik, S. *Inorg. Chem.* **2010**, *49*, 4049–4062.
- ²⁰ Ryabov, A. D.; Sukharev, V. S.; Alexandrova, L.; Le Lagadec, R.; Pfeffer, M. *Inorg. Chem.* **2001**, *40*, 6529–6532.
- ²¹ Fetzer, L.; Boff, B.; Ali, M.; Xiangjun, M.; Collin, J.-P.; Sirlin, C.; Gaiddon, C.; Pfeffer, M. *J. Chem. Soc., Dalton Trans.* **2011**, *40*, 8869–8878.
- ²² Beley, M.; Collin, J.P.; Sauvage, J.P. *Inorg. Chem.* **1993**, *32*, 4539–4543.
- ²³ Sullivan, B. P.; Calvert, J. M.; Meyer, T. J. *Inorg. Chem.* **1980**, *19*, 1404–1407.
- ²⁴ Boutadla, Y.; Al-Duaij, O.; Davies, D.L.; Griffith, G.A.; Singh, K. *Organometallics* **2009**, *28*, 433–440.
- ²⁵ Ceron-Camacho, R.; Morales-Morales, D.; Hernandez, S.; Le Lagadec, R.; Ryabov, A.D. *Inorg. Chem.* **2008**, *47*, 4988–4995.
- ²⁶ Minick, D.J.; Frenz, J.H.; Patrick, M.A.; Brent, D.A. *J. Med. Chem.* **1988**, *31*, 1923–1933.
- ²⁷ Pomper, M.J.; Vanbrocklin, H.; Thieme, A.M.; Thomas, R.D.; Katzenellengogen, J.A. *J. Med. Chem. Soc.* **1990**, *33*, 3143–31550.
- ²⁸ D'ambroise, M.; Hanai, T. *J. Liq. Chromatograph.* **1982**, *5*, 229–244.

Appendix



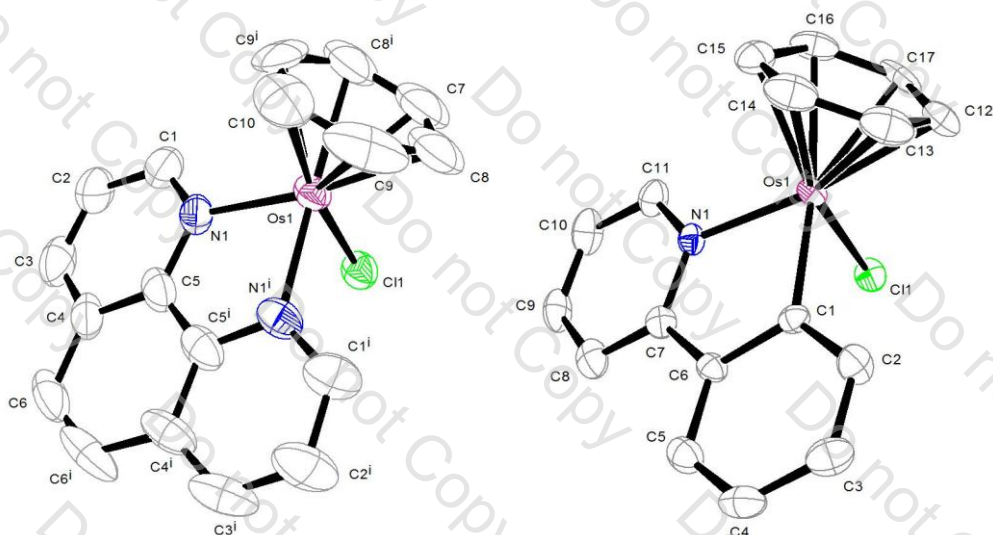


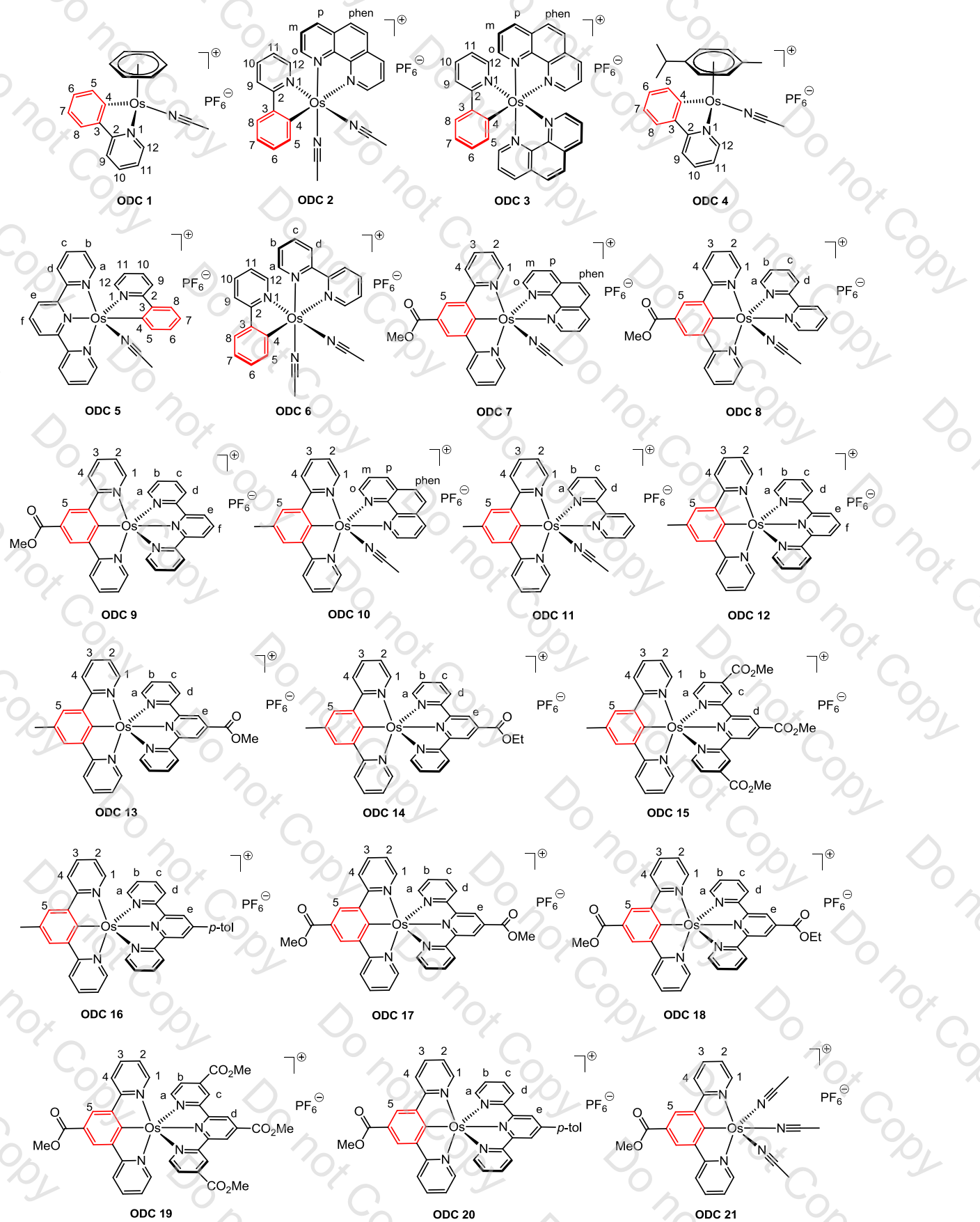
Figure 1: ORTEP diagram of the molecular structure of ODC 25 (left) and ODC 38 (right). Ellipsoids are drawn at a probability level of 50%. Hydrogen atoms, counter anions and solvent have been omitted for clarity.

Compound reference	ODC 25	ODC 38
Chemical formula	C ₁₈ H ₁₄ ClN ₂ Os•F ₆ P	C ₁₇ H ₁₄ ClNOs
Formula Mass	628.93	457.94
Crystal system	Orthorhombic	Triclinic
<i>a</i> /Å	11.5853(6)	10.2487(4)
<i>b</i> /Å	11.2542(6)	12.0186(4)
<i>c</i> /Å	14.6348(5)	12.5330(3)
α /°	90.00	70.610(2)
β /°	90.00	77.258(2)
γ /°	90.00	75.119(2)
Unit cell volume/Å ³	1908.13(16)	1391.77(8)
Temperature/K	193(2)	173(2)
Space group	<i>Cmc</i> 2 ₁	<i>P</i> -1
No. of formula units per unit cell, <i>Z</i>	4	4
No. of reflections measured	6703	12900
No. of independent reflections	2241	6353
<i>R</i> _{int}	0.0506	0.0709
Final <i>R</i> _{<i>i</i>} values (<i>I</i> > 2σ(<i>I</i>))	0.0614	0.0470
Final <i>wR</i> (<i>F</i> ²) values (<i>I</i> > 2σ(<i>I</i>))	0.1645	0.1269
Final <i>R</i> _{<i>i</i>} values (all data)	0.0665	0.0512
Final <i>wR</i> (<i>F</i> ²) values (all data)	0.1701	0.1353

Table 1: Details for the X-ray crystal structure determination of ODC 25 and ODC 38

ODC 25	ODC 38		
C7 – Os1	2.17(3)	C1 – Os1	2.077(6)
C8 – Os1	2.17(2)	C12 – Os1	2.202(8)
C8 ⁱ – Os1	2.17(2)	C13 – Os1	2.180(8)
C9 – Os1	2.172(17)	C14 – Os1	2.185(9)
C9 ⁱ – Os1	2.172(17)	C15 – Os1	2.162(8)
C10 – Os1	2.14(2)	C16 – Os1	2.271(7)
C11 – Os1	2.380(4)	C17 – Os1	2.245(7)
N1 – Os1	2.092(13)	N1 – Os1	2.104(6)
N1 ⁱ – Os1	2.092(13)	Cl1 – Os1	2.4315(17)
N1 – Os1 – N1 ⁱ	78.1(8)	C1 – Os1 – N1	77.5(2)
N1 ⁱ – Os1 – Cl1	82.1(4)	C1 – Os1 – Cl1	87.64(19)
Cl1 – Os1 – N1	82.1(4)	N1 – Os1 – Cl1	82.04(16)
Os1 – N1 – C5	114.8(11)	Os1 – C1 – C6	115.5(5)
N1 – C5 – C5 ⁱ	116.2(9)	C1 – C6 – C7	115.2(6)
C5 – C5 ⁱ – N1 ⁱ	116.2(9)	C6 – C7 – N1	113.8(6)
C5 ⁱ – N1 ⁱ – Os1	114.8(11)	C7 – N1 – Os1	117.6(5)

Table 2: Selected bond length (Å), angles (°) for ODC 25 and ODC 38

**Figure 2: Overall view of 1st and 2nd generation ODC complexes**

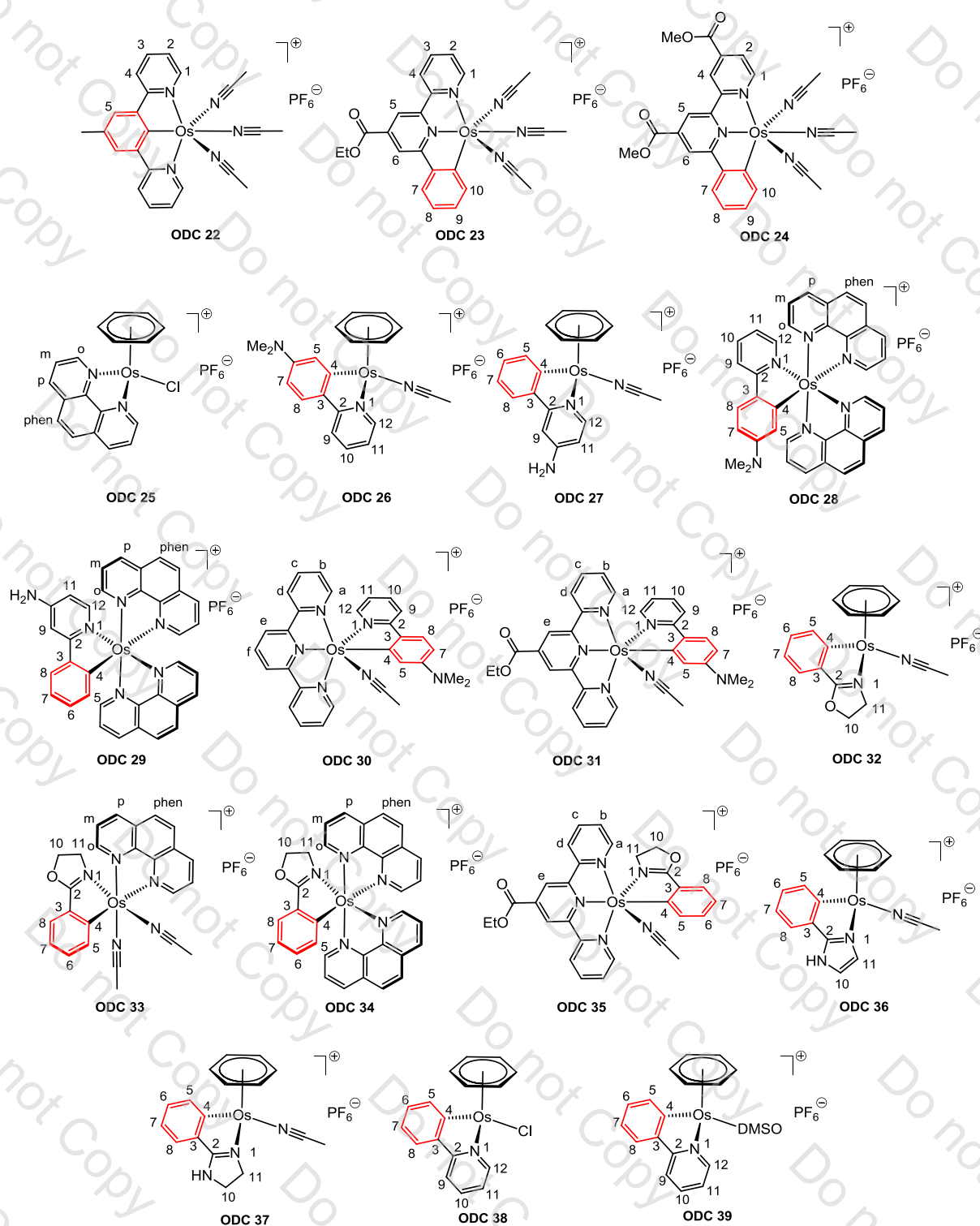


Figure 3: Overall view of 1st and 2nd generation ODC complexes (continued)

Summary of chemical properties for new ruthenium and osmium complexes:

Ru compounds	Formula	MW (g/mol)	MS (ES, m/z)	MS found (ES, m/z)	Elem. Anal.			Elem. Anal. found		
					C (%)	H (%)	N (%)	C (%)	H (%)	N (%)
RDC 55	C ₃₂ H ₂₄ F ₆ N ₅ O ₂ PRu	756.6000	612.0974	612.095	50.80	3.20	9.26	50.55	3.25	9.26
RDC 56	C ₃₁ H ₂₄ F ₆ N ₅ PRu	712.5905	568.1075	568.107	52.25	3.39	9.83	52.18	3.35	9.78
RDC 49-Cl	C ₂₁ H ₂₂ ClNRu	424.9291	425.0484	425.048	59.36	5.22	3.30	59.24	5.27	3.41
RDC 49-DMSO	C ₂₃ H ₂₈ F ₆ NOPSRu	612.5742	467.6095	467.609	45.10	4.61	2.29	45.28	4.68	2.31

Table 3: Chemical data for new RDC complexes

Os compounds	Formula	MW (g/mol)	MS (ES, m/z)	MS found (ES, m/z)	Elem. Anal.			Elem. Anal. found		
					C (%)	H (%)	N (%)	C (%)	H (%)	N (%)
ODC 1	C ₁₉ H ₁₇ F ₆ N ₂ POs	608.5459	465.1007	465.101	35.98	2.79	4.30	36.15	2.85	4.38
ODC 2	C ₂₇ H ₂₂ F ₆ N ₅ POs	751.6913	608.1490	608.149	41.59	2.92	8.82	41.69	2.91	8.64
ODC 3	C ₃₅ H ₂₄ F ₆ N ₅ POs	849.7927	706.1647	706.165	46.26	2.80	7.49	46.36	3.22	7.69
ODC 4	C ₂₃ H ₂₅ F ₆ N ₂ POs	664.6522	521.1633	521.164	41.56	3.79	4.21	41.64	8.85	4.21
ODC 5	C ₂₈ H ₂₂ F ₆ N ₅ POs	763.7020	620.1490	620.154	44.04	2.90	9.17	43.81	2.89	8.97
ODC 6	C ₂₅ H ₂₂ F ₆ N ₅ POs	727.6699	584.1490	584.158	41.26	3.05	9.62	41.05	2.95	9.52
ODC 7	C ₃₂ H ₂₄ F ₆ N ₅ O ₂ POs	845.7594	702.1545	702.159	45.44	2.86	8.28	45.25	2.91	8.18
ODC 8	C ₃₀ H ₂₄ F ₆ N ₅ O ₂ POs	821.7380	678.1545	678.150	43.85	2.94	8.52	43.55	2.91	8.39
ODC 9	C ₃₃ H ₂₄ F ₆ N ₅ O ₂ POs	857.7701	714.1545	714.155	46.21	2.82	8.16	46.05	2.83	8.06
ODC 10	C ₃₁ H ₂₄ F ₆ N ₅ POs	801.7499	658.1647	658.165	46.44	3.01	8.74	46.25	3.02	8.65
ODC 11	C ₂₉ H ₂₄ F ₆ N ₅ POs	777.7285	634.1647	634.166	44.79	3.11	9.00	44.45	3.08	8.95
ODC 12	C ₃₂ H ₂₄ F ₆ N ₅ POs	813.7606	670.1647	670.163	47.23	2.97	8.61	46.93	2.98	8.61
ODC 13	C ₃₄ H ₂₆ F ₆ N ₅ O ₂ POs	871.7973	728.1701	728.163	46.84	3.01	8.03	46.78	3.01	8.05
ODC 14	C ₃₅ H ₂₈ F ₆ N ₅ O ₂ POs	885.8239	742.1858	742.187	47.46	3.19	7.91	47.35	3.33	7.97
ODC 15	C ₃₈ H ₃₀ F ₆ N ₅ O ₆ POs	987.8694	844.1811	844.184	46.20	3.06	7.09	46.10	3.08	7.12
ODC 16	C ₃₉ H ₃₀ F ₆ N ₅ POs	903.8837	760.2116	760.212	51.82	3.35	7.75	51.57	3.34	7.80
ODC 17	C ₃₅ H ₂₆ F ₆ N ₅ O ₄ POs	915.8062	772.1600	772.157	45.90	2.86	7.65	45.56	2.91	7.69
ODC 18	C ₃₆ H ₂₈ F ₆ N ₅ O ₄ POs	929.8328	786.1756	786.174	46.50	3.04	7.53	46.40	3.07	7.58
ODC 19	C ₃₉ H ₃₀ F ₆ N ₅ O ₈ POs	1031.8784	888.1709	888.167	45.39	2.93	6.79	45.76	3.31	6.88
ODC 20	C ₄₀ H ₃₀ F ₆ N ₅ O ₂ POs	947.8927	804.2014	804.199	50.68	3.19	7.39	50.19	3.25	7.50
ODC 21	C ₂₄ H ₂₂ F ₆ N ₅ O ₂ POs	747.6579	604.1388	604.143	38.55	2.97	9.37	38.54	3.01	9.43
ODC 22	C ₂₃ H ₂₂ F ₆ N ₅ POs	703.6485	560.1490	560.153	39.26	3.15	9.95	39.16	2.35	9.86
ODC 23	C ₂₅ H ₂₄ F ₆ N ₅ O ₂ POs	761.6845	618.1545	618.154	39.42	3.18	9.19	39.56	3.38	9.09
ODC 24	C ₂₆ H ₂₄ F ₆ N ₅ O ₄ POs	805.6940	662.1443	662.144	38.76	3.00	8.69	38.96	3.10	8.75
ODC 25	C ₁₈ H ₁₄ ClF ₆ N ₂ POs	628.9643	485.0460	485.047	34.37	2.24	4.45	34.45	2.26	4.55
ODC 26	C ₂₁ H ₂₂ F ₆ N ₃ POs	651.6137	508.1429	508.145	38.71	3.40	6.45	38.60	3.42	6.40
ODC 27	C ₁₉ H ₁₈ F ₆ N ₃ POs	623.5605	480.1116	480.110	36.60	2.91	6.74	36.32	2.87	6.69
ODC 28	C ₃₇ H ₂₉ F ₆ N ₆ POs	892.8605	749.2069	749.207	49.77	3.27	9.41	49.53	3.31	9.41
ODC 29	C ₃₅ H ₂₅ F ₆ N ₆ POs	864.8074	721.1756	721.176	48.61	2.91	9.72	48.53	3.04	10.12
ODC 30	C ₃₀ H ₂₇ F ₆ N ₆ POs	806.7698	663.1912	663.192	44.66	3.37	10.42	44.63	3.40	10.43
ODC 31	C ₃₃ H ₃₁ F ₆ N ₆ O ₂ POs	878.8324	735.2123	735.211	45.10	3.56	9.56	45.08	3.65	9.34
ODC 32	C ₁₇ H ₁₇ F ₆ N ₂ OPOs	600.5239	457.0956	457.094	34.00	2.85	4.66	34.24	2.88	4.82
ODC 33	C ₂₅ H ₂₂ F ₆ N ₅ OPOs	743.6693	600.1439	600.144	40.38	2.98	9.42	40.48	3.20	9.35
ODC 34	C ₃₃ H ₂₄ F ₆ N ₅ OPOs	841.7707	698.1596	698.160	47.09	2.87	8.32	47.33	3.13	8.08
ODC 35	C ₂₉ H ₂₆ F ₆ N ₅ O ₃ POs	827.7426	684.1650	684.164	42.08	3.17	8.46	42.24	3.21	8.54
ODC 36	C ₁₇ H ₁₄ F ₆ N ₃ POs	597.5232	454.0959	454.098	34.17	2.70	7.03	34.12	2.71	7.05
ODC 37	C ₁₇ H ₁₈ F ₆ N ₃ POs	599.5391	456.1116	456.109	34.06	3.03	7.01	34.16	3.02	7.07
ODC 38	C ₁₇ H ₁₄ ClNOs	457.9828	459.0430	459.040	44.58	3.08	3.06	44.46	3.07	3.13
ODC 39	C ₁₉ H ₂₀ F ₆ NOPSOs	645.6274	502.0880	502.089	35.35	3.12	2.17	35.30	3.01	2.12

Table 4: Chemical data for new ODC complexes

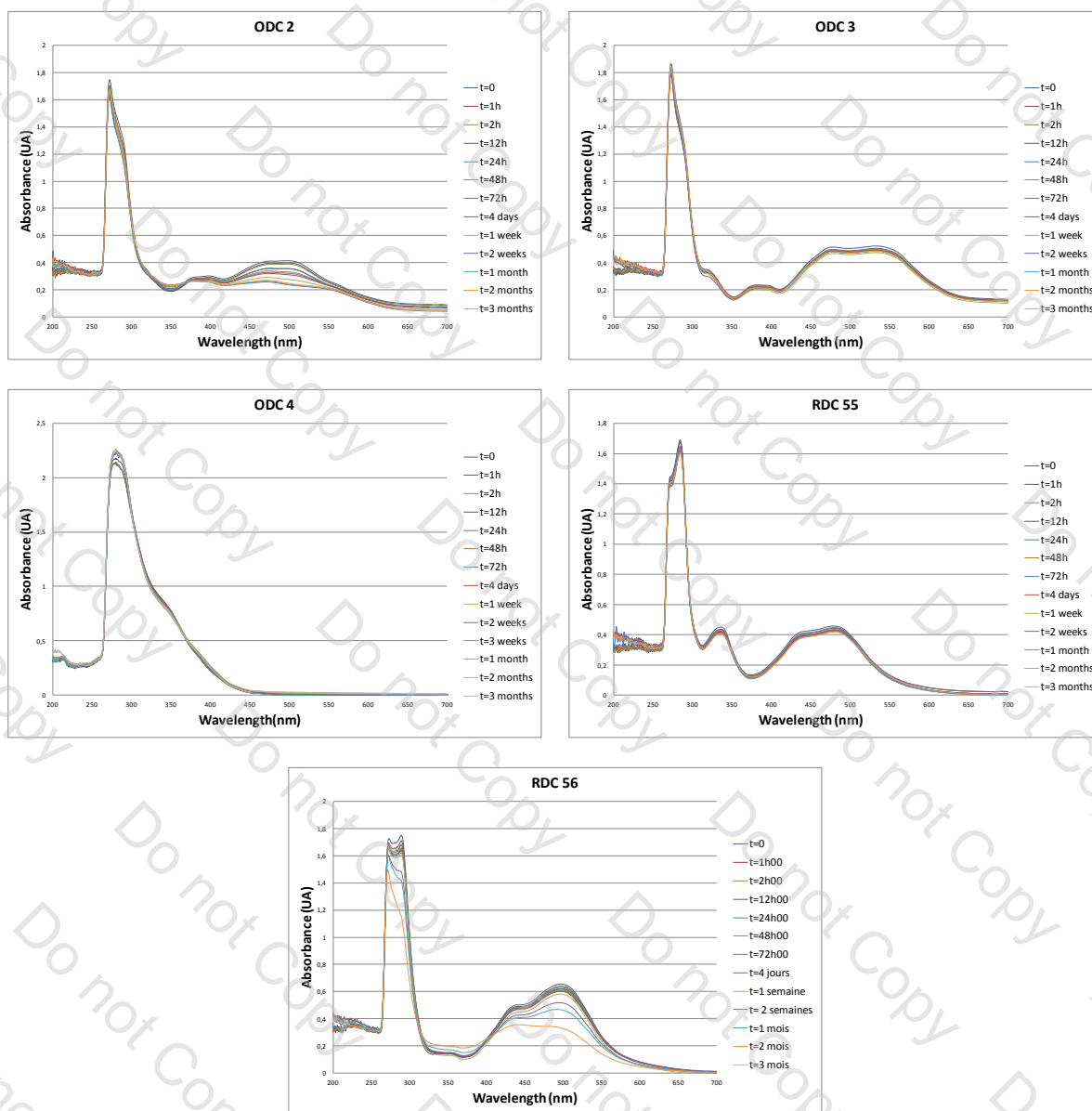


Figure 4: UV spectra of different compounds in MeCN at R.T. exposed to ambient light

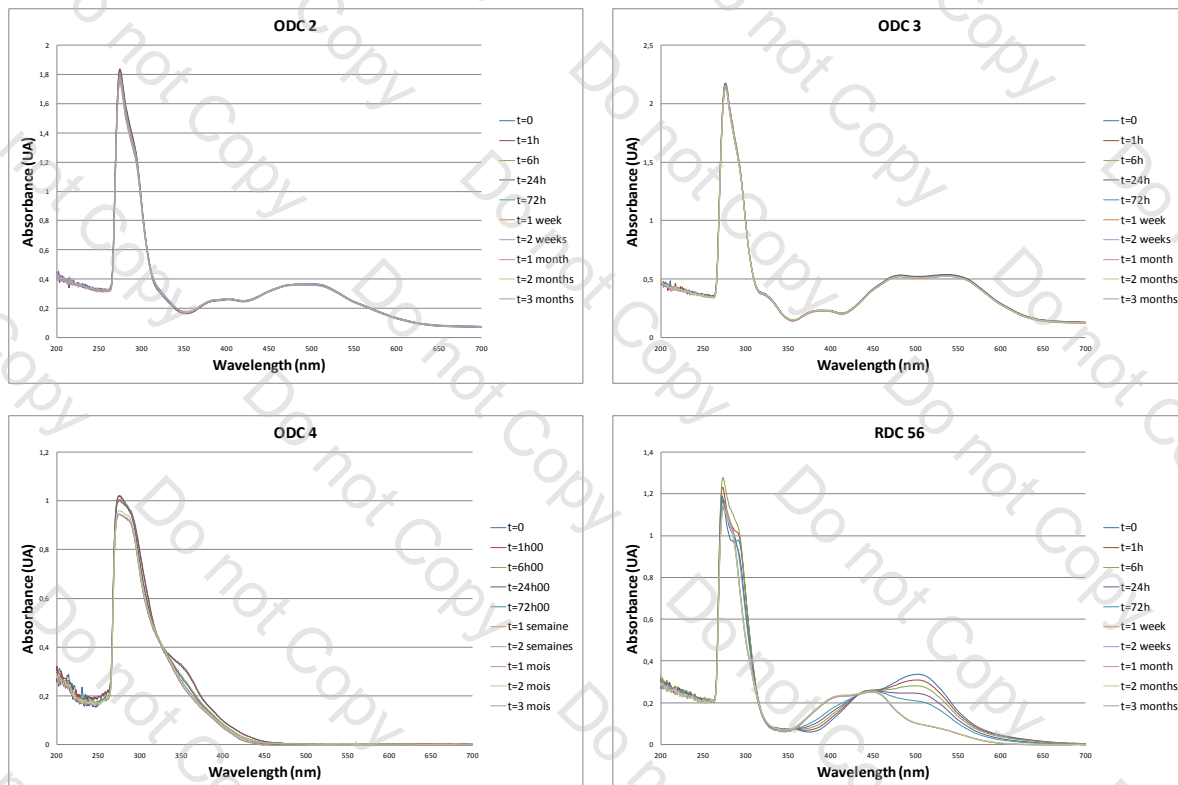


Figure 5: UV spectra of different compounds in DMSO at -15°C in the dark

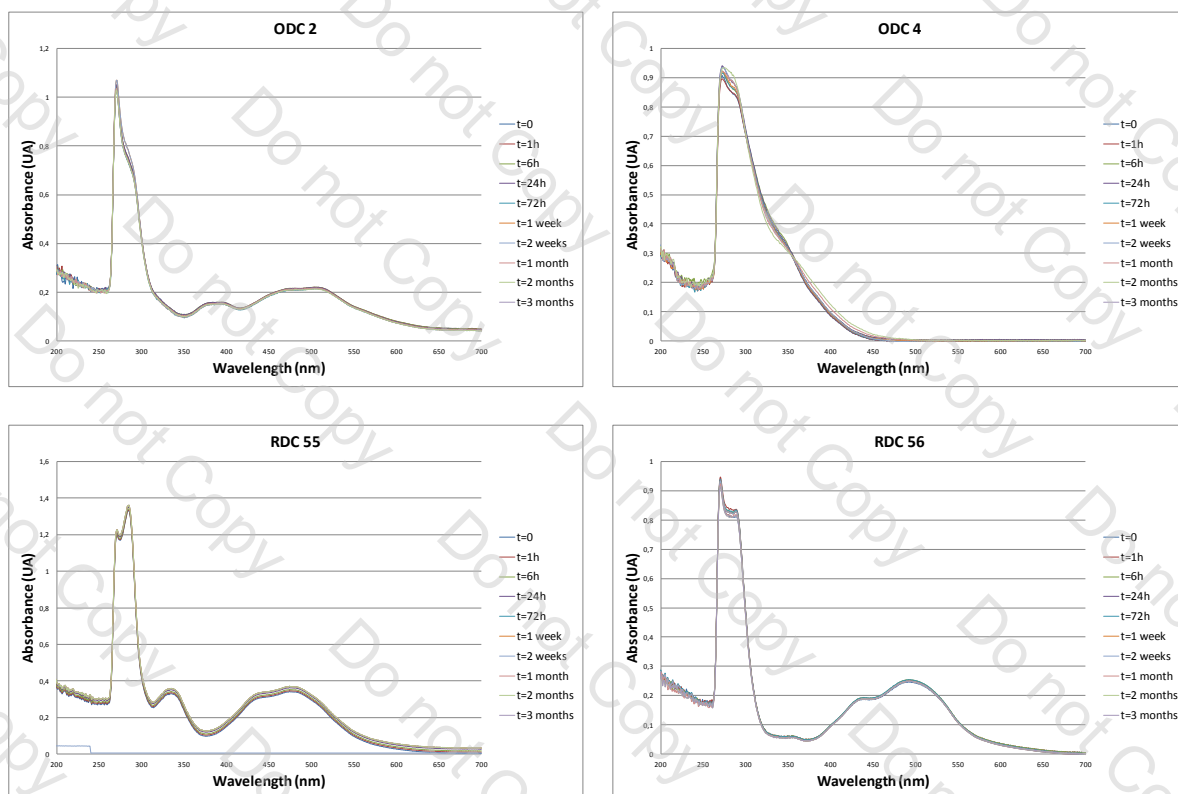


Figure 6: UV spectra of different compounds in EtOH at -15°C in the dark

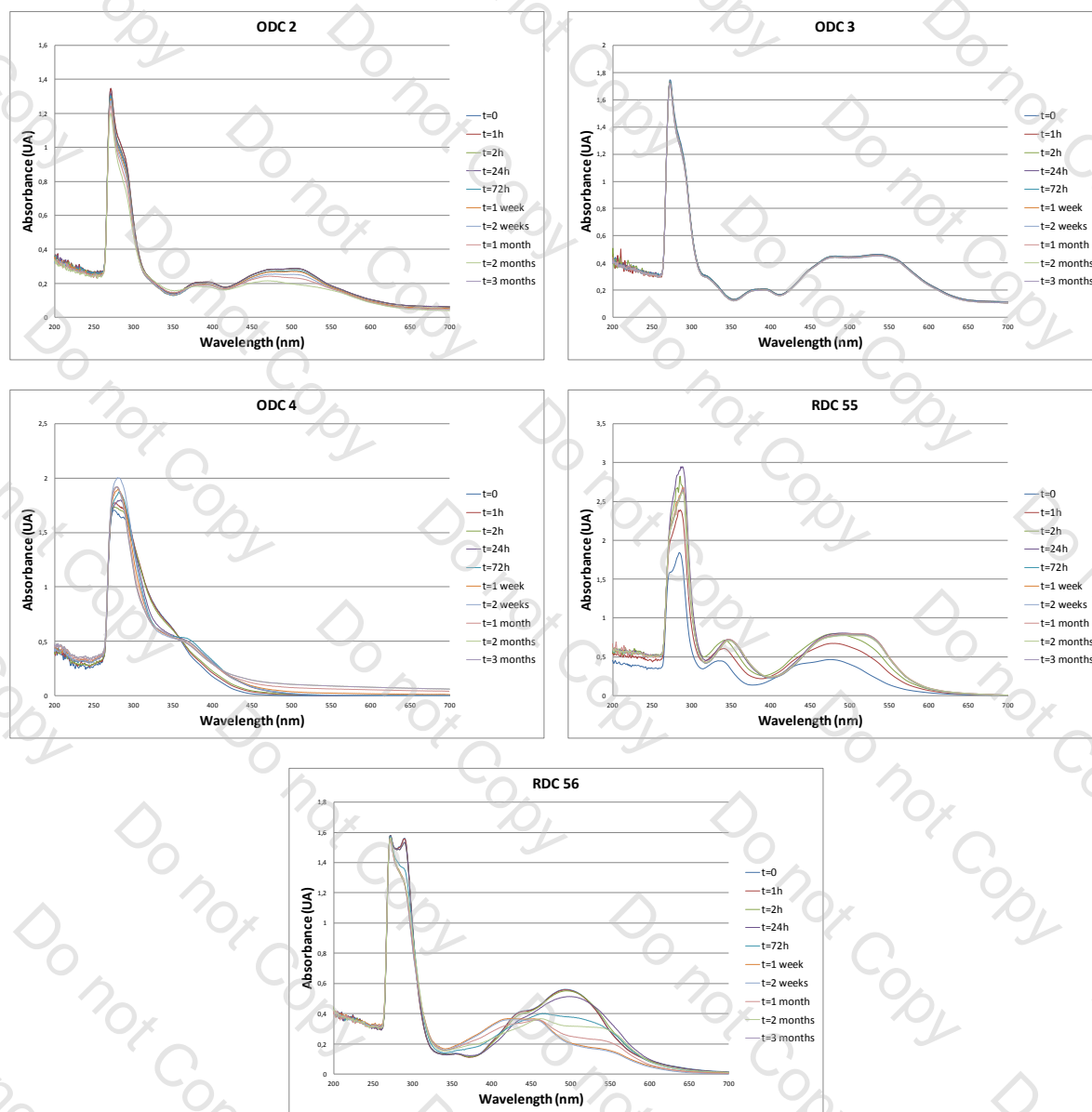


Figure 7: UV spectra of different compounds in EtOH at R.T. exposed to ambient light

3D non-linear regression using Maple programming software:

```
> with(LinearAlgebra) : with(Optimization) :
> Digits := 20 :
```

New data Z->IC50 Y->REDOX X->LIPO

```
> X := [ 1.2, 2.45, 1.8, 0.9, 2.9, 2.4, 2.25, 2.3, 2.35, 2, 2.5, 2.1, 2.95, 2.05, 2.05, 2.2 ] :
> Y := [ 0.56, 0.38, 0.595, 0.2, 0.310, 0.41, 0.52, 0.6, 0.66, 0.65, 0.62, 0.72, 0.71, 0.69, 0.62, 0.43 ] :
> Z := [ 3, 0.8, 1.7, 5, 3, 0.5, 0.6, 0.6, 1, 1.2, 1.2, 1.5, 0.9, 0.5, 1, 0.5 ] :
```

Optimization problem solving

```
> N := nops(X) :
> s := [ [ 0, 0 ], [ 1, 0 ], [ 2, 0 ], [ 0, 1 ], [ 0, 2 ], [ 1, 1 ] ] :
> Nb := nops(s) :
> A := Matrix( [ seq( [ seq( X[i]**s[j][1]*Y[i]**s[j][2], i = 1..N ), j = 1..Nb ] ) ] :
> C := A.Transpose(A) :
> det := Determinant(C) ;
```

$$\det := 0.013056264643088885701 \quad (2.1)$$

if the determinant C is non-zero, the optimization problem admits a unique solution.

```
> SOL := C**(-1).A.Vector(Z) ;
```

$$SOL := \begin{bmatrix} 11.795936598727576557 \\ -7.0103203434638224282 \\ 1.9726429101817551967 \\ -10.945674989394128379 \\ 19.015310059657703435 \\ -4.2237828279660482193 \end{bmatrix} \quad (2.2)$$

```
> sensib := Norm(C**(-1).A, 2) ;
```

$$sensib := 22.973603998797341690 \quad (2.3)$$

Polynomial solution

```
> P := add(SOL[j]*x**s[j][1]*y**s[j][2], j = 1..Nb) ;
P := 11.795936598727576557 - 7.0103203434638224282x + 1.9726429101817551967x^2
- 10.945674989394128379y + 19.015310059657703435y^2 - 4.2237828279660482193xy
```

$$(3.1)$$

Error computing

```
> errV := [ seq( (Z[j]-subs(x=X[j], y=Y[j], P))**2, j = 1..N) ] ;
errV := [ 0.048135990306214571762, 0.099573878461011647735, 0.18986052317382716361,
0.010881506078787635663, 0.094270021467868339690, 0.14910063186640644534,
0.0068254867901326104488, 0.0018690811461933696343, 0.076485065290132897273,
0.011187370478138178164, 0.39005366048653270716, 0.018520428755769530733,
0.12242436743398423343, 0.54899844270436445723, 0.017017086705267991997,
0.054950653702217071918 ]
```

$$(4.1)$$

```
> err := sqrt(add((Z[j]-subs(x=X[j], y=Y[j], P))**2, j = 1..N)) ;
err := 1.3565228324089679146
```

$$(4.2)$$

Correlation factor R²

```
> Zbar := add(Z[i], i = 1..N) / N ;
> SStot := add((Z[i]-Zbar)**2, i = 1..N) ;
SStot := 22.877500000000000000
```

$$(5.1)$$

for i to N do

```
ZZ[i] := subs(x=X[i], y=Y[i], P) ;
```

od:

```
> SSerr := add((Z[i]-ZZ[i])**2, i = 1..N) ;
SSerr := 1.8401541948468488517
```

$$(5.2)$$

```
> R2 := 1.-SSerr/SStot,
```

$$R2 := 0.91956489149396355145 \quad (5.3)$$

Computation of minimum of P

```
> MiniP := Minimize(P);
MiniP := [0.487881540305757475, [x = 2.3663831217306967916, y = 0.55062902781102200593]] (6.1)
```

```
> GradP := [diff(P, x), diff(P, y)]:
> HessP := Matrix([ [diff(P, x, x), diff(P, x, y)], [diff(P, x, y), diff(P, y, y)] ]):
> ValeursPropresP := Eigenvalues(HessP);
ValeursPropresP := [ 3.429682982575693166 + 0.1 I
                    38.546222957103224098 + 0.1 I ] (6.2)
```

if the eigenvalues are strictly positive, the minimum of P cancel the gradient.

```
> solve(GradP); subs(op(%), P);
{x = 2.3663831217306967916, y = 0.55062902781102200593}
0.4878815403057574740 (6.3)
```

Graphical representation of optimization

```
> with(plots) : with(Statistics) :
IC50 := [3, 0.8, 1.7, 5, 3, 0.5, 0.6, 0.6, 1, 1.2, 1.2, 1.5, 0.9, 0.5, 1, 0.5];
REDOX := [0.56, 0.38, 0.595, 0.2, 0.310, 0.41, 0.52, 0.6, 0.66, 0.65, 0.62, 0.72, 0.71, 0.69, 0.62, 0.43];
LIPO := [1.2, 2.45, 1.8, 0.9, 2.9, 2.4, 2.25, 2.3, 2.35, 2, 2.5, 2.1, 2.95, 2.05, 2.05, 2.2];
N := nops(IC50);
pts := [seq([LIPO[i], REDOX[i], IC50[i]], i = 1..N)];
G1 := pointplot3d(pts, axes=normal, axis[2]=[color=black],
axis[3]=[color=black], thickness=3, font=[HELVETICA, BOLD, 11],
title="", color=red,
symbol=sphere, labels=["", "Red-Ox potentiel (V)", "IC50 (micro M)"]);
IC50 := [3, 0.8, 1.7, 5, 3, 0.5, 0.6, 0.6, 1, 1.2, 1.2, 1.5, 0.9, 0.5, 1, 0.5]
REDOX := [0.56, 0.38, 0.595, 0.2, 0.310, 0.41, 0.52, 0.6, 0.66, 0.65, 0.62, 0.72, 0.71, 0.69, 0.62, 0.43]
LIPO := [1.2, 2.45, 1.8, 0.9, 2.9, 2.4, 2.25, 2.3, 2.35, 2, 2.5, 2.1, 2.95, 2.05, 2.05, 2.2]
N := 16
pts := [[1.2, 0.56, 3], [2.45, 0.38, 0.8], [1.8, 0.595, 1.7], [0.9, 0.2, 5], [2.9, 0.310, 3], [2.4, 0.41, 0.5],
[2.25, 0.52, 0.6], [2.3, 0.6, 0.6], [2.35, 0.66, 1], [2, 0.65, 1.2], [2.5, 0.62, 1.2], [2.1, 0.72, 1.5], [2.95,
0.71, 0.9], [2.05, 0.69, 0.5], [2.05, 0.62, 1], [2.2, 0.43, 0.5]]
G1 := PLOT3D(...) (7.1)
> G2 := plot3d(P, x=-1..7, y=0..1):
display(G1, G2):
```

Do not Copy

Summary

Since the clinical success of platinum drugs (*cisplatin* and its derivatives) as anticancer agent, medicinal inorganic chemistry has become a field of growing interest because it offers an alternative for the design of therapeutic agents that are not readily available to organic compounds. Although *cisplatin* is one of the most widely used drugs in chemotherapy, it is not effective for all types of cancer. Moreover, platinum drugs are the cause of disabling side effects (neurotoxicity, nephrotoxicity, weight loss, nausea...) and their applicability is limited by innate or induced resistance to platinum in a narrow range of tumours. Therefore, this clinical success has promoted the search for cytotoxic compounds with enhanced activities and more acceptable toxicity profiles. This has stimulated interest in complexes containing other heavy metals of the platinum group such as ruthenium because these compounds show lower toxicity than drugs based on platinum. Some ruthenium compounds have already shown promising anticancer activity and two Ru^{III} complexes *trans*-[RuCl₄-(DMSO)(Im)]ImH (NAMI-A and *trans*-[RuCl₄(Ind)₂]IndH (KP1019) recently enter in clinical phase for their respectively antimetastatic and cytotoxic properties.

In the essential aim of increasing activity and reducing side effects of anticancer agents, the Laboratoire de Synthèses Métallo-Induites has developed for several years organometallic ruthenium compounds **RDC** (**R**uthenium **D**erivative **C**ompound) in which one of the ligand is strongly bound to the metal *via* a strong σ C-Ru bond and stabilized by an intramolecular N-Ru bond. This thesis presents the recent advances of the laboratory in this field and the development of a second generation **RDC** in which the cyclometallating ligand is stabilized by two N-Ru bonds. Thus, several complexes pass the symbolic barrier of the nanomolar range for their IC₅₀ indicating a critical improvement. At the same time, we decided to focus our studies on osmium heavier congener, not only to complete the **RDC** chemical library, but also to verify the impact of exchanging the metal. An extensive chemical library **ODC** (**O**smium **D**erivative **C**ompound) of forty cyclometalated osmium complexes was synthesized and evaluated *in vitro*. Biological studies on these **ODCs** showed that osmium is another metal that deserves attention for the development of new effective antitumour drugs. The measurements of physicochemical properties such as red-ox potential and lipophilicity ($\log(P_{o/w})$) allowed us to tentatively correlate these parameters to the level of activity, thus approaching a possible Property-Activity Relationship (P.A.R.). More insight into the role of the red-ox potential will probably become clearer as we progress into the mechanism of action of these species.

Keywords

ruthenium / osmium / organometallic complexes / cyclometallation / red-ox potential / lipophilicity / inorganic medicinal chemistry / cancer / anticancer agent / chemotherapy / stability / *in vitro* and *in vivo* evaluation / Property Activity Relationship (P.A.R.)